On the Extent and Spatial Profile of Visual Crowding

Kristian Paul Skoczek

Bsc (Hons) MCOptom

School of Optometry and Vision Sciences

Cardiff University

Presented for the degree of Doctor of Philosophy

January 2023

Thesis summary

Visual crowding is the deleterious effect of clutter causing interference in the perception of neighbouring targets. Crowding effects are particularly prominent in peripheral vision and are regarded as the main limiting factor in the perception of peripheral details. Crowding occurs when distractor elements are present within a particular spacing around a target of interest known as a crowding zone. Targets may take on aspects of the appearance of flankers or appear as an indistinct mixture of target and flanker features. These effects are strongest when flankers are immediately neighbouring the target and weaken as separation increases. Disruptions in target perception are also particularly strong when flankers are similar in appearance to the target. It is currently unclear how the influences of target-flanker similarity and target-flanker spacing lead to a combined influence on the perception of detailed targets.

This thesis presents four studies investigating the effects of target-flanker similarity on the spatial dependencies of visual crowding in orientation. Manipulating the relative orientation of targets and flankers modulates the span over which systematic shifts in target appearance occurred as flankers encroached on the target. However, this transitionary span is consistently centred at a fixed distance from the target, which increases with eccentricity. This work presents a novel model of these changes at the limits of crowding zones – 'the spatial profile of crowding'. This model reveals that common methods of estimating crowding zone extent (the target for a wide variety of crowding research) may overlook informative changes in how detailed perception of a target shifts in the presence of flankers, conflating aspects that are dependent and independent of flanker appearance. The spatial profile of crowding provides new insight into potential confounds in prior research and may aid the design of future work by strengthening associations between structural and psychophysical measures.

Acknowledgements

To begin, I must thank my supervisors Tony, Jennifer and John. My gratitude for all your support and advice cannot be overstated. Without any one of you, this thesis would not have achieved half the quality of work that it has, and it would not have been possible without your combined efforts. I truly could not have hoped for a more encouraging, inspiring and entertaining supervisory team. Diolch o waelod fy nghalon i chi.

Next, I want to thank my friends, all of whom have been ready to offer support and comradery whenever I have needed it. I'm too afraid of missing somebody out to name you all, but if you think I might mean you, then I probably do. You have all been there to remind me to have a life outside of work, often at times when I especially needed a reminder. I also want to make special mention of my office mates and colleagues, to whom all of the above equally applies, but who also had to put up with the noise of my lunch-shakes and coffee grinding. Thankyou for all the patience, and best of luck with your own projects and future.

I must also thank the College of Optometrists for funding the project and offering additional support after the delays and impacts of the COVID pandemic. I wear my MCOptom with pride. Thankyou.

Finally, to my family. Knowing I always had your support is what kept me going through all the highs and lows of my time during this project. I know the work I've been doing and why I've been doing it is hard to make sense of some times, but your love and patience truly mean the world to me. You might not read it, but I want to dedicate this work to you:

Mum, Dad, Kirst and all of my grandparents. I'm doing my best to be your little genius.

Table of Contents

Table of Figures

Chapter 1 Introduction

1.1 Section 1 – Visual crowding

It is well established that peripheral vision is limited compared to central vision [see Rosenholtz (2016) for a review], but one key limiting factor is 'visual crowding' - the deleterious effect of neighbouring details on the perception of a target in a cluttered scene (see Figure 1.1 for a demonstration). Peripheral targets that are visible in isolation become less identifiable and difficult to identify when 'flanked' by distractors, demonstrating crowding to be the primary limiting factor on perception in normal peripheral vision (Levi 2008; Whitney and Levi 2011). Therefore, the known reduction in acuity with increasing distance from central vision is eclipsed by the corrupting influence of nearby details, leading crowding to be considered by some as 'the most important factor in peripheral vision' (Rosenholtz 2016). Crowding has

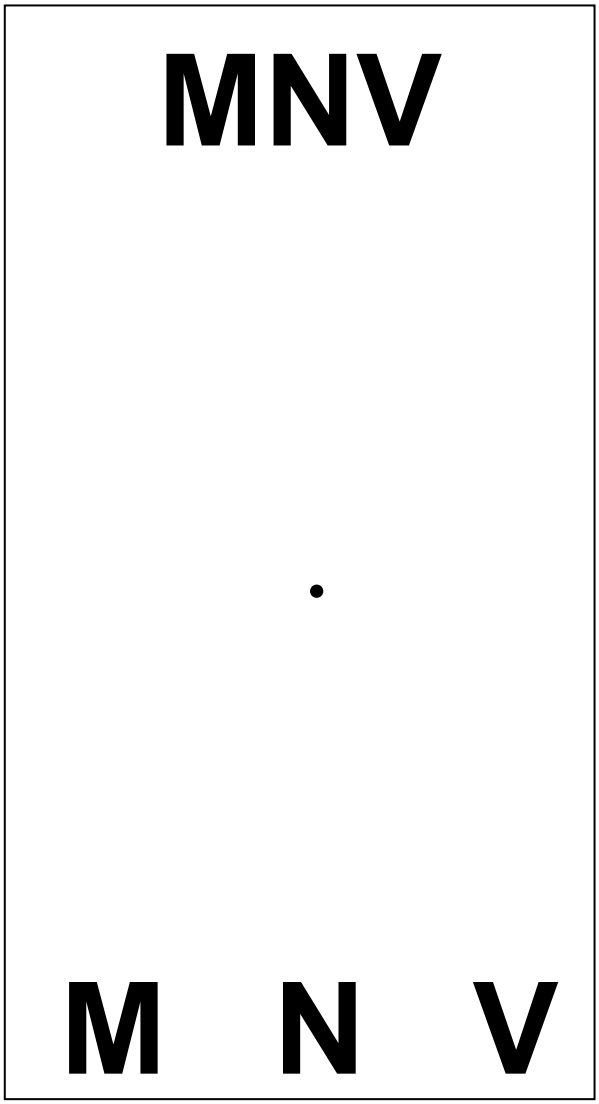

Figure 1.1 – Demonstration of crowding

When fixating the central spot, it will be easier to identify the centre letter of the lower trio of letters than the upper trio, despite both central letters, 'N', being identical. Reduced spacing in the upper trio makes identification of the central (crowded) letter more difficult, though it does not disappear entirely.

been found to influence perception of a wide range of stimuli from letters (Bouma 1970; Flom, Weymouth and Kahneman 1963) to faces (Kalpadakis-Smith, Goffaux and Greenwood 2018; Martelli, Majaj and Pelli 2005), and stimulus features including motion (Bex and Dakin 2005), colour/hue (van den Berg, Roerdink and Cornelissen 2007; Kennedy and Whitaker 2010) and orientation (Wilkinson, Wilson and Ellemberg 1997). Whilst much research focuses on crowding in normal peripheral vision, the effect has also been shown to be present in the fovea, though it has been a topic of debate as to whether or not foveal crowding is distinct from peripheral crowding (Coates *et al.* 2018; Lev, Yehezkel and Polat 2014; Levi, Klein and Hariharan 2002; Marten-Ellis and Bedell 2021).

The reported perceptual effects of crowding are wide-ranging. The earliest systematic studies of the effect often used letter stimuli and examined the proportion of correctly identified letters in the presence of bars or other letters that were placed at varying distances from them (Bouma 1973; Bouma 1970; Stuart and Burian 1962; Flom, Weymouth and Kahneman 1963). Later, more basic visual stimuli were used in a variety of setups, frequently following Strasburger, Harvey and Rentschler (1991) in measuring identification contrast thresholds and examining threshold elevations in the presence of flankers (e.g. Chung, Levi and Legge, 2001; Pelli, Palomares and Majaj, 2004; van den Berg, Roerdink and Cornelissen, 2007). Studies such as these noted that crowding has the effect of making target identification (as opposed to detection) more difficult. This highlights a key difference between visual crowding and similar effects such as lateral masking: crowding affects identification of target details, but not the detection of a target (Petrov, Popple and McKee 2007). Investigations allowing participants to report their perception of a target reveal that errors under visual crowding frequently follow the appearance of the flankers (Harrison and Bex 2015; Harrison and Bex 2017; Greenwood, Bex and Dakin 2010). This systematic nature of crowded errors will be utilised in this thesis to investigate spatial dependencies of crowding effects, and how these

effects may vary in ways that could be overlooked by common methods of investigating visual crowding.

1.1.1 Spatial selectivity of crowding

Some of the earliest mentions of 'crowding' were made in reports of the mechanisms of amblyopia (Stuart and Burian 1962), however its importance in normal vision was later identified. Stuart and Burian (1962) noted that the close spacing of letters on standard visual acuity charts led to reduced measures of acuity in comparison to isolated letters and termed this 'crowding'. However, similar phenomena were described earlier by Ehlers (1936, 1953) in relation to acuity, and by Korte (1923) in relation to Gestalt psychology. The effect of visual crowding may even have been the underlying subject of a 1738 essay by James Jurin, and was the likely origin of phenomena described by 11th century Islamic scholar Ibn al-Haytham (Strasburger and Wade 2015; Sabra 1989). Despite these early reports, much crowding literature begins by citing Bouma (1970) and the description of what was later termed 'Bouma's law' – that letters must be spaced by roughly half their eccentricity to avoid

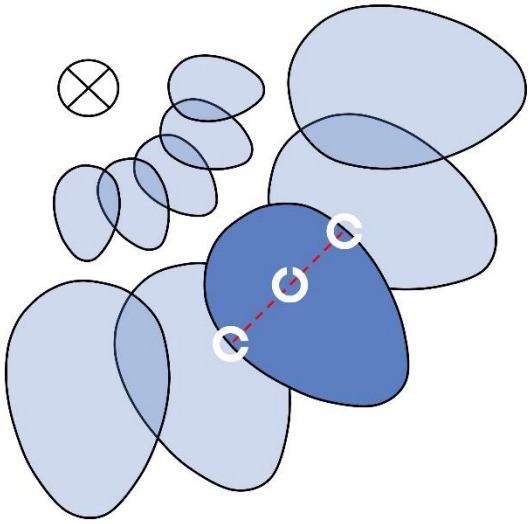

Figure 1.2 – Illustration of crowding zones

A 'crowding zone' is the spacing from a target (up-oriented C) within which flankers (right-oriented Cs) cause interference with the perception of target features. Zones increase in extent proportionally with target eccentricity (Bouma's law) and are elongated in the radial axis (direction of eccentricity) compared to the tangential axis (red dashed line).

interference in identification. Though better understood as a ‘rule of thumb’ rather than a true law unless several caveats are considered, see Strasburger (2020), this linear relation with eccentricity has proven particularly persistent in observations of crowding in subsequent decades (Toet and Levi 1992; Gurnsey, Roddy and Chanab 2011; Tripathy and Levi 1994; Strasburger, Harvey and Rentschler 1991; Pelli, Palomares and Majaj 2004; van den Berg, Roerdink and Cornelissen 2007). Frequently, studies investigating the span of crowding interactions will report a ‘Bouma constant’ linking the span of crowding effects to target eccentricity, typically around 0.4 - 0.5 (Pelli, Palomares and Majaj 2004; Bouma 1970; Andriessen and Bouma 1976) but varying between as much as 0.1 and 0.6 depending on experimental setup and stimuli used (Pelli and Tillman 2008; Bernard and Chung 2011). Crowding effects have also been observed at target-flanker separations with even greater Bouma constant (greater than 0.6) when the target is simultaneously masked and crowded (Vickery et al. 2009).

Crowding zones also show inward-outward anisotropy (see Figure 1.2). Flankers located further from fixation than target have been shown to be more disruptive to target appearance than equally spaced flankers located closer to fixation (Bex, Dakin and Simmers 2003; Chastain 1982; Banks, Larson and Prinzmetal 1979). Some reports have suggested the presence of this inner-outer difference could be considered a diagnostic factor of crowding particularly in comparison to surround suppression where no such difference is seen (Petrov, Popple and McKee 2007). However, other reports observe a reversal of anisotropy, meaning more central flankers are more disruptive, when a secondary attention-demanding task is required of observers (Petrov and Meleshkevich 2011b). Competing explanations for the effect have included differential cortical magnification of the spacing between inner and outer flankers (Pelli 2008; Motter and Simoni 2007) and differential weighting of responses to inner and outer flankers as a result of increasing cortical receptive field size with eccentricity

(Shechter and Yashar 2021; Dayan and Solomon 2010), though the effect may vary considerably with a range of experimental manipulations (Chakravarthi *et al.* 2021).

The ubiquity of Bouma's law gives rise to the concept of the 'crowding zone' – the area of visual space around a target within which flanking elements may influence perception of the target, illustrated in Figure 1.2 (Bouma 1970; Toet and Levi 1992; Levi, Klein and Aitsebaomo 1985). Investigations of crowding commonly seek to quantify the span of visual crowding and estimate the effect of experimental manipulations on this span, including target eccentricity (Toet and Levi 1992), target movement (Bex, Dakin and Simmers 2003) and presentation time (Tripathy, Cavanagh and Bedell 2014). However, studies in the literature utilised many varying definitions of what represents the limit of the crowding zone. Threshold-based definitions related to the psychophysical task (that is, the level of spacing necessary to achieve a threshold level of performance) are widespread (Levi, Hariharan and Klein 2002b; Ogata *et al.* 2019; Kwon and Liu 2019; Greenwood *et al.* 2012). These are useful for comparing data acquired with the same (or a sufficiently similar) task, but comparing data acquired with different tasks may be hampered by different definitions of threshold performance which are often determined by the task. For example, the number of permissible observer responses to a task will alter the threshold performance level, as this is typically fixed to the point halfway between best performance (100% 'correct', or lower if accounting for lapses in responses) and random guessing (or 'chance'). In a 2-alternative task (2-AFC), if task ability is degraded to random guessing, responses will be correct approximately 50% of the time, so threshold is defined as the spacing resulting in 75% 'correct' responses, whereas a 4-alternative task (4-AFC) may have an associated chance level of 25%, so threshold performance is 62.5% 'correct' responses. Several investigators have noted that differing estimation methods and definitions of spatial extent impact on the resulting measures of crowding extent (Gurnsey, Roddy and Chanab 2011; Harrison and Bex 2017),

which weakens comparisons between studies. Methodological decisions have also been demonstrated to confound results within experiments using the same estimation methods and definitions – in a 10-AFC letter identification task, being unable to report flanker identities improved estimates of crowding extent (Reuther and Chakravarthi 2020), which other studies had attributed to high-level knowledge of target and flanker set membership (Zhang *et al.* 2009). Alternative forced choice approaches are revisited in the context of the aims of this thesis in section 1.3.1 below).

1.1.2 Critical spacing

An alternative definition of the limit of the crowding zone, popularised by Pelli, Palomares and Majaj, (2004), is 'critical spacing' (see Figure 1.3). Adapted from the definition used by Levi, Hariharan and Klein (2002), 'critical spacing' was defined as the smallest spacing between a target and flankers which causes no increase in a task threshold [such as contrast letter-identification threshold (Pelli, Palomares and Majaj 2004)]. This definition may be more comparable between different tasks as it is independent of the task itself, relying only on the presence of a difference in result from that of an unflanked condition. As such, these measures of crowding extent represent a delineation between spacings where no

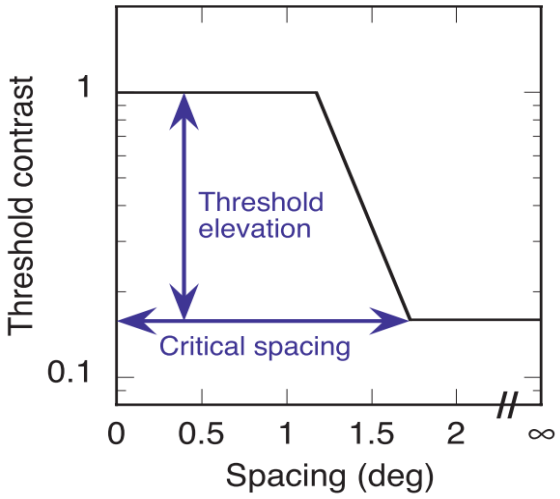

Figure 1.3 – Schematic figure of a 'Clipped-line' model from Pelli, Palomares and Majaj (2004).

Threshold contrast to identify Sloan letters was elevated with reduced target-flanker spacing. The ratio of max threshold elevation was taken as an indicator of crowding magnitude. 'Critical spacing', the maximum target-flanker separation to affect threshold estimates, is commonly used as a measure of crowding zone extent.

crowding effect is observed and spacings where the effect of crowding is present, which may be possible to infer from a wide range of experimental setups. This method also defines ‘crowding magnitude’ as the ratio of the maximally-crowded threshold level (typically at the smallest target-flanker separation) to the threshold level observed in the absence of flankers (or ‘uncrowded’). Estimating these points may be achieved with the fitting of a ‘clipped-line’ model (Pelli, Palomares and Majaj 2004) to threshold elevation data plotted against target-flanker separation (see Figure 1.3), though Gaussian functions have also been used to describe the shape of changes (Levi, Hariharan and Klein 2002b). The systematic elevation of thresholds as flankers are situated closer to a target in these instances highlight that crowding effects are not constant within the crowding zone. Yet it remained unclear as to the effect a smaller flanker spacing has on the perceived appearance of the target. A systematic alteration in target appearance towards that of the flanker elements is indicated by several proposed models of crowding (explored in Section 2 - Proposed mechanisms and models of visual crowding below), but a different experimental approach is required to investigate the perceptual effects of crowding in more detail.

1.1.3 Defining target-flanker spacing

As visual crowding is dependent on the spatial separation between targets and flankers, questions have been raised as to how this spacing should be defined. Early studies measured the empty spacing between targets and flankers (Flom, Weymouth and Kahneman 1963; Bouma 1970; Andriessen and Bouma 1976), which would later be called 'edge-to-edge' separation, but it has since become far more common for experiments in peripheral vision to measure the centre-to-centre distance between elements (Pelli, Palomares and Majaj 2004; Strasburger, Harvey and Rentschler 1991; Pelli and Tillman 2008), see Figure 1.4. In a key study comparing these definitions of spacing, Levi and Carney (2009) varied the size of flankers by altering the inner and outer radii of annular wedge shaped flankers, which either altered the edge-to-edge spacing (fixed outer radius) or maintained this spacing (fixed inner radius). Their data in both cases, and of a third experiment varying centre-separation while maintaining flanker size, were aligned when expressed in terms of centre-to-centre separation, indicating that centre-to-centre separation is the key determinant for crowding in peripheral vision. A later update to this assertion added that the location of details within a 'lopsided' object or flanker also determined the extent of crowding effects (Rosen, Chakravarthi and Pelli 2014). They proposed the critical spacing of parts, as opposed to whole objects, also offers an explanation for the 'self-crowding' of objects made up of several parts, such as faces (Martelli, Majaj and Pelli 2005). Crowding

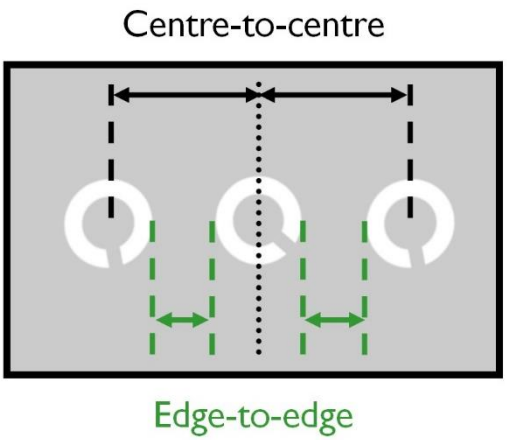

Figure 1.4 - Centre- and edge-separation

Target-flanker spacing may be defined either between the centres of target and flankers (black arrows) or in terms of empty space between stimulus elements (green arrows)

with simpler stimuli, including letters, are best described in terms of centre-to-centre separation (Levi and Carney 2009; Rosen, Chakravarthi and Pelli 2014; Martelli, Majaj and Pelli 2005).

1.1.4 Feature selectivity of crowding

Crowding effects are also affected by the similarity in appearance between targets and flankers (Ester, Zilber and Serences 2015; Kooi *et al.* 1994; Greenwood, Bex and Dakin 2010; Bernard and Chung 2011; Freeman, Chakravarthi and Pelli 2012). While crowding is observed between reasonably dissimilar stimulus elements, such as flanking bars around a Landolt-C target (Flom, Weymouth and Kahneman 1963), the effects of crowding are typically stronger when flankers are similar to the target in certain features, such as orientation (Ester, Zilber and Serences 2015; Põder 2012), colour (Manassi, France and Herzog 2012) and motion (Bex and Dakin 2005). This 'stronger' effect is has been interpreted as a larger crowding zone with similar targets and flankers, (Kooi *et al.* 1994), and this is predicted by 'grouping' models of crowding (Herzog *et al.* 2015), see 'Perceptual grouping' below. However, it is currently uncertain how the similarity-based strength of crowding may interact with established effects of weakening interference with increasing target-flanker separation (Harrison and Bex 2015). Explaining such potential interactions in terms of mechanisms of interference that produce crowding is also currently unclear (Kalpadakis-Smith *et al.* 2022; Ester, Zilber and Serences 2015), warranting further work into disambiguating the spatial- and featural-dependencies of visual crowding.

Crowding is most effective when flankers share several feature dimensions with the target (Põder and Wagemans 2007). For example, flankers will interfere with the perceived appearance of a target when elements are similar in both colour and orientation, than when they are similar in only one of these attributes. However, similarity in one attribute such as

colour may not predict crowding effects over another attribute such as direction of motion (Greenwood and Parsons 2020), highlighting the feature-specific nature of crowding effects. This featural interference in perception is sufficient to induce a perceived orientation in a noise target where no orientation information exists (Greenwood, Bex and Dakin 2010). Crowding may therefore act to promote the perception of consistency in features present in neighbouring areas of the visual field (Greenwood, Bex and Dakin 2010).

A range of experiments have tasked participants with reporting detailed stimulus features in the presence of crowding effects (Harrison and Bex 2017; Harrison and Bex 2015; Freeman, Chakravarthi and Pelli 2012; Ester, Zilber and Serences 2015), as opposed to comparing thresholds obtained with a simpler task such as tilt detection (Andriessen and Bouma, 1976; Mareschal, Morgan and Solomon, 2010a; Van der Burg, Olivers and Cass, 2017), Vernier acuity (judging the relative position of two lines) (Francis, Manassi and Herzog 2017) or other forced-choice methods (Wilkinson, Wilson and Ellemberg 1997). An early study focussing on contrast thresholds in number identification tasks (Strasburger, Harvey and Rentschler 1991) noted that for a peripherally viewed target, 42% of 'incorrect' responses corresponded to the identity of a flanker, far greater than the 20% as would be expected by chance for their task. Since then, numerous studies have investigated this 'substitution' effect of crowding with a range of stimuli (Freeman, Chakravarthi and Pelli 2012; Hanus and Vul 2013; Ester, Zilber and Serences 2015) though other types of errors relating to summary statistics, including averaging, have also been reported (frequently in combination with substitution effects) (Parkes *et al.* 2001; Greenwood, Bex and Dakin 2009; Dakin *et al.* 2010; Balas, Nakano and Rosenholtz 2009). These are explored further and compared with other reported mechanisms and models in Section 1.2 below).

1.1.5 Visual crowding in atypical vision

Beyond normal vision, visual crowding has also been explored in the context of a range of visual conditions. Abnormal visual crowding with amblyopia has been a longstanding topic of research interest (Stuart and Burian 1962), characterised particularly by a wider extent of foveal spatial interactions compared to typical vision (Levi and Klein 1985; Greenwood *et al.* 2012; Song, Levi and Pelli 2014). The pattern of errors made under crowding with amblyopic and developing vision have been shown to be similar to the pattern of errors made in the near-periphery with normal vision, indicating normal, developing and amblyopic crowding may all involve a common mechanism (Kalpadakis-Smith *et al.* 2022).

Elevated crowding has also been demonstrated with nystagmus (Chung and Bedell 1995; Pascal and Abadi 1995). In this condition, the eyes involuntarily drift and quickly resume their position, leading to a constant flicking motion, typically horizontally (Van Vliet 1982). A recent study suggests that the spatial extent of crowding zones in infantile nystagmus may be uniquely affected by this motion (Tailor *et al.* 2021). After measuring elevations in threshold acuity with Landolt-C stimuli crowded by flankers positioned vertically and horizontally, crowding zones in participants with nystagmus were found to be elongated horizontally. This specific elongation was not seen in participants with amblyopia in this study (Tailor *et al.* 2021) or in similar studies (Levi and Carney, 2011), suggesting this difference is primarily due to relocation of the image to more peripheral retinal locations. This evidence of elongation in crowding effects, along with simulated effects of nystagmus motion in typical participants, indicated that that crowding with nystagmus presents effects that are distinct from those of crowding in amblyopia and typical vision. Some uncertainty remains as to whether a sensory deficit arising from long-term degradation of the retinal image (due to constant eye movements) may also contribute to abnormal crowding in nystagmus observed in the study.

While amblyopia and nystagmus are primarily related to congenital and developmental issues, evidence has also been found for abnormal crowding in acquired conditions such as cerebral visual impairment in childhood (Pike *et al.*, 1994; Jacobson *et al.*, 1996; reviewed in Huurneman *et al.*, 2012), posterior cortical atrophy in older adult participants (Crutch and Warrington 2007) and recently in glaucoma (Ogata *et al.* 2019; Stringham *et al.* 2020; Shamsi, Liu and Kwon 2022). In participants with glaucoma, these studies found increased critical spacing (see Figure 1.3) in crowded letter identification tasks. Given that glaucoma is primarily associated with degeneration and death of retinal ganglion cells (Chang and Goldberg 2012; Tribble *et al.* 2019), the authors speculated that the crowding evidence indicates that disrupted retinal input may be associated with changes in how receptive fields are combined cortically (Ogata *et al.* 2019; Stringham *et al.* 2020; Shamsi, Liu and Kwon 2022). Indications of cortical reorganisation in the presence of glaucomatous damage has also been found outside of crowding studies (King *et al.* 2006; Redmond *et al.* 2010a; Zhou *et al.* 2017).

Investigating visual crowding in atypical vision has provided new insight into both the pathophysiology of studied conditions, and clues as to how visual crowding arises in normal vision. However, researchers continue to debate the mechanisms contributing to the perceptual and spatial effects of crowding (explored in section 1.2 below). Frequently used experimental methods have focused on either the perceptual effects of crowding [e.g., by comparing observers' performance at a task when flankers at a fixed target-flanker separation are manipulated, as in Ester, Zilber and Serences (2015)] or the extent of spatial interactions [e.g., by varying target-flanker spacing until a defined 'threshold' level of performance at a task is achieved, as in Toet and Levi (1992)]. Less frequently, perceptual and spatial influences may be studied together (Pelli, Palomares and Majaj 2004; Harrison and Bex 2015; Harrison and Bex 2017), and a complete account for visual crowding remains elusive.

Understanding how spatial and non-spatial factors interact to simultaneously influence the perception of a target may help to close the gap between contending explanations for crowding presented in the literature.

1.2 Section 2 - Proposed mechanisms and models of visual crowding

This section will explore proposed mechanisms and models of visual crowding in more detail. There will be a brief introduction to some underlying visual functions that are necessary for crowding, specifically those which are particularly targeted by common methods used in crowding research such as contrast sensitivity and orientation perception. Presented literature may be split into two broad categories: 'bottom-up' processing approaches (which are frequently inspired by more basic neurophysiological mechanisms relating to low-level stimulus features such as orientation and contrast), and 'top-down' mediation of target recognition (often invoking higher-level visual areas which consider targets in wider context with regard to global configurations of stimuli and attentional effects). How these differing proposals explain spatial and featural influences of crowding will be explored and compared.

1.2.1 Visual functions contributing to crowding

'Visual perception' encompasses a range of mechanisms which contribute to the perception of the world. While it is beyond the scope of this thesis to describe every possible process, this section will highlight the key functions which will contribute to the tasks commonly used to assess visual crowding, before proposed models and mechanisms of visual crowding are reviewed. Exploring how changes to the underlying functions which are sampled in order to detect and measure crowding is a key concept of the thesis, as this may aid the translation

of experimental findings into predictions of how a target is actually perceived under crowded conditions.

1.2.1.1 *Light detection and spatial summation*

Detection of light and sensitivity to contrast arises from summation – the process by which photons of light incident on the retina are integrated over space (spatial summation) and time (temporal summation) in order to produce a single percept (Baumgardt 1959; Barlow 1958; Owen 1972). This summation represents an early stage in cortical processing of visual stimuli (Pan and Swanson 2006) and is the fundamental process being (incidentally) tested by standard perimetric measures of differential light sensitivity (Redmond *et al.* 2010a). Ricco's law (Riccò 1877) states that the area and intensity of a stimulus are directly and inversely proportional for sufficiently small stimuli at detection threshold. The largest stimulus size for which this is true is termed 'Ricco's area'. This area increases with eccentricity (Wilson 1970; Volbrecht *et al.* 2000; Vassilev *et al.* 2003) and has been investigated alongside crowding zone extent (Kwon and Liu 2019), as the extent of both may be associated with retinal ganglion cell density. Ricco's area and crowding zone extent have also both been observed to be enlarged with glaucoma (Redmond *et al.* 2010a; Ogata *et al.* 2019), potentially hinting at a link between summation at the level of point stimuli and whole objects.

1.2.1.2 *Contrast perception*

Ricco's law and Bloch's law both describe summation of light within a simple point stimulus, whose appearance may be defined by its 'Weber contrast' (a ratio of the difference in luminance in comparison to the background luminance, formulated mathematically by Fechner (1860)). Larger, more varied stimuli such as gratings and Gabor patches can also be used to measure pattern contrast sensitivity, but are better defined by the 'Michelson

contrast' (Michelson 1927) of maximum and minimum luminance within the pattern. At zero Michelson contrast, the pattern fades to the mean luminance of the stimulus, typically this is kept equal to the background luminance so that when the pattern can no longer be discriminated, there is no detectable stimulus. If the mean luminance of the pattern were greater than the background luminance, a bright area may be detected even when the pattern detail (e.g., the orientation of a Gabor stimulus) cannot be discriminated. The distinction between stimulus detection and detail discrimination is important, as this is part of the fundamental difference between 'masking' (which affects detection) and crowding (which affects perception of detail, thus identification) (Pelli, Palomares and Majaj 2004). Contrast threshold elevations (indicating reductions in contrast sensitivity) for identification of numerical stimuli were demonstrated to be a good indicator of the presence of crowding by Strasburger, Harvey and Rentschler (1991) and similar contrast threshold measures have been used in other crowding experiments (Pelli, Palomares and Majaj 2004).

1.2.1.3 Feature perception

An observer's ability to discriminate detail may be described in terms of contrast sensitivity or acuity. Contrast sensitivity may be measured by altering the contrast of a stimulus pattern at a fixed spatial frequency to determine the threshold level of contrast – 'how much contrast is necessary for this spatial frequency to be perceived?'. Alternatively, measures of acuity will typically fix the level of contrast and alter the spatial frequency of the target – 'what is the smallest level of detail that can be resolved at this contrast?'. While related, these are not synonymous measures and both approaches have been utilised in crowding research (Strasburger, Harvey and Rentschler 1991; Song, Levi and Pelli 2014; Barollo *et al.* 2017). Acuity and sensitivity represent different methods of probing the contrast sensitivity function (CSF), which links spatial frequency and contrast of details at the threshold of perception (De

Valois, Morgan and Snodderly 1974). The effect of crowding on measures of acuity has been shown to vary with stimulus contrast (Kothe and Regan 1990; Simmers *et al.* 1999), and shifts in peak sensitivity towards higher spatial frequencies have been found in the presence of flankers (Chung and Tjan 2007), highlighting the importance of considering differences in stimulus characteristics and methodological approach when comparing crowding studies.

Orientation and spatial frequency information (which are frequently the basis of crowding stimuli e.g. in Wilkinson, Wilson and Ellemberg (1997)) are processed as early as V1 (Hubel and Wiesel 1962) and closely related to RGC density (Thibos, Cheney and Walsh 1987; Anderson, Zlatkova and Demirel 2002) but other stimuli and features are believed to follow distinct pathways in the visual cortex (Livingstone and Hubel 1988). Indications for the separation of feature and positional pathways have been found in crowding experiments (Strasburger 2005), and the ventral stream (or 'what' pathway) has received particular attention with regards to crowding (Freeman and Simoncelli 2011) and its potential relationship with texture perception. There is division in the crowding literature as to whether crowding effects originate at the early processing of stimulus parts or features (Rosen, Chakravarthi and Pelli 2014) or if the combination of features into object representations then determine crowding via 'perceptual grouping' mechanisms (Herzog *et al.* 2015).

1.2.2 Possible neural loci of crowding

Crowding was established as a cortical phenomenon by the finding of an effect when targets and flankers were presented separately to right and left eyes (Flom, Heath and Takahashi 1963). Andriessen and Bouma (1976) conceived an early suggestion that lateral inhibition of cortical complex cells may contribute to the interference effects they observed, but subsequent research has expanded on the various potential cortical origins of visual crowding. After the assertion that the size of crowding zones may correspond to a fixed

spacing in millimetres of cortical surface (Tripathy and Levi 1994), this separation was calculated by Pelli (2008) to be 6mm at V1 in the radial direction, and 1mm in the tangential direction (assuming a 'Bouma constant' of 0.4). Further psychophysics-based research posited that receptive field properties in visual area V4 could account for crowding interactions observed in visual search tasks (Motter and Simoni 2007), and the reduction of crowding when flankers are presented across the vertical meridian (Liu *et al.* 2009). Evidence that the spatial-dependence of visual crowding relates to perceived, over physical, location of flankers (Dakin *et al.* 2011) also supports the idea that crowding effects could originate in later visual areas as earlier areas (V1 and V2) are believed to be primarily directed by physical locations of stimuli (Fischer, Spotswood and Whitney 2011). Conversely, a model developed to explain the characteristic anisotropies of crowding zone extent places the origin of crowding in V1 as the result of lateral interactions that were not sufficiently explained by V4 receptive field anisotropies (Nandy and Tjan 2012). Research characterising visual crowding as a statistical summary of areas of visual space (reviewed further in section 1.2.3.2.2 below) proposed spatial properties of crowding which aligned with neural pooling properties of visual area V2 (Freeman and Simoncelli 2011). More recent electrophysiological measurements in Rhesus monkeys have also suggested neural activity in V4 indicates receptive field properties which match patterns featural selectivity observed in crowding (Motter 2018).

The advent of technology enabling direct of imaging of cortical activity concurrent with crowding stimuli and tasks has provided a new approach to determining the possible neural origins of crowding. Functional magnetic resonance imaging (fMRI) techniques such as measuring the blood-oxygen-level-dependent (BOLD) response, which infers neural activity from regionally increased blood flow (Kim and Ogawa 2012), have been popular in such experiments. Crowding of a target has been associated with suppression of corresponding fMRI BOLD responses as early as V1 (Kwon *et al.* 2014), though similar evidence has been

used to propose crowding occurs at multiple levels through the visual system (Anderson *et al.* 2012) or that influences from higher areas cannot be ruled out (Millin *et al.* 2014).

Population receptive field (pRF) mapping, which maps the visual field area corresponding to each 'voxel' (3-dimensional pixel) of fMRI data, has also been utilised in crowding research. V4 reoccurs as a proposed potential origin of crowding in studies comparing psychophysical estimates of critical spacing with cortical map area sizes by one research group (Kurzawski, Pelli and Winawer 2021; Kurzawski *et al.* 2021; Himmelberg *et al.* 2021). Population receptive fields in V2 have been found to be correlated with the magnitude of crowding effects, including modulation of both measures with the addition of a separate task with additional attentional demand and perceptual learning (He, Wang and Fang 2019).

Several potential origins and explanations for crowding have been put forward in the literature, and a unifying consensus is yet to be reached. The heart of the discourse appears to be whether sufficiently strong evidence exists to explicitly single out areas as being the sole origin, or mostly uninvolved, with mechanisms that produce crowding effects (Kwon *et al.* 2014; Nandy and Tjan 2012; Millin *et al.* 2014; He, Wang and Fang 2019). Variations in approaches, both in terms of imaging and psychophysical methods, may pose unique obstacles to targeting specific areas. For example, while V4 has received particular attention in several studies (Kurzawski, Pelli and Winawer 2021; Liu *et al.* 2009; Motter and Simoni 2007), fMRI BOLD responses (which underpin pRF mapping) corresponding to V4 may be selectively hindered by its proximity to veins and sinuses within the brain (Boyd Taylor *et al.* 2019). This may lead to additional difficulty in retinotopic mapping of V4 in comparison to earlier visual areas, hindering comparisons between them. Meanwhile, psychophysical approaches are hugely varied in terms of task and stimulus used, leading some investigators to attempt to mathematically quantify the effect of target-kind in a model predicting critical spacing (Kurzawski *et al.* 2021). Alternatively, if appearance-related and spacing-related

effects of crowding could be effectively disentangled and measured separately, a new line of investigation may be opened. Relating separated psychophysical measures of spatial and featural dependencies of crowding to imaging-based measures of receptive field properties could help to indicate the cortical areas involved in crowding effects.

1.2.3 Perceptual and spatial predictions of proposed crowding models

In reviewing proposed models of crowding, particular attention will be given to the predictions these models make with regard to perceptual outcomes of crowded tasks (i.e., what errors are made in the presence of flankers) and the predicted spatial extent of these effects. There is considerable variation in experimental stimuli used to develop the current frameworks pertaining to crowding, and attempts to directly compare different models with the same sets of stimuli have seen limited success (Doerig *et al.* 2019).

1.2.3.1 Types of responses observed in crowding

Early studies of stimulus interactions proposed stimulus identity was lost in the presence of flankers, either by direct inhibition from neighbouring letters (Chastain 1982) or due to coarse resolution of attention (He, Cavanagh and Intriligator 1996). However, early evidence indicated that the appearance of a crowded target was systematically influenced by the appearance of the flankers, as opposed to degrading target appearance in a way that would lead to random responses (Strasburger, Harvey and Rentschler 1991; Wolford 1975). In these studies using alphanumeric stimuli, it was noted that participants frequently reported the flanking letter or number in place of the target, rather than a non-presented character – termed a 'substitution' error. Substitution may occur between whole objects (Strasburger 2005; Huckauf and Heller 2002), or stimulus features (Nandy and Tjan 2007; Põder and Wagemans 2007). These types of errors may be the result of a misdirection of attention

(Strasburger 2005), or a heavy weighting of flankers in a combined response to crowded stimuli (Greenwood, Bex and Dakin 2009).

Later studies with more basic stimuli uncovered another type of error that may occur in crowded conditions – feature averaging (Parkes *et al.* 2001). Where substitution-based crowding would predict the irretrievable loss of orientation information in the target, Parkes *et al.* found that the average orientation of a group of stimuli could still be reliably reported even when the orientation of a specific target could not. They argue this supports the idea that observers have access to the combined (or 'pooled' – see below) appearance of crowded targets but not specific signals. Subsequent reports of 'averaging' type errors (alternatively called 'assimilation' errors) have continued to indicate that 'weighted averaging' could explain distributions of detailed reports under crowding (Greenwood, Bex and Dakin 2009; Dakin *et al.* 2010; Hanus and Vul 2013).

1.2.3.2 Bottom-up processing of stimulus features

Theories of crowding mechanisms may be termed 'bottom-up' where observations seen in crowding experiments are related primarily to low-level stimulus features such as orientation, contrast and spacing. This contrasts with 'top-down' mechanisms relating to influences based on the perception of targets and flankers as whole objects, which frequently invoke 'grouping' stages to explain effects of crowding seen with more complicated stimulus arrangements.

1.2.3.2.1 Pooling

Pooling theories propose that perceptual information from targets and flankers are combined to influence the final perception of a crowded target (Parkes *et al.* 2001). In a study involving judgements of the position of parts of 'cross-like' stimuli, Greenwood, Bex and Dakin (2009) found participant responses were better predicted by a model utilising a 'weighted average' of target and flanker appearance, than a model of probabilistic substitution. This study

highlighted the benefit of a fine-grain continuous response scale (as opposed to an m-alternative forced choice paradigm with fewer options) in order to be able to differentiate the effects of possible substitution- and averaging-type mechanisms. This averaging model was also able to produce substitution-type effects when flankers are weighted heavily, indicating nonlinear weighting of stimulus features may also explain similarity- and spacing- based differences in crowding effects (later explored with orientation-defined stimuli by Ester, Zilber and Serences (2015) and Harrison and Bex (2015)). Differential weighting of flanker elements could also underpin radial-tangential anisotropy (Greenwood *et al.* 2017; Van Den Berg, Roerdink and Cornelissen 2010).

Pooling models have been combined with the idea of 'population coding' (Zemel, Dayan and Pouget 1998; Pouget, Dayan and Zemel 2000), to mathematically characterise crowding as response of groups of neurones (as opposed to individual neurones) tuned to the properties of stimuli used (Van Den Berg, Roerdink and Cornelissen 2010). In this framework, 'averaging' and 'substitution' may be considered descriptors of portions from a continuous range of responses, rather than necessarily being the result of specific substitution or averaging mechanisms (Harrison and Bex 2015). Using 'Landolt-C like' stimuli, Harrison and Bex (2015, 2017) found that a range of reported effects of crowding (specifically 'substitution' and 'averaging', as well as 'accurate' reports) can be explained with a weighted combination of responses to nearby stimulus elements. The later report (Harrison and Bex 2017) in particular indicated a constant proportion of 'averaging' type responses as target-flanker spacing increased, while 'accurate' and 'substitution' response types showed opposing trends. At greater flanker distances, participants more accurately reported the target orientation, while at smaller separations a greater proportion of responses clustered around the flanker orientation ('substitution'). They propose this is the result of spacing-dependent

weighting of target and flanker responses within a Gaussian ‘weighting field’, inspired by the action of neural response fields (Ringach 2002).

The ‘weighting field’ proposed by Harrison and Bex (2015) has been criticised for not fully explaining some effects of crowding demonstrated with identical stimuli. In return, Pachai, Doerig and Herzog (2016) argued that the presented weighting field is inadequate as it does not accurately predict participant reports when multiple concentric flankers of the same orientation are present. They propose that a ‘grouping’ mechanism is necessary to explain why observers can more accurately report the orientation of a target when more flankers are added, suggesting that crowding is lessened when flankers ‘group’ separately to the target.

Figure 1.5 - Population pooling from Harrison and Bex (2015)

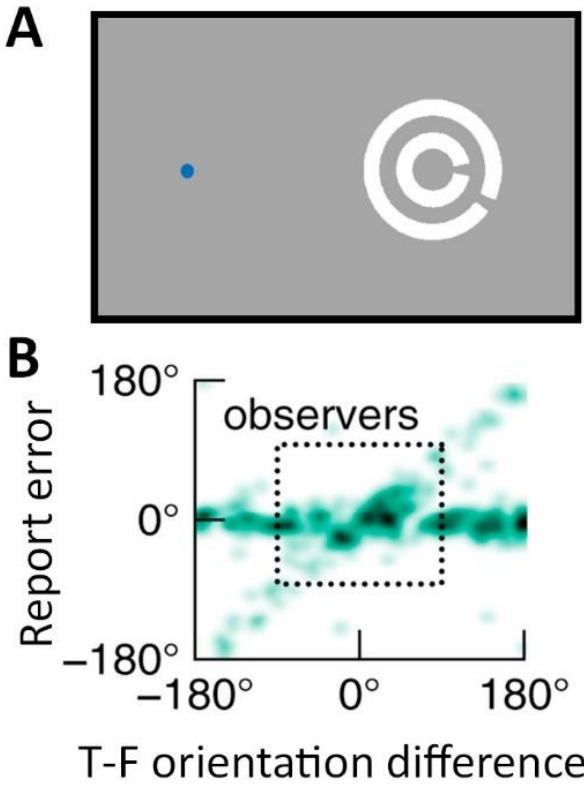

Panel A shows the ‘Landolt-C like’ stimuli used in the study – participants were tasked with reporting the orientation of the central target while the outer flanker was varied in diameter and relative orientation difference. Panel B shows observers’ reports with the smallest diameter flanker. Two clear trends are seen: accurate reports producing a horizontal line around a report error of 0°, and a diagonal line approximately matching the orientation of the flankers. Within the dotted box (where targets and flankers are most similarly oriented), predictions of ‘substitution’ and ‘averaging’ type mechanisms are hard to distinguish.

In response, Harrison and Bex instead propose the presence of texture boundaries may also influence the weighting of responses in the population code (Harrison and Bex 2016). Additionally, Agaoglu and Chung (2016) hypothesised that the Gaussian form of the weighting field arose from Harrison and Bex's method of defining the target as the inner-most C stimulus. They claimed that the weighting field as presented by Harrison and Bex (2015) would imply that the most central stimulus element would always be weighted more heavily in the population code. However, their data suggest participants are more precise in reporting the outermost C in both of their experimental conditions ('flanker inside' and 'flanker outside'). It should be noted that in their experiment, observers were not directed to one particular C as a 'target', and were asked to report the orientation of both Cs. This slight difference in experimental method could be the source of the apparently opposing findings between the two papers, as other studies have found similarly altered crowding effects with broad- vs directed-attention (Rummens and Sayim 2021; Petrov and Meleshkevich 2011b). Overall, the balance of evidence appears to be in favour of the weighting field mechanism, though finer aspects as to how weightings may vary with target-flanker similarity remain to be explored (Kalpadakis-Smith *et al.* 2022).

While the systematic nature of feature (i.e., relative orientation difference) dependent action is evident from the raw data of Harrison and Bex (2015), the data present along a diagonal line in Figure 1.5B, the authors do not factor orientation difference into the weighting stage of their weighted pooling model. This likely follows from their decision to randomise target-flanker orientation difference across trials, rather than presenting fixed levels of orientation difference, so their data covered the entire range of possible target-flanker orientation differences. As examining target-flanker similarity was not their primary aim, Harrison and Bex weighted flankers only by their distance from the target, predicting flankers of similar and dissimilar orientation at the same distance would contribute equally to the pooled response.

This results in stronger averaging with similarly oriented flankers (where population responses to target and flanker orientations overlap) but otherwise no predicted difference in processing, or spatial extent, with regards to orientation difference. The authors posit this stronger averaging is an origin of similarity effects, though in the region where primarily substitution-type errors are predicted (>90° orientation difference), the only difference is the orientation at which substitution errors are placed, not their relative proportion. Other studies have been primarily focused on flanker orientations less than 90° (Ester, Zilber and Serences 2015; Andriessen and Bouma 1976; Põder 2012). One study that did investigate greater orientation differences (Ester, Klee and Awh 2014) only reported a slightly greater incidence of substitution-errors with a 60° orientation difference, but do not mention a difference between their 90° and 120° difference conditions.

1.2.3.2.2 Summary statistics and texture processing

An elaboration on the pooling approach to crowding posits that crowded stimuli are processed as a continuous texture wherein image statistics are used to summarise stimuli within regions of the visual field (Keshvari and Rosenholtz 2016; Balas, Nakano and Rosenholtz 2009). Balas, Nakano and Rosenholtz (2009) utilised a texture-synthesis algorithm (Portilla and Simoncelli 2000) to generate ‘mongrels’ of crowding stimuli – images whose physical appearance was degraded but whose summary statistics (e.g., orientation and location information) were the same. These ‘mongrels’ were then presented to human observers in an image sorting task designed to be analogous to the crowding task associated with the original stimuli (a 4-AFC letter identification task). The authors found a significant association between human performance in the crowded letter identification task and mongrel sorting task (and also between human performance under crowding and computer classification based on image statistics). From this they propose local summary statistics within patches of peripheral vision can predict crowding task performance. Therefore, they argue, crowding is

the result of the visual system condensing visual input by encoding key statistical features under cluttered conditions. This approach has come to be called a 'texture tiling model', with several iterations being presented in the literature (Keshvari and Rosenholtz 2016; Freeman and Simoncelli 2011; Rosenholtz *et al.* 2012; Rosenholtz, Yu and Keshvari 2019).

The texture tiling model is compatible with pooling approaches to crowding, demonstrated by Freeman and Simoncelli (2011) whose 'metamers' (similar to 'mongrels') were generated using pooling properties of V1 cells projecting to V2. This study generated synthesised images wherein peripheral patches of a real image were decomposed in line with the action of 'V1-like' oriented receptive fields, then underwent weighted averaging of local features. By varying the eccentricity-dependent scaling of the size of these peripheral patches, the study found synthesised images were perceptually identical to human observers when patch sizes were similar to the pooling properties observed in physiological studies of V2 (in humans and macaques). The authors found an eccentricity-scaling parameter of 0.5, in line with Bouma's proposed constant (Bouma 1970).

While taken as an indicator of the link between scene perception, texture processing and visual crowding (Movshon and Simoncelli 2014), this inference has been called into question by the finding that much smaller eccentricity-related scaling is required for such synthesised images to be perceptually identical to unaltered natural scenes (Wallis *et al.* 2019). It has also been proposed that a step involving segmentation or grouping of image content is necessary to adequately represent peripheral vision (Doerig *et al.* 2019; Manassi, Sayim and Herzog 2013).

1.2.3.3 Top-down mediation and 'perceptual grouping'

Experimental evidence has challenged many bottom-up models of crowding, particularly in how they struggle to fully explain some observed effects of crowding observed with more

complicated arrangements of stimuli at greater spacings around a target (Pachai, Doerig and Herzog 2016; Doerig *et al.* 2019; Manassi, France and Herzog 2012). In such instances, mechanisms featuring 'top-down' mediation of crowding mechanisms have been proposed, invoking higher visual areas to modulate the final perception of a target after lower-level processing in earlier areas. 'Grouping' mechanisms are a persistent component of top-down modulation theories (Francis, Manassi and Herzog 2017; Manassi, Sayim and Herzog 2013), while attention has been associated with a range of experimental observations (Strasburger, 2005; Dakin *et al.*, 2009; Mareschal, Morgan and Solomon, 2010a).

1.2.3.3.1 Attention and crowding

Attentional accounts of crowding have proposed that positional uncertainty in the visual periphery (Rentschler and Treutwein 1985; Levi and Klein 1990; Levi, Klein and Yen Lee Yap 1987) may lead to additional difficulty in directing attention (Strasburger, Harvey and Rentschler 1991; Strasburger 2005). This account predicts substitution-type errors in instances when the 'spotlight of attention' (Eriksen and St. James 1986) is misdirected to a flanker instead of the target, but there is no integration of information from both target and flanker stimuli (Zhang *et al.* 2012). This is difficult to reconcile with evidence of weighted averaging models exceeding probabilistic substitution models in predicting observer's reports (Greenwood, Bex and Dakin 2009).

Alternatively, a coarser resolution of attention in the periphery has been proposed as a cause of the spatial extent of crowding effects (He, Cavanagh and Intriligator 1996; Intriligator and Cavanagh 2001). In this framework, the 'spotlight of attention' is not misdirected towards a flanker, but is instead too large to be able to select the target from other stimuli within the spotlight area. This would cause a mixture of feature and positional information to be perceived and subsequent breakdown in target identification, but the exact perceptual outcome is difficult to predict. Nevertheless, this approach may be able to explain different

crowding effects observed with varying target-flanker similarity (Kooi *et al.* 1994; Ester, Zilber and Serences 2015; Põder 2007) as an interaction of several, feature-based forms of attention (Kravitz and Behrmann 2011).

Attention has also been reported to have an influence on the ability to perform a crowded task that is dissociable (thus, separate) from the effects of crowding in a pooling framework. Dakin *et al.* (2009) found that the addition of an attention-demanding foveal task to a peripheral crowded task only affected how the peripheral stimuli were sampled, not the process by which they were subsequently integrated (i.e., crowding). They propose being able to direct additional attentional resource to a particular task may reduce thresholds obtained in the task by improving the global access to peripheral stimuli but does not affect the local process by which nearby stimulus elements are combined, and that therefore crowding is distinct from attention.

1.2.3.3.2 Perceptual grouping

'Perceptual grouping' refers to a phenomenon whereby elements of a stimulus array are perceived as being part of a common group (Herzog 2018), often when Gestalt principles (such as proximity and closure) are observed (Wertheimer, 1923; *translated in* Ellis, 1938). With regards to crowding, perceptual grouping has been proposed to determine which elements of a group of stimuli will undergo crowding (Malania, Herzog and Westheimer 2007; Manassi, France and Herzog 2012). In this hypothesis, crowding occurs when a target is grouped with flanking elements, and not when flankers group separately. This is posited to explain observations of 'uncrowding' – whereby perception of a crowded target is improved when additional flankers are added to a stimulus array and cause flankers to group separately to a target (Manassi, Sayim and Herzog 2013). Pachai, Doerig and Herzog (2016) used similar stimuli to Harrison and Bex (2015) to argue that their 'weighting field' model of

population pooling would not produce the ‘uncrowding’ effect seen in perceptual reports (see Figure 1.6).

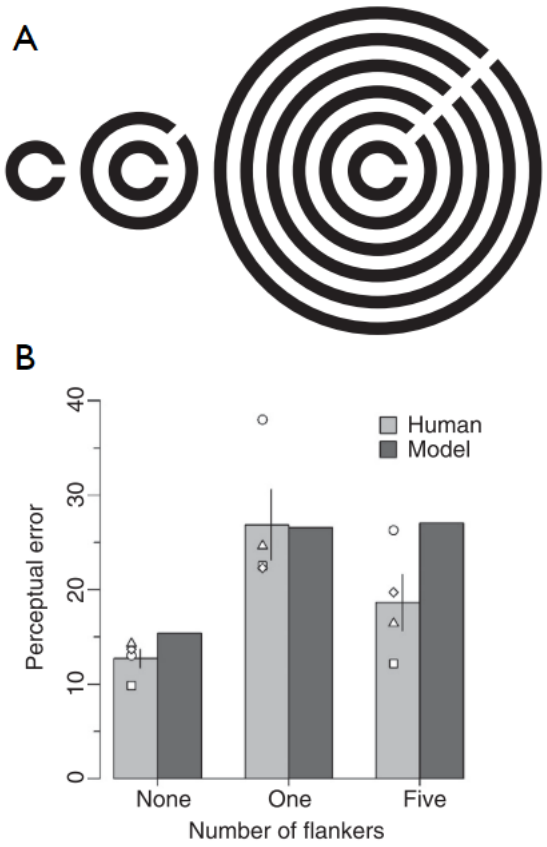

Figure 1.6 – ‘Uncrowding’ from Pachai et al. (2016)

Panel A shows stimulus arrangements used by Pachai et al. (2016) to produce ‘uncrowding’ seen in their results (Panel B). Perceptual error (related to spread) of target orientation reports is reduced (indicating less crowding) when additional flankers with the same orientation are present (light grey bars). Dark grey bars show the perceptual error predicted by their interpretation of the ‘weighting field’ pooling model by Harrison and Bex (2015).

The neurological underpinnings of grouping effects may be indicated by a model of the action of laminar layers of V1 and V2 (Raizada and Grossberg 2001), a model of which (LAMINART – Laminar Active Resonance Theory (Raizada and Grossberg 2003; Cao and Grossberg 2005)) has been extended with respect to crowding effects by Francis, Manassi and Herzog (2017). In this model, boundary signals spread across representations of flankers and (if sufficiently similar) to the target. Flankers group separately when this boundary signal is unable to connect with the representation of the target stimulus, segmenting the neural representations. The second stage attempts to match a template of possible responses to the segmented or grouped signals of the stimuli. In the authors’ worked example based on an earlier experiment (Malania, Herzog and Westheimer 2007), a Vernier acuity task requires

two templates – a left offset and a right offset. In a recent comparison of a range of models (Doerig *et al.* 2019), the LAMINART model was the only one able to reproduce uncrowding in a range of stimuli, though it was also the only model of those tested to include an explicit grouping stage. Critics of grouping approaches note a lack of objective means by which to measure grouping (Doerig *et al.* 2019), and that stimulus arrangements in which grouping is reported may provide more generic cues which influence the decision-making stage of perceptual reports, rather than featural processing (Rosenholtz, Yu and Keshvari 2019). For example, in Figure 1.6A the additional flanking Cs may lessen crowding by grouping separately to the target, or by providing a cue that the odd-one out of the array is in fact the target, thus reducing uncertainty. Further, Gestalt properties may arise from bottom-up processing (Roelfsema and Houtkamp 2011), suggesting a grouping-like effect of similarity may not necessarily require top-down mediation.

1.2.3.4 Spatial predictions of reviewed proposals

Pooling and texture perception related models typically posit that crowding mechanisms occur within zones that increase approximately linearly with eccentricity, and may be influenced by methods and form of stimuli used to estimate the extent of interaction (Rosenholtz, Yu and Keshvari 2019). Attention-based proposals may refer to the 'zoom-lens' model of attention (Eriksen and St. James 1986; Stoffer 1994), suggesting crowding may occur over wider or smaller spans depending on attentional focus and demands (Dayan and Solomon 2010; Petrov and Meleshkevich 2011b). Grouping mechanisms operate over large spans of the visual field, making predictions of a relevant spatial extent difficult. Such mechanisms may modulate crowding within zones that would only be apparent when grouping effects are minimal, corresponding to the resolution of the template matching step (Francis, Manassi and Herzog 2017). This template matching step follows earlier

interpretations of target identification as template matching (Levi, Klein and Carney 2000; Mareschal, Morgan and Solomon 2008), wherein participants compare the cortical representation of the stimulus to internal representations of potential responses, and choose the one most similar. It is at this template comparison and selection step that the presence of flankers may affect the sensitivity with which participants compare the internal templates to the stimulus, producing uncertainty and adding to the internal 'evidence' towards particular responses. However, the authors of the LAMINART grouping model note that this step could instead reflect alternative interpretations of the same process of interference (such as pooling).

Estimates of the spatial extent of crowding are varied across experiments (Pelli, Palomares and Majaj 2004; Bouma 1970; Andriessen and Bouma 1976; Pelli and Tillman 2008; Bernard and Chung 2011; Levi, Hariharan and Klein 2002b), and a complete theory to explain this variation remains to be elaborated. Methods incorporating detailed perceptual reports have been useful in differentiating between proposed mechanisms that predict similar perceptual outcomes (Greenwood, Bex and Dakin 2009; Harrison and Bex 2017), so investigating the change in reports made as target-flanker spacing is altered may help to develop theories of the spatial dependencies and limits of crowding. Essentially, rather than probing the crowding zone 'from the outside in' to find the greatest spacing at which performance at a crowded task is affected (the 'critical spacing' (Pelli, Palomares and Majaj 2004)), such an approach would traverse the entire edge of the crowding zone to observe spatial-dependency of the reported appearance of the target. A weighted pooling model would predict higher flanker weighting at small target-flanker spatial separations that then falls as spacing is increased, possibly following a Gaussian-shaped function of space (Harrison and Bex 2015). However, these weighting factors are simultaneously influenced by other factors such as target-flanker similarity in appearance (Kalpadakis-Smith *et al.* 2022), which would also alter the distribution

of responses made (Harrison and Bex 2015; Ester, Zilber and Serences 2015; Põder 2012; Ester, Klee and Awh 2014). Several questions then arise from these results: Are the spatial (flanker distance) and non-spatial (flanker appearance) influences on reported target appearance independent from one another? Or should flankers that are similar in appearance to the target operate over a different spatial extent to flankers that are dissimilar in appearance? Could extricating the effects of stimulus appearance (which may vary considerably across experimental methods present in the literature) provide new insight into the spatial extent of crowding interactions?

1.2.4 Summary

Reports of the perceived appearance of a crowded target may be well described by weighted pooling model in a variety of instances (Kalpadakis-Smith *et al.* 2022; Harrison and Bex 2015; Harrison and Bex 2017; Greenwood, Bex and Dakin 2009). More complicated arrangements of stimuli may garner the assertion of higher-level grouping effects (Manassi, France and Herzog 2012; Pachai, Doerig and Herzog 2016) or alternatively introduce cues and actions which may affect the responses given via mechanisms other than crowding (Dakin *et al.* 2009; Harrison and Bex 2016; Harrison and Bex 2017; Rosenholtz, Yu and Keshvari 2019). Weighted pooling models may also be particularly beneficial in predicting the perception of a target under crowded conditions, and support generalisable models to explain wider aspects of vision (Rosenholtz, Yu and Keshvari 2019).

However, some aspects remain uncertain. Target-flanker similarity has a notable influence on the weighting of pooled responses to target and flanker orientations (Kalpadakis-Smith *et al.* 2022), as does target-flanker separation (Harrison and Bex 2015; Harrison and Bex 2017). It remains unclear how target-flanker separation and similarity interact to alter the perception of a target as flankers traverse the limits of the crowding zone. The limited evidence available

indicates that large differences between target and flanker appearance may result in significantly different psychometric functions of crowding (Kooi *et al.* 1994). The influence of finer degrees of dissimilarity (such as relative orientation difference) is obscured in the present literature as insufficient data is available to ascertain the spatial dependencies of such crowding arrangements.

Whether similar and dissimilar flankers operate on the same patterns of spatially dependent weighting appears to be an important question that remains unanswered. If the pattern of flanker weighting across target-flanker spacing is the same for similar and dissimilar flanker is the same, then observed similarity effects remain unaccounted for (Kalpadakis-Smith *et al.* 2022). If the pattern of flanker weighting differs, how does this difference arise? For example, which parameters of the gaussian weighting field (Harrison and Bex 2015) may vary with flanker appearance, and what is the impact on perceived target appearance. This thesis will investigate the effects of target-flanker similarity on the spatially dependent weighting of responses to stimuli defined in orientation, in order to seek answers to these questions.

1.3 Section 3 – Methods of investigating visual crowding in orientation

This thesis will explore detailed reports of the appearance of crowded targets defined by orientation (Landolt-Cs). Orientation perception tasks have been a longstanding feature in crowding research (Flom, Heath and Takahashi, 1963; Solomon, Felisberti and Morgan, 2004; Baldassi, Megna and Burr, 2006; Gheri and Baldassi, 2008; Mareschal, Morgan and Solomon, 2010a; Greenwood *et al.*, 2012; Põder, 2012; Ester, Zilber and Serences, 2015; Kalpadakis-Smith *et al.*, 2022), and even Vernier tasks have been examined with an orientation-related template (Francis, Manassi and Herzog 2017). This section will review the potential approaches that have been used to investigate spatial- and perceptual- related influences of crowding effects in orientation perception, along with predictions from previous literature and proposed models of crowding.

1.3.1 Alternative forced-choice methods

Alternative forced-choice methods (abbreviated to m-AFC, where 'm' is the number of possible responses) are a common tool in psychophysical research – participants are presented with a stimulus, then tasked with identifying the stimulus from a fixed number of response option. In crowding research, such methods often utilise either two alternatives (as in a tilt-detection task (Mareschal, Morgan and Solomon, 2010a)) or four alternatives (as in a typical Landolt acuity task (Flom, Heath and Takahashi 1963)). A letter acuity task could be considered a 26-alternative forced choice method, though researchers may restrict the available options to a subset of the potential alphabetic characters in order to control relative legibility of stimuli (Pelli, Palomares and Majaj 2004; Shamsi, Liu and Kwon 2022), or use numbers for a 10-alternative task (Strasburger, Harvey and Rentschler 1991).

In a task to investigate the spatial-dependencies of crowding, the target-flanker spacing may be altered, and the proportion of correctly identified targets at varying spacings can be compared (method of constant stimuli). This has the potential to introduce a lower-bound of observable task performance – if the observer has no access to any information to identify the target and is reduced to guessing, they may still produce a 'correct' response in a subset of trials. Theoretically, this chance rate should be the inverse of the number of alternatives (e.g., 25% in a 4-AFC task), so may be reduced with greater numbers of response options, though this may increase task difficulty. As a result, these methods are typically used to determine a 'threshold' spacing – the spacing at which the proportion of correct responses is half-way between 100% and chance performance (e.g., 62.5% in a typical 4-AFC task).

Threshold spacing is frequently taken as an indicator of the spatial extent of crowding (Kwon and Liu 2019; Ogata *et al.* 2019; Greenwood *et al.* 2012), yet this would always be smaller than the 'critical spacing' used elsewhere (Pelli, Palomares and Majaj 2004; van den Berg, Roerdink and Cornelissen 2007). Determining critical spacing may require more intensive data collection as it requires threshold estimation at several target-flanker spacings in order to reliable determine the point at which threshold elevation becomes apparent (Pelli, Palomares and Majaj 2004). Neither threshold-spacing nor critical spacing are themselves able to convey the types of responses being made by observers. Limited response options has also been highlighted as a potential confounding influence on the inferences and predictions gained from alternative forced choice methods in crowding research (Reuther and Chakravarthi 2020).

1.3.2 Primer on circular statistics

This section provides a brief introduction to circular statistics and the 'von Mises distribution' as this will be referred to repeatedly in the modelling procedures of the thesis. This distribution is also known as a 'circular normal' distribution, and has been used to model distributions in orientation data in crowding (Harrison and Bex 2015; Ester, Zilber and Serences 2015; Tkacz-Domb and Yeshurun 2021; Van Den Berg, Roerdink and Cornelissen 2010). This distribution is analogous to the 'normal' or 'Gaussian' distribution (Jammaladak 2001), and is well suited for use with orientation data as it is continuous around a circle (i.e., it is able to treat +180° and -180° as the same orientation, rather than opposite ends of a linear scale). There are two key identifying parameters: the mean (or 'location') corresponding to the peak of the distribution, often denoted by μ. The second parameter is the concentration, indicating how heavily the data are grouped around the mean. Concentration is typically denoted by κ, where a high value of κ indicates a narrow spread of values around the mean, and κ=0 signifies a uniform distribution. 1/κ is analogous to the variance (σ^2) of the normal (linear) distribution.

1.3.3 Modelling response errors

A more informative, but more intensive, approach (in comparison to AFC methods) is to examine the types of errors being made more directly. Early indications of the systematic nature of crowding effects (Strasburger, Harvey and Rentschler 1991) noted that the impact of these systematic effects on threshold estimates remained unknown at the time. More recent studies have been conducted to characterise the types of errors made under crowding, leading to more nuanced mechanisms being proposed (reviewed in Section 2 - Proposed mechanisms and models of visual crowding). Studies modelling report errors commonly task

participants with reporting the perceived orientation of a crowded target using a continuous scale (i.e., the full range of possible orientations), as opposed to a limited number of options in m-AFC paradigms (Ester, Zilber and Serences 2015; Põder 2012; Kalpadakis-Smith *et al.* 2022; Harrison and Bex 2015). These data can then be used to construct a frequency distribution of responses, from which more detailed models can be developed.

An example of a response distribution shown in Figure 1.7 from Kalpadakis-Smith *et al.*, (2022) who modelled responses at a range of target eccentricities and 2 levels of target-flanker orientation difference. Uncrowded responses (panel A) are centred around 0° error (the target orientation) with a small spread, while +30° flankers (panel B) produce a wider spread in responses and shift the peak of the distribution to between the target and flanker orientations (indicated by the vertical dashed lines), which may indicate averaging-type responses. Flankers at a greater orientation difference (panel C) produce a distinctly bimodal distribution, indicative of both accurate- and substitution-type responses in a proportion of trials. In their modelling (solid black line), noisy responses to orientation signals from the target and flankers are combined in a weighted population pooling model. This study indicated flanker weighting in a population pooling model could vary with target-flanker similarity and target eccentricity, while data presented in other studies indicate target-flanker spacing would also contribute to this weighting (Ester, Zilber and Serences 2015; Harrison and Bex 2015), consistent with the idea of spacing-dependent crowding ‘strength’ (Pelli, Palomares and Majaj 2004; Petrov and Meleshkevich 2011a; Bouma 1970; Levi, Klein and Hariharan 2002; Pelli and Tillman 2008; Strasburger, Harvey and Rentschler 1991). How these influences (spacing, similarity and eccentricity) may interact to influence flanker weighting remains unclear at present.

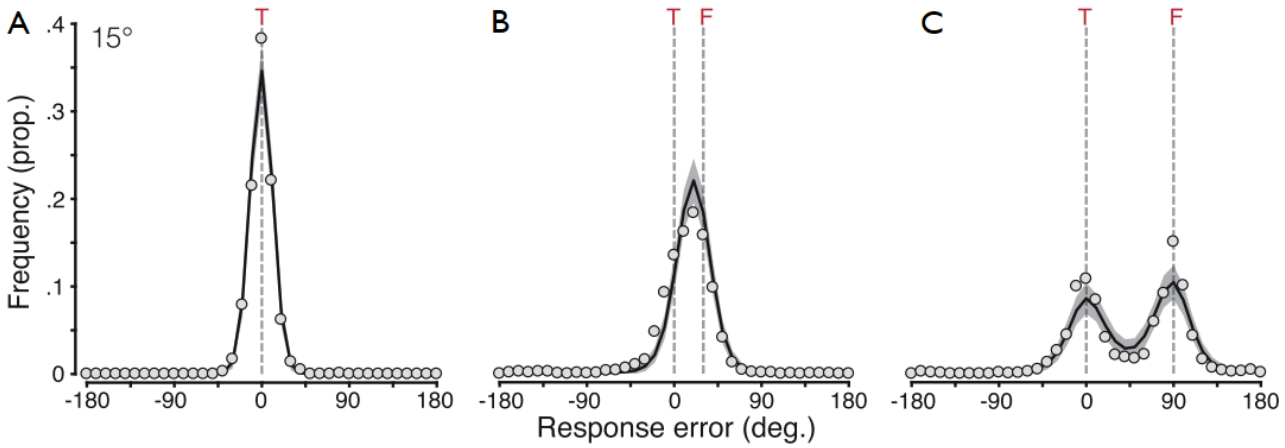

Figure 1.7 - Probability distributions of orientation responses from Kalpadakis-Smith et al. (2022)

Distributions of response errors (difference between response and presented target orientations) under three stimulus conditions. A) Target-only ('uncrowded') B) Target crowded by 4 flankers oriented at +30° relative to the target C) Target crowded by 4 flankers oriented at +90° relative to the target. Relative target-flanker orientation alters the shape of the distribution of responses, and the relative weighting of target and flanker responses in a weighted population pooling model (solid black lines).

1.3.4 Thesis rationale

Weighted pooling models have been shown to be informative in a number of studies (Harrison and Bex 2015; Kalpadakis-Smith *et al.* 2022; Greenwood, Bex and Dakin 2009). Although there is disagreement on underlying mechanisms (Ester, Zilber and Serences 2015), crowded responses can be well described by this class of model. However, the driving forces behind the differences in weighting factors observed between experiments remains to be

explored. Of particular interest is whether changes in weighting factors with varying target-flanker spacing may be extricated from changes arising from varying stimulus appearance.

Studies with the potential to investigate interactions between target-flanker spacing and orientation difference have either been hampered by combining data obtained with a range of target-flanker orientation differences (Ester, Klee and Awh, 2014 (specifically, their experiment 3); Harrison and Bex, 2015, 2017) or focused on comparing straightforward (i.e., non-weighted) averaging with probabilistic substitution models (Ester, Zilber and Serences 2015). The data of Ester, Zilber and Serences (2015) indicate a higher probability of substitution-type errors with flankers at 60° orientation difference than at 15° difference, particularly at the smaller target-flanker separation, though their statistical tests only indicated a significant main effect of orientation difference and no interaction with spacing. This may be due to their method of simultaneously presenting clockwise and anticlockwise oriented flankers at each trial, meaning the model fitted to response errors required a trimodal form to characterise reports corresponding to the orientations of the target, clockwise flanker and anticlockwise flanker. If the authors had instead modelled absolute magnitude of error (aligning clockwise and anticlockwise errors), the difference in fitted parameters corresponding to probability of substitution errors would be greater and may have revealed a statistically significant interaction. Recent evidence using a weighted pooling model has suggested differing weighting factors for small and larger orientation differences better describes the pattern of responses observed (Kalpadakis-Smith *et al.* 2022), but differences in weighting over a range of target-flanker spacings remain unexplored.

Disentangling these spatial and non-spatial (or, featural) dependencies may provide new insight into the spatial dynamics of crowding. Simultaneously examining the distribution of errors made due to crowding and the spatial dynamics of these effects may improve our understanding of crowding mechanisms in normal vision. If beneficial, this approach may also

have potential to elucidate the changes underlying altered crowding in abnormal vision (Kalpadakis-Smith *et al.* 2022; Ogata *et al.* 2019; Tailor *et al.* 2021), where it remains uncertain whether apparently enlarged estimates of crowding zone extent are the result of true increases in the spatial extent of crowding, or corruptions of the underlying processes resulting in crowding, or a combination of both.

1.4 Section D – Thesis outline

Weighting factors used in weighted pooling models can describe the contribution of flankers to the pattern of responses made under typical crowding conditions, but are simultaneously influenced by flanker appearance and spacing (Kalpadakis-Smith *et al.* 2022; Harrison and Bex 2015; Harrison and Bex 2017). Investigating the co-effects of flanker separation and appearance may reveal new insights into the underlying mechanisms and physiological structures involved in producing crowding effects. This may also help to determine clearer measures relating to the spatial extent and perceptual effects of crowding, potentially identifying key features of peripheral vision and benefiting clinical measures of elevations in crowding.

The experiments described in this thesis sought to investigate visual crowding by assessing perceptual reports of target appearance when flankers were located at different spacings within the crowding zone. The overall aim was to study spatial aspects of visual crowding (i.e., zone extent and spacing-related modulation of effects) through assessing detailed patterns of responses. The main experimental method was initially developed with the intent to conduct experiments with non-psychophysically experienced participants and a clinical cohort with abnormal vision. Later, studies pivoted to a new research question, investigating visual crowding with a smaller number of psychophysically experienced participants and

more intensive data collection (for reasons expanded on in Chapter 4). This section provides an outline of the thesis, giving the aims and rationale of each chapter.

Chapter 2 contains logistical information that applied to all subsequent experimental chapters. All participants were screened to confirm normal vision, using procedures and criteria presented in this chapter. The basic experimental task and equipment were also consistent across studies – participants were tasked with reporting the orientation of a Landolt-C target using a rotating dial. This chapter introduces the experimental setup, stimulus presentation and response collection methods, including images and technical details that are referenced in later chapters.

The first experimental chapter (Chapter 3) asks whether the visibility of stimuli scaled to participant's peripheral acuity influences estimates of the spatial extent of the crowding zone. Stimuli were sized individually as multiple of each participant's acuity measured with Landolt-Cs at the target location. The invariance of crowding zone extent to exact target size when above acuity limits is well established (Tripathy and Cavanagh 2002; Pelli, Palomares and Majaj 2004; Levi, Hariharan and Klein 2002b; van den Berg, Roerdink and Cornelissen 2007; Gurnsey, Roddy and Chanab 2011). However, it remained unexplored whether subsequently increasing stimulus size further may affect task performance (by increasing spatial frequency of the target gap) or effective target-flanker spacing (if edge-to-edge separation were more relevant than centre-to-centre separation) in such a way as to influence final estimates of zone extent. This study was also designed to inform how stimuli should be scaled to participant acuity in later experiments.

Chapter 4 describes a significant shift in experimental design and approach from that intended at the outset of the PhD. While the project initially aimed to investigate crowding in a clinical cohort with abnormal vision, the decision was made to pivot to continue investigating

visual crowding with normally-sighted participants (specifically, psychophysically experienced participants). This was primarily a result of pandemic-related impacts on the ability to recruit and test the intended participant group. However, the change of direction also required more intensive data-collection methods to be implemented. This chapter explains in more detail why these changes were required, what changes were made and the benefits to subsequent experimental chapters. The chapter also details the development of a novel characterisation of the edge of the crowding zone – the 'spatial profile' which is used in later studies to disentangle the impact of spatial and featural characteristics of flankers on perceived targe appearance.

The second experiment, presented in Chapter 5, consisted of two studies with related research questions: is the characteristic in-out anisotropy of crowding zones related to cortical magnification of radially located flankers. Cortical magnification of spacing between stimuli has been examined as a contributory factor to this phenomenon (Motter and Simoni, 2007; Pelli, 2008; Mareschal, Morgan and Solomon, 2010b), however, the unequal cortical magnification of flankers remained unexplored. The studies in this chapter utilised radially located flankers that were scaled in diameter to counteract cortical magnification. The first study was conducted before the change in experimental approach detailed in Chapter 4, while the second study utilised the revamped experimental approach and individual fMRI-derived measures of cortical magnification to scale stimuli individually for each participant.

Chapter 6 directly investigated the co-effects of target-flanker similarity, spacing and eccentricity to systematically compare their effects on target and flanker contributions in a pooling model of crowding effects. Through constructing 'spatial profiles' of crowding effects induced by flankers of differing relative orientations, the impacts of flanker appearance and flanker spacing on pooled responses were disambiguated and explored independently. This was conducted at three levels of target eccentricity, permitting the examination of a previous

assertion that similarity-based modulation of crowding may be reduced with target eccentricity (Kalpadakis-Smith *et al.* 2022).

The final experiment, presented in Chapter 7, sought to investigate the potential contribution of early structural organisation (retinal ganglion cell density) to the newly disentangled measures of the spatial extent of crowding. This connection was proposed by an earlier study (Kwon and Liu 2019), though their experimental findings were not conclusive. By disentangling the influence of flanker appearance, a novel indicator of spatial extent was found that showed a closer association to physiological structures than has been seen with widely used threshold-spacing. This study utilises estimates of retinal ganglion cell receptive field density derived from recent literature regarding structural measures (Montesano *et al.* 2020) and estimates derived from psychophysical measures in the recruited participants to explore individual differences and compare the present findings with previous studies.

Chapter 8 reviews the findings of the studies presented in the thesis and proposes a model of how spatial and featural aspects of flanking stimuli may interact to produce psychophysically observed crowding effects in the framework of a weighted pooling model. The potential for the experimental and analytical approach developed in the thesis to be applied in other contexts is discussed and potential avenues for future work are outlined. It is hoped that this work will aid research in identifying the limitations and confounds of current methods to investigate elements of visual crowding and help inform the design of future studies of crowding in typical and atypical vision.

Chapter 2 Experimental and technological setup

This chapter will cover the decisions and considerations made while developing the experimental method. The first section will present the eligibility criteria applied to recruitment of all participants, and the methods used to ensure these criteria were met. The second section provides an overview of the technological setup and equipment used in the experiments presented in later studies. The baseline method described at the end of the chapter is intended to be a reference, introducing aspects of the method which are common to the majority of the experiments presented in this thesis and defining terminology used in several chapters. As such, some finer details such as exact stimulus size and flanker orientation are left unspecified here and will be detailed in the relevant chapter. Instead, the relevant differences will be stated and explained in each chapter.

2.1 Participant recruitment

2.1.1 Ethical approval

Ethical approval was granted by the Cardiff University School of Optometry and Vision Sciences Research Ethics Committee (ref. #1507). This permitted the recruitment of up to 20 normally sighted participants to undertake psychophysical testing using commercially available equipment, covering all studies presented in this thesis. All participants gave informed consent before any experimental procedures. The psychophysical data presented in this thesis was collected at the School of Optometry and Vision Sciences, Cardiff University, Cardiff.

Functional magnetic resonance imaging (fMRI) data utilised in Chapter 5 was used with permission from a lab colleague (Wright 2021). This data was collected by Melissa Wright as part of a separate research project under a different ethical approval. All fMRI data collection was conducted at Cardiff University Brain Research Imaging Centre.

2.1.2 Participant eligibility criteria

The criteria presented in Table 1 were chosen to ensure all participants were normally sighted, and to exclude participants in whom abnormal vision or crowding may be encountered. Each participant underwent several checks to ensure these eligibility criteria were met, detailed in section 2.1.3.

	Inclusion criteria	Exclusion criteria
Refraction	≤ ± 6.00 DS ≤ ±1.50 DC	> ± 6.00 DS > ±1.50 DC
Corrected acuity	6/9 or better	Worse than 6/9 in either eye
Ocular health	Normal ocular health Normal visual fields IOP < 21 mmHg	Diagnosis of amblyopia Fixation instability Family history of glaucoma

Table 1 - Participant inclusion and exclusion criteria

2.1.3 Methodology to ensure participant eligibility

A short clinical interview was carried out to confirm normal ocular history, any medication currently taken and normal general health. The absence of any diagnosed ocular conditions or family history of glaucoma was also confirmed verbally during the interview. Visual correction was permitted in the form of spectacles or contact lenses, provided these were ≤ 6.00 spherical dioptres (DS) and ≤ 1.50 cylindrical dioptres (DC) in power. Corrected visual acuity was measured with either Snellen or ETDRS chart at 6 meters. Ocular dominance was tested with +2.00 DS lenses. Subjective refraction was carried out to ensure no significant uncorrected refractive error was present.

A short ocular health check was also carried out. Clear ocular media and cornea were confirmed with slit lamp biomicroscopy. Binocular indirect ophthalmoscopy with a Volk lens was used to examine the posterior eye and confirm normal appearance of the optic nerve head, macula and retina in both eyes. Intraocular pressure (IOP) was measured with non-contact tonometry in each eye, taking the average of three measurements from either a Topcon CT-80 (Topcon (Great Britain) Medical Limited, Newbury, UK), or Pulsair IntelliPuff (Keeler UK, Windsor, UK) tonometer.

Visual field examination was carried out with a Humphrey automated perimeter 3 (Carl Zeiss Meditec, Dublin, CA), utilising the SITA-standard algorithm and 24-2 test pattern. Participants were excluded if any points of statistically abnormal sensitivity were indicated in repeated tests, or if fixation stability was consistently poor (indicated by >20% fixation losses, >15% false positives or >30% false negatives).

2.2 Experimental equipment and setup

2.2.1 Crowding setup

Stimulus generation and presentation was conducted with MATLAB (version R2019a; The MathWorks Inc., Natick, MA, USA) using PsychToolbox (Brainard, 1997) and the Eccentric Vision Toolbox (Greenwood 2021). Crowding stimuli were always presented on a Sony Trimaster OLED (organic light emitting diode) screen (SONY PVM-A250 Trimaster EL; Sony corp. Tokyo, Japan). Resolution 1920 x 1080, screen dimensions 543.4 x 305.6 mm, 60Hz refresh rate. The screen was gamma corrected using the 'CalibrateGamma' MATLAB script provided by the Eccentric Vision Toolbox (Greenwood 2021), and screen luminance was measured using a ColorCal MKII photometer (Cambridge Research Systems, Kent, UK). The screen was turned on for a minimum of 30 minutes before any data collection to allow the screen to warm up. Generated stimuli were always white (141 $cd.m^{-2}$) on a flat grey background (10 $cd.m^{-2}$). Responses were collected using a consumer keyboard and volume dial connected via USB. Figure 2.1 shows the experimental setup as it would appear to participants during a typical crowding trial. The screen could be raised, or seat height lowered, to ensure the centre of the screen was at participants' eye level.

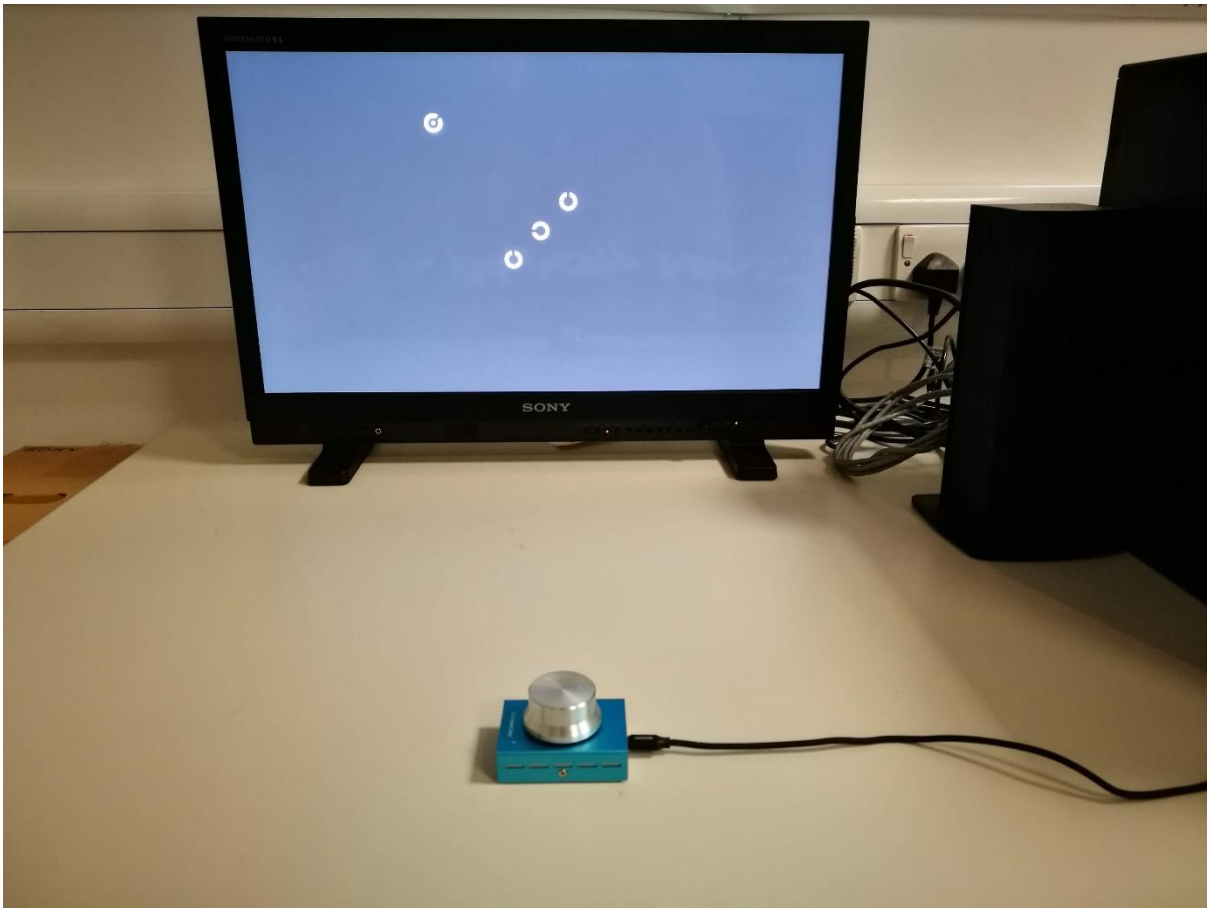

Figure 2.1 - Photograph of equipment setup for crowding tasks

Stimuli were presented on a Sony Trimaster OLED screen situated on a table. A consumer volume dial (shown) or standard keyboard (not shown) were placed at the front of the desk for participants to register responses. During data collection, room lights would be turned off and participants were adapted to the luminance of the screen before trials began.

2.2.2 Perimetry setup

Contrast threshold data was collected for one study (Chapter 7) using an Octopus 900 perimeter (Haag-Streit UK, Essex, UK) shown in Figure 2.2, controlled using scripts programmed in R (R Core Team 2021) utilising the Open Perimetry Interface (OPI) (Turpin, Artes and McKendrick 2012). The OPI allows custom test procedures to be programmed and carried out on compatible commercially available perimeters such as the Octopus 900, permitting precise stimulus control. Spot stimuli could be projected at standard Goldmann sizes I to V, up to 90˚ eccentricity in any meridian and at up to 3,185 cd.m^{-2} maximum luminance (0 to 47 dB). Participants wore optical correction if needed, or correcting lenses could be placed in a fold-out lens holder to sit in front of the eye being tested.

Figure 2.2 - Octopus 900 perimeter

Data collection using the Octopus perimeter mirrors standard automated perimetry (SAP). A stimulus is projected at a particular field location and participants press a response button to indicate if the stimulus was seen. Participants rest their chin on the chin and forehead against the blue rests and eye position can be adjusted by the operator using the buttons at the front of the machine.

2.2.3 Data analysis

Collected data were analysed with scripts programmed with R (version 4.1.2, 2021-11-01) (R Core Team and Team, 2021). The ‘circular’ package (Agostinelli and Lund 2022) was used for functions relating to von Mises distributions and calculating circular statistics. Data processing and graphical presentation also utilised the ‘tidyverse’ collection of packages (Wickham *et al.* 2019). Data processing pipelines are described in each chapter.

2.3 Experimental method development

2.3.1 Rationale

Crowding of different stimulus features can be dissociated, as demonstrated in colour and motion by Greenwood and Parsons (2020), suggesting stimulus aspects may be subject to crowding in separate pathways despite arising from the same object. The effects of crowding on perceived orientation of a target has been the focus of a range of studies (Põder 2012; Ester, Zilber and Serences 2015; Ester, Klee and Awh 2014; Greenwood, Bex and Dakin 2010) and several investigations have utilised Landolt-C stimuli or ‘Landolt-C like’ stimuli (Harrison and Bex 2015; Harrison and Bex 2017; Greenwood *et al.* 2012; Kalpadakis-Smith *et al.* 2022) see Figure 2.3, which are likely to be comparable in results. Orientation of a Landolt-C stimulus is beneficial as it can be continuously modulated through a full 360°, giving added flexibility to experimental design in comparison to gratings or Gabor patches which may only be perceptibly oriented through 180°.

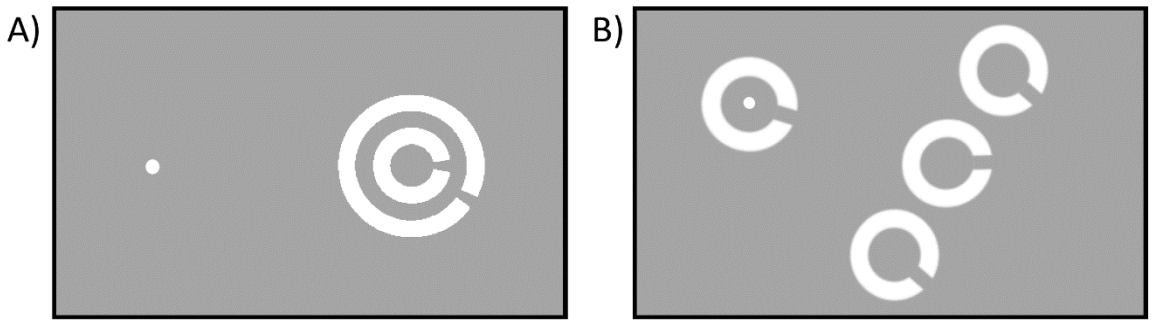

Figure 2.3 – Comparison with crowding stimuli used by Harrison and Bex (2015, 2017)

The stimuli in Harrison and Bex's studies were described as 'Landolt- like' as their gap size was kept constant, not proportional to the overall stimulus diameter. This allowed the experimenters to vary target-flanker separation by changing the flanker diameter, without altering the spatial frequency of the gap which defines the orientation of the flanker. The studies in this thesis will use standard Landolt-Cs and instead vary target-flanker separation in terms of centre-to-centre distance between the target and flankers.

2.3.2 Illustration of a typical crowding trial

Where studies measure the extent of visual crowding, the method is an adjustment of the steps laid out briefly here:

Participants fixate a spot on the screen throughout the experiment. A Landolt-C stimulus (the 'target C') is presented at a fixed peripheral location and a random orientation, and a second Landolt-C (the 'response C') is presented around the fixation spot also at a random orientation. In each trial, participants control the orientation of the response Landolt-C with a dial and are tasked with reporting the orientation of the peripheral target Landolt-C as closely as possible. The target Landolt-C may be

presented alone (the ‘unflanked’ condition) or neighboured by (usually) two further Landolt-Cs (the ‘flankers’) as in Figure 2.4 below. The flanker Cs will be presented at a fixed orientation relative to the presented target C, randomly clockwise or anticlockwise, and were always identical in orientation to the other flanker(s). The spacing between the target and flankers is controlled and altered throughout each experiment, though different studies followed different strategies to control target-flanker spacing, so this is described in the methods section relating to each experiment.

During crowding tasks, participants reported the orientation of the target with a consumer volume dial, shown in Figure 2.1. Turning the dial rotated the response C in the corresponding direction, and participants were instructed to press down on the dial when the response C matched the perceived orientation of the target. This button press submitted the final orientation of the response C and began the following trial. Trials were conducted in blocks with regular breaks. Participants could also take additional breaks at any point by withholding a response (these trials were skipped and conducted again later in the block of trials).

Across the studies presented in the thesis, several aspects of this base method are manipulated to investigate the effect of these changes on the pattern of responses gained, including the relative orientation difference between target and flankers, and the sizes of stimuli used. Studies developed later in the project also utilised a finite stimulus presentation time, so target and flankers were presented for the required interval before being replaced by only the response C at fixation (this is described in more detail in the methods sections of trials where finite presentation times were used).

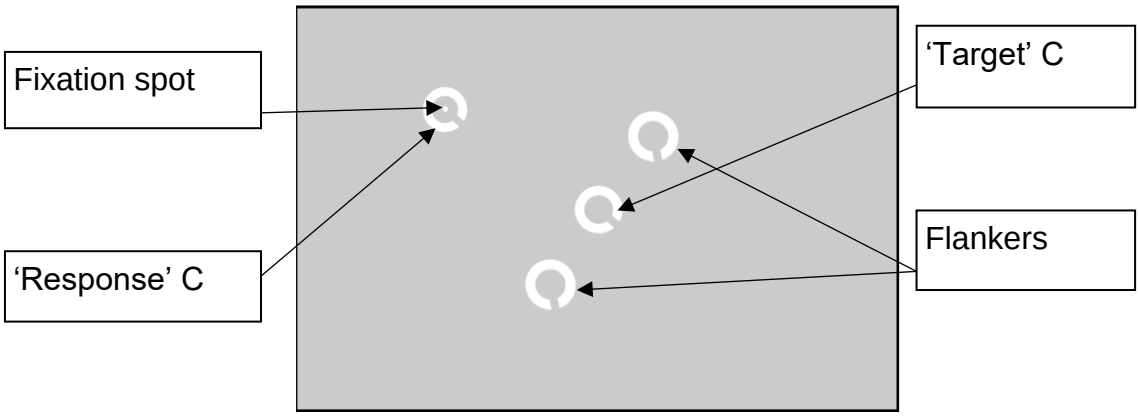

Figure 2.4 - Labelled illustration of trial elements

Stimulus elements were presented on a flat grey background (shown to scale). Boxes and arrows label the stimulus elements as they are referred to in the thesis. The target was always in the centre of the screen and the fixation spot was moved in order to change test location and eccentricity.

2.4 Summary

This chapter provides a technical background and introduction to the methods utilised in the thesis. The protocol to ensure recruited participants had normal vision was conducted with all recruited participants, so additional detail is given here in order to reduce repetition across chapters. Similarly, the experimental setup was the same for all crowding studies, so the description provided here is intended to help visualise how trials described in later studies were conducted, though specific details and arrangements of stimuli may differ. Stimulus and procedural descriptions provided in individual chapters are specific to each study, so should take precedence over any descriptions here. Any technical details not mentioned in a chapter should otherwise correspond to those given above.

Chapter 3 The effect of stimulus visibility on crowding extent

3.1 Introduction

Bouma's early studies with peripherally viewed letters (1970) produced what has come to be known as 'Bouma's law': that perception of a letter presented at a certain eccentricity will be affected by other letters presented within a distance of half the eccentricity around the target letter. A number of studies were undertaken to investigate whether factors other than eccentricity also contribute to the/this? effect, using a variety of methods and stimuli (Tripathy and Cavanagh 2002; Pelli, Palomares and Majaj 2004; Gurnsey, Roddy and Chanab 2011; van den Berg, Roerdink and Cornelissen 2007). Their findings largely support Bouma's guideline that the size of the crowding zone is more closely related to eccentricity than stimulus size, though investigators are conscious that Bouma's assertion is more of an approximation than a true 'law' (Strasburger 2020). Gurnsey, Roddy and Chanab (2011) in particular report that crowding may not be completely independent of stimulus size, reporting that performance at a crowded task may be simultaneously influenced by the size of the target as well as the distance between the target and flanking stimuli. These simultaneous effects of target size and stimulus spacing were most apparent with the smallest stimuli and most central target eccentricities. As target eccentricity increased, the effect of target size on task thresholds diminished and an independence from target size was observed.

One interpretation that appears unaddressed is that identical stimuli may not necessarily be equally visible by two normally sighted observers, even when

suprathreshold. Two observers might not find it equally easy to identify a target if it is only just above one observer's acuity threshold, but several times larger than the other's threshold. This effect of 'visibility' of a target is presently unknown and could be influential in experiments requiring detailed reports of fine stimulus features. Studies recruiting inexperienced participants may also encounter a wider range of acuities and abilities to complete psychophysical tasks, so investigators may decide to scale stimuli to the acuity level of individual participants. For example Greenwood *et al.* (2012) scaled stimuli in a crowding task to 2.5x the stimulus size at acuity threshold for each participant, which ensured stimuli were suprathreshold to the same amount for all participants, though absolute stimulus size varied. Conversely, studies utilising a fixed stimulus size for all participants are common and may mean that 'visibility' of the target (in terms of multiples of individual acuity) may vary.

Varying the amount of such scaling to individual acuity (and thus visibility) could influence the ability of participants to identify the target under crowded conditions. The study presented here will investigate the potential effect of stimulus visibility on estimates of crowding zone extent. Visibility will be controlled by scaling the size of stimuli to set multiples of the stimulus size at each participant's measured acuity threshold. This study also intended to inform the design of subsequent studies by determining whether scaling of stimuli to individual acuity was suitable (i.e., did not influence estimates of crowding zone extent) and what level of scaling would be most beneficial.

3.2 Methods

3.2.1 Participants

Twelve healthy participants were recruited from students attending the School of Optometry and Vision Sciences, Cardiff University. Participants gave informed consent and underwent the protocol to ensure inclusion criteria were met, detailed in section 2.1.3. Ethical approval was granted by the Cardiff University School of Optometry and Vision Sciences Research Ethics Committee (ref. #1507).

3.2.2 Stimuli and experimental setup

Participants were first adapted to a flat grey background of 10 cd/m^2 luminance for at least three minutes. Stimuli were white Landolt-Cs generated using a custom script programmed in Matlab (version R2019a; The MathWorks Inc., Natick, MA, USA) utilising Psych Toolbox (Brainard 1997) and the Eccentric Vision toolbox (Greenwood 2021) presented on a Sony Trimaster OLED screen (SONY PVM-A250 Trimaster EL; Sony corp. Tokyo, Japan) with gamma correction, at a distance of 60 cm. Target stimuli were presented at 9° temporal and 9° inferior (12.73° inferotemporal) to the right eye of all participants, using refractive correction where necessary, and an opaque eye patch over the left eye.

3.2.3 Peripheral acuity task

Participants first undertook a measurement of peripheral acuity in a 4-alternative forced choice (4AFC) task with an isolated Landolt-C presented at the test location, oriented to one of the four cardinal directions (up, down, left, or right). Participants

fixated a white spot towards the upper left of the screen while stimuli were located at the centre (12.73° inferotemporal eccentricity, as described above.) Participants were instructed to use the arrow keys on a keyboard to orient the response C to one of the four possible stimulus orientations and press the space bar when the response C matched their perceived orientation of the target C. Stimulus size was controlled by a QUEST algorithm (Watson and Pelli 1983) set to converge on a 62.5% correct threshold for 30 trials. The outcome of the test (threshold stimulus size) was used to set the size of all following stimulus elements. Stimuli for each of the subsequent sets of tasks were generated by taking the stimulus size at acuity threshold and multiplying by a factor selected from 1.5x, 2x, 2.5x and 3x in a random order.

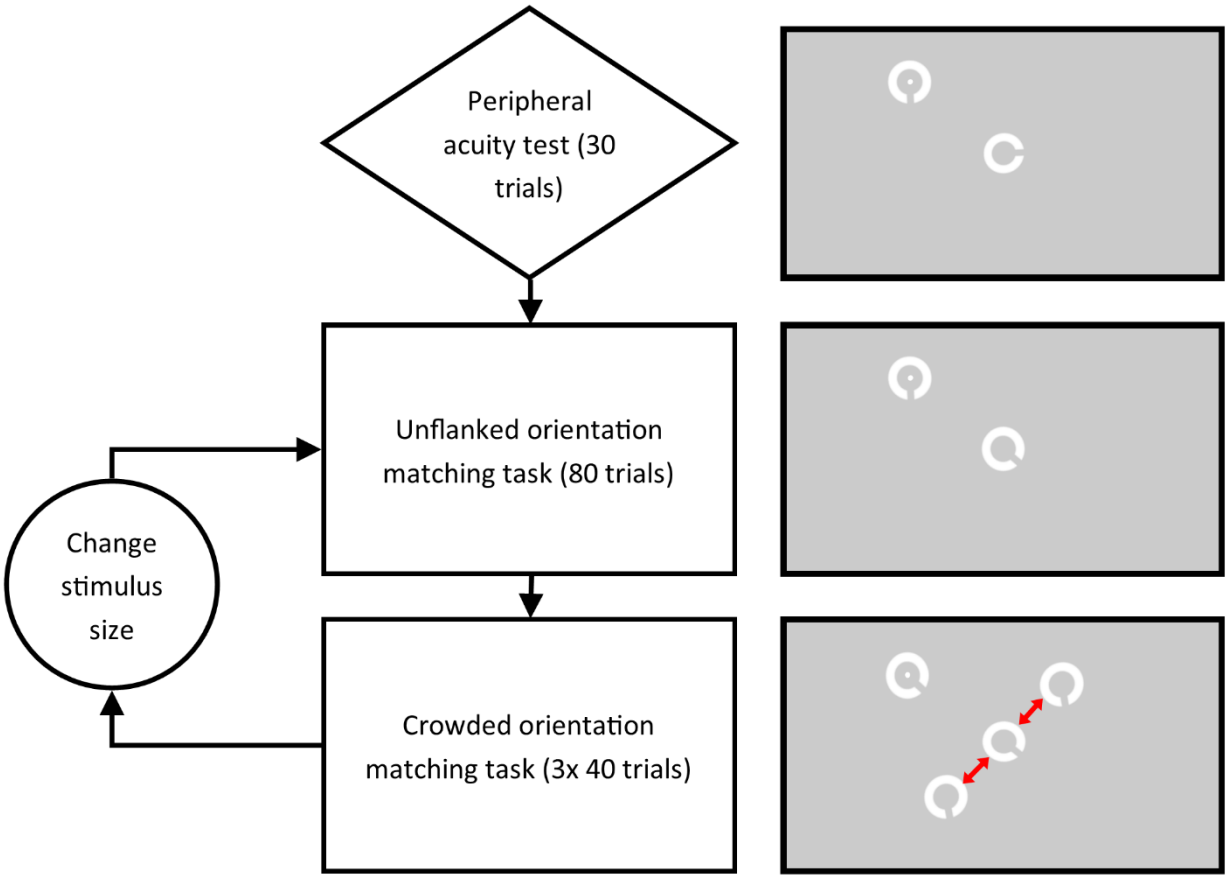

Figure 3.1 – Flow diagram of experimental methods and illustration of stimuli

Participants fixated the white spot (upper left) throughout the tasks and controlled the orientation of the 'response' Landolt-C (upper left, centred on fixation). The 'target' Landolt-C remained at the centre of the screen for all tests. The red arrows indicate the direction of change in target-flanker separation between trials of the crowded task and never appeared during the task.

3.2.4 Unflanked orientation matching task

The generated stimuli were first used in an unflanked orientation matching task to determine the limits for a 'correct' response during the crowded task.

The target Landolt-C was presented at the same location (12.73° inferotemporal to fixation) at one of 12 possible orientations randomly selected from a range each 30° apart (i.e., positions of a clock face). The response Landolt-C was presented surrounding the fixation spot at a random orientation between 0° and 360°. Participants controlled the orientation of the response C a by rotating a dial, rotating the C in 1° steps to match the perceived orientation of the target C as closely as possible. Pressing the dial down registered the response and presented the next trial. No feedback on performance was given.

Eighty trials of the unflanked task were conducted, and the difference in orientation between the target and given response at each trial was calculated. The standard deviation of the signed differences for the final 40 trials was calculated and used to inform the threshold for the crowding measurement task (see below).

3.2.5 Crowded orientation matching task

The crowding measurement setup was identical to the unflanked matching task except that the target Landolt-C was now flanked by two identically sized Landolt-Cs along the axis tangential to the target deviation from fixation (see Figure 3.1, in this experiment one flanker was located above and to the right of the target, while the other was below and to the left). The flankers were equally spaced from the target, at a distance controlled by a QUEST algorithm and measured from the centre of each element. The task was also identical to the unflanked paradigm – participants rotated the response Landolt-C at fixation, to match the perceived orientation of the peripheral target C. Flanker orientation was yoked to 24° from the orientation of the presented target at each trial, randomly clockwise or anticlockwise.

The criteria for determining whether a response was correct or incorrect was determined using the standard deviation (SD) of errors from the preceding unflanked task, conducted with stimuli at the same size. Responses within the range of target orientation ±2x the SD of unflanked errors were recorded as 'correct'. This is the range of responses expected when there is no influence of flankers and the target is 'uncrowded', and responses outside this range are therefore considered an 'error'. The ranges of 'correct' responses for each crowded task are shown in Table 2 and are reviewed in section 3.4.

The algorithm was updated at each trial. The flanker separation for the following trial was calculated by adding the QUEST calculated quantile of the algorithm's posterior probability density function (a suggestion of the most informative flanker separation to test at, recommended by Pelli (1987)) to an amount of noise selected from a normal distribution of mean of 0 and SD 39.4 (pixels, approximately 1.06° of visual angle). Responses deemed 'correct' would contribute to reducing the flanker separation recommended by QUEST, while 'incorrect' responses would contribute to increasing the separation. (Note: as QUEST is an adaptive algorithm, not a staircase, even participants familiar with a staircase paradigm would not be able to gain definitive feedback on prior performance from the next presentation.) Flankers never exceeded the screen dimensions (giving a maximum possible flanker separation of 20.6°, depending on stimulus size) nor overlapped the target C (thus a minimum possible separation of 1 stimulus size). No feedback on performance was given. A test consisted of 40 trials, after which a break was given, and the algorithm was reset. Three repeats were undertaken giving 120 trials for the crowded task at each stimulus size.

A set, consisting of one unflanked task and 3 crowded tasks, was conducted at each of the possible stimulus sizes in a random order. Rest breaks were also given between each set.

3.2.6 Data processing

Data were processed in R (R Core Team 2021). Responses from the crowding task were collected into 6 bins covering the range of target-flanker separations presented (All trials from the unflanked orientation matching task were included in one separate bin). The distribution of numbers of trials across target-flanker separations was examined and range chosen programmatically to attempt to separate trials into approximately even numbers across the bins. Note: some datasets were more heavily clustered around a small range of target-flanker separations, so some bins contained much fewer, or even 0, trials.

3.2.7 Analysis

For each trial, response error was calculated as the difference between the orientation of the presented target and the given response. The distribution of these errors was then modelled as a von Mises distribution with a fixed mean of 0° (i.e. the target orientation) while the concentration parameter was permitted to vary. ‘Perceptual error’ was taken as the spread of the distribution, calculated as the square root of the inverse of the concentration parameter. Perceptual error is inversely related to the concentration of errors; therefore a greater perceptual error value corresponds to a wider spread of errors. The calculated perceptual error from each bin of trials was then plotted against the mean target-flanker separation of the binned trials and fit with a two-phase ‘hinged line’ model – see Figure 3.2 for illustration. This follows the methods

of Harrison and Bex (2015), who give more detail in their supplementary information. The unflanked perceptual error value was added to the crowded task data, with a nominal value of target-flanker separation set to 30 degrees of visual angle, to aid model fitting. This separation is far beyond the proximity at which any crowding influence could reasonably be expected at this level of target eccentricity, so is considered representative of the unflanked condition.

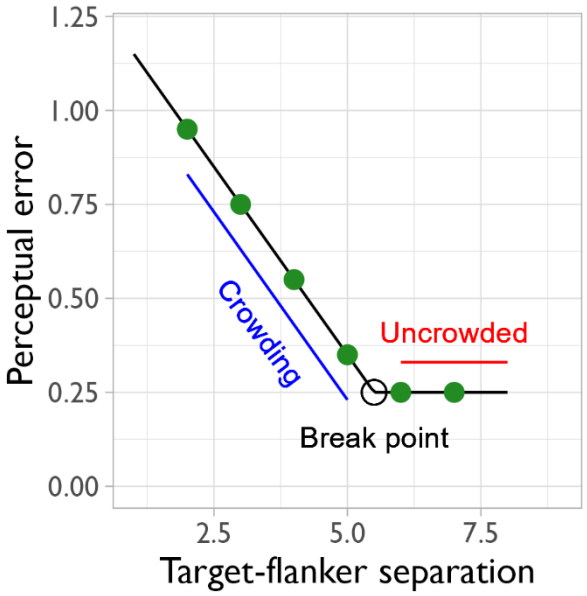

Figure 3.2 – Illustration of a hinged line model

Artificial data, illustration only. The hinged line model (black) contains two phases. Phase 1 (parallel to blue line) shows raised perceptual error due to crowding when flankers are within the crowding zone. Phase 2 (parallel to red line) shows perceptual error approximately equal to the unflanked condition, indicating flankers are outside the crowding zone. The break point between phases (black circle) is taken as an estimate of the extent of the crowding zone.

The hinged line model describes the decrease in spread of errors as target-flanker separation increases (phase 1), until a point at which flankers exert no effect on target perception (the breakpoint) and errors are only the result of participant imprecision, not crowding (phase 2). The model has three free parameters: the slope of the first 'descending' phase the height of the second (horizontal) phase, and the break point

between the phases. This break point was then taken as an estimate of the extent of the crowding zone as flankers presented at a greater separation did not worsen participant performance, indicating no effect of flanker presence.

Extracted estimates of the break point were then compared across stimulus size, defined in multiples of the stimulus size at each participant's acuity threshold. This categorical comparison was appropriate as stimulus size was linked to local acuity, so participants with worse estimates of local acuity were tested with larger stimulus sizes overall (see Table 2). As crowding zone extent has been suggested to be associated with acuity (Flom, Weymouth and Kahneman 1963; Yehezkel *et al.* 2015; Greenwood *et al.* 2012; Levi and Klein 1985), it follows that participants with coarser local acuity at the same eccentricity may show larger crowding zones than those with finer acuity even in the absence of any potential effect of stimulus size. Therefore, categorical comparison with multiples of acuity threshold may avoid the potentially misleading appearance of raw comparisons with stimulus size in degrees, illustrated in Figure 3.3.

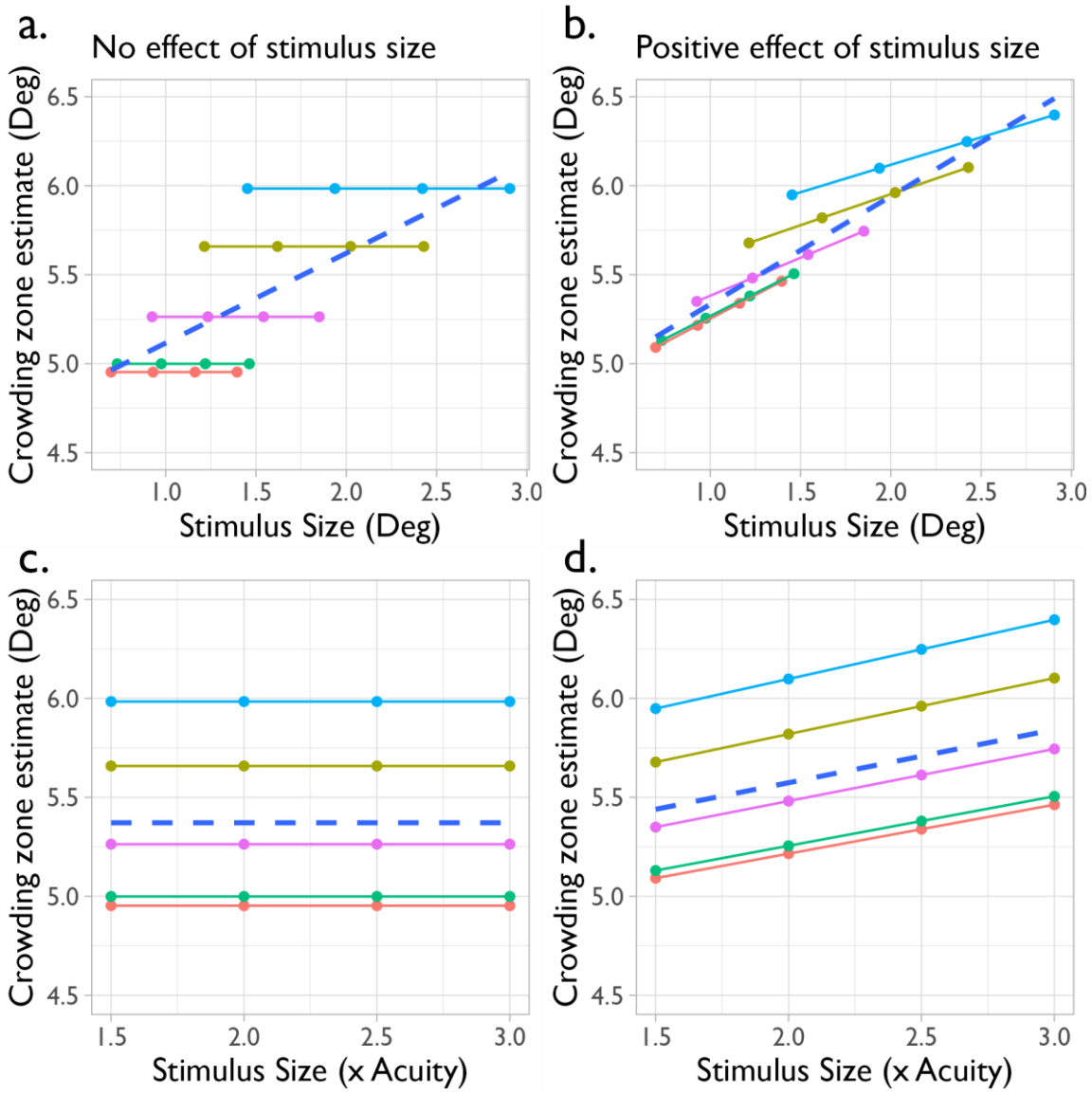

Figure 3.3 – Illustration of comparisons against size in raw degrees and multiples of acuity

Artificial data, illustration only. Panels a. & b. compare estimates of crowding zone extent against raw stimulus size in degrees for five 'observers' (coloured points). Panels c. & d. show the same data, but size is converted to a multiple of stimulus size at acuity threshold for each simulated participant. Left panels (a. & c.) illustrate data with no effect of stimulus size while right panels (b. & d.) show a positive association of crowding zone extent estimate with stimulus size (or visibility). Note the similarity in trend lines (blue dashed) between panels a. & b. compared with the differing trendlines between c. & d. Comparisons across size categories may avoid misleading results.

3.3 Results

Participants consisted of 1 Male, 11 Females, further characteristics are presented in Table 2, including the size of stimuli at threshold peripheral acuity at the test location (obtained from the peripheral acuity task), stimulus sizes subsequently used at each size condition and the criteria for marking crowded responses determined by the unflanked orientation matching task. Stimulus diameters across all size multiples from all participants ranged from 0.95 to 5.89 degrees of visual angle. Criteria determining a 'correct' response during the crowded task ranged from ±9.53° to ±80.52° around the orientation of the target. These ranges were calculated within the stimulus presentation script and were utilised by the QUEST algorithm during the crowded task, which in-turn controlled target-flanker separation. While derived from the same response data, unflanked perceptual error was calculated after data collection and fitting of a von Mises model to the errors (see Figure 3.4). As such, trial criteria data may not necessarily be directly reflected in the perceptual error data. Figure 3.5 shows the standard deviation of errors recorded during the unflaked task. Values of standard deviation are directly related to perceptual error (and show an identical pattern when plotted), so SD values are presented here as degree units are more intuitive.

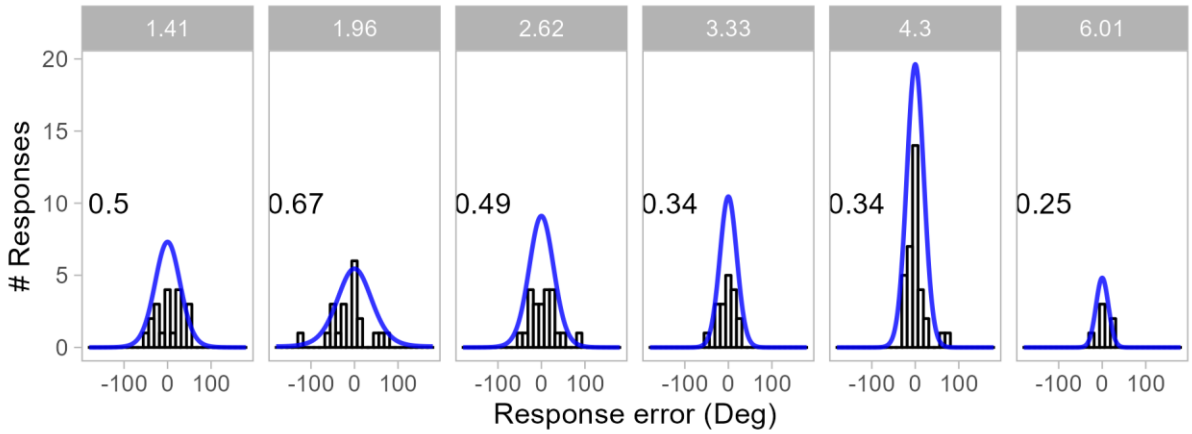

Figure 3.4 – Example distributions of response errors

Data shown are from one data set (Participant 4, stimulus size 2x acuity). Each panel represents one bin, mean target-flanker separation of binned trials (degrees) is shown at the top of each panel. Blue line indicates fitted von Mises distribution of fixed mean 0. Perceptual error (derived from concentration) is shown in each panel. Responses become more concentrated (smaller perceptual error) with increasing target-flanker separation.

Participant No.	Age (years)	Minimum angle of resolution (Degrees)	Stimulus size (Degrees)					Trial criteria per condition (°± relative to target orientation)			
			Acuity threshold	1.5x	2x	2.5x	3x	1.5x	2x	2.5x	3x
1	18	0.22	1.12	1.67	2.24	2.81	3.38	38.46	27.46	24.56	18.08
2	21	0.24	1.19	1.78	2.38	2.97	3.56	34.76	47.26	29.00	28.73
3	20	0.21	1.05	1.57	2.11	2.62	3.13	43.05	41.79	23.40	27.12
4	20	0.14	0.70	1.05	1.40	1.75	2.11	72.37	28.24	24.67	19.49
5	28	0.39	1.96	2.94	3.92	4.91	5.89	65.05	24.89	27.72	48.40
6	22	0.12	0.62	0.94	1.24	1.57	1.86	37.68	17.73	31.48	22.95
7	18	0.20	1.02	1.51	2.02	2.54	3.05	42.39	45.16	37.12	80.52
8	19	0.18	0.92	1.38	1.84	2.29	2.75	29.76	31.63	13.61	9.53
9	20	0.12	0.62	0.94	1.24	1.57	1.86	49.04	35.38	26.31	24.79
10	20	0.24	1.18	1.75	2.35	2.94	3.54	39.56	34.75	27.81	26.02
11	19	0.20	1.01	1.51	2.02	2.54	3.02	34.04	28.13	14.62	17.28
12	24	0.23	1.13	1.70	2.24	2.81	3.38	16.42	18.94	16.75	58.41

Table 2 - Characteristics of recruited participants

Participant acuity threshold at the target location is shown as minimum angle of resolution (MAR) in degrees of visual angle. The diameter of the Landolt-C at this acuity threshold is 5x the MAR by definition. This stimulus diameter at acuity threshold was then multiplied by a factor (1.5x, 2x, 2.5x, or 3x) to give the diameter of Landolt-C stimuli used during the experiments. Trial criteria were used to define a 'correct' response during the crowded task and were calculated as 2x the standard deviation of responses errors during the unflanked task. Issues arising from defining trial criteria this way are explored in the discussion.

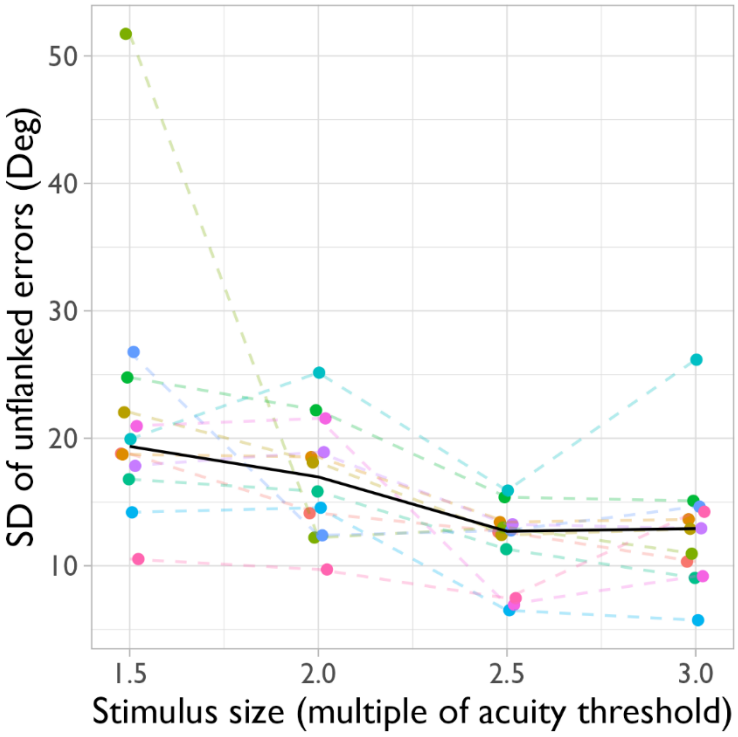

Figure 3.5 – Standard deviation of unflanked errors

Coloured points show individual participant data, while black lines indicate median perceptual error value at each stimulus size. The standard deviation of errors are directly related to values of perceptual error, which show an identical pattern when plotted.

Figure 3.6 shows the crowded perceptual error data and fitted hinged line models for all participants, at each level of stimulus size. Some data sets contain fewer points than others due to clustering of the target-flanker separations presented. Though these still represent the same total number of trials, more trials were counted within each bin, shown by a larger point size. There is a general trend across the datasets of decreasing perceptual error with increasing target-flanker separation, until this meets approximately the value of the unflanked perceptual error. The black lines on each plot show the hinged-line model fitted to each data set. Some models can be seen to be more representative of the form of the data than others (for example, the models fit to the data from participant 4 almost exactly match the shape of the data at all but the smallest stimulus size). One data set failed to achieve optimized model parameters and no model could be fit (Participant 12 stimulus size 3x local acuity threshold).

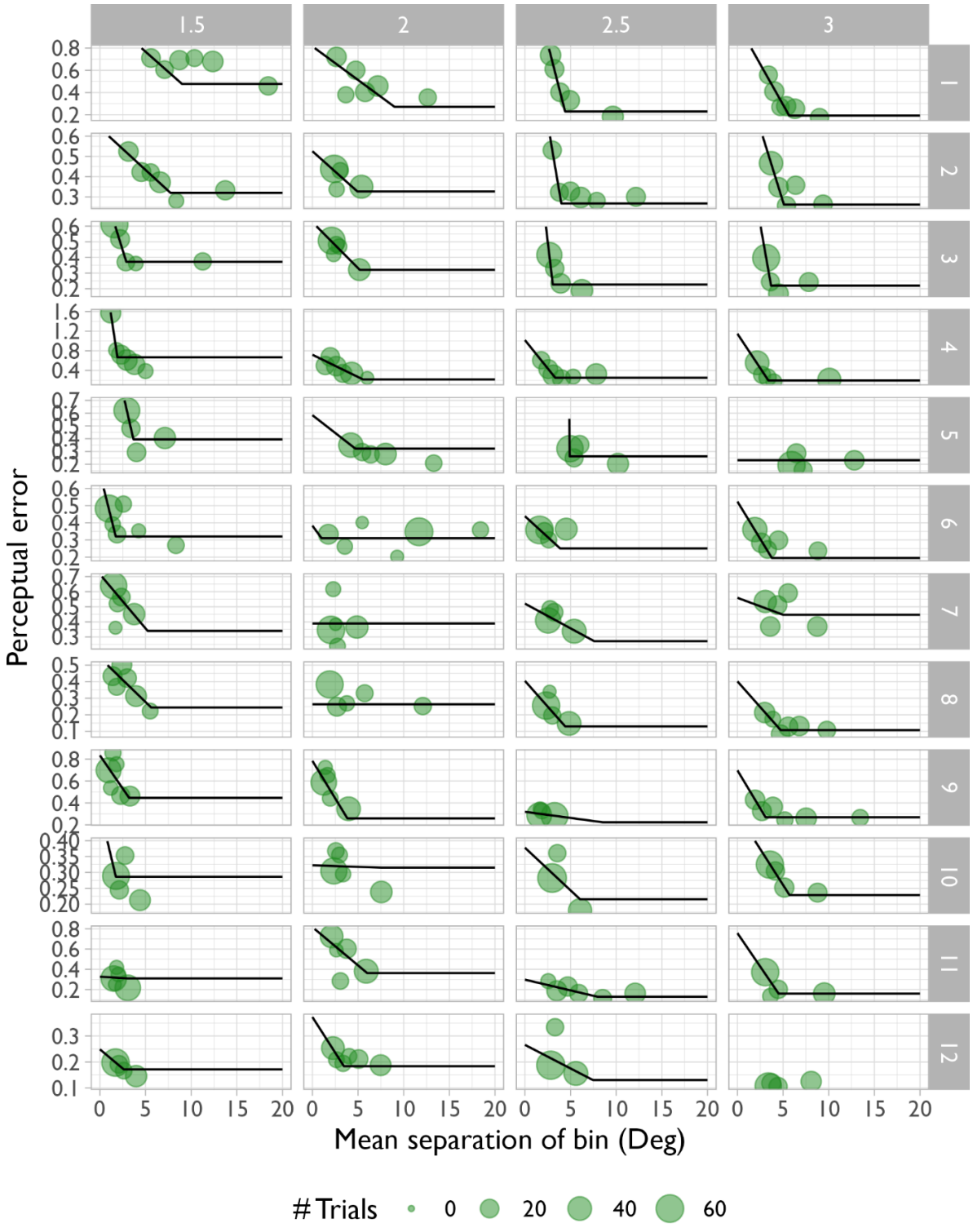

Figure 3.6 – Hinged line models fit to perceptual error data

Perceptual error was calculated from the spread of responses to crowded trials at each stimulus size (increasing across columns, multiples of size at acuity threshold). Point size indicates the number of binned trials. Fitted hinged lines are shown in black, modelling the fall in perceptual error (increase in precision) with increasing target-flanker separation.

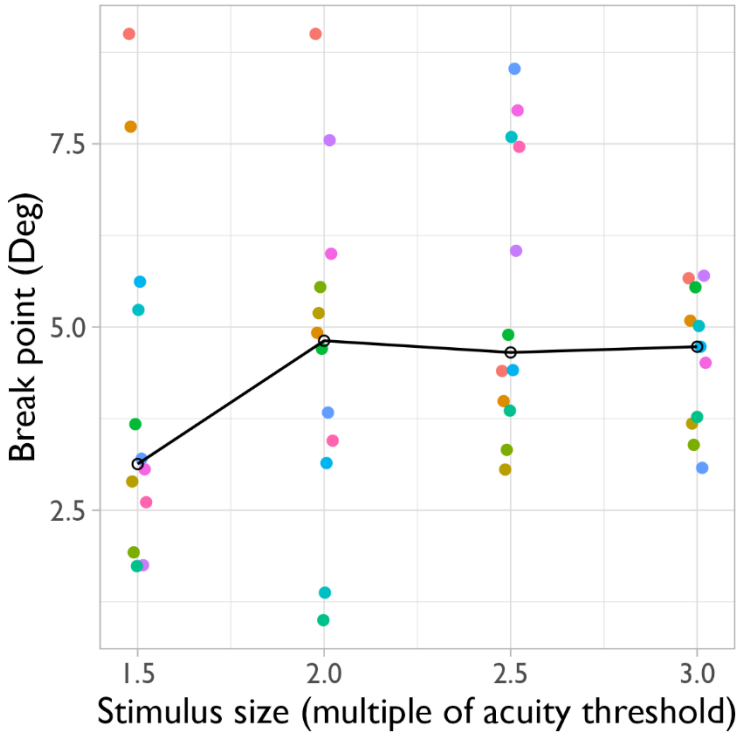

Figure 3.7 – Hinged line break points across stimulus sizes

Coloured points show individual participant data, black circles joined by a line indicate median break point of each stimulus size group. No statistically significant effect of stimulus size was found.

Figure 3.7 shows the extracted break points from the fitted hinged line models. Break points (measured in degrees) are compared with stimulus size in terms of multiples of stimulus size at local acuity threshold. The median of the smallest stimulus size group (1.5) is lower than the other three groups (2.0, 2.5, 3.0). The spread of the break points reduces with increasing stimulus size, potentially influenced by the reduced range of possible target-flanker limitations with larger stimulus diameter. There was no statistically significant trend in breakpoint estimate with increasing stimulus size indicated by a repeated-measures ANOVA $F(3,30) = 0.639$, $p=0.596$, however the 1.5x group estimates are not normally distributed, as indicated by Shapiro-Wilk test ($W = 0.861$, $p = 0.05$), so this assertion may be unreliable. The smaller median break point of the 1.5x group may be a reflection of the greater spread of unflanked errors with smaller stimuli, leading to higher value for the 2nd (horizontal) limb of the hinged model, which would meet the descending portion at a smaller target-flanker

separation. Nevertheless, a paired t-test between the smallest stimulus size groups did not indicate a statistically significant increase in break point values ($t(11)=-0.743$, $p=0.764$, the normality of differences was confirmed with Shapiro-Wilk test, $W=0.980$, $p=0.983$). A second repeated-measures ANOVA was conducted with only the three normally distributed groups (2x, 2.5x, 3x) which also indicated no statistically significant trend among these, $F(2,20) = 0.454$, $p = 0.64$. Mauchly's test of sphericity indicated the variance between the groups was sufficiently similar to meet the ANOVA assumption of equal variance in both instances (however, it should be noted that Mauchly's test is intended for normally distributed data).

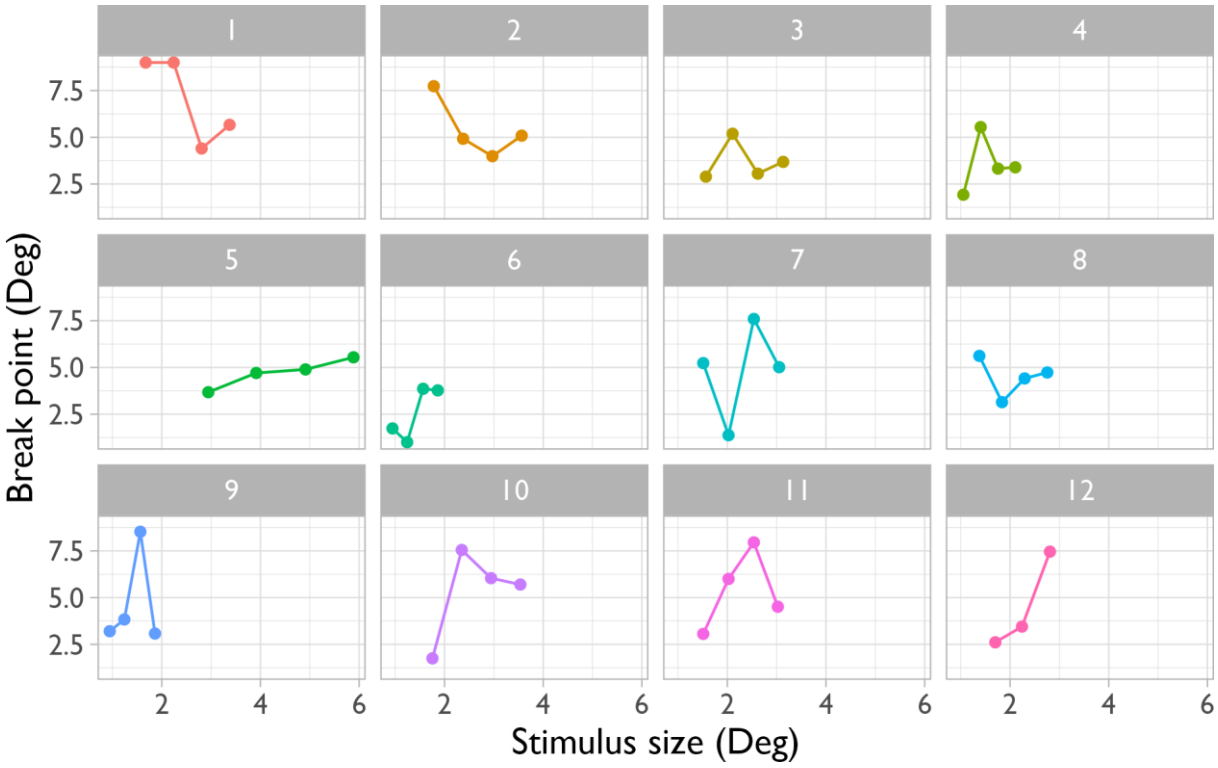

Figure 3.8 – Break point estimates for each participant

Break points extracted from fitted hinge line models indicate the smallest target-flanker separation at which reports of target orientation are predicted to be similar to the unflanked condition. As plots are separated for individual participants, stimulus size can be shown in degrees of stimulus diameter. One data point for participant 12 is missing as no hinged line model could be fit to the perceptual error data.

Break point estimates shown in Figure 3.8 are separated for each participant and compared with raw stimulus diameter in degrees of visual angle. The apparent trends of the data are quite different between individual participants. Break point estimates across stimulus sizes are also more variable for some participants (e.g., participant 7) than others (e.g., participant 5).

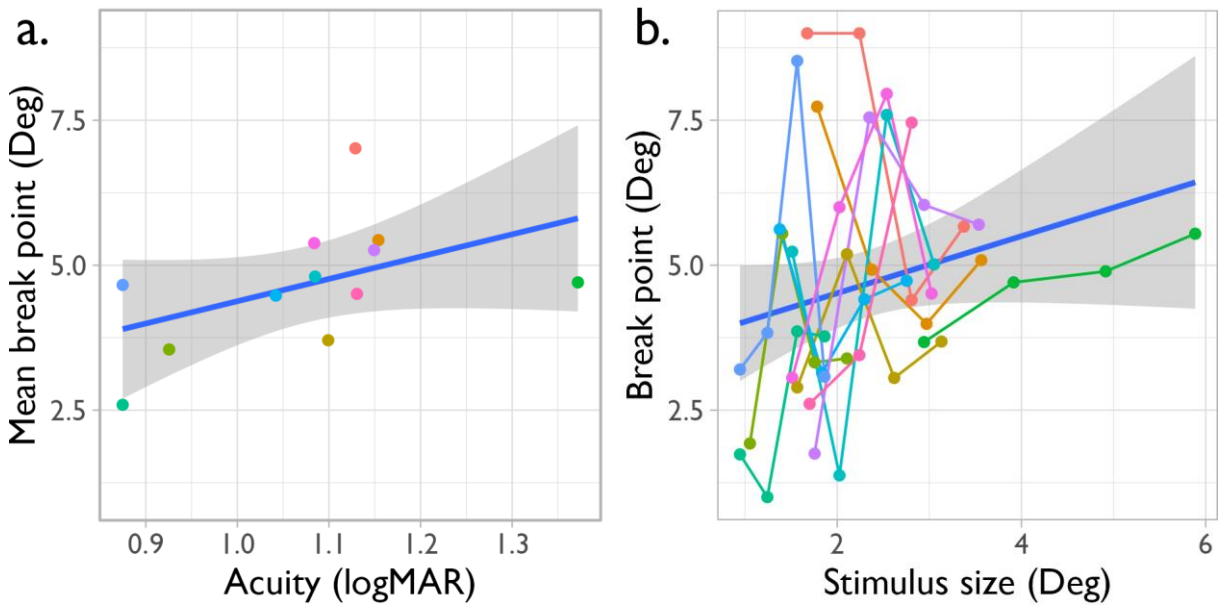

Figure 3.9 – Association with visual acuity

Panel a shows mean break point for each participant against acuity (log(MAR), measured with a Landolt-C 4AFC task). Panel b shows each break point estimate against the stimulus size used in degrees (as opposed to multiple of stimulus size at acuity threshold). The linear models fit to each data set (blue line, shaded area indicates 1 standard error) are subjectively similar, highlighting the potential for misleading interpretations if comparisons were made with raw stimulus size. Note the similarity between panel b here and Figure 3.3b and d above.

Figure 3.9a shows estimated acuity threshold at the target location converted to log(MAR). Figure 3.9b should be compared with the illustrated prediction in Figure 3.3b above. The positive trends may be being biased by data points at either end of the acuity and stimulus size scales, and these comparisons were not the intended aim of the study, so causal or physiological inferences are not to be drawn. This figure is intended only to justify the use of categorical comparisons of stimulus size as a multiple of stimulus size at acuity threshold (or, visibility), as opposed to direct comparisons with stimulus size in degrees.

Figure 3.3 illustrates the potential for misleading conclusions with such direct comparisons.

3.4 Discussion

The study found little evidence for any systematic influence of stimulus visibility (in terms of stimulus size) on estimates of crowding zone extent. This aligns with reports that the raw size of a suprathreshold stimulus does not influence visual crowding (van den Berg, Roerdink and Cornelissen 2007; Pelli, Palomares and Majaj 2004; Tripathy and Cavanagh 2002). Ruling out stimulus visibility as a potential influence would validate the findings of previous studies that used a consistent stimulus size across all participants (Martelli *et al.* 2009), studies that scaled stimulus to participant acuity (Greenwood *et al.* 2012) and studies that simultaneously varied stimulus size and spacing (Kalpadakis-Smith *et al.* 2022; Song, Levi and Pelli 2014). While participant acuity at a peripheral field location can be highly variable, any method ensuring the stimulus is supra-threshold for all participants may be sufficient to prevent potential acuity-related issues confounding results.

Figure 3.3b shows the anticipated, but potentially misleading, association between raw stimulus size in degrees and estimates of crowding zone extent. Indeed, Figure 3.9a shows the predicted positive correlation between peripheral acuity and estimated crowding zone extent. These figures validate the methodological decision to define stimulus size in terms of multiples of peripheral acuity, rather than raw degrees. See Figure 3.3 for the illustrated predictions of the data form in the presence and absence of a true effect of visibility, and note that the experimental data in Figure 3.7 most closely resemble Figure 3.3c which illustrates no effect of stimulus size.

Examining each participant's estimates of crowding zone extent in Figure 3.8, both the estimates themselves and the apparent trends across stimulus sizes between participants are highly variable. This suggests that the method is sensitive to sources of uncertainty, creating variability in the estimates acquired particularly with smaller stimulus sizes. The variability in these estimates could potentially obscure small true effects of stimulus visibility on estimates of crowding zone extent. However, the appearance of the present data suggest that if such an effect were truly present, it is likely such a small effect that accounting for stimulus visibility may not be beneficial.

The hinged line model-based analyses used here are sufficient to estimate crowding zone extent as the break point of the fitted model. Close examination of the errors collected in some bins with high perceptual error (and other pilot data – see Figure 4.1) suggested systematic patterns of errors being made, with responses tending to cluster around either the orientation of either the target or the flanker. A more detailed analysis pipeline was later developed to exploit this clustering of responses and quantify visual crowding (detailed in section 4.4). However, attempts to apply this type of analysis to the present data were unsuccessful. This is likely due to two main design decisions in the present study. Firstly, the implementation of the QUEST adaptive algorithm, and secondly, the fine-grain levels of potential target-flanker separations used in stimulus presentation leading to trials being conducted at slightly different levels of target-flanker separation, rather than having repeated trials at the same level. Collecting these trials into bins was sufficient for the present analyses but created an additional source of error in more detailed analysis of the data. This also led to some bins containing more trials than others which would affect the reliability of inferences from more in-depth analyses. Bins at greater target-flanker separations tended to contain too few trials for deeper analysis. Subsequently, the fitting of 'spatial profiles'

(section 4.5) used in later analyses would frequently fail to find reasonable estimates of crowding parameters which are explored later in the thesis. Models which did not fail to fit were also subject to considerable potential biases due to the clustering of data points (Wichmann and Hill 2001). These limitations are discussed and resolved in Chapter 4 towards the analysis of later studies.

The present method of adapting the range of responses considered ‘correct’ by the adaptive algorithm also tended to lead to high numbers of trials being conducted at small target-flanker separations. A spuriously wide trial criterion would cause the QUEST algorithm to tend to present smaller target-flanker separations, as a greater proportion of trials are counted as ‘correct’. However, this may not necessarily affect estimates of hinged-line model break points due to the addition of noise to the value of the algorithm’s posterior probability density function when determining target-flanker separation for the following trial (see Method). This step, as well as starting each repeat of the crowded task at a wide target-flanker spacing ensured that not all trials were conducted at small target-flanker separations. After being collected into bins for calculation of perceptual error and combined with the unflanked perceptual error, most datasets held sufficient information to fit a hinged line model. However, datasets for which there were fewer data points beyond the estimated break point would be particularly subject to possible errors in estimation of the break point.

3.4.1 Implementations and future work

As no systematic influence of stimulus visibility on crowding zone extent is suggested, smaller suprathreshold stimuli may be preferable in order to provide a larger range of potential target-flanker separations to be examined. Note, the range of possible target-flanker separations are limited by stimulus diameter at a minimum (to ensure stimuli do not occlude one another) and the screen size at a maximum, which varies with viewing distance from the screen. Provided stimuli are sufficiently larger than the acuity threshold at the test location, further enlargement of the stimuli is not useful. This could be achieved by either using a constant (reasonably large) stimulus for all participants, or by scaling stimulus size to some multiple of each participant's measured acuity as demonstrated by this study. Using one stimulus size for all participants would require validating that each participant is able to resolve the stimuli with an acuity task and may lead to exclusion of participants if too small a stimulus size is chosen. The present study suggests scaling stimuli to participant acuity would not confound results by virtue of the stimulus size used. This would potentially allow a larger range of participants (with a greater range of peripheral acuities) to be examined. Post-hoc examination of effects against acuity may be useful to determine or rule-out any potential effects arising from a greater range of acuities examined.

Chapter 4 Developing the spatial profile of crowding

4.1 Introduction

Following analysis of the data collected in section 3.3 it was concluded that the method required development to better explore how crowded targets are perceived. While perceptual error-based analysis could estimate the extent of observed crowding effects, details of the perception of the target within the crowding zone were obscured. In light of this, the aims of following experiments were altered to shift focus onto investigating the changes in distributions of reported target perception as flankers when flankers are located within the crowding zone, rather than determining the limit of the crowding zone (as achieved by the perceptual error analyses detailed in 3.2.6 and discussed in 4.3.2). By refining the experimental method, and implementing a novel analysis technique, the patterns of errors made within the crowding zone could be more thoroughly investigated.

It was at this stage that the COVID-19 pandemic began and necessitated a change in the overall aims of the project. The later stages of the project had planned to investigate crowding effects in participants from a clinical cohort and the general public, but the impact of the COVID-19 pandemic (explored below) eventually led to the decision to pivot towards continuing investigating normal visual crowding in a small number of experienced participants recruited from the University. These new aims would also be better achieved with a change in experimental design and related analysis method. Additionally, the change in participant group (from inexperienced members of the public to psychophysically trained participants from the University)

also permitted the required methodological changes which may not have been suitable for the initially planned participant group.

This Chapter will review the method to estimate the extent of crowding effects used in Chapter 3 (and Study 1 of Chapter 5, section 5.2), highlighting its limitations before describing the rationale and design of a new method used in later Chapters. This new method removes the implementation of an adaptive algorithm, and instead conducts a fixed number of trials at several pre-determined target-flanker spacings. The patterns of collected responses are then able to be explored more thoroughly with a population-pooling model and the fitting of a novel 'spatial profile' of crowding.

4.1.1 Pandemic-related impact on participant recruitment

The COVID-19 pandemic led to a significant change in participant recruitment protocols. Participant-facing research was halted for several months, and a number of safety protocols were put in place in order for research activities to resume. The effects were compounded by uncertainty over the prospect of future lockdowns and further delays to the ethical approval process within the local health board. As a result, recruiting large enough cohorts of untrained participants in the required timeframe was deemed unfeasible for the remaining studies planned.

The research aims were adapted to explore crowded perception in normal vision, rather than a clinical cohort. This reduced the number of participants that would need to be recruited, as well as allowing data collection to continue while participant recruitment from the general public was not permitted under COVID-related rules mandated by the University.

4.2 Rationale behind the change in method

The general experimental design pivoted to conducting a higher number of trials in a smaller number of experienced participants. This permitted more intensive data collection as these highly trained participants were familiar with psychophysical methods and experiments involving high numbers of trials. As a result, more data could be collected while mitigating potential learning and fatigue effects. The methods used so far (Chapter 3and Study 1 of Chapter 5, section 5.2) were designed with inexperienced observers in mind, including a few compromises and assumptions that can now be revised, which are explored below.

4.3 Review of experiment components being changed

4.3.1 Use of an adaptive algorithm

The method presented in Chapter 3and Study 1 of Chapter 5 (section 5.2), features an adaptive algorithm (QUEST (Watson and Pelli 1983)) which is used to set the target-flanker spacing dynamically between trials. The adaptive algorithm is supplied with an '*a priori*' distribution of expected performance (proportion of 'correct' vs 'incorrect' responses) over the extent of possible stimulus placement (meaning target-flanker spacing in this implementation), which is a best guess based on prior information. The algorithm is then set to estimate the target-flanker separation required to achieve a provided level of performance – the 'threshold' level.

The implementation of QUEST here requires three decisions to be made which will impact its effectiveness: the shape of the 'prior' distribution of performance over target-

flanker spacings, the level of performance at which to estimate the associated stimulus spacing, and the criteria of a ‘correct’ versus ‘incorrect’ response.

The closer the *a priori* distribution is to the observed participant performance, the fewer number of trials will likely be required by QUEST to arrive at an estimate of target-flanker spacing at threshold (dependent on participant ability to complete the task). In some instances, this may be easily obtained (where available from the literature or previous experiments) but this is more difficult in relation to crowding. Determining the best parameters for the *a priori* distribution is complicated by the wide range of crowding effects reported in the literature, even with similar stimulus arrangements.

The performance level that an adaptive algorithm is set to estimate is typically related to the psychophysical task being conducted. For example, a seen/not-seen detection task (such as standard automated perimetry) would give an associated threshold performance level of 50% seen – halfway between perfect performance (100% seen) and ‘poorest’ performance (0% ‘seen’). Similarly, a 2 alternative forced-choice (2AFC) task is typically interpreted with a 75% ‘correct’ threshold, falling hallway between 100% ‘correct’ responses and 50% ‘correct’ (where participants resort to guessing). A ‘continuous-report’ paradigm (method of matching, (Farell and Pelli 1998)) does not have an associated level of threshold performance as responses are not a forced choice between a small number of alternatives. Performance does not fall to a level of random guessing, rather to a ‘maximally crowded’ state in which responses are centred on the flanker orientation (in this these data). In visual crowding research there is no defined level of performance which is uniformly accepted as the limit of the crowding zone, so the decision is ultimately up to the researcher. A level towards the upper end of performance (e.g. 80% ‘seen’ as in Kalpadakis-Smith *et al.* (2022)) is logical to indicate the spacing at which crowding begins to affect perception, but may

be confounded by other factors (discussed further in 6.4.3). The pre-set threshold level of performance will also affect the difficulty of the task, as this implementation of QUEST will typically determine spacings close to that associated with the 'threshold' level of performance as being the most informative – especially as more trials are conducted. A high 'threshold' performance level could lead to a subjectively easy task as most trials are weakly crowded at greater target-flanker separation (Harrison and Bex 2015), and fewer trials being conducted at smaller target-flanker spacings.

For an adaptive algorithm to operate, it must be supplied with two key pieces of information on each trial: the target-flanker spacing used and whether the response was 'correct' or 'incorrect'. In the example of standard perimetry, this definition of a 'correct' trial is obvious (i.e. the stimulus is seen, so the response button is pressed). For a continuous-report method, the delineation of 'correct' and 'incorrect' is less obvious. In the previously described method, an 'incorrect' response is defined as being outside 2 standard deviations of the estimated distribution of responses during an initial unflanked task (equating to the 2.3% and 97.7% percentiles). This would be adequate on the assumption that 'crowded' trials would provide responses outside this range. However, as 'crowded' responses are centred around the flanker orientation, this only holds for larger target-flanker orientation differences. If flankers are oriented sufficiently similarly to the target orientation, or if participants are inaccurate enough, some 'crowded' responses could fall within the previously defined range and be counted as 'correct'. This may then lead QUEST estimations of the participant's performance distributions astray, limiting its use as an indicator of crowding behaviour in these instances.

This might be avoided by reducing the range of responses considered 'correct'. As participant accuracy in reporting perceived orientation can vary considerably (see

Figure 3.5 of perceptual error in the uncrowded task) it may still be preferable to set this level individually as above, rather than setting an arbitrary limit to 'correct' responses for all participants. However, setting too small a range may have the opposite effect – indeed the previously used definition could still indicate 4.6% of unflanked responses were 'incorrect', despite the absence of flankers.

Additionally, this difficulty of determining a level of 'correct' vs 'incorrect' responses would persist if a simpler 'staircase' type algorithm were used. These do not use any behind-the-scenes estimation of underlying distributions and instead would vary the target-flanker spacing according to the evaluation of previous responses (Leek 2001). To systematically explore perception of crowded targets, it would be preferable to use a method that does not change in response to participant responses. Instead, a number of fixed target-flanker spacings are pre-selected and tested over a set number of trials with the collected data being analysed separately after the fact. This would allow the categorisation of 'crowded' and 'uncrowded' responses to be explored with no inherent bias in the data arising from the experimental setup.

4.3.2 Outcome measure and analysis method

The main outcome measure of the previous method (Chapter 3and Study 1 of Chapter 5, section 5.2) was an estimation of the extent of the crowding zone – taken as the target-flanker spacing at which responses deviate from unflanked responses. This was estimated by collecting trials within determined ranges of target-flanker separations (a 'bin') and modelling the errors in responses as a single von Mises distribution (similar to the method of Harrison and Bex (2015)). Note: the Von Mises distribution is

analogous to the normal distribution in linear statistics but is more suitable for circular data such as orientation – for example, +180° and -180° would be correctly treated as the same orientation, rather than opposite ends of a linear scale. The standard deviation of these distributions was then taken as a measure of perceptual error and modelled against the mean target-flanker separation of the collected trials. These 'hinged-line' models provided an estimate of crowding zone extent as the level of target-flanker spacing at which the spread of responses increased above the spread of responses when no flankers were present. This is in line with methods described in the supplemental materials of Harrison and Bex (2015).

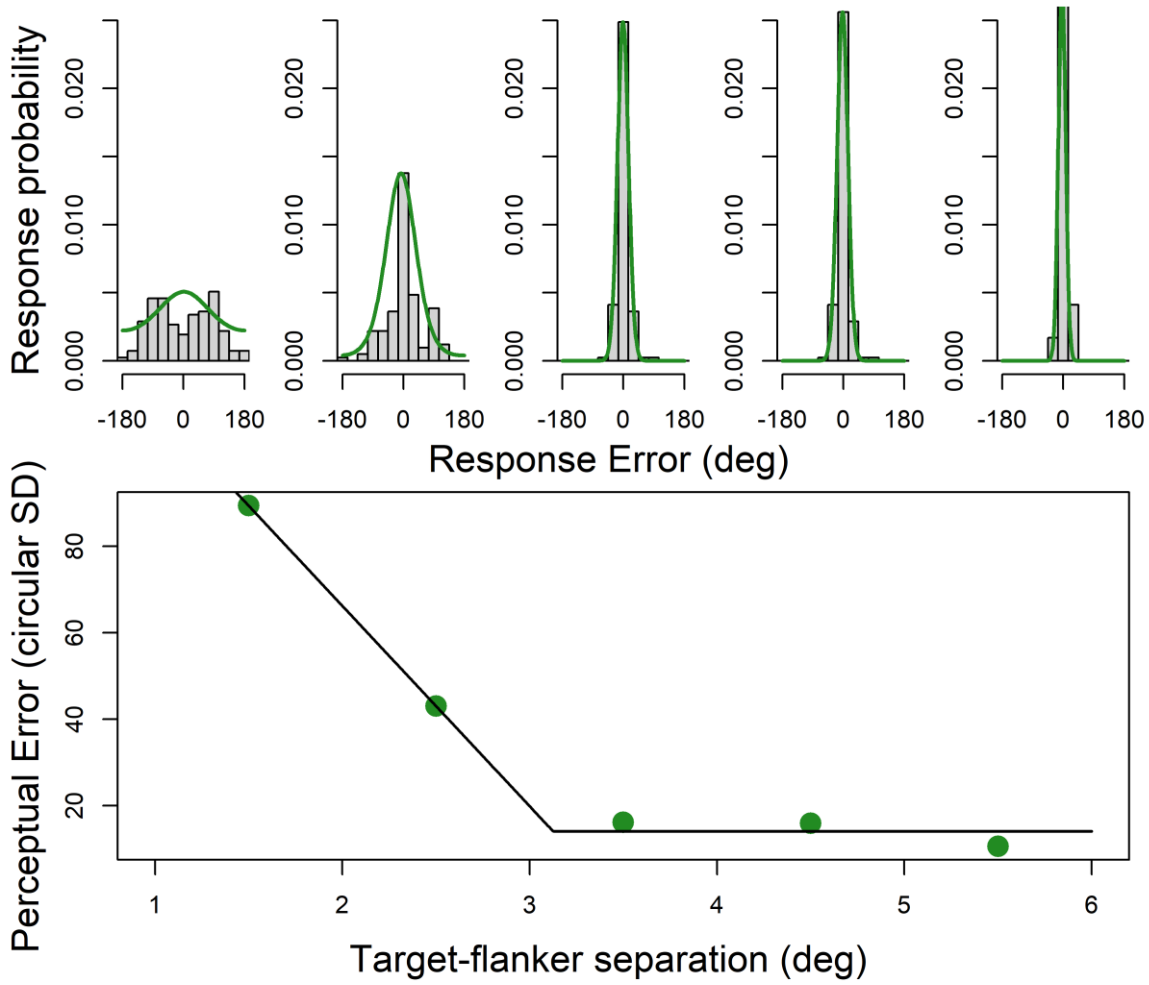

Figure 4.1 - Distributions of errors and the hinged line model

The row shows distributions of errors from a pilot experiment plotted with increasing target-flanker spacing from left to right. The green lines show the fitted von Mises distributions. The lower plot shows the 'perceptual error' (circular standard deviation of errors) plotted against target-flanker separation. The black line shows the fitted 'hinged line' model. Note while most of the distributions show responses primarily cluster around 0° (i.e. the target orientation) the left most plot shows two peaks at +90° and -90°. These are the relative flanker orientations (90° clockwise or anticlockwise to the target). While this analysis does show the departure from uncrowded patterns of responses (right-most distributions), a more in-depth analysis would provide more detail on the types of errors being made.

Though this is a reasonable definition of the limits of a crowding zone that can be estimated from the data, the estimation of this limit is all the information this method can provide. The value of 'perceptual' error does not confer any further insight beyond whether it is approximately the unflanked value, therefore it does not give any indication of what participants perceive. From the distributions of errors (such as in Figure 4.1), more information may be accessible with a different approach. Clear groups of errors around 0° (indicating 'uncrowded' responses) and at values corresponding to the amount of target-flanker orientation difference are visible in trials in which crowding is evident. Modelling these errors as a single von Mises distribution leads to a wide distribution in order to capture the two 'flanker' centred peaks either side of 0°. If larger target-flanker orientation differences were used, these 'flanker' peaks would be further separated in peak orientation and a higher value of perceptual error would be produced – even if the proportions of 'crowded' trials were the same. The above analysis does not explore the pattern of responses in a meaningful way, rather it only provides an indication of whether crowded responses are present in the collected trials. Attempts to analyse the distribution of errors in the studies presented in Chapter 3and Study 1 of Chapter 5 (section 5.2) with more informative methods proved difficult due to factors arising from the adaptive nature of the experiment design. Specifically:

1. Some bins of trials to be analysed together were conducted over a range of target-flanker spacings. This hampered associations between response patterns and target-flanker spacing, particularly when these ranges were large

2. Some bins contained too few trials to adequately assess

3. In some datasets, large proportions of trials were conducted at similar levels of target-flanker spacing. This meant response distributions could be well determined at some (often small) levels of target-flanker separation, but too few trials were subsequently conducted at other separations to provide useful insights

Conducting a pre-determined number of trials at pre-determined levels of target-flanker separation (as is typical of psychophysical research, especially before staircase/adaptive methods were commonplace) would alleviate these issues and potentially provide rich insight. The main disadvantage to this type of design is that it will necessitate a higher number of trials overall. This would be disproportionately high if a single estimate of stimulus spacing (i.e., threshold level) is the intended outcome measure. The benefit of these additional trials is the ability to assess the underlying function relating target-flanker spacing to any measure of performance that can be derived from the obtained data – thereby a psychometric function of visual crowding. Consequently, the outcome measure of the experiment is no longer a single level of target-flanker spacing to be taken as the limit of the crowding zone. Instead, a sufficiently constructed psychometric function would be able to predict participant performance at any level of target-flanker spacing. Comparing psychometric functions between conditions could also indicate other changes in response characteristics that may be overlooked when comparing threshold measures – see Figure 4.2 below for an illustrated example. As experienced observers would be more able to tolerate additional trials, changing the experimental method and associated analysis may potentially enable much more significant insights.

The remainder of this Chapter will explain the new experimental design and any associated decisions and considerations. The difference between the two methods in the context of an experiment will be explored in the next Chapter, as Study 1 of

Chapter 5 (section 5.2) had already been conducted using the experimental design outlined above.

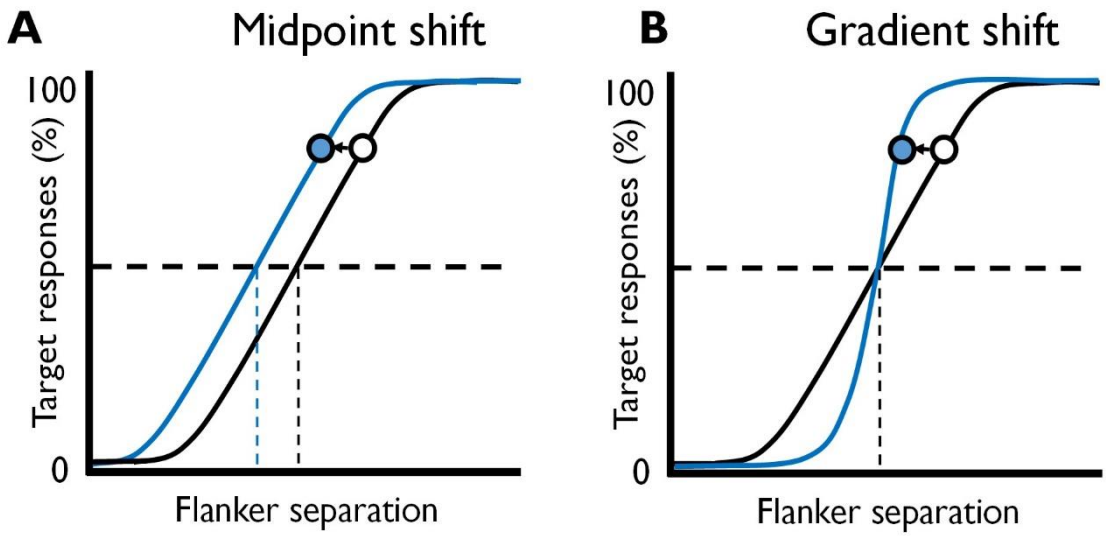

Figure 4.2 - Illustration of different changes in psychometric function which could explain the same shift in threshold level

Consider an experiment sampling the psychometric function at one level, producing the white data point. Next, a second experimental condition produces the blue data point. Based on these data alone, this difference in threshold level could equally be the result of two very different psychometric functions (blue line). One explanation is that the function has steepened, but not shifted along the x-axis (panel A) whereas an alternative explanation is that the function is identical in shape but has shifted along the x-axis (panel B). These explanations could have dramatically different interpretations when related to underlying physiology but could not be distinguished from a single threshold comparison.

4.4 New experimental method

The fundamental change in experiment design is the removal of the adaptive algorithm, which has knock-on effects: levels of target-flanker spacing will now need to be pre-determined, and the primary outcome measure is no-longer limited to a single level of target-flanker spacing. From a participant perspective, the experimental task remains identical – to report the perceived orientation of a target by rotating a 'response' Landolt-C using a response dial.

4.4.1 Pre-determining target-flanker spacings

Pre-determining the target-flanker spacings to be examined poses a conceptually similar problem to providing parameters of an *a priori* distribution to the QUEST algorithm (discussed above). Sampling a sufficient number of appropriately set target-flanker spacings is necessary to minimise bias in estimations of the underlying psychometric function (Wichmann and Hill 2001). However, no knowledge of the shape of the underlying function is particularly necessary, only its approximate range which levels can then be evenly spaced across. At a minimum, flankers must be spaced at least 1 stimulus-width from the target to avoid covering (or 'masking') the target as this would confound the observed effects. The maximum of this range should be just beyond the maximum target-flanker spacing which is expected to give rise to crowding effects. An approximation of this may be taken from Bouma's law: the span of the crowding zone is approximately half the eccentricity of the target. Despite its name, it is typically better understood as a rule of thumb, unless several caveats are considered (Strasburger 2020). Nevertheless, this gives a reasonable level of target-flanker spacing to consider an approximate maximum. The largest target-flanker

spacing utilised in a particular experiment would be close to half the spacing between the fixation point and the centre of the target stimulus. Testing at levels above this is likely to render largely uncrowded distributions of errors, which gives little additional information over an unflanked condition. Five target-flanker spacings was determined to be adequate to permit linear regression. An additional unflanked condition will also be assessed, which could be taken as a 6th target-flanker spacing with flankers at an infinite distance from the target.

4.4.2 Number of trials

While the number of trials was still pre-determined in the previous adaptive method, these were (often unevenly) spread across the range of target-flanker spacings examined. In this new method, a decision is required as to the number of trials needed to adequately characterise a pattern of responses at each target-flanker spacing. As this could not be estimated from previously collected data, an initial conservative choice of 150 trials per condition (Chapter 6, Study 1, section 6.2) was later revised to 105 trials per condition (Chapter 5, study 2, section 5.3), and to 80 trials per condition (Chapter 6, study 2, section 6.2) to prevent prohibitively long data collection sessions.

4.4.3 Trial blocks and experiment repeats

As in the previous method, trials were conducted in blocks with enforced breaks at specific intervals. Trials of different target-flanker spacings were shuffled together and presented in a random order, including unflanked trials. Three repeats of the experiment procedure were conducted and the order of trials was randomly shuffled at each repeat. This was done to permit longer breaks between repeats and break up

the data-collection while minimising the risk of data loss should an error occur (no refreshing of any algorithm was needed).

4.5 Constructing the spatial profile of crowding

This analysis method was initially developed for use with the data from the previous experiment. The aim is to characterise the distribution of responses from two fundamental sources: a 'target' response and a 'flanker' response. This proved difficult due to the issues mentioned above, but the rich data obtained with a non-adaptive method works well with this in-depth analysis. The main steps, and associated considerations, are explored here.

4.5.1 Calculating response error

Report error was calculated as the difference between the presented target orientation and the orientation provided by the participant in response to each trial. A response at exactly the target orientation for a given trial would have a response error of 0°. The sign of response errors collected on trials with anti-clockwise flankers were flipped, such that positive errors now always indicated responses towards the orientation of the flanker, and errors away from the orientation of the flanker were negative. For example: If a target were presented at 90° and flankers at 135°, a response given at 100° would be given a response error of +10°. If the flankers were presented at 45°, the response error would be -10°, as the response was oriented 'away' from the orientation of the flanker.

4.5.2 Modelling distributions of responses

A frequency distribution of response errors for each unique condition was constructed by summing the number of trials that produced each possible report error. These sums were then divided by the total number of trials conducted under this condition to give a distribution of probabilities such as in Figure 4.1 In crowded trials there were typically two peaks: one centred at 0° corresponding to the 'target' response, and a second centred at the level of target-flanker orientation difference (the 'flanker' response), as in the left-most distribution of responses in Figure 4.1.

These distributions were well described (in most instances) by a bimodal model consisting of two overlapping von Mises distributions. These responses are then individually weighted and combined to produce a bimodal model of the probability of potential errors, with peaks centred at 0° (the 'target' response) and the target-flanker orientation difference (a 'substitution' type response). The concentration parameters of the distributions (related to the width of the peaks produced by the final model, and indicative of the precision of responses) were allowed to vary individually for the target and substitution responses, as well as their weighting constants which relate to the height of each peak in the combined distribution. The end result is a 'population pooling' model, which can be interpreted as the weighted output of a population of orientation-selective neurons to the particular stimulus arrangement (Harrison and Bex 2015; Kalpadakis-Smith *et al.* 2022).

The weighting of a particular response error (θ) predicted by the model can be expressed mathematically in Equation 4.1 below, where f() is a von Mises distribution function.

$$P_{(\theta)} = w_T \times f(\theta \mid 0, k_T) + w_F \times f(\theta \mid \theta_F, k_F)$$

Equation 4.1– Bimodal mixed von Mises distribution

θ = Response error
W = Weighting factor (Target, Flanker)
θ_F = Flanker orientation (relative to Target at 0°)
k = Concentration parameter (Target, Flanker)

An important assumption in this model is that there are no other sources of response orientations. Some authors using similar methods report the use of an additional element to quantify 'random' errors (Ester, Klee and Awh 2014). However, the data collected for these analyses contained very few responses that could not be reasonably captured by the 'target' and 'flanker' response elements. Quantifying these few responses would require an additional model parameter – a weighting factor to determine the height of a uniform von Mises distribution (concentration = 0, no true mean). When attempted, this 'trimodal' model frequently failed to determine optimised values of the free parameters and estimated very low proportions of random responses in the few instances it did succeed. As this gave no more useful information, it was decided to continue with the assumption of responses consisting only of 'target' and 'flanker' elements, and use the bimodal model described above.

The four free parameters (weighting constant and concentration parameter for each of the target and substitution responses) were optimised using a nonlinear least-squares method. The calculated circular standard deviation of the unflanked trials was used to determine initial estimates of the concentration parameter of each population response and was allowed to vary between the concentration of unflanked trials at a

maximum (narrowest peak) and 8 at a minimum. (Note: A von Mises distribution of concentration=8 has 95% quantiles at approximately ±40°). Initial estimates of the weighting parameters were set to 0.1 and allowed to vary between 0.001 and 10, though the final values rarely exceeded 0.1.

4.5.3 Calculating proportions of target and flanker responses

Optimised weighting factors for target and flanker responses in the fitted bimodal model for each bin were extracted. Participant performance for each condition was then expressed as the ratio of the target weighting factor to the sum of the target and flanker weighting factors. This value indicates the relative proportion of target responses observed, alternatively abbreviated to p(Target), which can also be interpreted as the probability of a response being centred around the target orientation under the crowding conditions used. This produces a performance scale ranging from 1 (all responses contained within the target peak) to 0 (all responses contained within a peak around the flanker orientation, i.e. substitution type responses).

An important caveat of this method is that the concentration parameters (related to peak width) are not used in the calculation of p(Target). The spread of the peak still reflects the proportion of responses it contains (a wider peak of equal height would encompass a greater proportion of responses), but this inference is lifted from only the weighting parameters. This is illustrated in the error distributions in Figure 4.3 below. Note: identical results were obtained when comparing areas under the curves of each peak as a confirmatory analysis. The result of this is that p(Target) is a good indicator of the relative proportion of target responses, but no inference of response precision can be made on these values.

Analyses of the fitted concentration parameters to investigate response precision were inconclusive. No consistent pattern or interaction could be seen, and some datasets were fitted with concentration parameters at the floor and ceiling limits of the optimisation algorithm. Altering (or removing) the limits of the parameter optimisation did not improve model fitting, and frequently led to models either failing to be fit or illogical parameters being suggested. For example, some datasets with few flanker-centred responses suggested the response to the flanker was more precise than the unflanked trials by an order of magnitude. With defined limits, these datasets were more reasonably characterised as being low in magnitude (i.e. peak height as determined by the weighting factor) and a concentration parameter (controlling spread) at the lower limit, equal to the unflanked trials.

In some datasets where there was no peak in responses centred at the orientation of the flanker, the bimodal model failed to be fit. In this case, a unimodal model centred at a responses error of 0° (i.e. the target orientation) was used instead and only one weighting factor was optimised, so the p(Target) value was defined as being 1. This is appropriate for instances where flankers were present but the flanker response was so weak that all responses were concentrated around the target orientation, or where flankers were absent.

4.5.4 Fitting the spatial profile of crowding

Values of p(Target) under each condition were then combined and modelled by a logistic function using the self-starting logistic model provided by the SSLogis function in R and optimised with a second nonlinear least squares optimisation.

It is an assumption that the spatial profile follows a logistic curve, but this appears to describe the data presented in later chapters well. Another important aspect is that the logistic functions were constrained to plateau at p(Target) values of 0 and 1. An upper level of 1 is logical as flanker response should reasonably drop off at a sufficient level of target-flanker separation, which is also evident in most of the datasets with larger separation values. A lower level of 0, while evident in most datasets, may not be so universal. Indeed, in some data sets the smallest permissible target-flanker spacings still produced a small proportion of target responses.

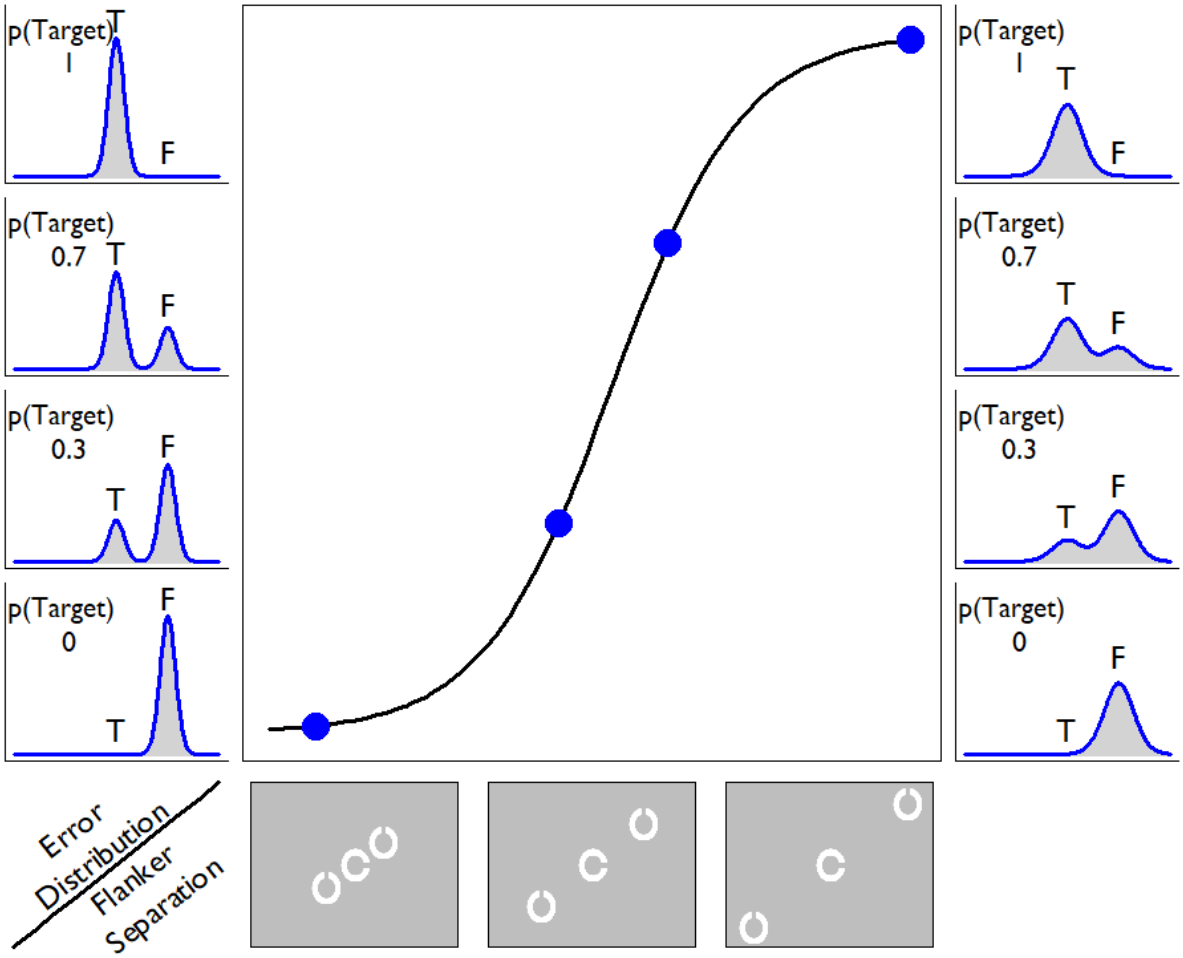

Figure 4.3- Illustration of error distributions and the spatial profile of crowding

The central curve is a characteristic 's-shaped' logistic function linking p(Target) values (y-axis) with target-flanker spacing (x-axis). The value of p(Target) (blue points) is a ratio of responses centred at the target orientation vs. the flanker orientation, calculated from the fitted bimodal model (blue lines). Thus, a p(Target) of 0 shows all the responses were centred at the flanker. The left- and right-most columns show distributions of errors producing a range of p(Target) values and illustrate how the precision of target and flanker responses are not reflected in the value calculated.

4.5.5 Parameter analysis and comparisons

The spatial profile is defined by two parameters:

Location of the midpoint – the level of target-flanker separation at which responses are equally shared between being centred at the target and flanker orientations, so p(Target) = 0.5. This is a measurement of distance with units in degrees of visual angle (°)

Gradient at the midpoint – the steepness of the function relates to rate at which the proportion of responses shifts when target-flanker separation is altered. This value is steepest at the midpoint and flattens towards the upper and lower limits of p(Target). A steeper function indicates small changes in target-flanker separation will result in larger shifts in the distribution of responses, whereas a shallower function suggests large changes in target-flanker spacing would be needed to produce a change. This is a measurement of rate of change, so will have units of change in p(Target) per change in spacing (δp/δ°)

These two parameters describe two key aspects of visual crowding which may be disentangled with this method. The distance measurement (location of the midpoint) is interpreted as being an indicator of the spatial extent of visual crowding. The rate of change (gradient at the midpoint) describes separate aspect of crowding which controls the span of the transitionary zone between minimal and maximum effects of crowding. Disentangling potentially conflated aspects of crowding has been previously suggested as potentially informative (Pelli and Tillman 2008) but methods so far have been limited to examining shifts in threshold elevations (Pelli, Palomares and Majaj 2004; van den Berg, Roerdink and Cornelissen 2007) rather than examining changes

to the underlying psychometric functions. This is expanded on in the discussion of Chapter 6, in relation to experimental findings.

4.6 Summary

After reviewing distributions of responses collected in earlier experiments (presented in Chapter 3 and Study 1 of Chapter 5) it was noted that deeper analysis of the types of responses being made could be more informative. An analysis pipeline was developed to further exploit the observed tendency of responses to cluster around the target and flanker orientations and explore systematic shifts in the pattern of responses, also reported elsewhere (e.g. Harrison and Bex 2017; Harrison and Bex 2015; Ester, Zilber and Serences 2015). Applying these analyses to previously collected data was hampered by the implementation of the QUEST algorithm tending to set target-flanker spacing at or near the algorithm's threshold estimate, leading to an uneven distribution of target-flanker spacings sampled.

A new method for subsequent experiments was designed without any adaptive algorithm, instead conducting fixed numbers of trials at pre-set target-flanker spacings. Removing the QUEST algorithm also relieved several assumptions and experimenter-decisions which may have influenced the experiment outcome (explored above). The new experiment method is more in-line with classical psychophysics methods and permits the fitting of a spatial psychometric function of crowding. This 'spatial profile of crowding' relates target-flanker spacing to the proportion of responses centred at the orientation of the target (i.e. 'uncrowded' responses). Fitting a logistic psychometric function in this way will allow spatial and non-spatial aspects of crowding to be disentangled, which was not possible with the previous method. The parameters of

the fitted logistic function can then be extracted and compared between stimulus conditions to better explore what factors influence the spatial and non-spatial aspects of the crowding zone. Disentangling these aspects has been proposed in the literature (Pelli and Tillman 2008), but previous studies aimed at disentangling these effects have been restricted by the assumptions and limitations inherent in adaptive algorithms and threshold-estimates as primary outcome measures (Pelli, Palomares and Majaj 2004; van den Berg, Roerdink and Cornelissen 2007).

Chapter 5 The effect of scaling radial flankers to counter cortical magnification

5.1 Introduction

Visual crowding is well understood to be a chiefly cortical phenomenon, evidenced by the presence of the effect when stimuli are presented dichoptically (Flom, Heath and Takahashi 1963; Tripathy and Levi 1994) and by a reduction in crowding when flankers are cortically distant despite being in close physical proximity (Liu *et al.* 2009). While a common neural locus for various forms of crowding remains elusive, cortical organisation and function are frequently referenced in models of crowding mechanisms (He, Wang and Fang 2019; Mareschal, Morgan and Solomon 2010b). One established proposal is that critical spacing between stimulus elements (i.e., the limits of the crowding zone in visual space) may map to a fixed distance on the cortical surface independently of eccentricity. This distance is reported as 6mm by Pelli (2008), and is further supported by experimental findings (Motter and Simoni 2007; Mareschal, Morgan and Solomon 2010b). Note: this prediction relates to locations away from the fovea, but the mathematical derivation was generalized to extend to foveal vision (Strasburger 2022) which showed the critical cortical separation may be much lower for targets closer to the fovea. A (mostly) fixed cortical spacing would produce the characteristic increase in crowding zone extent with eccentricity due to cortical magnification of the central visual field. A distance across the cortical surface corresponding to the central field would translate to a much smaller portion of the

visual field compared to the same distance across the cortical surface corresponding to the peripheral field (Horton and Hoyt 1991).

The in-out anisotropy of radial estimates of crowding zone extent is another characteristic aspect of visual crowding (Banks, Larson and Prinzmetal 1979; Bex, Dakin and Simmers 2003; Pelli 2008). Peripheral, rather than central, flankers have a stronger influence on target perception. For example, Chakravarthi *et al.* (2021) showed that in groups of letters, the outer flanker is more effective at crowding a target than the inner flanker, larger critical spacings for peripheral (or, distal) flankers have been found experimentally (Petrov and Meleshkevich 2011a) and effects of the outermost distractor were even noted among the earliest evidence of crowding (Mackworth 1965).

Cortical magnification of the distance between flanking elements has been suggested to contribute to the in-out anisotropy of crowding (Motter and Simoni 2007; Pelli 2008), but it remains unexplored whether unequal magnification of radially located flankers may also have an influence. If two flankers located along the radial axis are of equal sizes in visual space, the inner flanker will be magnified (and thus occupy greater cortical area) compared to the more peripheral flanker – illustrated in Figure 5.1. This unequal cortical representation may contribute to the difference in crowding effects, a hypothesis which may be investigated by altering the physical size of flankers to counteract cortical magnification. It has been demonstrated that when flankers differ in physical size compared to the target, crowding effects are largely unchanged, if the centre-to-centre separation between targets remains the same (Levi, Hariharan and Klein 2002b; Levi and Carney 2009). When considering unequal cortical representation of radial flankers, the representation of an inner flanker ‘grows’ more rapidly than an outer flanker ‘shrinks’ for each equal increase in spatial separation (in

opposite directions) from the target. This is due to the shape of the cortical magnification function – the log of the level of magnification of the visual field falls with eccentricity at a stable rate according to most models (Harvey and Dumoulin 2011; Horton and Hoyt 1991). Therefore, an inner flanker may sooner reach the level of spacing (and concurrent magnification) needed to escape crowding and reveal the inner limit of the crowding zone, than an equally displaced outer flanker. This could theoretically result in the characteristic in-out anisotropy of crowding.

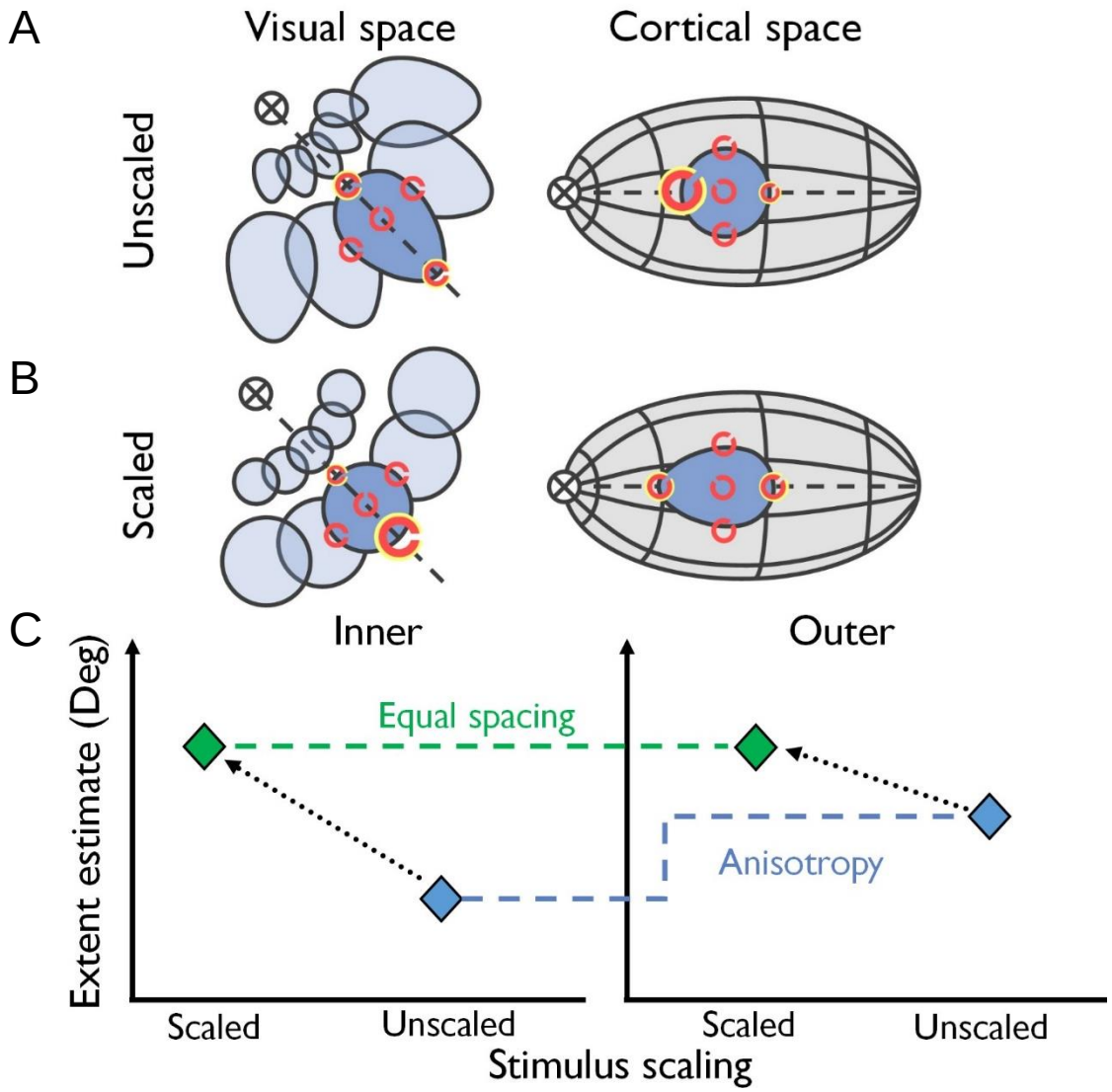

Figure 5.1 - Illustration of the hypothetical effect of flanker scaling

Panel A - The 'unscaled' visual space left) is an illustration of what is typically found by estimates of crowding zone extent with unscaled stimuli. The associated 'cortical space' illustration (right) is a hypothetical prediction of the cortical projections of the stimuli, where the flankers are magnified and minified due to cortical magnification. Panel B – Illustrated visual and cortical space projections of hypothetical effect of flanker scaling. M-scaled radial flankers (yellow edge) theoretically occupy equal cortical surface area. If flankers vary only in target-flanker separation and not also occupied surface area, crowding effects may extend over greater separations and reduce observed in-out anisotropy in visual space. Panel C – Hypothetical change in radial extent of crowding zones with scaled and unscaled flankers. If unequal cortical representation of flankers contributes to anisotropy (blue), this may be reduced or eliminated in the scaled condition (green). Note: stimuli shown in red for clarity in illustration only, task stimuli were always white.

To test this hypothesis, an experiment was designed whereby visual crowding was assessed with radial flankers that underwent scaling as a function of eccentricity to counteract cortical magnification. This M-scaling of radial flankers was intended to equate the area of the visual cortex stimulated by the target and flankers used, so flankers closer to fixation were made smaller while flankers further in the visual periphery were made larger. A control condition was also tested, in which target and flanker size was equal and constant. Three potential outcomes are anticipated: First, in-out anisotropy is found to be equal in both the scaled and unscaled conditions. This would support the proposals that radial anisotropy is the result of a fixed cortical spacing, and unequal cortical representation of flankers has no impact. Such a finding would also be in agreement with reports that centre-to-centre separation (in visual space) is more important than edge-to-edge separation (Levi and Carney 2009). Second is a reduction in radial anisotropy of crowding zone extent in the scaled condition, suggesting unequal flanker size in cortical space contributes to the observed anisotropy in the unscaled condition but is not the sole contributing factor. Third, radial anisotropy is eliminated in the scaled condition, suggesting unequal cortical representation flankers is the cause of radial anisotropy, not a fixed cortical spacing as previously reported. A reduction in anisotropy with flanker scaling would suggest that a more nuanced definition of target-flanker separation may be needed, for example with respect to separation of cortical representations of stimuli as opposed to centre-to-centre vs edge-to-edge definitions in visual space only.

Two studies were conducted, with the second intended to overcome some methodological limitations present in the first study while also approaching the research question slightly differently. The first study (Study 1) scales radial flankers according to a cortical magnification function derived from a separate cohort of

similarly-aged and normally sighted participants. The method to investigate visual crowding incorporates an adaptive algorithm and aims to estimate the extent of the crowding zone with inner and outer flankers. These estimates of crowding zone extent were then compared between the scaled and unscaled flanker conditions.

After the development of the more detailed method explained in Chapter 4, it was determined that this new method may be able to expand on this research question by disentangling previously confounded aspects of crowding, so was implemented in Study 2. Study 2 also utilises cortical magnification functions estimated from fMRI data obtained with the same participants. This then allowed stimuli to be scaled for each participant individually, rather than with a more generalised function. Relative proportions of responses to crowded stimuli were assessed systematically at a fixed set of target-flanker separations to permit fitting of spatial profiles to the data. Parameters of the fitted spatial profiles of crowding and appearance of response distributions could then be compared between scaled and unscaled conditions.

5.2 Study 1

In this study the radial extent of visual crowding was estimated in 10 participants at one visual field location, using the reported orientation of a crowded Landolt-C target. When present, flanking Landolt-Cs were varied in size as a function of their eccentricity (or were identical in diameter in the control condition) in order to investigate the effect of cortical representations of flankers on the extent of visual crowding. In this study, flanker scaling was controlled using a cortical magnification function derived from functional Magnetic Resonance Imaging (fMRI) data acquired in a separate study.

5.2.1 Methods

5.2.1.1 Measuring cortical magnification

The cortical magnification function was estimated from population receptive field (pRF) mapping fMRI data collected as part of another study by a lab colleague (Wright 2021). A young cohort (23 participants, mean age 20.8 years, range 18-22 years) of normally sighted participants underwent fMRI scanning with a SIEMENS 7 Tesla (7T) MRI scanner (Siemens Medical Systems, Erlangen, Germany) and 'natural scene' visual stimuli presented to the central and inferotemporal quadrant of the right eye visual field. These CMF data were already collected and accessible at the outset of the psychophysical experiments. It was decided that using estimates derived from these data would be beneficial, as the participant groups would be highly similar in potentially relevant characteristics such as age and refractive error.

The fMRI data were used to calculate the cortical surface area corresponding to 1 squared degree of visual area of the visual field at the imaged visual field eccentricities. These cortical magnification data were pooled from all participants and the median values from each level of eccentricity were modelled with a function for areal cortical magnification adapted from (Horton and Hoyt 1991).

$$M_{area} = \frac{A}{(E + e2)^2}$$

Equation 5.1

M = *Cortical magnification (mm^2/deg^2)*
A = *Cortical scaling factor*
E = *Eccentricity*
e_2 = *Eccentricity at which a target stimulates half the amount of cortical area stimulated by an identical target presented foveally*

5.2.1.2 Psychophysical tasks

Perceived orientation of a crowded Landolt-C target was assessed in twelve healthy, normally-sighted participants, aged 18-28 years. None were experienced in completing psychophysical tasks prior to the study. Normality was confirmed with a short health interview, direct examination of the anterior and posterior segment of both eye by slit lamp biomicroscopy and ETDRS or Snellen letter-chart acuity measurement (further details of the eligibility criteria and screening protocol given in section 2.1.3).

Throughout data collection, stimuli were presented to the participants' right eye and a black eye patch was worn over their left eye. Targets were presented at 12.72° inferotemporal to fixation, generated using Psychtoolbox (Brainard 1997) and the Eccentric Vision Toolbox (Greenwood 2021) for MATLAB (version R2019a; The MathWorks Inc., Natick, MA, USA) presented using a gamma-corrected Sony Trimaster OLED screen (SONY PVM-A250 Trimaster EL; Sony corp. Tokyo, Japan)

at a viewing distance of 60 cm. Responses were given using a keyboard (acuity task) and a consumer volume dial (crowding tasks).

5.2.1.2.1 Step 1 - Local Landolt acuity

Acuity at the test location was measured using Landolt-C stimuli in a 4 alternative forced-choice (4AFC) task, to determine a suitable target size for the crowding tasks to follow. Participants rotated a central 'response' Landolt-C (presented at fixation) through 4 alternatives (i.e. gap up/down/left/right) until it matched the target Landolt-C at 12.72° inferotemporal eccentricity, then submitted their response. Stimulus diameter (and hence spatial frequency of the target gap) was altered using a QUEST algorithm for 30 presentations to determine the 62.5% correct threshold. Stimulus diameter for all subsequent tests was set to double this diameter for each participant individually. This ensured all stimuli were an equivalent level above each participant's local acuity threshold – thus any influence of local acuity on subsequent tests would be equivalent between participants and could be discounted as a cause of any differences.

5.2.1.2.2 Step 2 - Unflanked orientation matching task

An unflanked orientation matching task was carried out to assess each participant's precision in the absence of flankers and determine the limits of 'correct' responses used to inform the adaptive algorithm in the crowded tasks. A randomly oriented Landolt-C was presented indefinitely at the target location, and a randomly oriented response C of equal diameter was presented surrounding the fixation spot. Participants were instructed to maintain fixation on the white spot throughout the task and rotate the response C using the dial until the orientation of the response C matched the perceived orientation of the target. The response was then submitted by pressing the dial. In this task, the response C could be rotated through 1° steps.

Responses were collected for 40 trials before beginning the crowded tasks and response error for each trial was calculated by subtracting the orientation of the presented target from the orientation of the response given. The standard deviation of these unflanked responses errors was then doubled to give the magnitude of the upper and lower bounds of responses to be considered 'correct' for the adaptive algorithm in the following crowding tasks (equating to the 2.3% and 97.7% percentiles).

5.2.1.2.3 Step 3 - Crowding with tangential flankers

The next series of tests aimed to determine suitable tangential flanker separation in the final series of tests (crowding with radial flankers). The target Landolt-C remained at 12.72° inferotemporal, neighboured only by two tangentially separated flankers. All presented Landolt-Cs (at this step) were fixed in diameter at double the previously determined peripheral acuity threshold. The participant was asked to rotate the response Landolt-C (again surrounding fixation) until it matched the perceived orientation of the target Landolt-C using a rotating dial, which was pressed to submit the response when these matched. The target and response Cs were again always presented at random orientations, while the flanker Cs were always yoked to a 24° offset (randomly clockwise or anticlockwise) from the orientation of the target. Target orientations (and permitted response orientations) were limited to multiples of 5° to balance test fidelity with the burden of labour to rotate the response C through possible orientations in each response. The separation between the target and tangential flankers was altered with a QUEST algorithm for 40 presentations set to converge on the 80% correct threshold (see note below). Three repetitions of this test, with a refreshed algorithm for each, produced 3 final flanker separations. The median of these 3 distances was selected to be the tangential flanker separation in the next series of tests (Step 4).

An important note here is that this test is not intended to estimate the tangential limits of the crowding zone. The QUEST algorithm was set to settle the tangential flankers at a distance allowing 80% correct responses so that the tangential flankers in Step 4 would be fixed at a distance to induce a small crowding effect. This aims to ensure the tangential flankers have an equal influence on the crowding behaviour of each individual participant, while allowing the radial flanker some scope to further influence the perception of the target. A lone radial flanker was not expected to produce a strong crowding effect, while too small a separation between the target and tangential flankers may cause them to dominate the observed effects of crowding, obscuring the effect of a radial flanker.

5.2.1.2.4 Step 4 - Crowding with radial flankers

This step determined radial crowding zone limits in the presence of tangential flankers. The task was the same as in Step 3 – the participant rotated the central 'response' Landolt-C until it matched the perceived orientation of the target C using a dial and pressed the dial down to register their response. However, in this task the target was flanked by a third, radially located flanker in addition to two tangentially located Landolt-Cs at a separation determined by Step 3. The position of the third Landolt-C was shuffled throughout trials, being presented both 'inner' (between the target and fixation) or 'outer' (further than the target from fixation) - see Figure 5.2 for an illustration. The target Landolt-C was again always presented at 12.72° inferotemporal to fixation. Targets, tangential flankers and the response C were fixed at a diameter of double that of the target at orientation resolution threshold determined in Step 1.

Radial flankers in the scaled condition were resized according to their eccentricity, using Equation 5.1 to calculate the cortical representation of the target, and then a rearrangement of this formula to calculate the flanker area expected to produce an

equal cortical representation. Flankers closer to fixation were decreased in size and flankers presented more peripherally were increased in size, utilising the cortical magnification parameters fitted to the fMRI data acquired from a separate cohort (see 5.2.1.1. A control condition was also conducted, in which radial flankers (when presented) were the same diameter as the target, regardless of their eccentricity. See Figure 5.2 for an illustration of all stimulus conditions used.

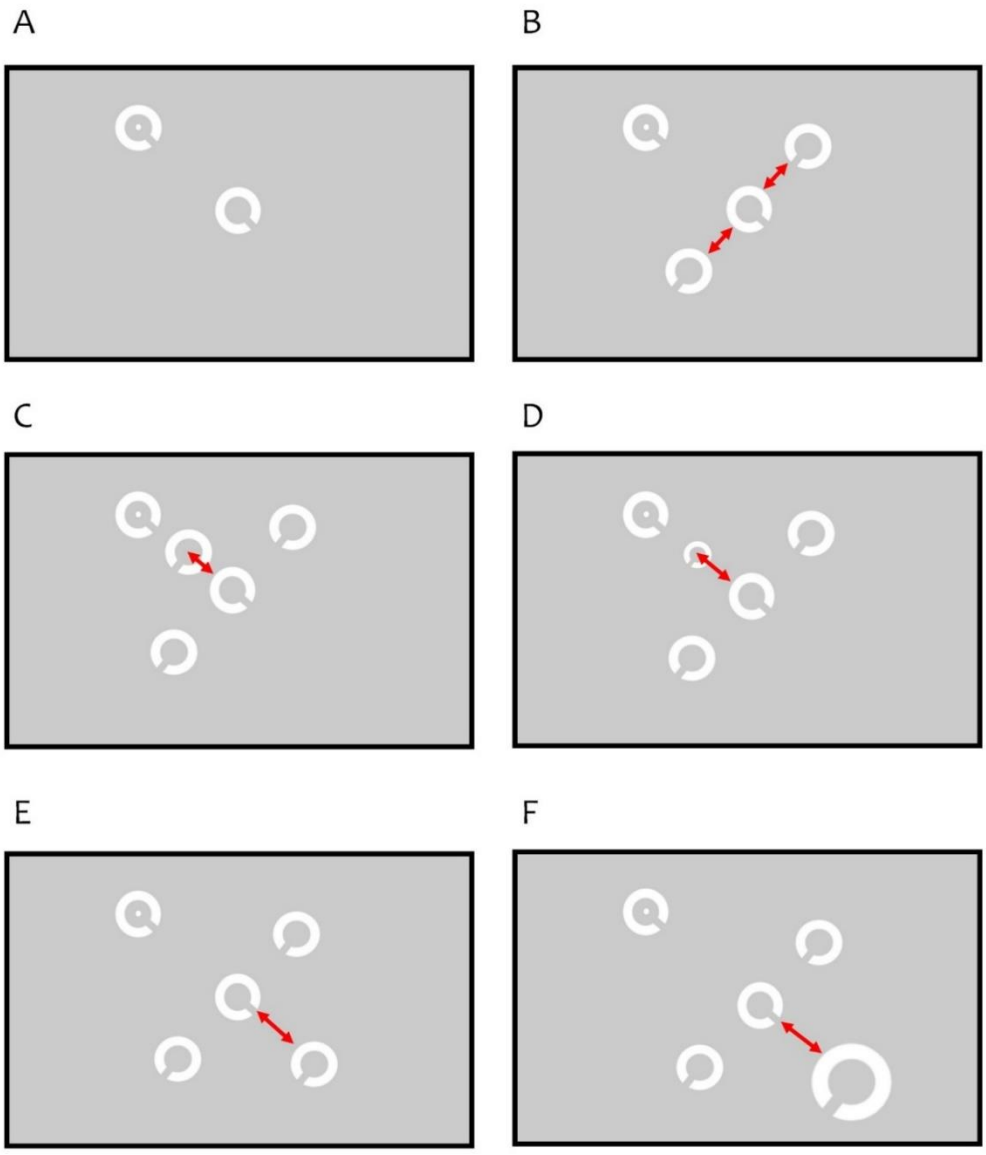

Figure 5.2 – Illustrated stimulus conditions

All illustrations show the fixation spot toward the upper left of the display, surrounded by the rotatable response Landolt-C. The response C was rotated by the participant to match the orientation of the target C presented at the centre of the screen. Red arrows indicate the axis of target-flanker separation for the purposes of the schematic but are not shown during the experiment.

A) Target only - the 'unflanked' condition

B) Target and tangential flankers - 'tangential-only' condition

C) Unscaled inner flanker - all flankers identically sized

D) Scaled inner flanker - radial flanker is smaller than the target

E) Unscaled outer flanker - all flankers identically sized

F) Scaled outer flanker - radial flanker is larger than the target

5.2.2 Analysis

The analysis followed the same method as the study presented in Chapter 3, detailed in 3.2.6. Responses were converted to response errors by subtracting the orientation of the response given from the orientation of the target presented. The range of target-flanker separations examined was divided into six bins and responses were collected into these bins for subsequent analysis. The divisions between bins were determined programmatically to result in approximately even numbers of trials within each bin (though this was not always possible in cases of heavy clustering of target-flanker separations.) Responses to trials where the target was presented in isolation ('unflanked' trials') or with only the tangentially located flankers ('tangential-only') were also collected into their own bins for the same analyses.

Response errors within each bin were combined and fitted with a von Mises frequency distribution. The mean of the distribution was fixed at 0 (indicating the target orientation) and the concentration parameter controlling the spread of the distribution was permitted to vary. 'Perceptual error' of each bin was defined as the square root of the inverse of this concentration parameter, as in the method used by Harrison and Bex (2015). This is analogous to the standard deviation of the responses, with a greater value indicating responses were more widely distributed around the target orientation.

For bins of trials from the crowded task, mean target-flanker separation of the binned trials was paired with the value of perceptual error from the same trials. This perceptual error data was then fitted with a hinged line model for each crowding condition examined with each participant (see Figure 5.2 for an illustrated overview of conditions). The model contains two linear phases: an initial downward gradient

showing the predicted fall in perceptual error with increasing target-flanker separation, and a horizontal 2nd phase where perceptual error is at approximately the unflanked level. The break point between the two phases is the minimum target-flanker separation at which performance at the crowded task is similar to that seen in the unflanked task, so is taken as an estimate of crowding zone extent. Figure 3.2in Chapter 3 and Figure 4.1 in Chapter 4 give further details on the hinged line model. Break point estimates for the inner and outer radial flanker locations were compared between scaled and unscaled conditions.

5.2.3 Results – Study 1

The cortical magnification function fitted using Equation 5.1 in (see 5.2.1.1) is shown in Figure 5.3. These data were collected as part of a separate study by a lab colleague (Wright 2021). The participants were normally sighted and were of similar age range to the participants recruited for this crowding study. For comparisons to Study 2, it is important to note that while the participants whose data are shown in Figure 5.3 shared similar group characteristics to the those who participated in Study 1, they are a different participant group. No individual participant was included in both groups.

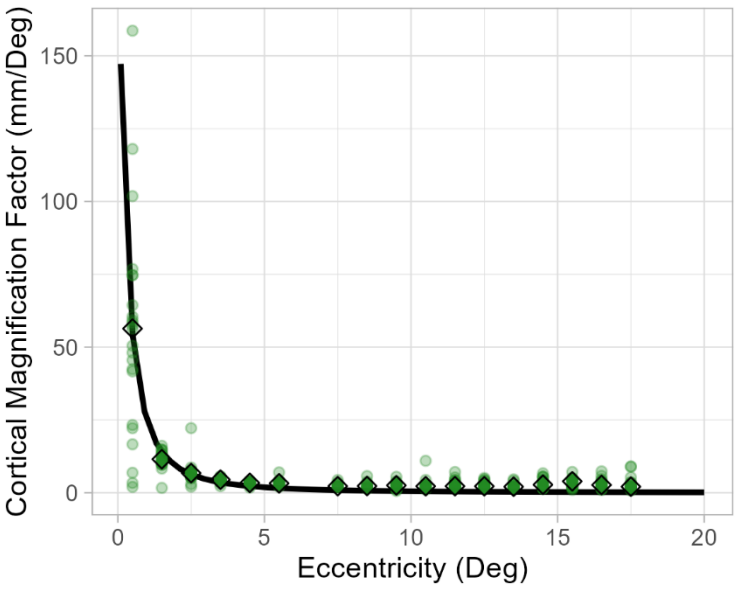

Figure 5.3 – Cortical magnification function fitted to data from 23 participants

Green data points show individual estimates of cortical magnification at each eccentricity. Median magnification factor at each eccentricity shown as black diamonds. The black line shows the cortical magnification function fitted to mean factor values, following Equation 1. This function was used to resize radial flankers according to their eccentricity in the 'scaled' condition of Study 1.

Table 1 shows the characteristics of participants recruited for the study. Note that all 10 participants participated in the previous study (Chapter 3), the remaining 2

participants who were recruited in the previous study could not attend the data collection session for this study due to the coronavirus pandemic lockdown.

Participant	Age (Years)	Target diameter (Degrees visual angle)	Acuity (logMAR)	Trial criteria (°± relative to target orientation)
1	18	1.94	1.07	25.4
2	21	1.86	1.05	31.8
3	20	1.78	1.03	24.5
4	28	1.92	1.06	43
5	18	2.02	1.08	31.6
6	19	1.7	1.01	18.9
7	20	1.3	0.89	19.4
8	20	2.24	1.13	29.7
9	19	2.02	1.08	25
10	24	2	1.08	25.5

Table 1 – Characteristics of recruited participants for Study 1

All but two participants recruited for the study presented in Chapter 3 also participated in Study 1 here (note: participant numbers may not be identical across studies). Acuity was measured using Landolt-C stimuli in a typical 4AFC task. Target diameter was set to double the diameter of the stimulus at threshold acuity (10x the minimum angle of resolution). Trial criteria were determined from the responses collected in the unflanked orientation matching task (2x standard deviation of responses). During the crowded task, responses that were oriented away from the presented target by more than the trial criterion were counted as 'incorrect' to inform the adaptive algorithm.

A computer error affecting flanker scaling calculations was identified during analysis of the data. This occurred during conversion of flanker position to eccentricity, which was then used to determine flanker scaling, and caused flankers to be smaller than intended. For some participants this was a minimal difference, but for others some

outer flankers were presented smaller than the target on a number of trials where they should have been larger. An example of each of these instances is shown in Figure 5.4. Affected trials (499 in total across all participants) were filtered out before further analysis.

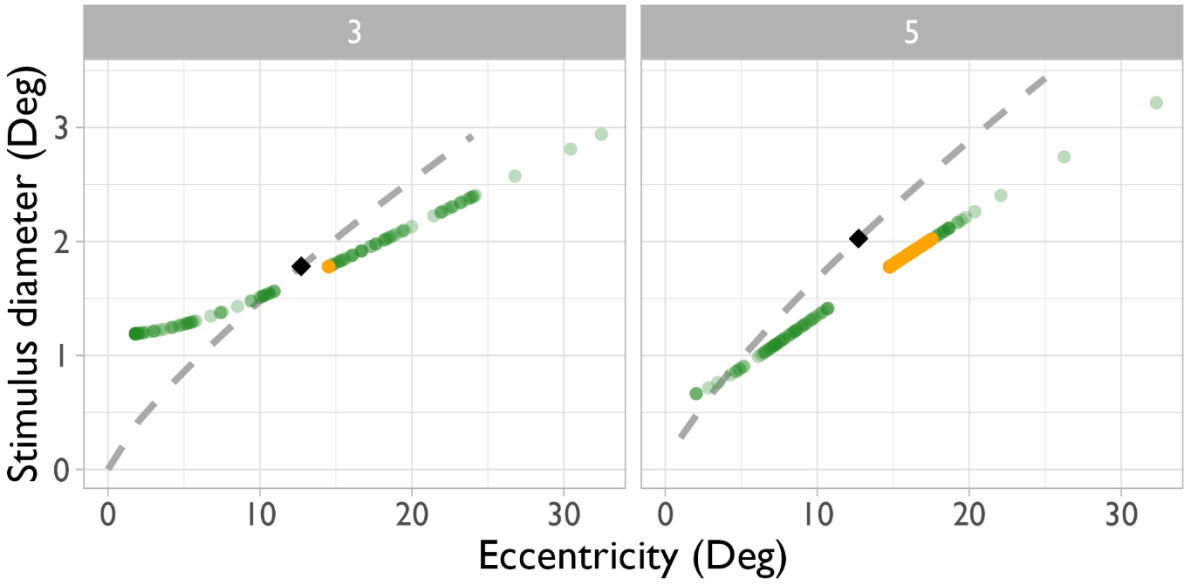

Figure 5.4 – Scaled flanker sizes did not exactly match the expected function

The diameter of scaled radial flankers displayed at varying eccentricities is shown by the green data points for two participants (3 and 5). The target diameter is indicated by the black diamond at 12.72° eccentricity. Flanker sizes were expected to follow the dashed grey line (scaled flanker diameter calculated using equation 1). A programming mistake affecting the calculation of flanker eccentricity at each trial caused flanker scaling to underestimate the diameter of the scaled flanker, leading some outer flankers to be incorrectly smaller than the target (orange points). This affected more stimulus presentations for some participants (e.g. 5 above right) than others (3 above left).

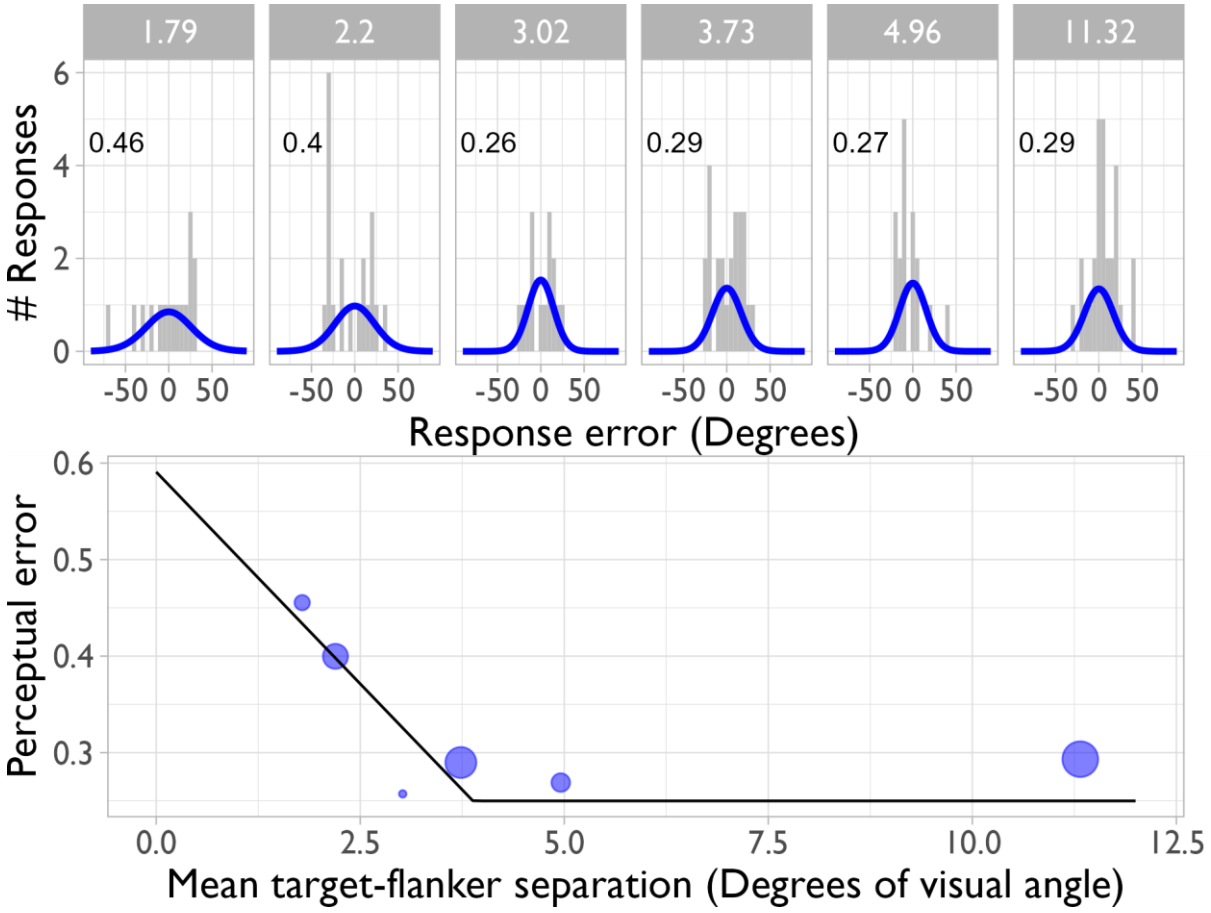

Figure 5.5 – Binned response errors, perceptual error and hinged line model fitting

The top row of panels show six bins of collected trials from one dataset (participant 3, outer unscaled flanker), and the mean target-flanker separation of the collected trials (grey header). Response errors (difference in orientation between target and responses) were modelled as a von Mises distribution centred at 0 (blue line). Calculated perceptual error is also shown on each panel (black number). The lower plot shows perceptual error values plotted against mean target-flanker separation of the binned trials and modelled with a hinged line (black line). The expected reduction in spread of responses can be seen in the upper panels and is reflected in the pattern of perceptual error data. Perceptual error value falls as target-flanker separation increases, down to a level approximately the same as responses in the unflanked condition – the 2nd, horizontal phase. The break point between the two phases of the model is taken as an estimate of the extent of the crowding zone.

Figure 5.5 shows an example of the distributions of binned response errors for one participant. Some datasets showed heavy clustering of target-flanker separations causing some bins to contain 0 trials. Hinged line fitting was still attempted on these datasets with fewer than 6 bins.

Figure 5.6 shows the perceptual error data for all participants and stimulus conditions, and all fitted hinged line models. Note that target-flanker separation was measured from the centre of the target to the centre of the radial flanker, and that two flankers located on the tangential axis were always present for these trials (see Figure 5.2). For an ‘inner’ radial flanker, the radial flanker is moved closer to fixation as target-flanker separation increases (away from the target), while an ‘outer’ flanker would be moved away from fixation and further into the peripheral field. As target-flanker separation increases, most datasets showed the expected fall in perceptual error, indicating responses became more concentrated around the target orientation. Where a plot is missing one or both lines, a hinged line model failed to be fit. This was usually due to a poor spread of target-flanker separations being tested, or where the data did not match the expected form (e.g. the inner scaled data for participant 3). While initial starting values for the model fitting specified the unflanked perceptual error as the height of the second (horizontal phase), this was permitted to vary, and some datasets were best fit with different heights despite the unflanked perceptual error being the same within each participant.

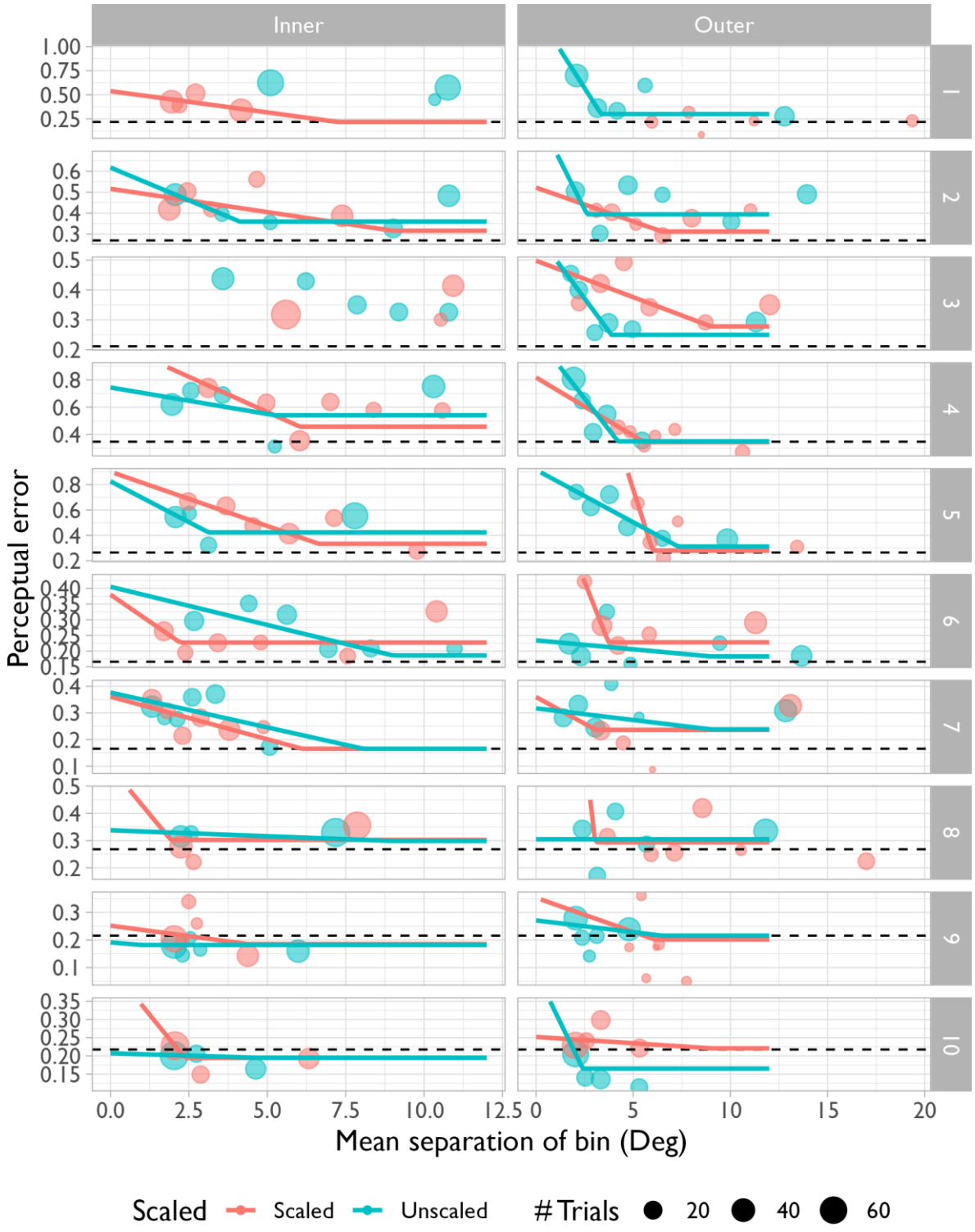

Figure 5.6 – Perceptual error and hinged line models for scaled and unscaled flankers

Lines show the fitted hinged line model for each set of perceptual error data. Both stimulus scaling conditions are shown on each plot for comparison (indicated by colour). Where a line is missing, the hinged line model failed to achieve optimised fitting parameters. Black dashed line indicates the unflanked perceptual error for each participant

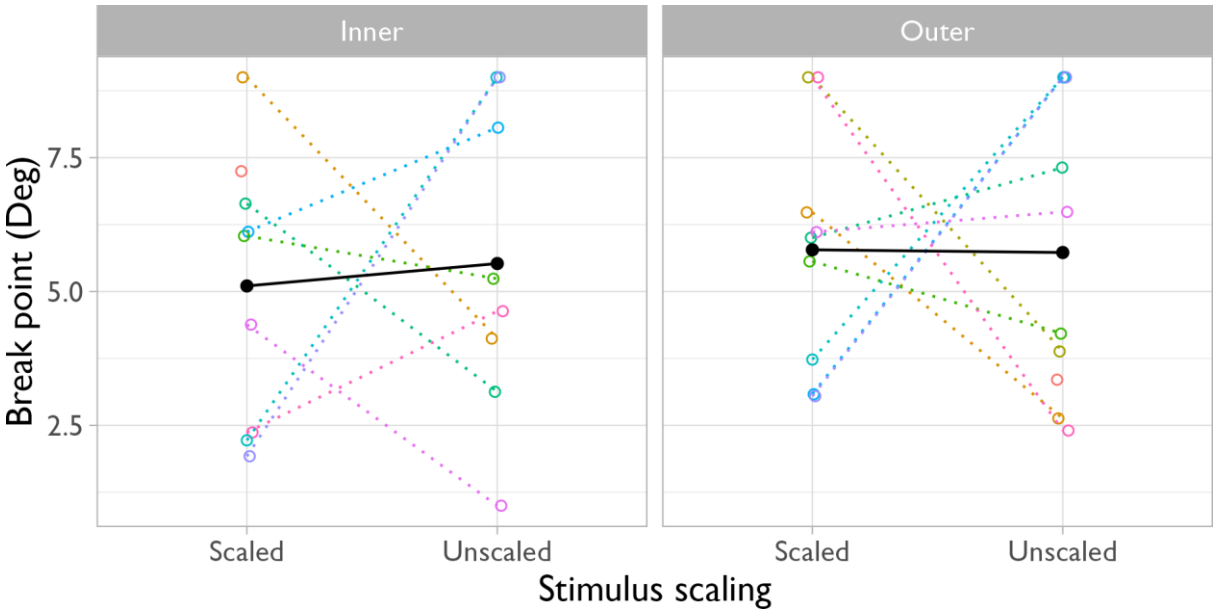

Figure 5.7 – Hinged line break point estimates

Break points extracted from fitted hinged line models. Black points (joined by line) indicate mean estimate for each group. Four sets of perceptual error data failed to be fit with a hinged line model (note missing lines in Figure 5.6), so fewer points are present.

Comparisons of break point estimates were made across scaling conditions for the inner and outer radial flankers separately, shown in Figure 5.7. Mean break point estimate (black circle) was slightly smaller with scaled stimuli for the inner extent, but mean outer extent estimates were almost identical and no statistically significant difference was found in either case (2-tailed paired t-test; inner: $t(7) = -0.420$, $p = 0.687$, outer: $t(8) = -0.133$, $p = 0.898$, normality confirmed with Shapiro-Wilk tests). As 4 sets of perceptual error data failed to be fit with hinged line models, comparisons could only be made for 8 pairs of inner extent estimates, and 9 pairs of outer extent estimates. In the case of one failed hinged line model (i.e. participant 1, inner), this participant's data were excluded from statistical testing for this location only.

No statistically significant difference was observed between the break point estimates for inner and outer flankers in either the scaling condition (2-tailed paired t-test; unscaled: t(7) = -0.758, p=0.473, scaled: t(7) = -0.504, p=0.63). No in-out anisotropy was observed in the data in either condition in this study.

5.2.4 Development of methods between studies 1 and 2

Other than the issues with stimulus scaling (see Study 1 results), the first study was limited by some aspects of experimental design which were addressed in the second study. Primarily, changing the experimental method and analyses (following the rationale explained in Chapter 4) allowed more detailed interpretations and confirmed that the patterns of errors due to crowding, not just the extent of crowding effects, are similar between scaling conditions. This is useful as more subtle changes to crowding effects apparent within the crowding zone may have been overlooked with the initial method used in Study 1.

Study 1 utilised a cortical magnification function obtained using averaged data from a different cohort of participants. Fitting individual cortical magnification functions for these participants (as in Study 2) was not possible due to the significant cost and time requirements involved with collecting fMRI data. In particular, there is a long waiting list for fMRI operators within the university, so acquiring this data would have been prohibitively long for 10 participants. Using fewer participants in Study 2 permitted the use of individual cortical magnification functions, so allowed flanker scaling to target cortical magnification in V1 within each participant and address a more nuanced research question.

5.3 Study 2

This study follows the same rationale as the study presented above – Visual crowding was assessed in the presence of flankers which were scaled as a function of eccentricity, to investigate the influence of cortical representation of flankers on crowding effects. There were two key differences: the experimental and analytical methods were different, in order to simultaneously assess spatial and non-spatial aspects of visual crowding, and flanker scaling was conducted using individually derived cortical magnification functions (rather than a shared function derived from a similar cohort of different participants). These changes were intended to overcome some limitations of the previous method (see Chapter 4, and discussion below) and address a more nuanced question: Does scaling flankers for *individual* measures of cortical magnification, thus equating their representation in V1 to that of the target, reduce the in-out anisotropy of crowding zones?

5.3.1 Methods

5.3.1.1 Participants

Three normally sighted participants aged 41-29 were recruited to participate in this study. All were psychophysically experienced but participant 3 was naïve to visual crowding research. All participants completed a short clinical interview and eye health check to ensure normal vision and eligibility (detailed in section 2.1.3)

5.3.1.2 Measuring cortical magnification

Cortical magnification for each participant was estimated from fMRI data collected by a lab colleague (Wright 2021) as part of an unrelated study. Participants underwent

structural and functional imaging with a SIEMENS 7 Tesla (7T) MRI scanner (Siemens Medical Systems, Erlangen, Germany). Visual stimuli consisted of drifting bar stimuli containing natural scenes for participants 1 and 2, and a radial checkerboard for participant 3 (the change in fMRI stimuli was the result of a change in protocol for the collection of fMRI data in the separate study). BOLD response data were used in a population receptive field (pRF) mapping procedure to estimate V1 cortical surface area activated by stimuli at central (0°-5°) and peripheral (7.7°-18.7°) visual field locations in the inferonasal quadrant. Associated r^2 values, a measure of the goodness-of-fit of the pRF model to the fMRI data, were also obtained. Cortical magnification was then calculated as the distance across the cortical surface corresponding to 1° visual angle separation in the visual field.

Cortical magnification values from each participant were then fit with an exponential model of cortical magnification adapted from (Horton and Hoyt 1991) linking cortical magnification and visual field eccentricity (Equation 5.2). Note, this equation differs from the CMF function used in Study 1 as it relates to distance over the visual field, as opposed to area, but it is otherwise the same relationship. Scaling the diameter, as opposed to the area, of the flanker produced the same result (i.e. the intended scaled Landolt-C) but saved additional calculation in the stimulus generation script and conversion to and from areal units was no longer needed.

$$M_{Linear} = \frac{A}{E + e_2}$$

Equation 5.2

M = Cortical magnification (mm/deg)

A = Cortical scaling factor

E = Eccentricity (Deg. visual angle)

e_2 = Eccentricity at which a target stimulates half the amount of cortical area stimulated by an identical target presented foveally

This model function was fit with a nonlinear least squares parameter estimation function with two free parameters (A and e_2). Parameter A was limited to >0.01 and e_2 was limited to >0.5 to prevent impossibly small parameter values, and no upper limits were imposed. Associated r^2 values for each magnification value were used to weight the model fitting of the cortical magnification function to reflect the stronger fit of the underlying pRF model and down-weight weaker pRF maps. The fitted cortical magnification function for each participant was then used to individually resize radially located flankers in the 'scaled' condition according to their eccentricity during the crowding experiment (below).

5.3.1.3 Psychophysical tasks

Stimuli were generated using Psychtoolbox (Brainard 1997) and the Eccentric Vision Toolbox (Greenwood 2021) for MATLAB (version R2019a; The MathWorks Inc., Natick, MA, USA) presented using a gamma-corrected Sony Trimaster OLED screen (SONY PVM-A250 Trimaster EL; Sony corp. Tokyo, Japan) at a viewing distance of 57cm, and responses were collected with a keyboard (4AFC acuity task) or response

dial (crowding task). Participants were adapted to the flat grey background (luminance 10 cd.m^{-2}) for three minutes before each testing session. Stimuli were presented to the right eye only. An eye patch was worn over the left eye throughout testing. The target was centred at 12.72° visual angle inferonasal to the right eye. Note: the inferonasal quadrant was used to align stimuli with the same quadrant (R inferonasal) assessed by the fMRI procedures. Regular breaks were given throughout the experiment, and participants were permitted to take additional breaks at any point by withholding a response (these trials were then reinserted into the remaining trials).

5.3.1.3.1 Local Landolt acuity

Participants first completed a 4AFC acuity task with Landolt-C stimuli. Participants were instructed to fixate a white spot while a lone (uncrowded) target Landolt-C was presented at 12.72° visual angle inferonasal to the right eye. Targets were randomly oriented to one of the four cardinal directions (up, down, left, right) and were not limited in presentation time. The diameter of the target was initially 1.5° visual angle, and subsequently set according to a QUEST adaptive algorithm converging on 62.5% correct threshold. A second 'response' Landolt-C was presented around the fixation spot. Participants controlled the orientation of the 'response' Landolt-C with the arrow buttons on the keyboard and instructed to match the orientation of the target C, submitting their response with the space bar. Responses (i.e. correct/incorrect) were supplied to the QUEST algorithm and the informative stimulus size suggested by the algorithm was used to set the diameter of the target C in the subsequent trial. This was repeated for 30 trials, and final estimates of Landolt-acuity at the target location were used to ensure local acuity was sufficient to adequately resolve the orientation of a 1.5° diameter target.

5.3.1.3.2 Crowding assessment

Participants were again instructed to fixate a white spot and report the orientation of a target Landolt-C presented at 12.72° visual angle inferonasal to the right eye. Targets were fixed in diameter (1.5° visual angle) and randomly presented at one of twelve equally spaced orientations (i.e. clockface directions). Presentation of target (and any flanking) stimuli was limited to 280ms (timing determined from piloting data presented in Appendix 2).

A short practice run was undertaken before beginning the crowded task and after any long breaks. Practice trials were unflanked (no flankers were presented) and responses were not recorded.

Several stimulus arrangements were presented throughout the crowding task (illustrated in Figure 5.2). Apart from the 'unflanked' condition, a pair of 1.5° diameter flanker Landolt Cs were always presented centred at 3.5° visual angle spacing from the target along the tangential axis. For a subsection of trials, only the tangential flankers were presented alongside the target (the 'tangential-only' condition). More frequently, a third flanker was presented centred at one of ten specific spacings along the radial axis. This radial flanker was either also 1.5° visual angle in diameter (the 'unscaled' condition) or scaled for cortical magnification dependent on the eccentricity of the flanker (the 'scaled' condition, explained below). Flankers in all locations were always identically oriented at 90° randomly clockwise or anticlockwise relative to the presented orientation of the target.

In the 'scaled' condition, the diameter of the radially located flanker was altered to scale for cortical magnification (also called M-scaling). This intends to produce equal representation for of the target and flanker Landolt Cs in terms of stimulated cortical

area, by altering the visual (and hence, retinal) area occupied by the stimuli. In effect, flankers presented closer to the fixation spot are made smaller proportionally to their reduced eccentricity, and flankers presented further peripherally than the target are made proportionally larger. This is to contrast with the 'unscaled' condition in which radial flankers were always 1.5° visual angle in diameter. Scaling was individualised by using each participant's fitted cortical magnification function, as detailed above. The cortical representation of the 1.5° diameter target at 12.72° eccentricity was calculated my multiplying the value of M predicted by the function at 12.72° eccentricity by 1.5. This cortical distance value was then reinserted into a rearrangement of Equation 5.2 (see section 5.2.1.1) to calculate the required diameter of radial flanker needed to stimulate an equal cortical distance at the intended eccentricity of the radial flanker:

$$D_F = C \frac{E_F + e_2}{A}$$

Equation 5.3

D_F = Diameter of flanker (Deg. visual angle)
C = Cortical distance corresponding to target (mm)
E_F = Eccentricity of flanker (Deg. visual angle)
A = Cortical scaling factor
e_2 = Eccentricity at which a target stimulates half the amount of cortical area stimulated by an identical target presented foveally

Stimulus condition (unflanked / tangential only / scaled / unscaled) and radial flanker location (when present) were shuffled and presented in a random order. Participants fixated a white spot throughout all trials. Stimuli (target Landolt-C and any flankers as

specified above) were presented for 280ms, followed by a random noise mask (static, grayscale, 1/F spectral density) at the location of any stimulus elements to disrupt any after-image effects (250ms). Next, a 1.5° diameter 'response' Landolt-C was presented centred at the fixation spot at a random orientation. Participants rotated this response C with a dial through 5° steps using a dial and were instructed to match the perceived orientation of the presented target C as accurately as possible. The participant then submitted their response with a button press (either pressing on the dial or the spacebar). A second random noise mask was presented centred at the fixation spot for 250ms before the next trial commenced. No feedback on trial-by-trial performance was given, and participants were monitored by the experimenter to ensure adequate fixation.

5.3.2 Analysis

'Response errors' were calculated as the difference between the presented orientation of the target and the orientation of the response given. These errors were corrected such that responses oriented towards the flanker orientation produced positive errors, and responses oriented away from the flanker produced negative errors. Response errors were then combined into a probability distribution of errors for each participant and each stimulus condition, ranging from +180° to -180°.

Errors from the unflanked condition were modelled as a single von Mises distribution with a mean fixed at 0°. The concentration parameter of the fitted distribution (related to the spread of responses) was used as a starting value in later model fitting steps for error distributions.

Errors from all other stimulus conditions (tangential-only, scaled and unscaled) were modelled as a mixed pair of von Mises distributions. The means of each distribution were fixed to 0° and +90°, corresponding to responses being centred at the target and flanker orientations respectively (after the sign of errors on anti-clockwise trials were flipped in order to align the responses, see 4.5.1). The fitted model parameters were then used to calculate the relative proportion of responses centred around the target orientation (error of 0°) made by each participant under each stimulus condition and level of radial flanker spacing. Additional details of this model fitting and calculation procedure are given in Chapter 4.4.

The proportions of target-centred responses were then modelled as a logistic function against the spacing between the target and radial flanker for each participant and scaling condition (i.e. scaled and unscaled for each participant). The upper plateau of each logistic function was fixed to the proportion of target-centred responses given by each participant under the tangential-only condition. This assumes that the proportion of target-centred responses in crowded conditions has an upper limit corresponding to the tangential-only condition, as the tangential flankers were always present at an identical location whenever radial flankers were presented. The tangential-only condition could be thought of as having an infinite spacing between the target and radial flanker.

5.3.3 Results

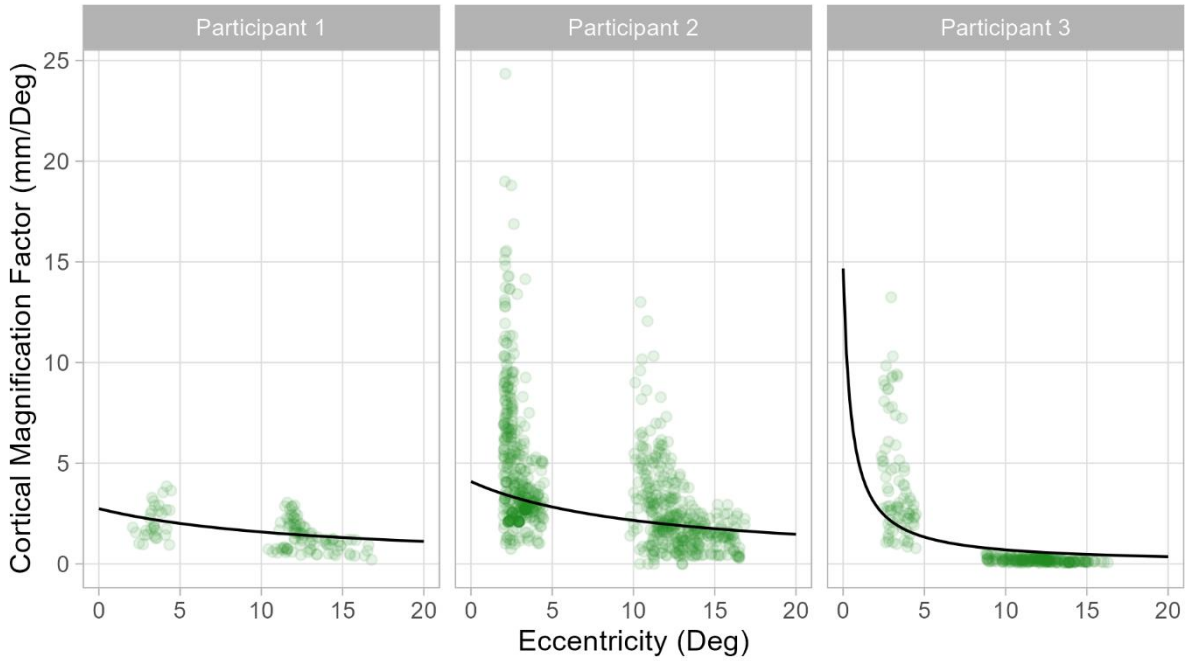

Figure 5.8 – Cortical magnification measures from population receptive field mapping

Each green point indicates one estimate of cortical magnification obtained from population receptive field (pRF) mapping, while each black line indicates the fitted cortical magnification function. Data point opacity signifies R2 values (pRF model goodness of fit). Darker areas are the product of many overlapping data points, and data with stronger pRF model fits, indicating areas where the cortical magnification function can be more precisely estimated.

Estimates of cortical magnification factor obtained from pRF mapping were modelled with Equation 5.2 (section 5.2.1.1) for each participant, to produce cortical magnification functions (Figure 5.8). The cortical magnification data for two participants appear much more variable due to a change in stimulus used during MRI data collection (participant 3 was shown checkerboard stimuli while participants 1 and 2 were shown natural scenes). It was not feasible for the MRI scans to be repeated due to the prohibitive cost of fMRI scans and length waiting lists caused by a shortage of trained operators.

All participants underwent a central (2°-5°) and peripheral (7.7°-18.7°) scan, which necessitates the gap in data between 5° and 7.7° eccentricity. The data for participant 1 contain fewer points (and less apparent noise), as the pRF mapping procedure filters out excessively poor pRF model fits. While more maps could be fit to the data for participant 2, the amount of noise present is also greater as a result. The fitted cortical magnification function (describing the change in cortical magnification factor across eccentricity) resulted in stimulus scaling for participant 3 that was slightly greater in magnitude (inner scaled flankers were smaller and outer scaled flankers were larger) than for participants 1 and 2, indicated in Figure 5.9.

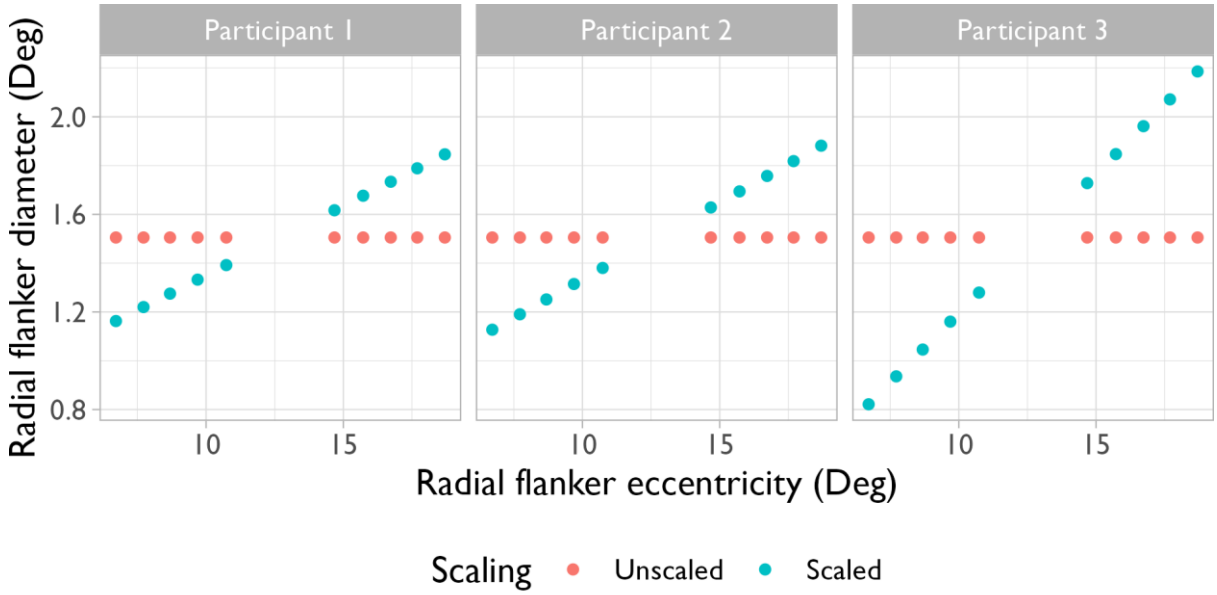

Figure 5.9 – Diameters of scaled and unscaled radial flankers

Radial flankers were either 1.5° in diameter regardless of eccentricity (unscaled, orange points) or scaled with eccentricity using each participant's fitted cortical magnification function (scaled, blue points). The target was presented at 12.72° eccentricity, flankers were smaller when presented more centrally, and larger when presented at greater eccentricity than the target. Scaling for participants 1 and 2 was similar, but the magnitude of scaling for participant 3 was greater, due to the difference in cortical magnification function shape.

Participants completed 105 trials of each unique stimulus condition. Figure 5.10 shows four sets of response error data from one participant. All data sets (except the 'unflanked' condition) showed clusters of responses centred at the target orientation (error = 0°) and the flanker orientation (error = +90°), which could then be fitted with the bimodal model. Each bimodal model produced one p(Target) value, indicating the ratio of target-centred responses to flanker-centred responses (Figure 5.10), which was then fit with a logistic model against target-flanker separation (Figure 5.11). Note that as in Study 1, two tangentially-located flankers were always present for the crowding task with a radially-located flanker. A distribution of responses under the 'tangential-only' condition is also shown in Figure 5.10.

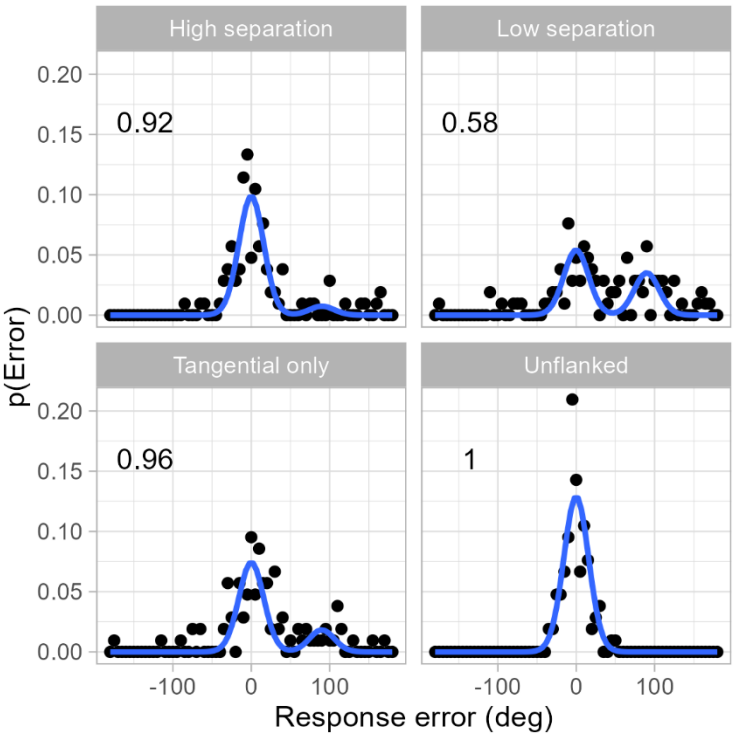

Figure 5.10 - Error distributions and bimodal models

Each panel shows the probability distribution of errors observed for one participant under four stimulus conditions – high and low target-flanker separation (from radial flanker, tangential flankers also present), tangential flankers only (no radial flanker) and unflanked (no flankers present). Blue lines indicate the fitted bimodal models. Peaks and spread were permitted to vary while means were fixed to 0° (target orientation) and 90° (flanker orientation). Each panel also shows the p(Target) value of the data, which is the ratio of target-centred responses to flanker-centred responses, or the probability of a response being centred at the target. The radial-crowding data (upper panels) are from trials with an inner, unscaled flanker, but the data from other stimulus conditions were similar in overall appearance.

The p(Target) data shown in Figure 5.11 are similar between stimulus scaling conditions in most instances. A high degree of accuracy (ability to centre a majority of responses on the target orientation, producing a higher p(Target) value) was evident in most of the data. No dataset spanned the range of possible performance, suggesting only minority of all responses were centred at the flanker orientation, even at the smallest target-flanker separation where crowding was expected to be strongest. All the data sets show an expected fall in p(Target) as the flanker encroaches on the target (lower target-flanker separation), but this effect was not strong in most instances. The notable exception is participant 3, who predominantly reported the flanker orientation when the radial flanker was more central than the target (inner).

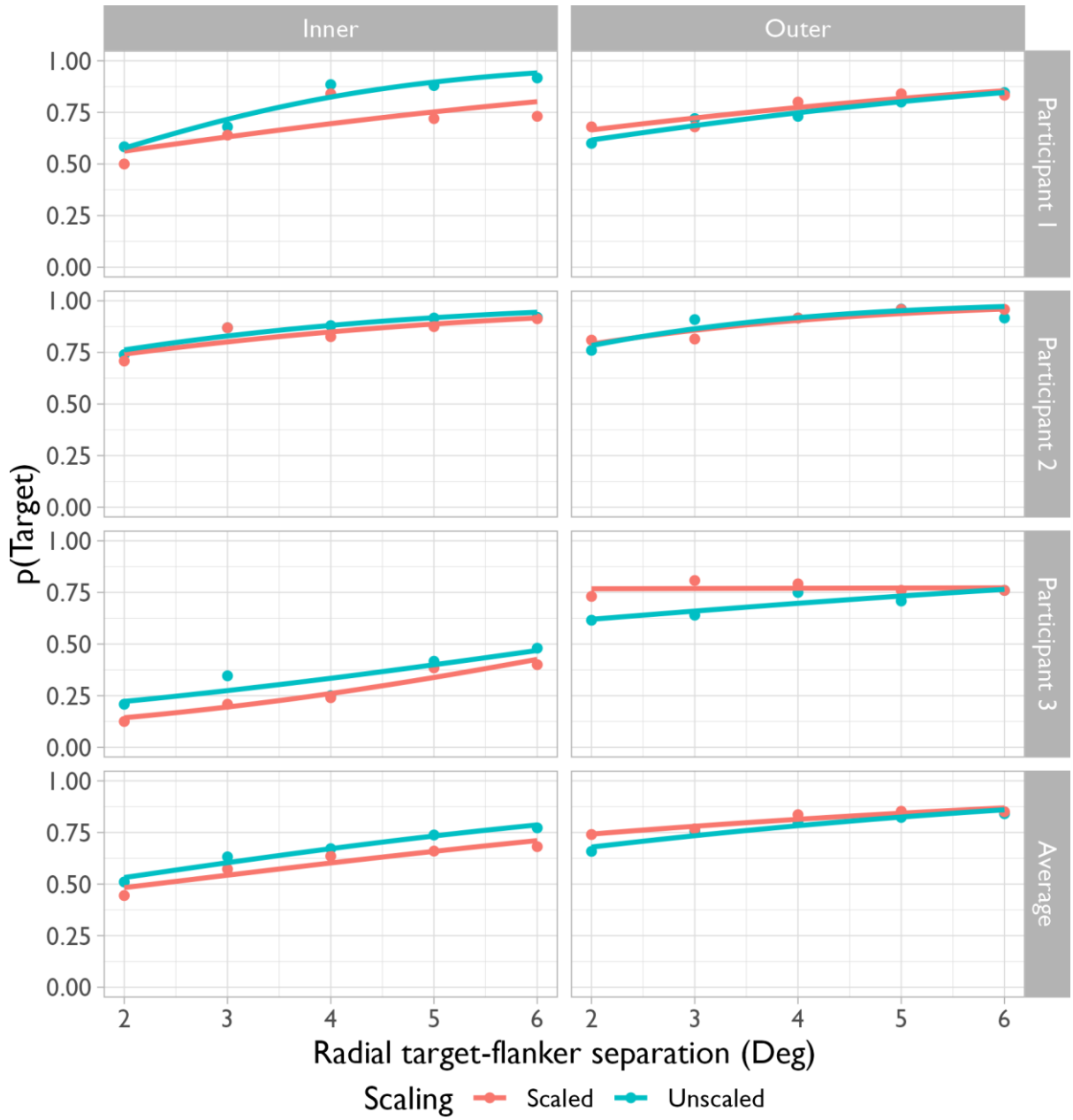

Figure 5.11 – Spatial profiles fitted to p(Target) data

Each participant's data is shown across each row and indicated by point shape. Both flanker scaling conditions are shown on each plot for comparison (indicated by colour). A higher p(Target) value indicates more responses centred on the target orientation, suggesting less crowding. The bottom row shows the average of the 3 p(Target) values at each level of separation and scaling, and the separate logistic model fitted to this averaged data.

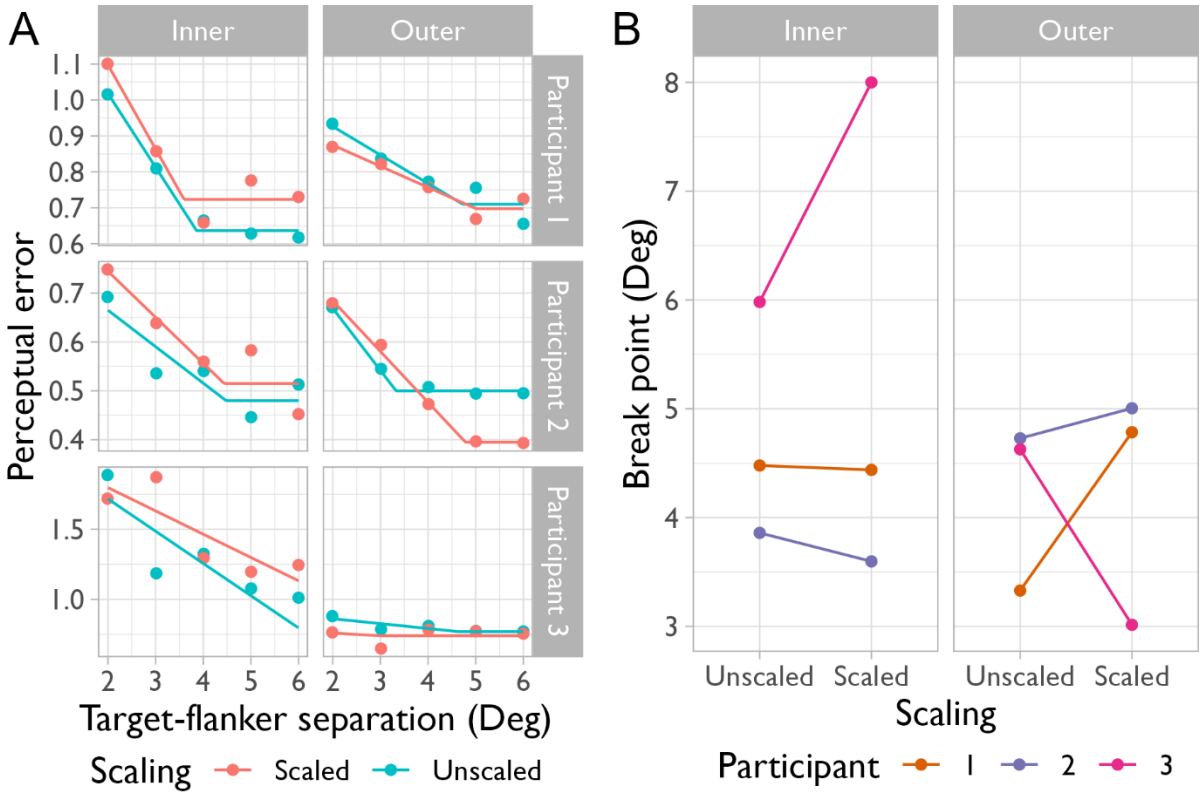

Figure 5.12 – Perceptual error analysis conducted on data from Study 2

Panel A shows individual perceptual error data and fitted hinged line models, following the same procedure as in Study 1. Panel B shows the extracted break point estimates for each participant under each condition. Perceptual error values are generally greater in this data than that of Study 1 due to the greater target-flanker orientation difference used. Stimulus scaling does not appear to affect break point estimates in a consistent way.

While spatial profiles could be fit to all the datasets (and appear to fit the data very well in most cases) extraction of midpoint and slope values was deemed inappropriate as no dataset showed a complete range of p(Target) values - see Figure 5.11. Perceptual error analysis was applied to the data collected in this study, shown in Figure 5.12. The fitted hinged line models describe the data well, but the extracted break points do not show any consistent effect of stimulus scaling. While Participant 2 showed

expected in-out anisotropy (a smaller break point estimate for the inner vs the outer flanker), this was seen in both the scaled and unscaled condition. Participant 1 showed anisotropy only in the scaled condition, while their unscaled data (and both scaling conditions for Participant 3) show the opposite pattern of anisotropy (larger break point estimates for inner vs outer radial flankers).

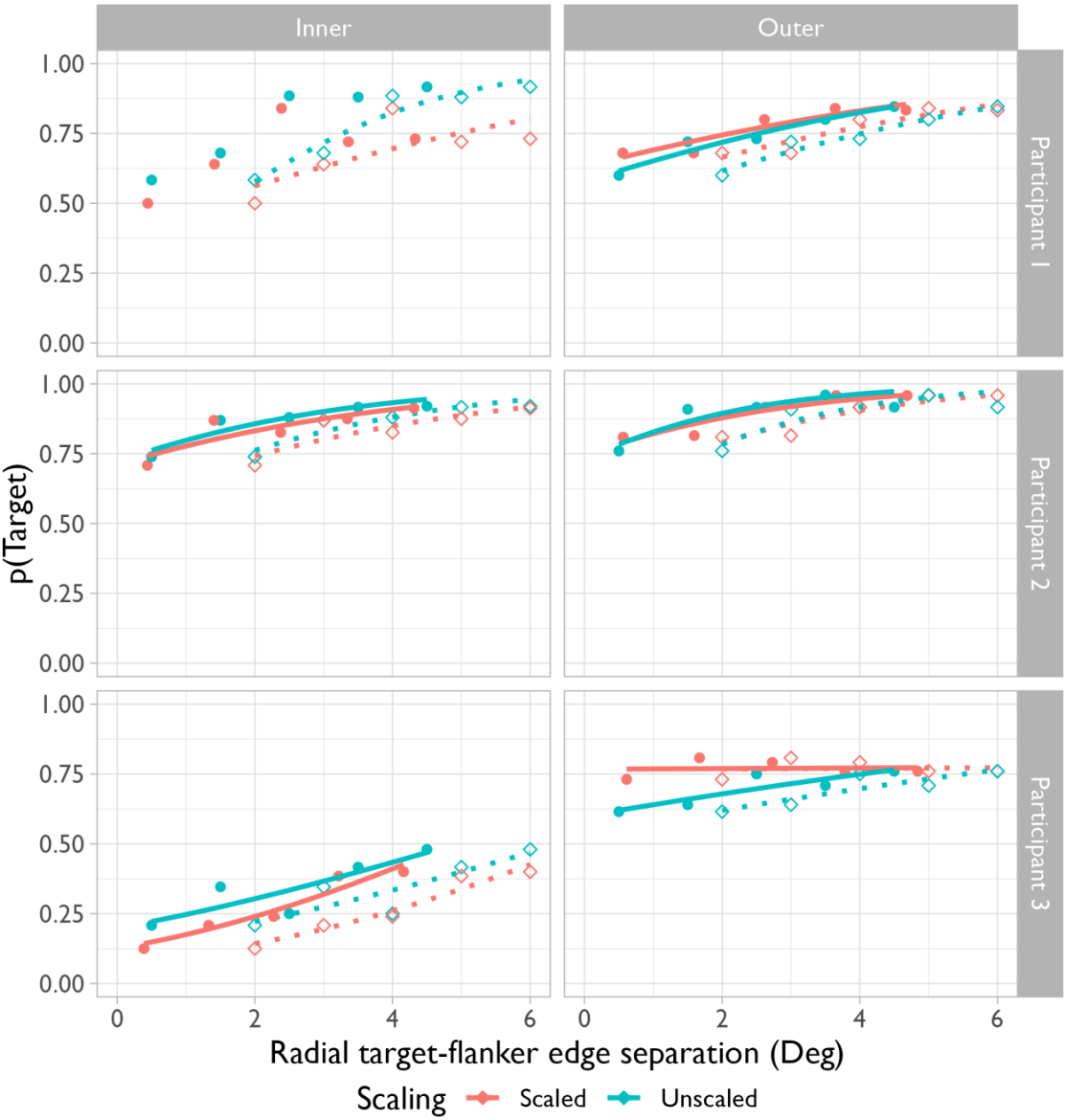

Figure 5.13 – Spatial profiles fitted to p(Target) data expressed in edge-to-edge separation

Each participant's data is shown across each row and indicated by point shape. The plot mirrors Figure 5.11 except target-flanker separation is converted to edge-to-edge separation (solid point and lines). Centre-to-centre data shown by hollow points and dotted lines for comparison.

5.4 Discussion

The present experiments did not find evidence that scaling flanker size with respect to eccentricity produces a significant change in observed crowding effect. Visual crowding was similar across stimulus conditions and flanker locations, both in terms of estimated extent of crowding (Study 1) and shifts in patterns of crowded responses (Study 2). These findings suggest that the span of cortical representations of flankers in V1 do not influence visual crowding. The results also provide further support to the proposal that it is the separation between these cortical representations that principally determine crowding effects. Despite not observing the intuitively expected results presented in the introduction, this study reveals some interesting characteristics of stimulus interactions under crowding.

The scaling manipulations used in these experiments align with the assertion that it is the centre-to-centre (not edge-to-edge) separation between objects that governs crowding, in agreement with other studies (Levi and Carney 2009; Rosen, Chakravarthi and Pelli 2014). A difference in effects between centre-to-centre and edge-to-edge separation has been reported with some stimuli (Hayashi and Ohnishi 2019), although this was a gap detection task rather than a detail discrimination task as more typically found in crowding research. An edge-separation effect may be expected particularly with Landolt-C stimuli, as the orientation information (i.e. location of the gap) is only present at the edge of the stimulus. The p(Target) data converted to edge-to-edge separation are shown in Figure 5.13. Flanker scaling had no impact on centre-to-centre separation, but edge-to-edge separation was different for inner (minimized) flankers and outer (magnified) flankers, as compared to the unscaled condition. If edge-to-edge separation was the determinant factor, a misalignment of

the crowding effects between scaling conditions would be expected when plotted with respect to centre-to-centre separation (as in Figure 5.11), which would then be aligned if plotted with respect to edge-separation. However, the opposite is observed in the current study: crowding effects are unaltered with respect to centre-to-centre separation (Figure 5.11) and are slightly more misaligned when separation is expressed as edge-to-edge separation, though the difference is very small.

The patterns of responses collected in Study 2 are largely similar between participants with the exception of the inner-flanker data obtained with participant 3 (Figure 5.11), who was psychophysically experienced but naïve to the expected outcomes of the experiment. Values of p(Target) are notably lower in both the scaled and unscaled condition, indicating a majority of responses tended to cluster around the orientation of the flanker. This is unlikely to be due to task confusion as the participant understood the task well and shows the expected increase in p(Target) with increasing flanker separation. That is, as target-flanker separation increased the participant gave more target-centred responses, despite the inner flanker approaching fixation. If the participant had adopted a strategy of simply reporting the closest flanker, the opposite pattern would be expected (an increase in flanker-centred responses, thus decrease in p(Target) as target-flanker separation increased and the inner flanker approached fixation). Comparing the inner and outer data for participant 3 suggests a stronger crowding influence from an inner flanker, the opposite of the expected appearance of radial anisotropy. Similar inversion of the expected pattern of anisotropy was reported by Petrov and Meleshkevich (2011b) when attention was biased centrally with a foveal, task-critical cue. There was no such central cue in the present task, only a fixation spot during stimulus presentation. The response C was presented centrally, but only after a noise mask following stimulus presentation, thus not concurrent with the stimulus.

An unintended central bias in attention (arising from the foveal location of the response C between stimulus presentations) could be a potential explanation both this specific inversion of radial anisotropy, and the general absence of anisotropy in the rest of the data collected (Petrov and Meleshkevich (2011b) reported a reduction in anisotropy in participants whose anisotropy was not reversed by the foveal cue). Alternatively, radial anisotropy has been shown to be reduced away from the horizontal meridian of the visual field (Petrov and Meleshkevich 2011a), so the target location may also have reduced the magnitude of anisotropy.

Inferences from the results of Study 2 are limited by the narrow range of crowding magnitudes (i.e. reductions in p(Target)) observed. This small range in crowding effect is likely a product of only the radial flanker being moved between conditions – tangentially located flankers were fixed in position throughout all trials involving a radial flanker. This was done to isolate the influence of the radial flanker while ensuring a measurable level of crowding was produced. A lone radial flanker would not be expected to induce as strong a crowding effect as was observed here, though further additional flankers may potentially have led to 'uncrowding' (Manassi, France and Herzog 2012), or a cue that the only misaligned C (all flankers were identical in orientation) was the target, reducing uncertainty and producing higher levels of p(Target).

Flanker scaling in these studies was intended to target cortical magnification in V1. Retinotopic maps of different visual areas are not identical, and studies have identified different visual areas as contributing to crowding effects in different ways (Shin, Chung and Tjan 2017; He, Wang and Fang 2019). One recent study in particular highlights V4h as being particularly relevant to crowding zone extent, in comparison to areas V1, V2 and V3 (Kurzawski *et al.* 2021). It is possible that it is the representation of stimuli

in higher cortical areas that produces anisotropy, so a greater difference in effects may be found if flankers are scaled to counter cortical magnification in those areas.

These results appear to disagree with reports of ‘uncrowding’ (or ‘ungrouping’) with differently sized flankers (Manassi, France and Herzog 2012). However, the reported experiment in particular used a Vernier acuity task flanked by vertical lines which were varied in length (also concurrently in number, but even the presence of one pair of differently size stimuli affected vernier thresholds). As well as allowing much smaller target-flanker separations, Vernier acuity may also be more sensitive to small magnitudes of crowding effects (Levi, Klein and Aitsebaomo 1985). It may also be the case that flanker length in their experiment is more relevant to their task than the diameter of flankers in the above method. Similarity modulations of stimulus features other than relative size (such as colour or luminance) may be expected to lead to varying crowding behaviour (Kooi *et al.* 1994; Greenwood and Parsons 2020), and the effect of target-flanker relative orientation is explored in the following Chapter.

5.4.1 Comparing perceptual error analysis and fitting spatial profiles of crowding

While the two studies produce similar conclusions, comparing the results between the two reveals the benefits of the updated experiment protocol. The greater number of trials and fixed levels of target-flanker separation permit more detailed analyses which could not be conducted with the data from Study 1. Perceptual error analysis can also still be conducted on the data from Study 2 (shown in Figure 5.12), the results of which further highlight a disadvantage of perceptual error as an indicator of visual crowding: Values of perceptual error are generally greater in the Study 2 data (Figure 5.12) than the Study 1 data (Figure 5.6) as a result of the different target-flanker orientation difference used in each study (24° in Study 1, 90° in Study 2). When a greater

orientation difference is used, flanker-centred responses (crowded) result in errors further from 0°, producing a wider spread in the fitted von Mises distribution and a greater value of perceptual error. As perceptual error also increases with the proportion of crowded responses (at smaller target-flanker separations), the value of perceptual error conflates greater orientation differences with stronger crowding, so cannot be used to directly quantify crowding effects. This conflation of effects is mitigated here by keeping target-flanker orientation difference constant (in Study 1) and, in other studies that use a similar method, by randomising target-flanker orientation difference between trials (Harrison and Bex 2015).

Values of p(Target) are a more direct and intuitive indicator of the pattern of responses being given, showing the proportion of all responses that were centred at the target orientation (uncrowded). With the assumption of no other sources of error, the proportion of crowded responses can also be easily discerned:

$$1 - p(\text{Target}) = p(\text{Flanker})$$

or the proportion of crowded responses. This assumption is supported by the form of the data, as responses at orientations far from either the target- or flanker- orientations were rare in these data. Other sources of error such as random responses would be accounted for with additional model parameters if these were observed (explained in section 4.5.3), but attempting to fit models including a random noise parameter led to more frequent failures in the model fitting stage (i.e. optimized model parameters could not be estimated), and frequently indicated near zero proportions of random-type responses when model fitting did not fail. The ability to fit functions analogous to a psychometric function of crowding may also allow spatial aspects of crowding (i.e., crowding zone extent) to be disentangled from other (non-spatial) aspects of crowding.

While the new systematic method necessitates additional trials for each crowding condition being investigated, the benefits of more intuitive and informative data are worthwhile in an experienced participant cohort. Potential future applications of this approach with an inexperienced cohort would benefit from further investigation into the minimum number of trials necessary to reliably quantify the proportions of different responses made under crowding. The greater potential for random-type errors in an untrained participant may necessitate more trials than would be needed by an experienced participant to quantify p(Target), but this may still be fewer trials than was utilised by this study (and those in following Chapters).

Chapter 6 The effects of target-flanker similarity and target eccentricity on the spatial profile of crowding

6.1 Introduction

Visual crowding is influenced by the perceived similarity between target and flanking stimuli used. Studies have investigated the difference in crowding effect when flankers are similar and dissimilar to a target in terms of letter shape (Estes, 1982), stimulus shape and contrast polarity (Kooi *et al.*, 1994). These were some of the first evidence that similar flankers exert a stronger crowding influence on targets than more dissimilar flanking stimuli. This difference was typically defined as elevations in threshold levels at a criterion set by the psychophysical method used - for example, stimulus spacing required to achieve 62.5% correct responses in a 4 alternative forced choice task as used by Kooi *et al.* (1994). Elevations in thresholds related to element spacing, i.e. flankers at a further distance leading to the same level of task performance, have been interpreted as being the result of larger crowding zones appearing in the presence of certain kinds of stimuli (Kooi *et al.*, 1994; Shamsi, Liu and Kwon, 2022). As crowding is a cortical-level phenomenon, with the suggested involvement of a number of visual areas and potential mechanisms (Anderson *et al.* 2012; Clarke, Herzog and Francis 2014), modulation in the apparent size of a crowding zone is not entirely unexpected. How this modulation arises, in terms of neural actions and resulting effect on perceived target appearance, remains uncertain.

Crowding is typically investigated in terms of crowding zones (Bouma 1970) and their extent. Investigations of crowding zone extent frequently rely on estimates of extent in the form of either 'threshold-spacing', the target-flanker spacing necessary to achieve a set threshold level of performance at a crowding task, or 'critical spacing' (Pelli, Palomares and Majaj 2004). 'Critical spacing' is similar to a 'threshold-spacing' estimate, except that rather than being related to a fixed level of task performance, the measure indicates the maximum target-flanker spacing necessary to elicit a change in task performance from an uncrowded level (Pelli, Palomares and Majaj 2004; van den Berg, Roerdink and Cornelissen 2007). Therefore, critical spacing may be considered a specific form of threshold-based estimation of crowding zone extent. Measures such as these have been used to infer key hallmarks of crowding such as radial-tangential anisotropy (Toet and Levi 1992) independence from target size (Levi, Hariharan and Klein 2002b) as well as in studies of crowding in atypical vision (Ogata *et al.* 2019; Tailor *et al.* 2021; Greenwood *et al.* 2012).

Threshold-related estimates of crowding zone extent only indicate the target-flanker spacing required to achieve a particular level of performance, but convey little more information about how perception of a target changes at other target-flanker spacings. The effects of crowding have been shown to vary with target-flanker spacing in a number of studies, being strongest at close spacings and reducing with increasing target-flanker distance (Flom, Weymouth and Kahneman 1963; Kooi *et al.* 1994; Harrison and Bex 2017). Threshold estimates therefore represent only a single sample of the underlying psychometric function linking spacing and task performance, so may overlook potentially informative changes in the appearance of the underlying function (see *Figure 4.1*). For example, Kooi *et al.* (1994) present a number of psychometric

functions obtained with a 4AFC task in different conditions of target-flanker similarity with a variety of thresholds and gradients. As the data were expressed as percentage of correct responses, threshold-separation was the primary outcome measure and little mention is made of the variability seen in the gradient of the psychometric functions. Chapter 4 of the thesis presented the concept of the 'spatial profile of crowding', which utilises the systematic nature of errors due to crowding (Harrison and Bex 2015; Harrison and Bex 2017) and describes shifts in the distribution of reports of target appearance as target-flanker spacing is varied. While analogous to a psychometric function of crowding, the gradient of the profile signifies the rate at which responses change as flankers approach the target. The gradient of the spatial profile may vary under experimental conditions, similar to psychometric data present in the literature (Kooi *et al.* 1994; Flom, Weymouth and Kahneman 1963), therefore the question of whether reports of changing threshold-extent arise from shifts in the gradient or location of the spatial profile remains unanswered.

Issues with conflating the spatial extent of crowding with a criterion-dependent level of performance (i.e. threshold) were noted by Pelli and Tillman (2008), who speculated that similarity effects could be the result of changes in 'amplitude' of crowding within an invariant spatial extent. Methods to disentangle 'amplitude' and 'spatial extent' of visual crowding have been reported before (Pelli, Palomares and Majaj 2004; van den Berg, Roerdink and Cornelissen 2007) with some key differences to the method proposed here. These studies estimated feature-identification thresholds for crowded stimuli using an m-alternative forced choice method (10-alternative by Pelli, Palomares and Majaj (2004), and 2-alternative method-of-limits style task by (van den Berg, Roerdink and Cornelissen 2007)), using the QUEST adaptive algorithm (Watson and

Pelli 1983) with the same initial gradient value. Feature-identification thresholds, such as tilt discrimination, were estimated at a range of target-flanker spacings and fit with a sigmoidal 'clipped' line. The 'amplitude' or 'strength' of crowding was defined as the ratio between the upper and lower horizontal sections of the fitted line (i.e. the threshold elevation). The 'critical spacing' was defined as the greatest flanker spacing to induce a change in threshold – the break point where the fitted line stops descending and reaches the floor level of performance. This was performed for crowding tasks varying letter contrast, grating orientation, colour hue and colour saturation. The general findings were that 'critical spacing' increases linearly with eccentricity but is unaffected by stimulus size, which Pelli, Palomares and Majaj (2004) regarded as distinguishing crowding from masking. The latter study also reports a difference in threshold elevation (and therefore crowding 'strength' in the author's interpretation) between different domains – a greater elevation in thresholds was observed in orientation and stimulus size than for colour hue or saturation (van den Berg, Roerdink and Cornelissen 2007). While enlightening, these findings ultimately relate back to changes in threshold estimates – samples of an underlying psychometric function linking changes in stimulus level (e.g., contrast or orientation) to performance at a task. The threshold elevations seen with reducing target-flanker spacing are the result of some change in these underlying psychometric functions which remain unclear in such methods. Such changes in psychometric function parameters are the key point of interest in this study, as these may be more directly related to changes in perceived target appearance than measures of identification threshold.

No study in the literature has systematically probed the psychometric function of crowding with a continuous report (as opposed to m-alternative forced choice)

paradigm while modulating target-flanker similarity along a continuous domain. Taking the approach of constructing 'spatial profiles' of crowding (detailed further in section 4.5) may reveal how target-flanker similarity influences the systematic shift in responses that is expected when changing target-flanker separation (Harrison and Bex 2015; Harrison and Bex 2017). Comparing spatial profiles collected at differing levels of target eccentricity will also explore how the shape of the spatial profile relates to expected changes in the apparent extent of the crowding zone with eccentricity (Bouma 1970; Pelli, Palomares and Majaj 2004), and whether influences related to flanker appearance remain consistent throughout the visual field.

Two studies were conducted with the aim of examining crowded perception of an oriented target by systematically altering both target-flanker orientation difference (therefore similarity) and target-flanker spacing. Study 1 examines crowding at one eccentricity (12.72°) with a wide range of target-flanker orientation difference (0° - 180°). Study 2 examines spatial profiles of crowding across a wider portion of the visual field by utilising two additional target locations (4.24° and 21.2° eccentricity) combined with data collected in study 1.

6.2 Study 1 – Spatial profiles of crowding at one eccentricity

6.2.1 Methods

Perceived orientation of a randomly-oriented Landolt-C target was measured under controlled levels of crowding, including the uncrowded condition. Participants reported the perceived orientation on a continuous scale using a dial to rotate a response

Landolt-C after each stimulus presentation. In crowding trials, the target was flanked by a pair of Landolt-C flankers, spaced along the tangential axis and identical to each other in orientation (offset from the orientation of the target). Ethical approval for the study was gained from the Cardiff University School of Optometry and Vision Sciences Ethics Committee (project #1507).

6.2.1.1 Participants

Three psychophysically trained participants (1 female, 2 male) were recruited to take part in the study. All participants gave informed consent and underwent checks to ensure normal ocular health, and visual system status (see 2.1.3). Refractive correction was required for one participant, who wore spectacles throughout data collection.

6.2.1.2 Experimental task

At each trial, participants fixated a Gaussian spot target (approx. 0.2° diameter) and a target Landolt-C was presented at 12.7° eccentricity below and right of fixation (inferotemporal), to the right eye of each participant. When crowded, two additional flanker Landolt-Cs were presented at a fixed distance (1.5° - 5.5°) from the centre of the target C along the axis tangential to the axis of eccentricity (see Figure 6.1). Unflanked trials were also randomly interleaved into blocks of trials. Flankers were both identically oriented at one of 5 possible orientations relative to the target: 0° (identical to the target orientation), 22.5°, 45°, 90° and 180°, randomly clockwise or anticlockwise. Each level of orientation difference was equally sampled, split evenly

between clockwise and anticlockwise rotations relative to the presented target orientation.

All stimuli (targets and flankers) were 1.5° in diameter and presented for 280ms to enhance crowding effects in experienced observers (see Appendix 2 for a comparison of longer and shorter presentation durations). Immediately following stimulus presentation, a 250ms random noise mask (static, grayscale, 1/F spectral density) was presented at the locations of the target and flankers to disrupt after-images. After each presentation and noise mask the response Landolt-C was presented surrounding the fixation spot.

Participants controlled the orientation of the response C through 5° steps with a consumer volume dial and submitted a response with a button press. After a response was given, a random noise mask was presented centred at the fixation spot for 250ms before the next trial began. Trials of all possible configurations, including the unflanked condition were randomly interleaved. Each participant undertook 3900 trials conducted in one session of less than 4 hours. Three repeats of the test procedure were conducted per participant, giving 150 responses per unique stimulus condition (combination of target-flanker spacing and orientation difference). Regular breaks were given, and additional breaks could be taken at any point by withholding a response. Participants were encouraged to be as accurate as possible without rushing.

Participants wore an eye patch over their left eye throughout data collection. Room lights were turned off and participants were adapted to the flat grey background (10

cd.m^{-2} luminance) for two minutes before beginning and after any breaks between blocks of trials.

Stimuli were presented at a distance of 57cm on a gamma-corrected OLED screen (SONY PVM-A250 Trimaster EL; Sony corp. Tokyo, Japan), calibrated with a ColorCal MKII photometer (Cambridge Research Systems, Kent, UK). Stimulus generation and presentation was conducted with MATLAB (version R2019a; The MathWorks Inc., Natick, MA, USA) using PsychToolbox (Brainard 1997) and the Eccentric Vision Toolbox (Greenwood 2021). Exported data were analysed with R (version 4.1.2, 2021-11-01) (R Core Team 2021) with the 'circular' package (Agostinelli and Lund 2022).

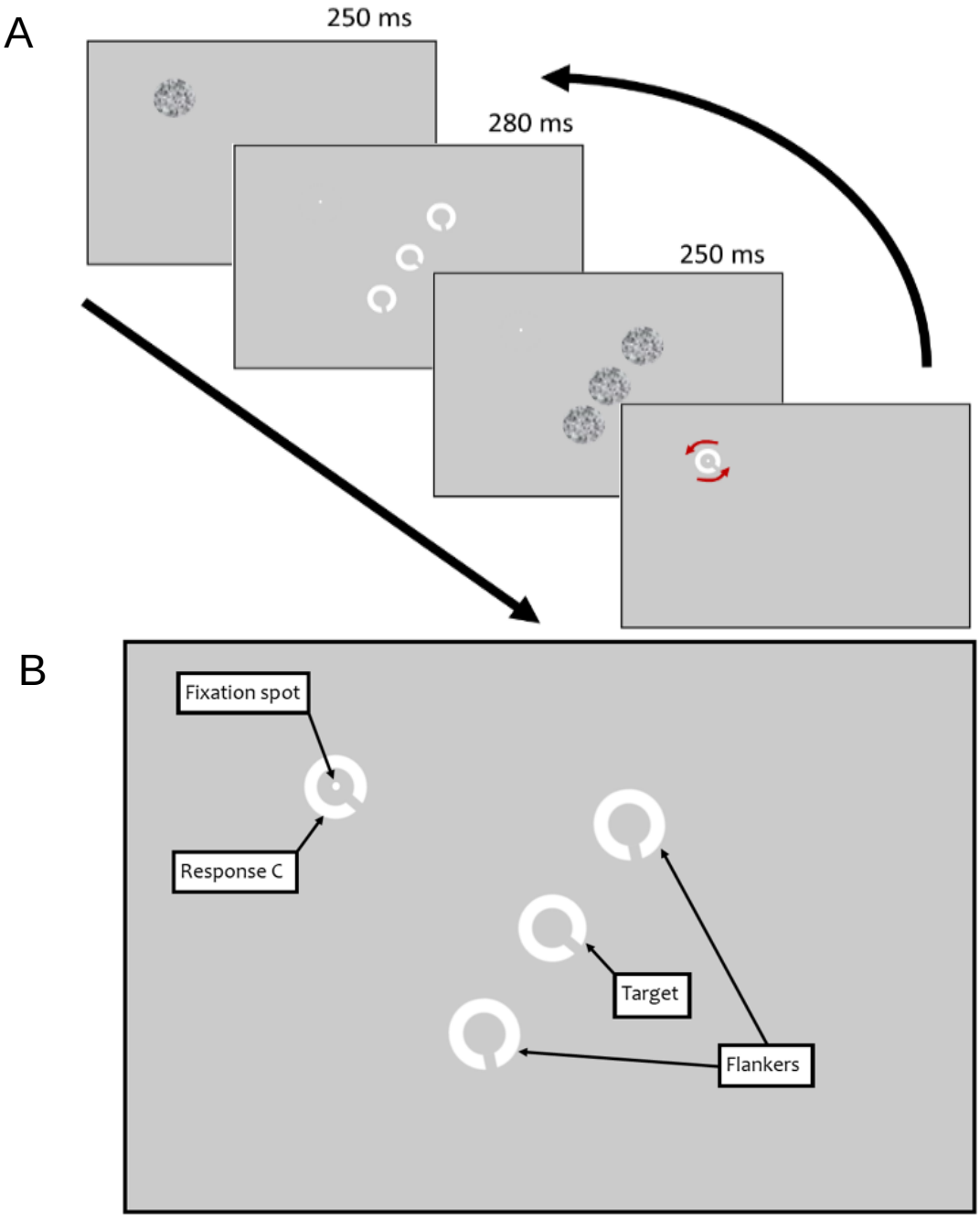

Figure 6.1 - Illustration of a crowded trial

Panel A shows the timeline of a typical crowded trial. A random noise mask is presented at the fixation spot to disrupt any remaining after-image of a previous response Landolt-C before stimuli are presented for 280ms. After stimulus presentation, a second noise mask is presented at the location of any presented stimuli. Finally, a 'response' Landolt-C is presented around the fixation spot. The orientation of the response C is controlled by the participant with a response dial (indicated by curved arrows, not presented during trial). After matching the perceived orientation of the target, the next trial begins. Panel B labels the main screen elements that appeared at various times through a trial (not to scale).

6.2.2 Data analysis

6.2.2.1 Calculating response error

Response errors made by each participant were calculated by subtracting the response orientation from the orientation of the target presented at each trial. The sign of errors made during trials with flankers oriented anti-clockwise to the target were flipped, meaning positive response errors always indicate a response towards the orientation of the flanker, whereas negative response errors signify responses away from the flanker orientation. For example, if flankers on a given trial were oriented clockwise relative to the target, a response 10° clockwise relative to the target orientation would give an error of +10°, whereas a response of 10° anticlockwise would give an error of -10°, and vice versa in the case of anticlockwise flankers. Note that for trials with flankers at 0° or 180° to the target, this transformation was not necessary as both clockwise and anticlockwise errors were equally 'towards' the flanker orientation, so signs of response errors were unaltered.

The probability of each possible error (-180° to 180° in 5° steps) being reported was calculated by summing the number of trials producing each error and dividing by the total number of trials conducted for each arrangement of stimuli (unique combination of target-flanker spacing and relative orientation difference).

6.2.2.2 Model fitting to distributions of responses

Unflanked data were fit with a single von Mises distribution centred at 0° with two free parameters corresponding to the height and spread (or concentration). For each crowded condition (target-flanker orientation-difference and spacing) the probabilities

of potential errors (the frequency of each error divided by the total number of trials) under each condition were then modelled as a weighted, mixed pair of von Mises distributions. These two distributions were centred at 0° ('target' responses) and the flanker orientation ('flanker' responses) respectively, with the explicit assumption that there are no other sources of potential responses which is supported by the data. Each distribution was fit with two free parameters: an optimised concentration parameter (related to its spread) and a weighting parameter (related the height of the whole distribution – not just the peak value) independently of the other distribution's parameters. Modelling responses as this mixture of two distributions permits calculation of the relative proportions of the responses made under different conditions by comparing weighting parameters for each of the 'target' and 'flanker' response distributions. The proportion of errors centred around 0° was taken as the probability of a giving a response centred at the orientation of the target, abbreviated to p(Target). A ratio of 1 indicates all responses were centred around the target orientation, while a ratio of 0 would indicate all responses were centred around the flanker orientation (See *Figure 4.3*).

6.2.2.3 Fitting spatial profiles of crowding

To quantify the effect of target-flanker spacing on the distributions of response errors, p(Target) values were then combined across the range of target-flanker spacings tested and modelled with a logistic function with two free parameters – location and gradient. This describes the spatial profile of crowding associated with each target-flanker orientation difference (see section 4.5for further detail). The location parameter (also called the 'inflection point' or 'midpoint') of this function indicates the target-

flanker separation at which responses switch from mostly target-centred to mostly flanker-centred. The gradient of the logistic function is steepest at the inflection point, and determines the span of the transition zone between minimal crowding (few flanker-centred responses) and maximum crowding (few target-centred responses). The span of the transition zone was estimated by predicting the target-flanker spacing associated with p(Target) values of 0.25 and 0.75 (indicating 25% and 75% of responses centred at the target orientation respectively) and calculating the difference between them. This meant shallower spatial profiles of crowding equated to a wider span of the transitionary zone.

A computer error during data collection affecting one repeat of the procedure was noticed during data analysis. During this run, the smallest target-flanker separation was incorrectly set to a value larger than the planned 1.5° visual angle. The incorrect separation was different for each participant, but all were between 1.5° and 2.0° (1.6°, 1.7° and, 2.0°). The remaining two repeats of the experiment were unaffected. Rather than discount the data, these were grouped individually alongside the other target-flanker separations and analysed as above. During logistic model fitting, the p(Target) values were weighted according to the number of trials included. This allowed the data to be kept and utilised but still accounted for the different target-flanker separations used. The number of trials contributing to each data point is indicated by the size of each point in Figure 6.6 and Figure 6.8.

6.2.3 Results – Study 1

Probability distributions of response errors are centred at 0°, corresponding to the target orientation. When present, the orientation of the flankers (both clockwise and anti-clockwise to the target) corresponds to the positive value of the target-flanker orientation difference, as the sign of errors in the presence of anti-clockwise flankers were flipped. As the data are circular (i.e., orientations on a continuous and repeating scale), the x-axis of these distributions wraps where x = ± 180°.

Response errors in the unflanked condition were concentrated around an error of 0°, shown in Figure 6.2. Fitted von Mises distributions described the data well and indicates participants were able to report the target orientation with reasonable accuracy. The greatest mean error (corresponding to the peak of the distribution) was -1.6°, suggesting there was no systematic bias in responses.

Responses in all crowded conditions tended to cluster around the target orientation (errors around 0°) and the flanker orientation (errors around the amount of target-flanker orientation difference) in varying proportions, as seen in Figure 6.3. Very few responses that would not fall under either of these two categories were observed, similar to findings mentioned in the alternative analyses of (Harrison and Bex 2015; Harrison and Bex 2017). The proportion of responses centred around the target was consistently greatest at further target-flanker separations and decreased when flankers were presented closer to the target (i.e., target-flanker spacing was reduced).

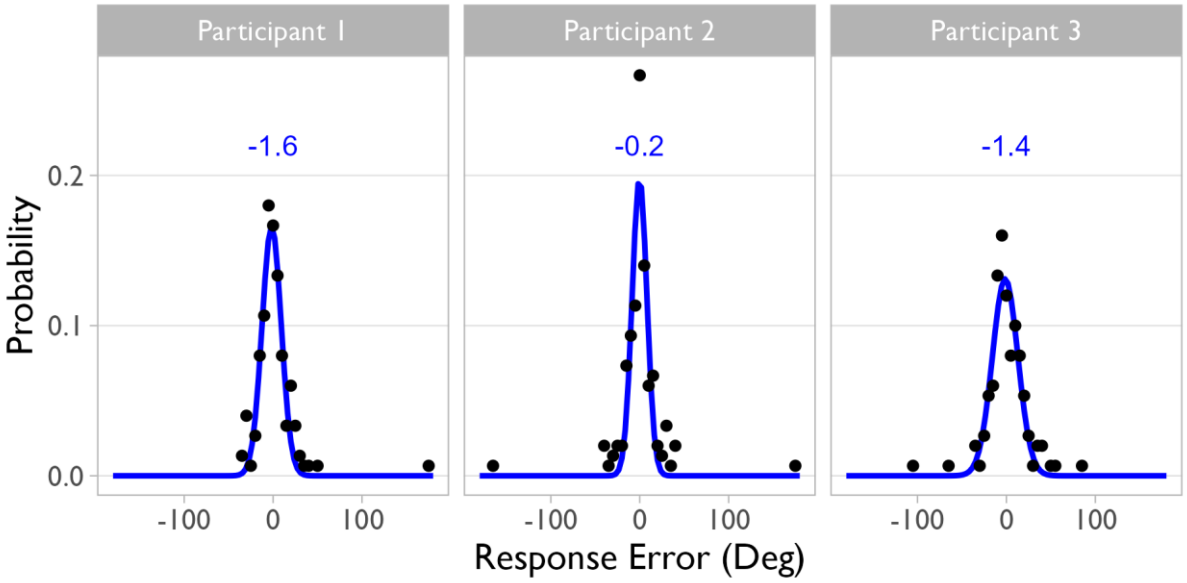

Figure 6.2 – Distributions of unflanked errors

The probability of each possible response error (difference between presented target orientation and response orientation) is indicated by the black data points. For clarity, points are not plotted where calculated probability was 0 (meaning no responses were given with this error). Each fitted von Mises distribution is shown by the blue line, and the mean error is given numerically (in degrees). Participants could report the target orientation with reasonable accuracy.

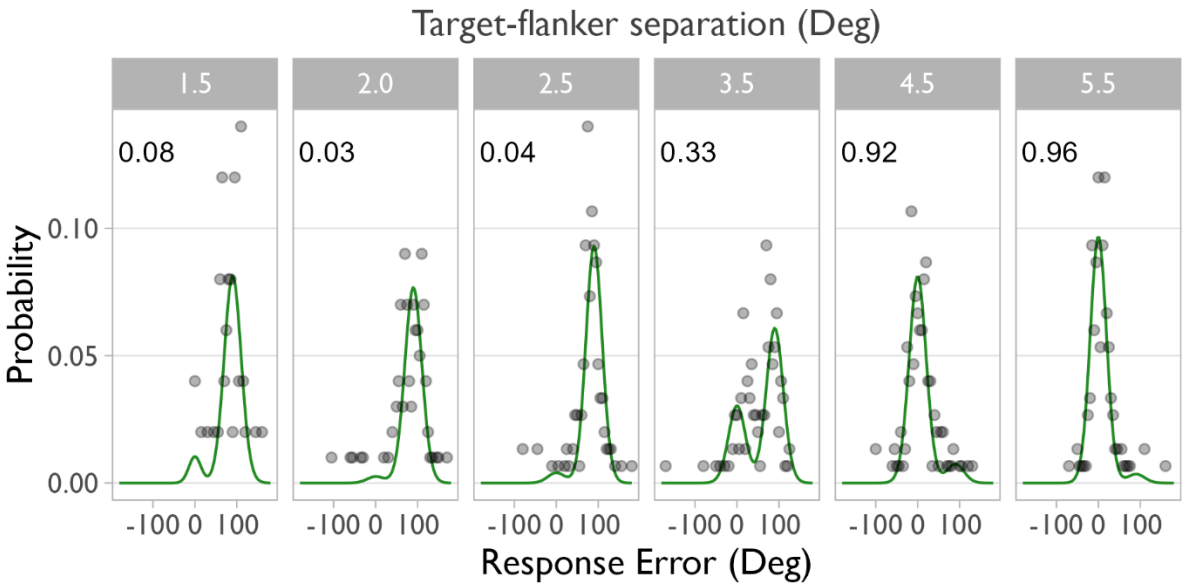

Figure 6.3 - Example distributions of crowded response errors

Probability distributions of response errors made by participant 3 with one target-flanker orientation difference (90°) are shown as they are representative of the form of the data from other participants and conditions. Panels from left to right correspond to target-flanker separation (shown in grey labels in degrees of visual angle). Data points show the probability with which each response error occurred and the fitted mixed von Mises model is shown in green. The calculated proportion of responses centred at the target orientation, p(Target), is shown numerically in each panel. Responses were concentrated around the target orientation (0°) at greater separations (right most panel) and shift in proportion towards mostly flanker-centred (around 90°) errors at smaller separation (left most panel). Six target-flanker separations were tested as a computer error affected flanker location in a subset of trials.

In the case of flankers that matched the orientation of the target (target-flanker orientation difference = 0), errors again cluster around 0° but do not shift towards a secondary orientation as target-flanker separation is reduced. Instead, the spread of the distribution (inversely related to the concentration parameter) increases when flankers are closest to the target, which can be seen in Figure 6.3. Modelling the data as a mixture of von Mises distributions was not possible, as the means of both distributions coincided, meaning calculation of p(Target) values was not possible.

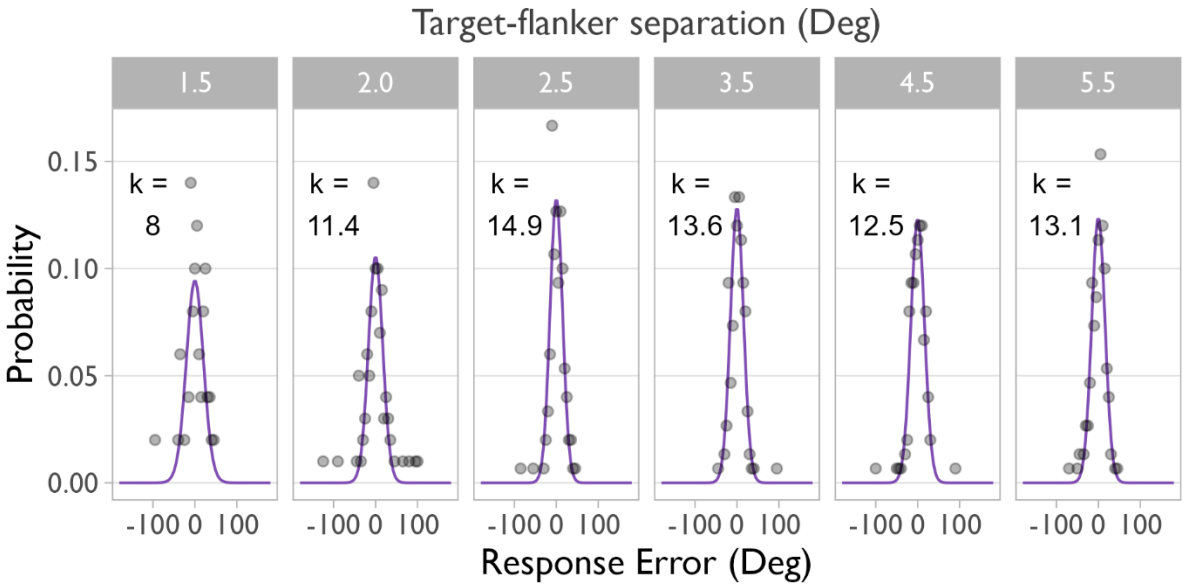

Figure 6.4 - Response errors when flankers match the target orientation

Data shown are from participant 3, though data from the other participants were similar. Purple lines show the fitted, single von Mises distribution. Grey labels at the top of each panel indicate target-flanker separation increasing left-to-right. When flankers are presented at the same orientation of the target, no secondary peak appears as flankers are presented at smaller spacings. The data become more concentrated (indicated by greater concentration parameter "k", shown numerically in black) when flankers are presented further from the target.

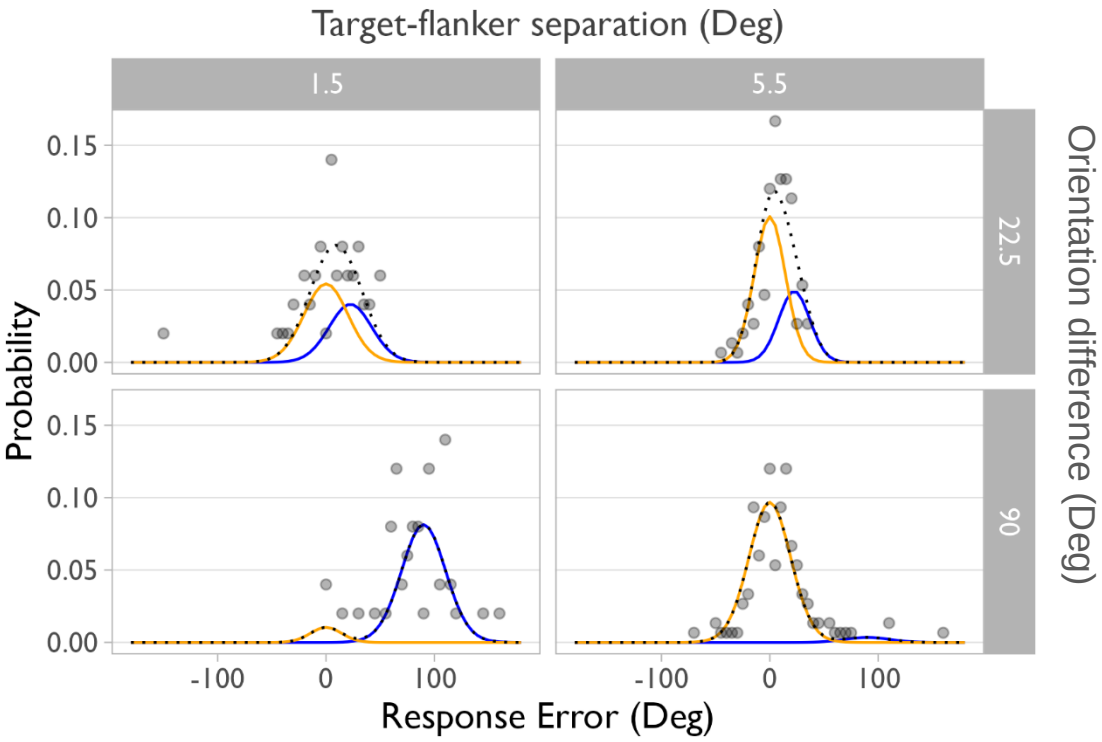

Figure 6.5 - Comparing error distributions over target-flanker orientation difference and separation

Example data from participant 3 to compare distributions of response errors at high and low target-flanker separation (columns left-to-right) and orientation difference (rows). Values of target-flanker separation (degrees of visual angle) and orientation difference (degrees of orientation) are given in grey labels. Individual fitted von Mises distributions are shown by solid lines, corresponding to the target- (orange, peak at 0°) and flanker (blue, peak at 22.5° or 90°) centred responses. The dotted lines show the fitted mixed von Mises model (sum of individual distributions). Where target- and flanker- centred distributions overlap (upper row), the peak of the mixed distribution occurs between the target and flanker orientations.

When flankers with smaller orientation difference were presented adjacent to the target such that the stimuli were just touching, a proportion of responses remained centred at the target orientation, compared to flankers of 90° or 180° orientation difference where flanker-centred responses dominate at the smallest target-flanker spatial separations. At greater spatial separations between stimuli, smaller orientation differences cause some flanker-centred errors, even where flankers with larger orientation differences do not. This is shown with example data in Figure 6.5.

Values of p(Target) were plotted for each participant at each target-flanker orientation difference against spatial separation in Figure 6.6. In general, the calculated proportion of responses centred at the target orientation, indicated by p(Target), falls as target-flanker separation decreases. The data show a systematically sharper decline in the proportion of target responses with increasing dissimilarity between target and flanker similarity. When flankers are presented with a greater orientation difference, this decline in performance occurs over a shorter range of spatial separation between target and flanker stimuli. Conversely, flankers presented with a smaller orientation difference from the orientation of the target cause a more gradual shift towards responses centred at the flanker orientation.

The midpoint of the spatial profiles (i.e. the spatial separation at which performance is exactly midway between perfect and maximally crowded responses) showed little variation with the changes in orientation difference – see Figure 6.7A. While the curve relating to 22.5° orientation difference reaches its midpoint at a slightly smaller separation, the other 3 orientation difference conditions all indicate a similar midpoint for each participant.

The span of the transition zone (difference in target-flanker spacing corresponding to p(Target) values of 0.25 and 0.75) is greatest with target-flanker orientation difference is smallest – see Figure 6.7B. With greater orientation differences the spatial profile of crowding is steeper (more ‘step-like’), indicating the shift in responses occurs over smaller range of target-flanker separations.

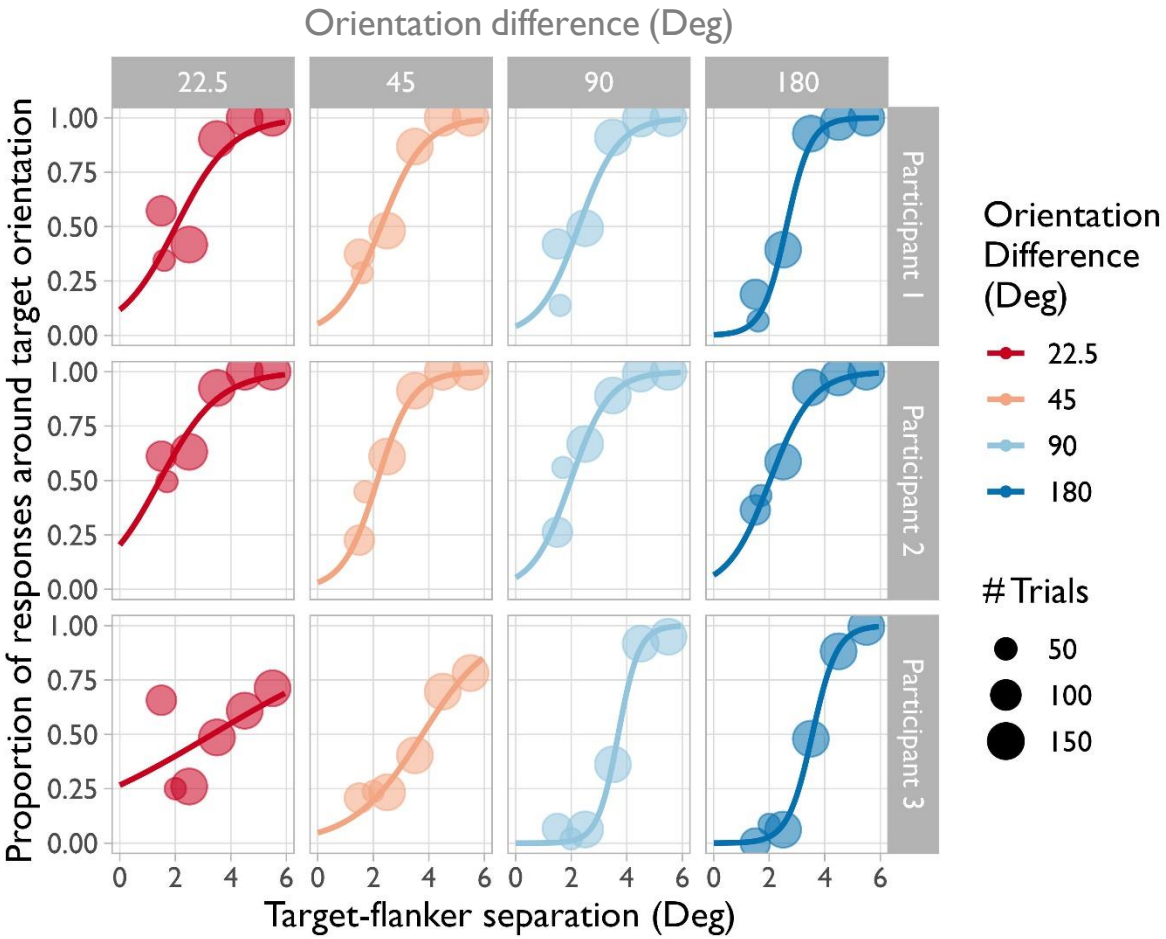

Figure 6.6 – Spatial profiles of crowding at one eccentricity

Each panel shows the proportion of responses centred at the target orientation, p(Target), plotted on the y-axis against target-flanker separation (x-axis). Solid lines show the fitted spatial profile of crowding. Data from each participant are shown separately in each row. Data corresponding to each target-flanker orientation difference are split across columns, increasing from left to right. Values of orientation difference are indicated by colour and shown in the upper grey labels of each column (in degrees). The size of each data point indicates the number of responses contributing to the distribution from which p(Target) was estimated. As target-flanker orientation difference increases (columns left to right), spatial profiles of crowding become steeper.

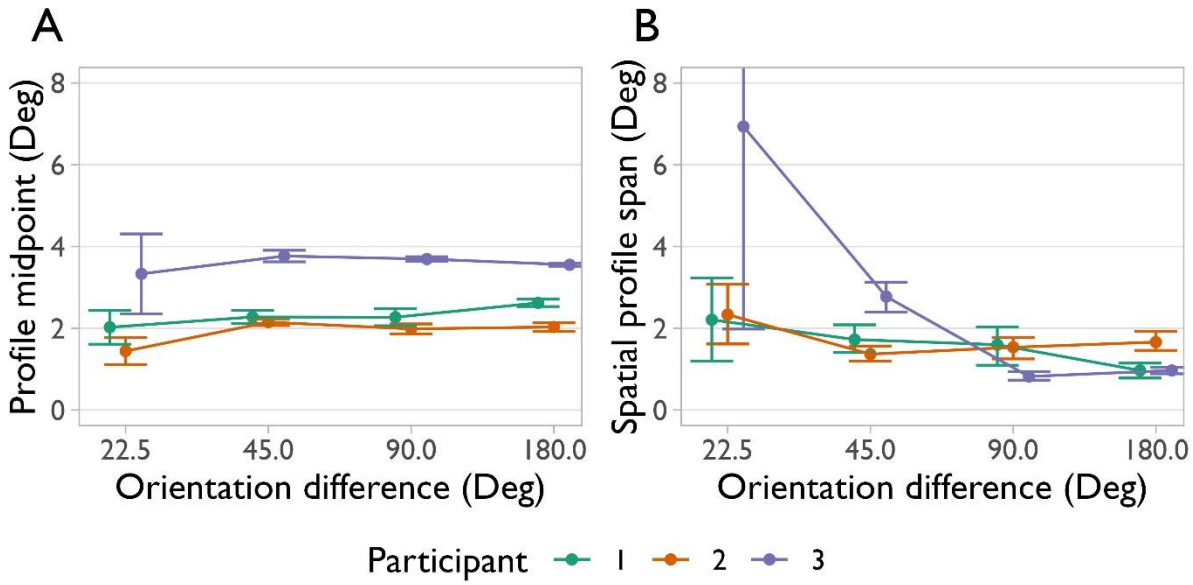

Figure 6.7 - Midpoint and span of spatial profiles at one eccentricity

Panel A shows the midpoint of spatial profiles of crowding fitted to data at each target-flanker orientation difference (x-axis) for each participant (indicated by colour). Panel B shows the span of the fitted spatial profiles, defined as the difference in target-flanker separations associated with 25% and 75% target-centred responses. Target-flanker orientation difference modulates the span of the spatial profiles (panel B) but the location of the spatial profile (indicated by the midpoint – panel A) is largely unchanged by changes in target-flanker orientation. Error bars indicate ±1SE.

6.3 Study 2 – Spatial profiles of crowding at multiple eccentricities

This second follow-on study investigated the effect of target eccentricity on the spatial profile. The same experiment as in Study 1 was undertaken ar two additional target eccentricities (4.24° and 21.2° eccentricity). The previous study showed that target-flanker similarity primarily modulates the span of the transitionary zone between minimum and maximum crowding, but it is unknown whether this modulation is consistent across the visual field. Finer acuity and smaller crowding zone extent in visual field areas closer to central vision could lead to different patterns of modulation compared with the coarser acuity and larger crowding zones of more peripheral locations. Some investigations have indicated a potentially positive correlation between eccentricity and crowding magnitude, as distinct from critical spacing, in terms of threshold elevation (van den Berg, Roerdink and Cornelissen 2007). How this may translate to the spatial profile of crowding is difficult to predict, but may appear as the midpoint of the spatial profile shifting further from the target while the profile simultaneously becomes shallower. This study sought to discover how aspects of the spatial profile of crowding change with eccentricity, and whether these changes occur equally in the case varying target-flanker similarity.

6.3.1 Methods

The participants recruited for study 1 also took part in study 2, see section 6.2.1.1 above for details. The same experimental method was used, except only three target-flanker orientation differences were employed (22.5°, 90° and 180°) and fewer trials per condition were undertaken (80 in study 2, 150 in study 1). These changes were

made to prevent data collection across the two additional target locations from becoming prohibitively long and potentially introducing fatigue effects. Trials were presented in distinct blocks at each additional eccentricity (4.24° and 21.2°) so that the locations of the fixation spot and target Landolt-C were constant within each block. Flanker appearance (relative orientation difference, target-flanker spacing and unflanked condition) were again shuffled and presented in a randomised order within each block. Stimulus diameter (for the target and flankers) was scaled for eccentricity at each location following the equation:

$$\text{Stimulus diameter} = \frac{(E + 1.77) \times 1.5}{12.72 + 1.77}$$

Equation 6.1

Here, E = target eccentricity in degrees of visual angle to equate stimulus size to that used in Study 1 (1.5° diameter at 12.72° eccentricity). This equation was adapted from (Horton and Hoyt, 1991) and uses parameters obtained from fitting their equation to fMRI data obtained from (Wright 2021) collected from a healthy cohort of similarly-aged controls, see section 5.2.1.1 for more information on this fMRI data. The calculated target diameters were 0.6° for targets at 4.24° eccentricity, and 2.4° in diameter when the target was at 21.2° eccentricity. Viewing distance from the screen was reduced to 40cm to permit the range of eccentricity and target-flanker spacings used (displayed stimulus sizes were scaled accordingly for this shortened viewing distance).

6.3.2 Analysis – Study 2

Participant responses were collected and analysed in an identical method to that described in section 6.2.2 above.

Target-flanker spacing was also subsequently transformed to 'Bouma-units' by dividing by the target eccentricity. This describes spacing as a proportion of eccentricity (Bouma 1970) and similar approaches have been used in other research (Greenwood *et al.* 2017). Logistic functions were then re-fit to make comparisons on equalised 'Bouma-unit' scales across levels of target eccentricity.

6.3.3 Results – Study 2

As in study 1, response-errors clustered around either the target or flanker orientations, with very few 'random' errors, similar to distributions shown in Figure 6.3 and Figure 6.5. The same general pattern of shifts in responses with increasing target-flanker spacing was also observed – errors centre around the flanker orientation when target-flanker spacing is low and shift towards mostly clustering around the target orientation when spacing is increased.

Modelling the spatial profiles of crowding also revealed similar patterns of similarity-based modulation as observed in study 1 – Figure 6.8 combines these functions for all examined field locations. The midpoints of the spatial profiles again appear invariant to target-flanker orientation difference, but the expected pattern of greater midpoint locations with increasing eccentricity can be seen. Low target-flanker orientation difference (i.e., similar target and flankers) tended to produce shallower logistic functions for each participant at all eccentricities. Whereas, higher target-flanker

orientation difference (dissimilar stimuli) produces steeper, more ‘step-like’ spatial profiles.

Locations of the spatial profiles (indicated by the midpoint - Figure 6.9 A) remain invariant to target-flanker orientation difference at all eccentricities. The span of spatial profiles (Figure 6.9 B) are generally wider at greater eccentricities, indicating spatial profiles were shallower than at more central target locations. As seen in study 1 (Figure 6.7), greater target-flanker orientation differences result in smaller spans of the transitionary zone at all eccentricities. Transforming these values to ‘Bouma-units’ (by dividing target-flanker spacing by the target eccentricity) greatly reduces the disparity between values seen across eccentricities and almost aligns the mean values - Figure 6.9 C and D. The span of the spatial profile in Bouma-units (Figure 6.9 D) is consistent across target eccentricities for each level of target-flanker orientation difference. This indicates the similarity-based modulation of the spatial profile is similar between the eccentricities used, when expressed as a ratio of the target eccentricity (i.e., Bouma-units).

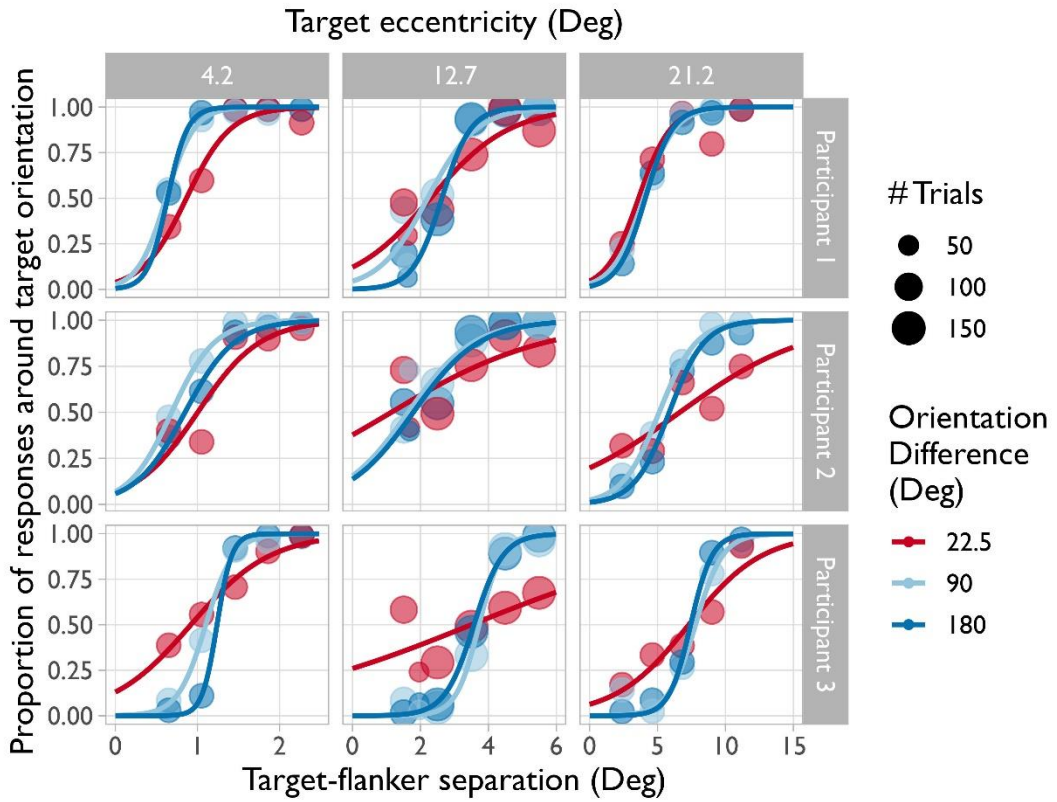

Figure 6.8 - Logistic functions of target-response probability against flanker spacing for all eccentricities

Data from each participant are arranged in rows and from each target eccentricity across columns. Only data from target-flanker orientation differences investigated at all eccentricities are included to aid clarity in comparisons. Note the difference in x-axis scales between eccentricities (columns). At all eccentricities, spatial profiles of crowding are shallowest with small target-flanker orientation differences (red lines).

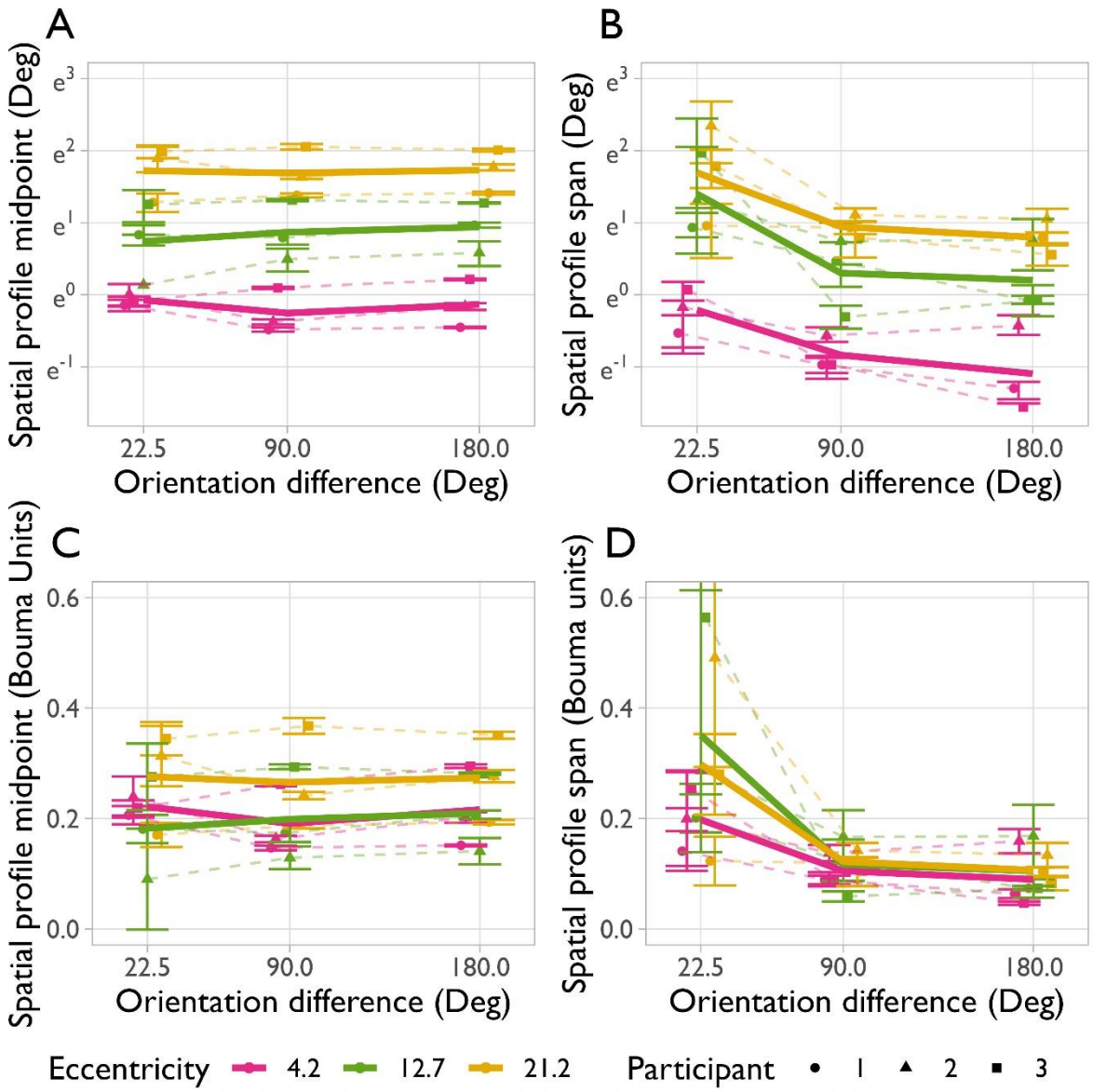

Figure 6.9 - Midpoint and span of spatial profiles at all eccentricities

Upper panels (A and B) show the midpoint and span of spatial profiles at all eccentricities (indicated by colour) in degrees of visual angle (y-axis) against target-flanker orientation difference (x-axis). Note: the y-axes of panels A and B are logarithmic scales to aid clarity over the range of data. Lower panels (C and D) show the same measures taken from spatial profiles fitted to p(Target) data where the associated target-flanker separation was converted to 'Bouma-units' by dividing by target-flanker eccentricity. Bold lines indicate the mean of participant data (dashed lines). The span of spatial profiles (right panels, B and D) decreases as target-flanker orientation difference increases, whereas midpoints (A and C) remain similar. When target-flanker separation is converted to Bouma-units, the variation in measures of midpoint and span are greatly reduced. Error bars indicate ±1SE.

6.4 Discussion

Target-flanker similarity modulates the span of the transitionary zone between minimum and maximum crowding effects, while the position of the spatial profile of crowding remains unaltered. Greater target-flanker orientation difference (reduced similarity) leads to a sharper transition between ‘no crowding’ and ‘fully crowded’ distributions of responses, compared to smaller orientation differences. Increasing target eccentricity has a dual effect of shifting the midpoint of the spatial profile of crowding further from the target and making spatial profiles generally shallower (thus giving a wider transitionary span). However, spatial profiles of crowding appear similar between eccentricities when target-flanker spacing is expressed as a ratio of target eccentricity (Bouma-units), indicating similarity-based modulation of the transitionary span, and similarity-independence of the midpoint, is preserved between the target locations.

6.4.1 Distributions of response errors

Shifting proportions of responses clustered primarily around the target and flanker orientations agrees with the findings of other researchers using similar paradigms which allow participants to report target appearance on a continuous scale (Harrison and Bex 2015; Harrison and Bex 2017; Põder 2012). Studies comparing distributions of responses at two levels of target-flanker separation (Ester, Klee and Awh 2014; Ester, Zilber and Serences 2015) noted greater proportions of substitution-type errors at nearer distances, which follows logically from earlier studies reporting spacing-dependent modulation of crowding strength (Tripathy and Levi 1994; Kooi et al. 1994;

Pelli, Palomares and Majaj 2004). However, it is difficult to infer whether these data agree with the present findings of similarity-based modulation in transitionary span due to the conflation of data from different target-flanker orientation differences (Harrison and Bex 2015; Harrison and Bex 2017) or the instantiation of a 'trimodal' population pooling model to describe the distributions of errors observed (Ester, Zilber and Serences 2015). These investigators' methodological decisions hamper the ability to differentiate the effects of target-flanker orientation difference with that of target-flanker separation in much of their data. Nevertheless, one report (Ester, Zilber and Serences 2015) does indicate a higher proportion of flanker-centred errors with flankers offset by 60° to the target compared those offset by 15°, at the smallest separation between target and flankers, while probabilities were equally low at the larger separation. This agrees with the findings of the p(Target) data presented above: that greater target-flanker orientation differences lead to smaller calculated proportions of target-centred responses at target-flanker separations smaller than the midpoint of the spatial profile, compared with flankers at smaller orientation differences.

6.4.2 The spatial profile of crowding

Fitting the two-parameter spatial profile of crowding revealed that target-flanker similarity has little influence on the midpoint of the spatial profile. Instead, the midpoint is primarily related to target eccentricity. The finding that similarity-dependent aspects of the spatial profile of crowding (the transitionary span) and similarity-independent aspects (location of the midpoint) can be differentiated in psychophysical data presents a new approach to investigating the edge of the crowding zone.

The shared midpoint of the spatial profile across different levels of target-flanker similarity may serve as an indication of low-level physiological structures that could contribute to the observed spatial extent of the crowding zone, such as retinal ganglion cell (RGC) receptive field density (Kwon and Liu 2019). If a critical number of underlying RGC receptive fields are associated with crowding zone extent (Kwon and Liu 2019), then it is less intuitive that this critical number should change when target-flanker orientation difference is manipulated. Rather, the fixed location of the midpoint could point towards an 'outer limit' of possible crowding interactions beyond the psychophysically observable extent that is also invariant of target-flanker similarity. The similarity-dependent weighting of responses to target and flanker features would then occur within this hypothetical outer limit at each target location. Flankers located close to this outer limit may contribute to the internal population response but be weighted so low as to be undetectable by present psychophysical techniques. The extent of this outer limit, being invariant of target-flanker similarity, could represent the maximum reach of the receptive fields of a critical number of RGCs. The midpoint of the spatial profile may then serve as an indicator of this similarity-independent outer limit, which would increase proportionally with eccentricity (following the observed changes in the midpoint in Figure 6.9 A) matching an identifying feature of crowding (Pelli, Palomares and Majaj 2004; Bouma 1970). This speculative hypothesis may be supported by an association between the midpoint of the spatial profile and RGC receptive field density, which is the aim of the experiment in the following chapter (Chapter 7).

As comparable psychometric functions with respect to spatial separation are less commonly presented in recent crowding research, it is difficult to predict how the

present findings may generalise to other types of target-flanker similarity, such as hue or flanker shape. In one example, Kooi *et al.* (1994) presented spatial psychometric functions obtained with a 4AFC task wherein observers reported the orientation of a rotated capital 'T'. When the target T was flanked by vertical or horizontal bars, the psychometric function was shifted towards smaller target-flanker separations in comparison to randomly oriented T flankers. Changes in gradient of the psychometric function are also seen in some, but not all, datasets. Interestingly, Kooi *et al.* also show a spatial psychometric function produced with capital 'H' flankers that, while qualitatively similar, did appear to be slightly steeper than to that produced with capital 'T' flankers in the same observer. These two functions also appear to intersect at close to 50% correct, despite the 4AFC paradigm giving a chance level (hence theoretical psychometric floor) of 25%. The participant in the experiment was also only tasked with reporting the orientation of a letter T, so could not have reported a letter H even if this were perceived at the target location (i.e., if substitution occurred). Nevertheless, the letters shared all necessary information to identify orientation (both horizontal and vertical bar parts conjoined perpendicularly), as opposed to only vertical or horizontal bars. With oriented bar flankers, the absence of a perpendicular junction in the flankers may have provided a cue to the target location. This would reduce positional uncertainty and improving identification ability, potentially explaining the shift in threshold location in figure 6 of their report.

6.4.3 Implications for present and future research

These findings have important implications in experimental design and when comparing crowding studies. Wider transitionary spans between minimum and

maximum crowding, as seen with greater target-flanker similarity, could well lead to a larger apparent extent of crowding when estimated with a criterion-level performance above 50% (such criteria are widely seen in the literature (Kooi *et al.* 1994; Kwon and Liu 2019; Greenwood *et al.* 2012; Ogata *et al.* 2019)) – see Figure 6.10 for an illustration. Conversely, if an experimental manipulation (or visual condition) were to cause an outward shift of the spatial profile of crowding, but without altering the gradient, this would also appear as a larger apparent extent of crowding. Figure 6.11 illustrates how these two different changes to the underlying spatial profile of crowding could produce the same shift in typical criterion-based measures. Concurrent shifts in midpoint and span of the spatial profile may also be possible, though not illustrated. Both the location of the midpoint and the span of the spatial profile of crowding could contribute to these apparently larger criterion-based estimates of the extent of the crowding zone, meaning these measures alone are unable to identify how the underlying psychometric function may be altered due to experimental manipulations. As either the midpoint or gradient of the spatial profile, or both, may be indicative of different features of crowding, establishing which one (or combination) of these is altered with experimental manipulations may lead to stronger inferences and associations with other measures.

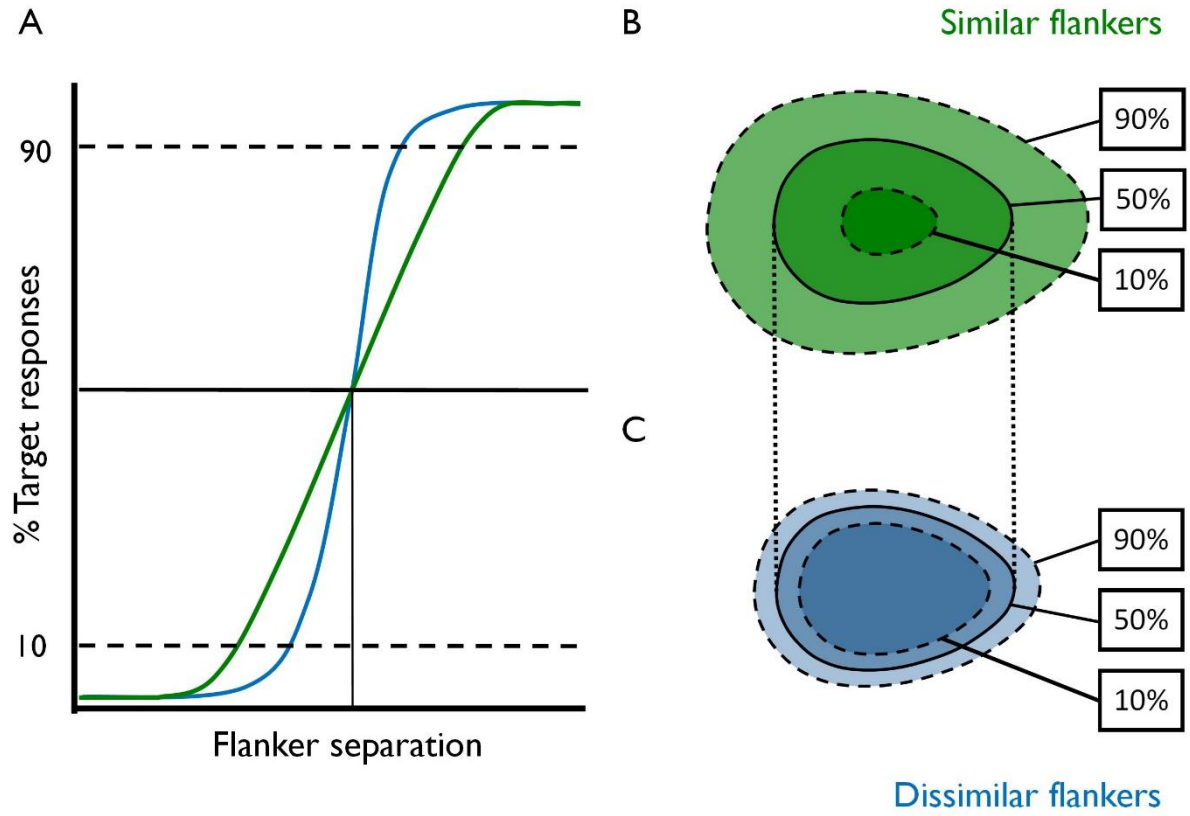

Figure 6.10 – Illustration of the link between the spatial profile of crowding and apparent crowding zone extent

Panel A Illustrates spatial profiles of crowding assessed with flankers that are similar and dissimilar to the target. The target-flanker separation (x-axis) corresponding to 50% responses centred at the target appearance is shared, while the gradient (thus, spread) of the profiles varies. Panels B and C illustrate crowding zones associated with similar and dissimilar target-flanker appearance by extrapolating samples of each spatial profile corresponding to 90%, 50% and 10% target-centred responses. Dotted lines indicate the shared midpoint-spacing while dashed lines highlight that different performance criteria produce varying measures of crowding zone extent. Crowding zones appear larger when flankers are more similar in appearance to the target, but the shared midpoint may suggest a common physiological origin of the extent of spatial interactions.

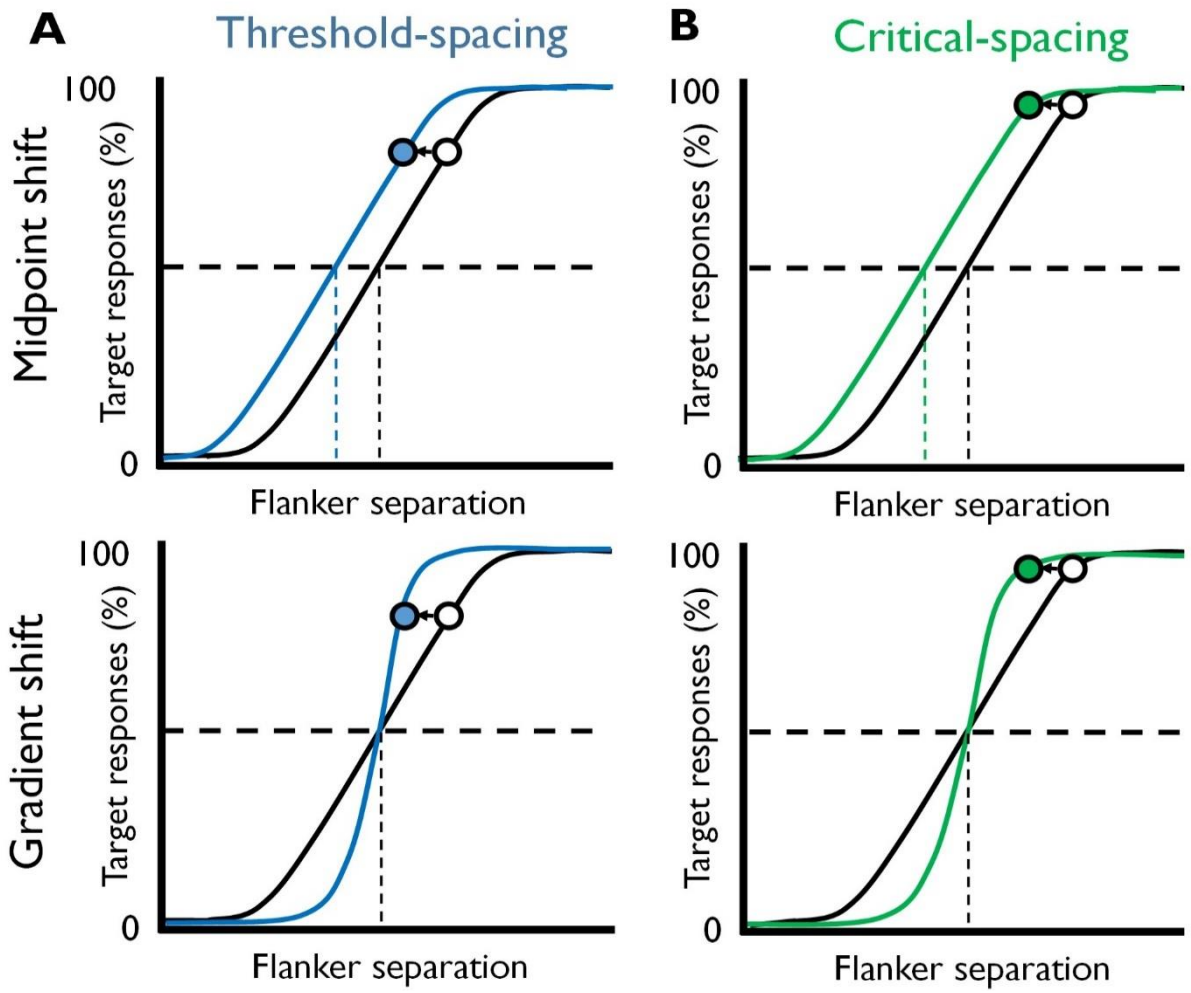

Figure 6.11 – Common estimates of crowding zone extent may obscure changes in the spatial profile of crowding

This schematic illustrates two potentially conflicting explanations for the change in crowding zone extent if estimated at a single point on the outer edge of the crowding zone. Common estimates of crowding zone extent such as threshold-spacing (panel A, blue) and critical-spacing (panel B, green) represent single samples from an underlying spatial profile of crowding (curved functions). Each pair of plots contrast opposing changes to the underlying spatial profile (upper and lower) which produce in the same change in estimated zone extent (circular data points). Critical-spacing differs from threshold-spacing in that it is not associated with a specified level of task performance (y-axis), but instead the smallest detectable deviation from 100% target responses (non-crowded), which may vary between experimental conditions.

One example of a study linking estimates of crowding zone extent to physiological structures proposed that a critical number of RGC receptive fields may determine the extent of crowding zones across the visual field (Kwon and Liu 2019). However, this is mainly supported by the investigators' simulation work, which is reliant on Bouma's law (Bouma 1970). Their experimental data showed a statistically significant association between RGC receptive field density and crowding zone area (estimated via critical spacing of letter-recognition contrast thresholds in a 10AFC task) between four quadrants of the visual field estimated at the same eccentricity, but not between different eccentricities. Critical spacing estimates the greatest target-flanker separation at which an elevation in threshold is detected, which is similar to sampling the spatial profile of crowding at a high level of task performance (i.e., equivalent to p(Target) slightly below 1, though the exact value is likely to vary between studies). The simultaneous increase of both the midpoint and span of the spatial profile of crowding with increasing eccentricity may well have resulted in underestimation of the intended measure of crowding (the 'outer limit' speculated on above). Such underestimation would worsen as the gradient of the spatial profile flattens with eccentricity, possibly leading to the negative trend present in some of data reported by Kwon and Liu (2019). Such a varying underestimation would weaken comparisons of measures over eccentricity but may be less impactful on comparisons at a fixed eccentricity where the gradient of the profile may be more similar between visual quadrants. This would mean the observed differences in critical spacing between quadrants are more likely to be the result of shifts in the midpoint of the spatial profile, which may be more closely related to RGC receptive field density. Solving the possible confound of variable gradient could resolve the apparent discrepancy in the

experimental data reported by Kwon and Liu, and may potentially be achieved by taking the midpoint of the spatial profile as an indicator of crowding zone extent.

6.4.4 Strengths and limitations

The ability of this study to reliably examine the gradient and position of the model curves as independent entities is made possible by the continuous-report paradigm of the experiment and analysis. By allowing participants to report the orientation they perceive, a much richer collection of data is obtained than if participants were forced to make a compromising choice between a restricted number of alternatives. Limiting response options has been demonstrated to have potentially misleading effects on results, especially if participants are unable to report a flanker identity (Reuther and Chakravarthi 2020). This type of data permits the fitting of weighted pooling models and individual examination of responses to target and flanker stimuli, even when individual responses fell between target and flanker orientations, and has been used in a number of recent studies (Harrison and Bex 2017; Harrison and Bex 2015; Kalpadakis-Smith *et al.* 2022). Some studies with similar approaches also include model parameters to quantify additional noise in reports (i.e., random errors not associated with the target or flanker orientation) (Ester, Klee and Awh 2014; Kalpadakis-Smith *et al.* 2022). However, adding an additional uniform (i.e., random) distribution to the mixed von Mises model yielded almost identical results in this study as very few such ‘random’ responses occurred. This is potentially a result of all three observers being experienced with psychophysical testing, reducing random errors.

One limitation of the analysis method is that it requires ‘crowded’ and ‘uncrowded’ responses to be sufficiently distinct in terms of report error. Some amount of overlap

is well accounted for by the mixed von Mises distribution models, but these struggle when both distributions centre on the same orientation (as is the case when flankers are identical to the target - 0° orientation difference). As a result, these data (and some datasets where absolutely no flanker-centred responses were recorded) failed to be fit with a bimodal model and instead are more successfully modelled by a single von Mises distribution centred on an error of 0°.

6.5 Conclusions

This study identifies that the parameters of the spatial profile of crowding can be differentially influenced by target-flanker appearance and eccentricity. The physiological correlates of the midpoint and gradient of the spatial profile remain to be explored. Nevertheless, the finding that the midpoint varies with target eccentricity (and not with target-flanker similarity) suggests that a closer association with structural determinants of the spatial extent of crowding could be possible, in comparison to reported associations with measures such as critical spacing. Investigating this potential association is the focus of the following chapter (Chapter 7). Critical spacing (and other criterion-based measures greater than 50% performance) may conflate changes in the midpoint and span of the spatial profile of crowding, weakening associations with other measures such as RGC receptive field density (Kwon and Liu 2019). In light of this, reports of weak (or absent) associations might in fact be the product of commonly used estimation methods that target portions of the spatial profile of crowding which are sub-optimal when seeking associations with physiological structures.

Target-flanker similarity was found to modulate the span of the spatial profile of crowding, and the pattern of this modulation was similar at all levels of eccentricity investigated. Therefore, the visuo-spatially dependent weighting of responses to flanker features in weighted pooling models is different for flankers that are similar in appearance to the target, than for those that appear dissimilar. Differential weighting of responses to flankers that are similar and dissimilar to the target has been indicated in a recent study (Kalpadakis-Smith *et al.* 2022) and could potentially be the origin of similarity effects noted elsewhere (Ester, Zilber and Serences 2015). The findings presented in this chapter add that the modulation of weightings according to orientation difference may be predictable across target-flanker spacings within the crowding zone, and that this pattern of modulation is similar across the levels of eccentricity investigated.

Chapter 7 The association between crowding zone extent and RGC density

7.1 Introduction

Estimates of crowding zone extent have been used in a wide range of studies with a variety of aims (e.g. Kooi *et al.* 1994; Greenwood *et al.* 2012; Tailor *et al.* 2021; Kwon and Liu 2019; Ogata *et al.* 2019). The ability to disentangle estimates of crowding zone extent from similarity-dependent influences, as demonstrated in 6.4.2, may benefit studies such as these by removing the potential for confounding effects. Indicators of the extent of crowding zone that are independent of similarity-based modulation may then provide stronger evidence for associations between crowding zone extent and other psychophysical or structural measures which are not subject to such confounds. Demonstrating this may provide a route to explore how low-level structures such as retinal ganglion cells relate to the extent of visual crowding.

7.1.1 Linking crowding to low level visual structures

Different methods of estimating crowding zone extent are used in the literature, such as estimating the target-flanker spacing equating to different 'threshold' performance criteria which are often defined as being above 50% accuracy (e.g., Toet and Levi 1992; Greenwood *et al.* 2012; Kooi *et al.* 1994). Such methods do not differentiate between aspects of crowding which are sensitive and insensitive to target-flanker similarity, both of which were demonstrated in 6.4.3 to contribute to psychophysical estimates of the observed crowding zone. While these methods are suitable for

determining the presence of a difference between experimental conditions, characterising the spatial profile of crowding allows differences to be related to specific parameters of the spatial profile (i.e., the midpoint and the gradient). Measures of critical spacing will also conflate the simultaneous shift in midpoint and widening of the spatial profile with increasing eccentricity. As the midpoint of the spatial profile of crowding is invariant to target-flanker similarity and primarily associated with eccentricity, this may be a useful alternative indicator of the spatial extent of crowding when seeking associations with physiological structures. By focussing on the midpoint of the spatial profile, stronger associations with underlying low-level structures may be found.

A number of hypotheses for the origin of visual crowding have been reported, some of which propose links between crowding zones and cortical receptive fields (Freeman and Simoncelli 2011; He, Wang and Fang 2019). While crowding is widely understood to be a cortical phenomenon, cortical receptive fields that map to areas of the visual field are sampling the output of retinal ganglion cells (RGCs). This leads to the idea that the spatial extent of crowding may be particularly explained by low-level structural factors, and an association with the pooling of retinal ganglion cells has already been proposed (Kwon and Liu 2019). Pooling of retinal ganglion cell output is the driving factor behind the area of complete spatial summation of spot stimuli, also called 'Ricco's area' (Redmond *et al.* 2010a). If pooling of a critical number of RGCs underlies the spatial extent of crowding, then trends of the calculated number of RGCs within crowding zones and Ricco's area across eccentricity would be similar in shape (i.e., a horizontal line if exactly constant), though at very different numbers of RGCs.

Kwon and Liu (2019) reported a significant portion of the difference in crowding zone extent across visual quadrants was associated with the underlying density of retinal

ganglion cell receptive fields. By combining estimates of crowding zone area with values of receptive field density at the same location, numbers of ganglion cell receptive fields subserving crowding zones were calculated. The authors suggested that a constant, critical number of retinal ganglion cells may be associated with the extent of crowding zones across eccentricity, though they find ganglion cell density does not completely account for the differences across eccentricity in their data. They attribute the remaining unexplained variation to high-level cortical processes, particularly as they find a higher proportion of the variance in Ricco's area (which is not believed to have such attentional influences) is explained by RGC density with this same method. However, as they defined crowding zone extent as critical spacing, their comparisons over eccentricity may have been subject to confounds identified in 6.4.3. The spatial profile of crowding shifts in midpoint and becomes shallower as eccentricity increases. This could lead to increasing misalignment between critical spacing and the extent of crowding zones that are related to low-level factors, which may be better indicated by the midpoint of the spatial profile. The apparent negative trend in their figures showing RGC count within crowding zones across eccentricity may arise from increasing underestimation of crowding extent, which would not occur in their comparisons between visual quadrants where eccentricity was fixed.

Taking the midpoint of the spatial profile of crowding as an indicator of crowding zone extent avoids the confounding effect of changes in the gradient of the spatial profile across eccentricity. This has the potential reveal an association between zone extent and the arrangement of underlying RGCs where Kwon and Liu reported no statistically significant association. This study sought to investigate the association between the midpoint of the spatial profile of crowding and the underlying density of RGC receptive fields by calculating the number of RGC receptive fields underlying crowding zones

across eccentricity. By comparing the number of RGC receptive fields calculated with estimates of the midpoint and estimated derived with a threshold criterion above the midpoint, the study also aims to establish whether the midpoint provides and indicator of crowding zone extent that are better predicted by RGC density.

7.2 Methods

This study utilised the measures of the midpoint of the spatial profile of crowding as an indicator of crowding zone extent that is disentangled from other potentially confounding influences, as discussed in section 6.4.3. These disentangled measures were compared with another form of visual pooling (spatial summation) and used to test the association between crowding zone extent and the density of RGC receptive fields. Numbers of RGC receptive fields within Ricco's area and crowding zones were calculated. The effect of eccentricity on RGC receptive field counts was investigated, and the amount of variance explained by the proposed fixed number of ganglion cells was quantified. The three participants who took part in the study presented in Chapter 6 (see 6.2.1.1 for participant characteristics) also underwent estimation of Ricco's area detailed below.

7.2.1 Ricco's area

Ricco's area was estimated at the same three visual field locations as the crowding data (4.2°, 12.7° and 21.2° visual angle inferotemporal to the right eye), similar to the method of (Redmond *et al.* 2010b). Detection thresholds for luminance contrast (hereafter 'contrast thresholds') with 5 different sized white spots (Goldman I-V) were measured at the locations of interest using a method of constant stimuli, programmed with R (R Core Team 2021) and presented on an Octopus 900 perimeter (Haag-Streit UK, Essex, UK), controlled using the Open Perimetry Interface (Turpin, Artes and McKendrick 2012). The background luminance was 10 $cd.m^{-2}$. Thresholds were plotted against stimulus area and fitted with a hinged line model constrained such that the slope of the first section was -1 (in accordance with Ricco's law) while the

intersection, break point and slope of the second section were permitted to vary (Seber and Wild 2005). These free parameters were optimised with a nonlinear least squares procedure, and the break point of the optimised hinged line model is taken as a measure of Ricco's area at the test location. This produced one estimate of Ricco's area at each target location for each participant.

7.2.2 Area of the crowding zone

Measures of the spatial extent of crowding were taken from the data collected in the study presented in Chapter 6. Participants reported the perceived orientation of a Landolt-C target at 3 eccentricities inferotemporal to fixation in the right eye (4.2°, 12.7° and 21.2° eccentricity). The target was flanked by a pair of Landolt-Cs of identical diameter, located along the axis tangential to the meridian of the test location (Figure 6.1). Flankers were spaced at five fixed levels of target-flanker separation along this axis, measured from the centre of the target to the centre of a flanker. The orientation of the flankers was identical to each other and fixed at one of three possible orientation differences relative to the orientation of the target (±22.5°, ±90°, or ±180°; ±45° was also examined at one eccentricity). Stimulus sizes and target-flanker spacings were scaled for each level of target eccentricity. Collected responses were modelled with a describing the increase in proportion of target-centred responses with increasing target-flanker separation (a spatial profile of crowding, see 6.2.2.3). The midpoint of these logistic functions (the level of target-flanker spacing predicted to result in equal likelihood of reporting either the target or flanker orientation) was taken as a measure of the spatial extent of crowding.

This measure of extent was used to calculate an approximate area of the crowding zone. The formula of the area of an ellipse (π x $radius_{minor}$ x $radius_{major}$) was used as

an approximation for the area of the crowding zone to account for radial-tangential anisotropy (Toet and Levi 1992; Nandy and Tjan 2012). anisotropy (Toet and Levi 1992; Nandy and Tjan 2012). The target-flanker spacing described above (signified by 'c' in Equation 7.1 below) was estimated along the tangential axis, so is used as the minor radius. This value was scaled up by 2 to serve as the major radius, giving Equation 7.1*:*

$$\text{Area} = \pi \times c \times (c \times 2)$$

Equation 7.1 - Area of an ellipse

Area = Area of the ellipse (degrees^2)

c = Spatial extent of crowding zone (degrees)

The area of the crowding zone was calculated with Equation 7.1 using the spatial extents estimated at each target eccentricity and each level of target-flanker orientation difference at all target locations (±22.5°, ±90° or ±180°). This was done on a by-participant basis. This gave three estimates of crowding zone extent for each participant at each target eccentricity.

7.2.3 Calculating ganglion cell receptive field count

Ganglion cell density data was acquired from the online tool provided by Montesano *et al.* (2020) which utilises the histological data of (Curcio and Allen 1990). The tool was supplied with a custom grid of 1° area stimuli at field locations along the inferotemporal axis (i.e., the same axis along which crowding zone extent and Ricco's area were measured). The tool assumes an axial length of 23.84mm (Drasdo and

Fowler 1974) and calculates the number of ganglion cell receptive fields covered by the stimulus at each location, after accounting for receptive field displacement from the ganglion cell body. These counts are then taken as the density of ganglion cell receptive fields at each level of eccentricity, as the number of receptive fields divided by a 1° stimulus area gives density in receptive fields per degree visual area.

The number of ganglion cell receptive fields covered by each area of interest (Ricco's area and crowding zone area) were then calculated by multiplying each area by the receptive field density at each target location. (Note: This assumes that the density is constant across the span of retinal area on which the stimulus is superimposed.) Calculated values of the number of ganglion cell receptive fields encompassed within Ricco's area and crowding zones were then plotted against target eccentricity.

7.2.4 Comparing accounts of ganglion cell density

Following the intuition of Kwon and Liu (2019), three predictions can be made for the resulting shape of the function of ganglion cell receptive field count across eccentricity for both Ricco's area and crowding zones: If the change in retinal ganglion cell density completely accounts for the change in span of these areas, the number of cells underlying the area would be constant with eccentricity and the resulting function would be a horizontal line with a y-intercept equal to the number of encompassed ganglion cell receptive fields. Alternatively, if the change in retinal ganglion cell density has no contribution to the change in area with eccentricity, underlying cell number would increase as a function of eccentricity resembling the association between area and eccentricity. Thirdly, the function may lie between these two predictions if the change in underlying retinal ganglion cell density is only partly associated with the change in area.

For further comparison with the findings of Kwon and Liu (2019), these analyses were repeated with values of ganglion cell receptive field density indicated by Drasdo *et al.* (2007). As values are only given by Drasdo *et al.* for the main visual meridians (i.e., directly superiorly, inferiorly, nasally and temporally of the fovea), values of constants utilised in their model linking ganglion cell receptive field density and eccentricity were taken as the mean of values for the inferior and temporal meridians. All other calculations and analyses were as described above. Analyses were also conducted with midget RGC receptive field densities obtained from Watson (2014), using his online tool to acquire density estimates at the test locations.

7.2.5 Comparing ganglion cell counts with midpoint vs upper threshold estimates of crowding zone extent

Next, the effect of implementing different definitions of crowding zone extent on associations with RGC receptive field density were investigated using the same crowding data. A nominal threshold of 90% target-centred responses (p(Target) = 0.9) was used and estimates of target-flanker spacing expected to produce this distribution of responses were obtained from the fitted logistic models (see Chapter 6 methods) by logistic regression. (Recall that the detail-report paradigm of the crowding task (detailed in Chapter 6) results in no specifically defined threshold level of performance, as would be the case in an m-alternative forced choice paradigm. Therefore a 90% threshold is 'conventional' in that it targets the upper part of the spatial profile of crowding as opposed to the midpoint (50%), though the actual value varies depending on experimental setup). These estimates, determined with two separate definitions of crowding zone 'extent' were then used to calculate crowding zone area with Equation 7.1 above.

Individual values for RGC density at each eccentricity were estimated from contrast thresholds measured with Goldman III stimuli acquired above (see Methods - Ricco's area). Thresholds were converted to instrument-specific perimetric sensitivity (in decibels) and used to derive RGC density using Equation 7.2 below (Redmond *et al.* 2013) based on the model published by Swanson, Felius and Pan (2004). Note: The definition of the decibel unit is the same between the Octopus 900 and Humphrey Field Analyzer instruments (i.e. 1dB = 10 × log(L_A), where L_A is luminance attenuation from the maximum available in the instrument) and the maximum stimulus luminance of the instruments is the same (3,185 cd.m^2, or 10,000 apostilbs). The definition of sensitivity (approximating 50% seen on the psychometric function using a 1-up/1-down staircase (Levitt 1971)) is also the same as the Full Threshold perimetry strategy used to obtain the data (Heijl, Lindgren and Olsson 1987) to which Swanson, Felius and Pan (2004) fitted their 'hockey-stick' model, so therefore converge to the same point.

$$\frac{RGC}{Deg^2} = \begin{cases} \dfrac{10^{0.1 \times (dB-16)}}{a_r} & \text{if } dB < 31 \\ \dfrac{10^{0.4 \times (dB-27.44)}}{a_r} & \text{if } dB > 31 \end{cases}$$

Equation 7.2 – RGC density from contrast sensitivity

dB = Contrast detection threshold of Goldman III stimulus (decibels)

a_r = Area of Goldman III stimulus (0.145 Deg.^{2})

Two equations were used, depending on the level of sensitivity, as a reflection of the two-phase function presented in the original paper (Swanson, Felius and Pan 2004). A value of 0.145 was used for a_r as this is the area of a Goldman III stimulus in

degrees^2. The critical value of 31 dB is the threshold sensitivity of a stimulus identical in size to Ricco's area, the maximum stimulus size to undergo complete spatial summation (Pan *et al.* 2006).

RGC count within Ricco's area and crowding zones was calculated at each target eccentricity for each participant. As crowding zone extent was estimated from data collected with three levels of target-flanker orientation difference, RGC counts within crowding zones could also be stratified by orientation difference used.

7.3 Results

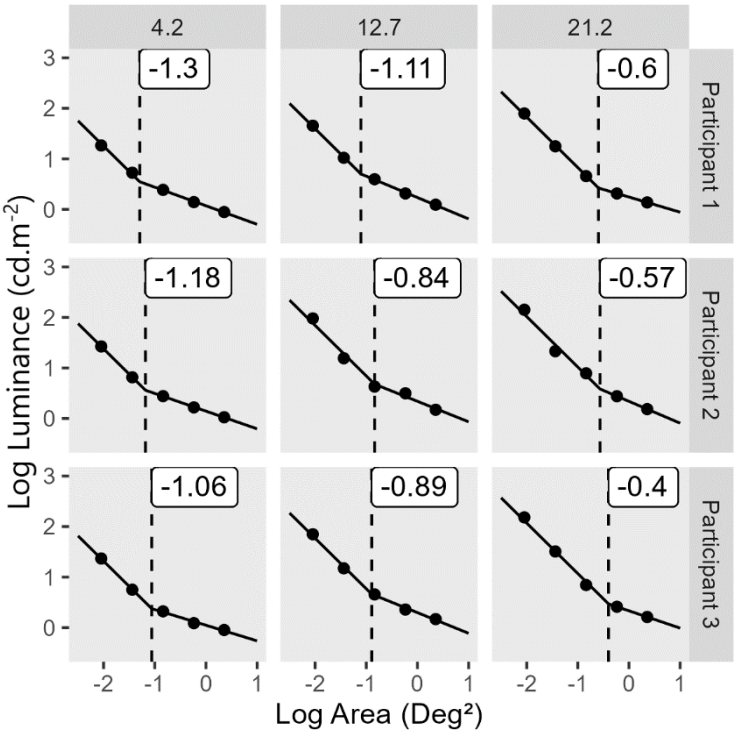

Figure 7.1 - Ricco's area estimated with two-phase linear regression

Threshold estimates for spot stimuli of Goldman sizes I-V (left to right) obtained in a seen/not seen task as in standard automated perimetry are shown by black data points. Plots are arranged by participant (rows) and for three levels of target eccentricity (columns, increasing left to right). Black lines show the fitted two-phase linear regression, wherein the slope of the first phase was fixed to -1 while the slope of the second phase and the breakpoint between phases weas permitted to vary. The breakpoint is taken as a measure of Ricco's area, the maximum area of complete spatial summation. Stimuli larger than this area undergo incomplete summation, giving a shallower slope. Log Ricco's area values are also shown in the white box within each panel.

Spot detection threshold data are shown in Figure 7.1 with the fitted two-phase linear regressions used to estimate Ricco's area. Each panel also gives the estimate for Ricco's area in degrees^2. Ricco's area can be seen to increase with eccentricity in a similar pattern for each participant in Figure 7.2 panel A.

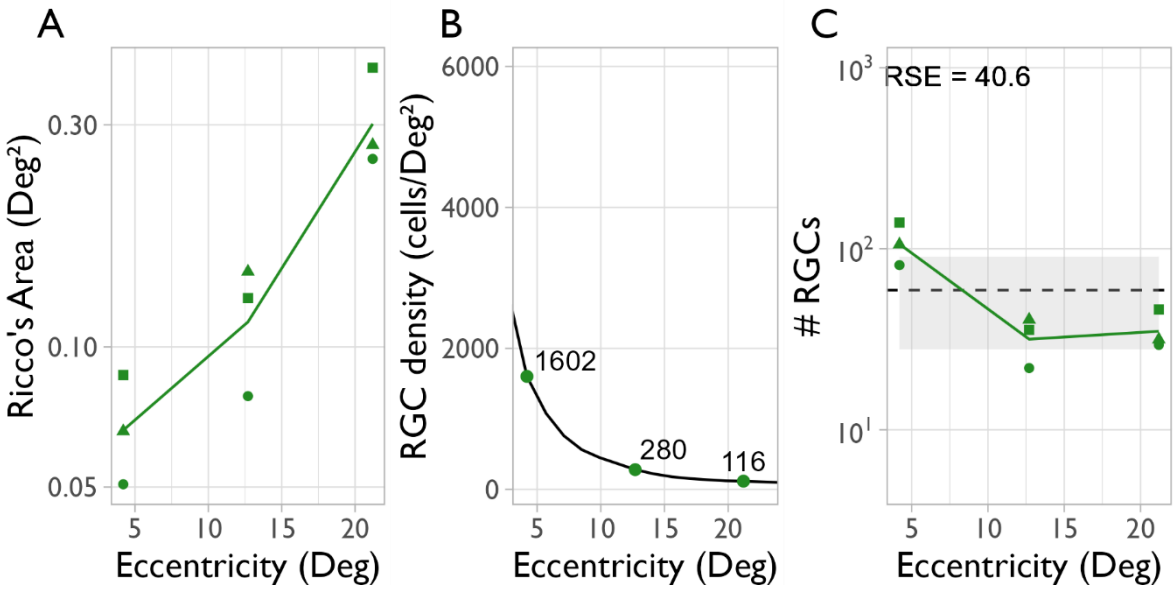

Figure 7.2 – Calculating the number of ganglion cell receptive fields underlying Ricco's area

A) Ricco's area estimated with two phase linear regression in three participants at three eccentricities. B) Retinal ganglion cell receptive field densities obtained from the online model of Montesano et al. (2020). C) Ganglion cell receptive field count calculated by multiplying Ricco's area estimate (panel A) by ganglion cell density (panel B). Green data points show actual receptive field count calculated with receptive field density values at each eccentricity. The dashed horizontal line shows the fitted linear model indicating a fixed number of ganglion cell receptive fields under Ricco's area obtained in this study (grey area indicates 95% confidence interval). Also shown is the residual standard error (RSE) of the model.

Values of retinal ganglion cell receptive field density, and subsequently calculated numbers of receptive fields encompassed within Ricco's area are also shown in Figure 7.2, panels B and C, respectively. The calculated numbers of receptive fields under Ricco's area (green data, panel C) are greatest at the smallest eccentricity (4.2° visual angle, mean 109 receptive fields). At the two further eccentricities, numbers of receptive fields underlying Ricco's area are similar to each other (mean 34 receptive

fields). The mean across eccentricities (black dashed line, Figure 7.2 panel C) indicated that 59 retinal ganglion cells would subserve Ricco's area under the hypothesis that this value was constant across the retina. However, the data at the smallest eccentricity appear to depart from this proposed relationship.

Figure 7.3 panel A shows the estimates of crowding zone area calculated with Equation 7.1 and the midpoint extents of logistic functions fitted to crowding data presented in Chapter 6. Three midpoint values were utilised from each participant at each eccentricity, obtained with three levels of target-flanker orientation difference (see 6.3.3). This gave 9 values of crowding zone area at each eccentricity (i.e., 3 from each participant). A confirmatory analysis using only the mean of each participant's midpoint values gave the same overall results, so all values of crowding zone area were utilised here. Figure 7.3C shows calculated numbers of RGC receptive fields underlying crowding zones at three eccentricities. Ganglion cell count (product of crowding zone area and receptive field density at each eccentricity) increases with eccentricity). The hypothetical fixed number of retinal ganglion cells subserving crowding zones (indicated by the fitted linear model) was 19,122 ganglion cells. However, the pattern of the data suggests ganglion cell density may only partly contribute to the change in crowding zone extent with eccentricity.

The analyses were repeated with density values indicated by Drasdo *et al.* (2007) and midget RGC density from Watson (2014), the results of which are shown in Appendix 1. The calculated numbers of RGC receptive fields within Ricco's area and crowding zones were lower (slightly with the Drasdo function and lower again with the Watson function of mRGC density). However, overall patterns of the data remain unchanged from that shown above.

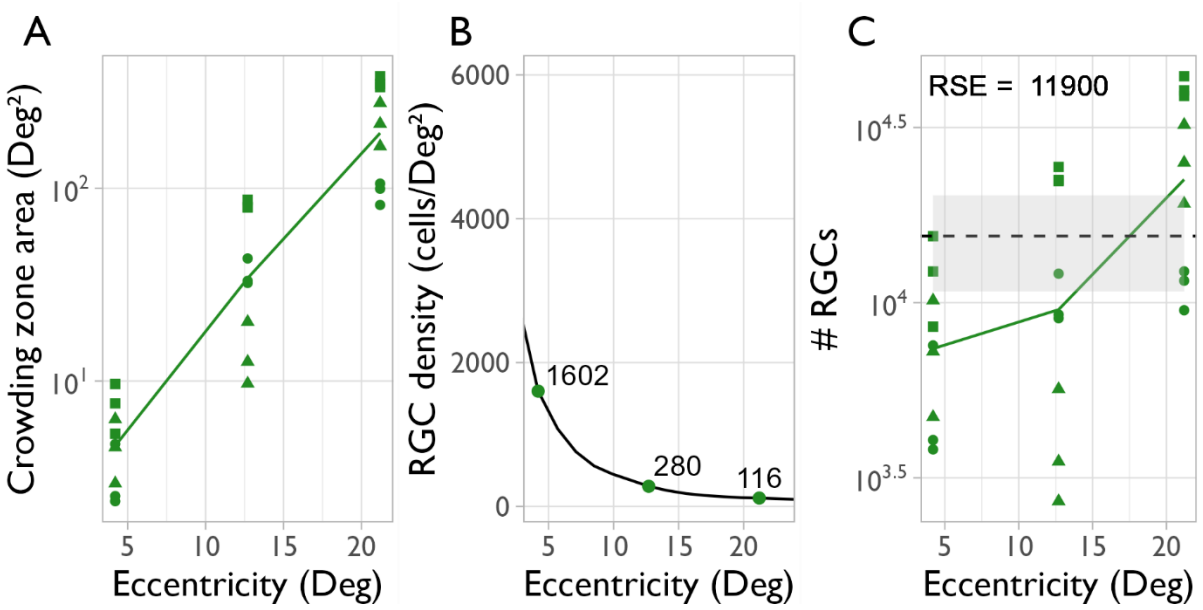

Figure 7.3 – Calculating the number of ganglion cell receptive fields underlying crowding zones

A) Crowding zone area estimated with Equation 1 and crowding zone extents estimated with 3 observers and 3 target-flanker orientation differences at 3 eccentricities. B) Ganglion cell receptive field densities obtained from the online model of Montesano et al. (2020). C) Ganglion cell receptive field count calculated by multiplying crowding zone area estimate (panel A) by ganglion cell density (panel B). Green data points show calculated ganglion cell count calculated with receptive field density values. The dashed horizontal line shows the fitted linear model corresponding to a fixed number of ganglion cell receptive fields under crowding zones obtained in this study (gray shading indicates the 95% confidence interval). Also shown is the residual squared error value.

Figure 7.4 A shows individual estimates of RGC density derived from contrast thresholds. Density values are generally lower than those of Montesano *et al.* (2020), but show a similar decrease with eccentricity. The number of RGC receptive fields

underlying Ricco's area (panel B) are approximately constant across eccentricity at 20 ganglion cell receptive fields.

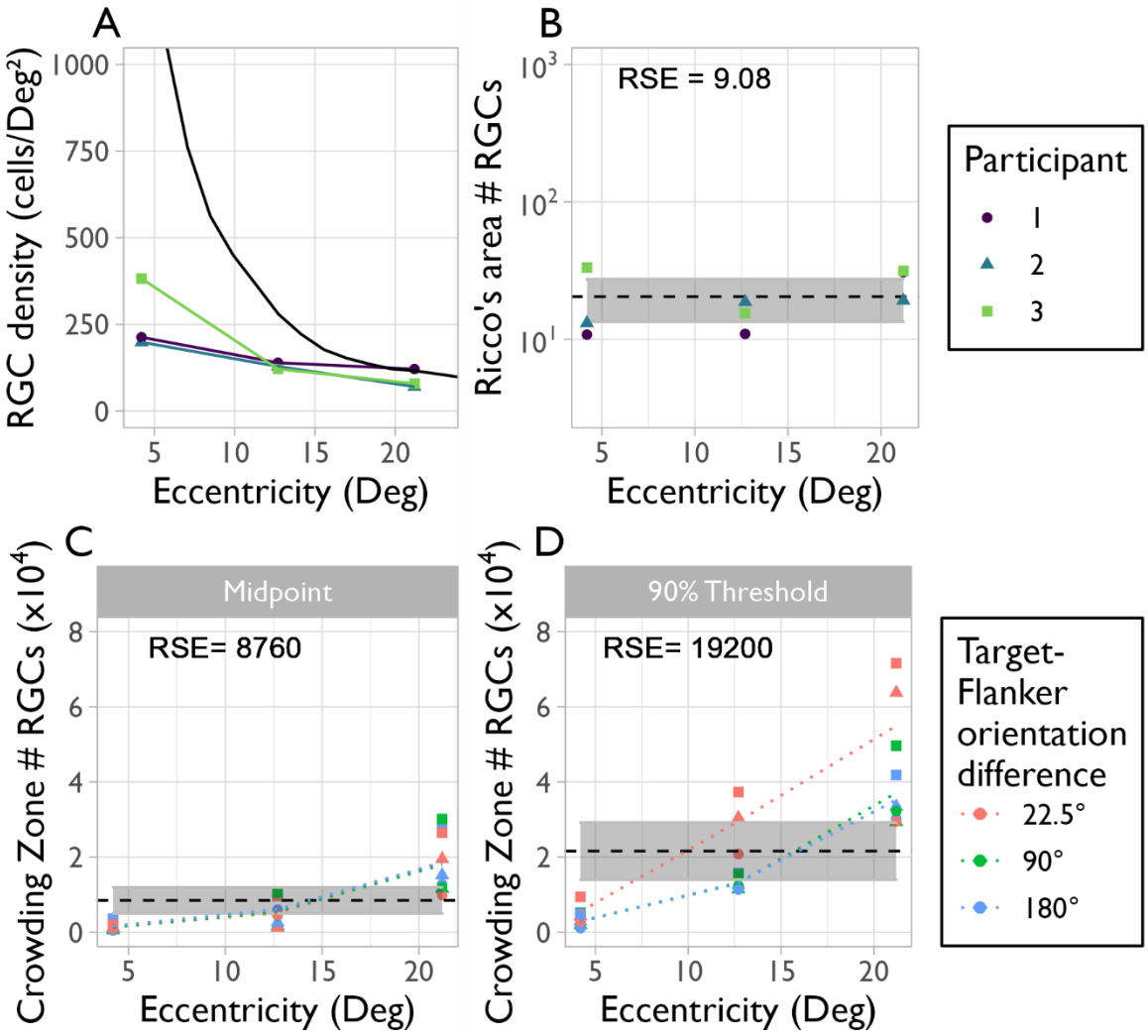

Figure 7.4 - Individual estimates of RGC count within Ricco's area, and crowding zones estimated with midpoint and 90% threshold extent measures

Panel A shows individual estimates of RGC density at each location estimated with a spot detection task. Coloured lines indicate each participant's own data and the black curve shows the values given by Montesano et al. (2020) for comparison. Calculated numbers of RGCs underlying Ricco's area (panel B) and crowding zones estimated with midpoint (C) and 90% threshold (D) measures of crowding zone extent. The dashed black line in each panel shows the fitted linear model which would indicate the fixed number of RGCs serving each area. Panels C & D also show dotted lines indicating mean RGC count stratified by orientation difference between target and flankers in the crowding task (see Chapter 6). Grey areas indicate 95% confidence intervals of fitted models, RSE = residual standard error.

Outcomes of implementing different definitions of crowding zone extent are shown in Figure 7.4 C and D. Greater numbers of RGC receptive fields underlying crowding zones were produced by the 90% threshold estimate data, as values of crowding zone area were larger. Both datasets indicate a positive trend, suggesting the number of RGC receptive fields underlying crowding zones increases with eccentricity, and thus only a partial contribution of RGC density to this change in both instances. Comparing the two panels, midpoint estimates of crowding zone extent produced RGC counts (panel C) which are closer to being constant over eccentricity (i.e., a horizontal line) than the 90% threshold estimates (panel D). While neither dataset show a perfect relationship, the steeper gradient seen in the mean trend line in panel D, and greater value of residual standard error in the fitted model, indicates a greater departure from association with RGC density.

Figure 7.4 panels C and D also show the mean trend lines stratified by target-flanker orientation difference used in the crowding task (dotted lines, coloured by level of orientation difference). With midpoint estimates of crowding zone extent (panel C), the data are well aligned. Conversely, 90% threshold estimates of crowding zone extent led to a separation in the trends of data obtained with different target-flanker orientation differences. In particular, the data obtained with the smallest orientation difference (i.e. greatest target-flanker similarity) led to larger estimates of crowding zone extent and subsequently greater numbers of RGCs within the crowding zones. These calculated numbers of RGCs also increased at a greater rate in the small orientation difference data than was seen in the large orientation difference data.

7.4 Discussion

The extent of Ricco's area and crowding zones could be (at least partially) associated with RGC sampling density. Using individual estimates of RGC receptive field density based on functional measures (Pan *et al.* 2006), and estimates of crowding zone extent that are free from confounding influences, similar trends are found in ganglion cell count underlying each area over eccentricity (Figure 7.4). The constant number of RGC receptive fields underlying Ricco's area agrees with the findings of previous reports (Vassilev *et al.* 2005). While the number of RGC receptive fields underlying crowding zones does not appear to be exactly constant in the present data, the association is much closer when the midpoint of the spatial profile is used as a measure of crowding zone extent, in comparison to the 90% threshold spacing. This is particularly shown by the steeper gradient in the 90% threshold data (Figure 7.4D) and the greater residual squared error of the model in comparison to the midpoint data (7.4C).

The results of this study suggest that midpoint estimates of crowding zone extent may indicate stronger associations with observations of related physiology. The increase in crowding zone area with eccentricity showed an association with the fall in retinal ganglion cell receptive field density, though the pattern of the data indicates only a partial contribution. Comparing midpoint estimates of crowding zone extent with 90% threshold estimates extracted from the same data revealed a closer association between midpoint extent estimates and underlying ganglion cell density. However, the calculated number of RGCs within estimated crowding zone area was not constant over the eccentricities examined. Nevertheless, this study suggests that disentangling estimates of crowding zone extent from non-spatial aspects of crowding may be useful

when relating observed effects of crowding to spatial aspects of visual physiology such as RGC density.

When estimates of crowding zone extent are disentangled from non-spatial aspects of crowding, subsequently calculated numbers of RGCs within the crowding zone area are more concentrated at each eccentricity and show a closer association with RGC receptive field density over eccentricity. This may indicate that the midpoint of the spatial profile of crowding is more closely associated with the physiological structures underpinning crowding than more conventional threshold-based estimates of crowding zone extent (i.e., associated with performance criteria >50%). As the number of RGCs within the crowding zone was not constant across eccentricity, this may suggest the spatial extent of visual crowding arises from the combined output of responses from cortical cells which themselves receive input from non-constant numbers of ganglion cells. Disentangling aspects of crowding which are frequently confounded may provide a route to better explore different stages of processing which may contribute to reported effects. For example, crowding zone extent could be compared with the pooling behaviour of different visual areas either directly with imaging techniques such as population receptive field mapping during crowding tasks (He, Wang and Fang 2019; Ozkirli *et al.* 2021) or indirectly through comparing psychophysical findings to confluence of the retinotopic map in different visual areas (Pelli 2008; Strasburger 2022; Kurzawski, Pelli and Winawer 2021).

Measures of the extent of crowding used in studies seeking associations with physiological measures may benefit from being separated from similarity-dependent aspects of crowding, as these may arise from different stages of visual processing. The steepness of the spatial profile of crowding (or the span of the transitionary zone – see 6.3.2) could be mediated by the action of a process separate to that which

determines the spatial extent of the crowding zone, and may even distort associations with physical structures. The results of the 90% threshold estimates of crowding zone extent indicate a greater number of RGCs may be involved when targets and flankers are more similar in appearance. Such a suggestion could infer a similarity-based modulation of the number of ganglion cell inputs, following a top-down style 'grouping' process (Malania, Herzog and Westheimer 2007). Alternatively, a pooling-based mechanism, by which the contribution of dissimilar flankers to the pooled response is more easily distinguished from that of the target (leading to a down weighting of flanker-centred responses in perceptual reports) could indicate that crowding interactions in fact occur over a wider, fixed distance. Within this 'maximum possible extent of spatial interactions', flankers that are more easily distinguished may appear to shrink the apparent crowding zone observed psychophysically by reducing the frequency of flanker-centred reports at larger target-flanker separations, though these may still invoke some perceptual representation these distances. Conventional threshold-based estimates of crowding (utilising criteria >50%) may weaken or obscure the associations between crowding extent and physical structures, as evidenced in the weaker association with RGC density in this study, as these non-spatial (possibly decisional) aspects influence the span of the transitionary area and confound estimates of crowding zone extent.

The link between crowding zone extent and RGC density should be considered carefully. Indeed, the suggestion of a fixed number of RGC receptive fields subserving Ricco's area and crowding zones across the visual field may not match the appearance of the data here. Focussing on the crowding zone data shown in Figure 7.3 and panels C and D of Figure 7.4, the calculated number of retinal ganglion cells appear to increase with eccentricity. This suggests that the change in RGC density

does not fully explain the change in crowding zone area over eccentricity seen in these data. A similar pattern was also seen with counts of midget retinal ganglion cells (Figure A1.2). Alternatively, crowding zone extent may better reflect the receptive field of some cortical processing unit which itself employs a non-constant number of retinal ganglion cells over eccentricity, possibly by sampling the retinotopic map of lower visual areas (Motter 2009).

Kwon and Liu (2019) reported a lower proportion of the variance in crowding zone area was explainable by the underlying RGC density than the variance in Ricco's area over the same change in eccentricity (81% vs 89% across eccentricity alone, 74% vs 90% when also compared across different visual quadrants). They attribute this difference to crowding zones being subject to high-level cortical factors also contributing to their estimates of crowding zone extent. The measures of extent used in this study have been disentangled from target-flanker similarity-dependent aspects of crowding (explained in 6.4.2). Using the equations stated by Kwon & Liu, the difference in contribution between variance in Ricco's area and crowding zones explained by underlying RGC density in this experiment was in fact much closer (95.4% and 99.6% respectively). While this could be taken as an indicator that underlying RGC density significantly contributes to crowding zone area, this may in fact be an artefact of experiment design. Variance in the 'zero-contribution' condition (where an artificially constant value of RGC receptive field density is used at all eccentricities – see Kwon and Liu (2019)) is particularly inflated at greater eccentricities (where greater variability in can be seen in the spread of data points in Figure 7.3 panel A) compared to more central locations. This is also exacerbated by a wider range of eccentricities being examined (4.2˚ to 21.2˚ in this study, 4.5˚ to 18.5˚ by Kwon and Liu (2019)) leading to a greater discrepancy between the 'actual' RGC

density at the greatest eccentricity and the value used to produce the 'zero-contribution' data. Together, these exaggerate the difference between $RSS_{ZeroContribution}$ and $RSS_{ActualResults}$, resulting in a larger apparent percentage contribution of RGC density in the present data. While these calculations are an indicator that crowding zone area follows a moderately similar trend to RGC density over eccentricity, comparisons beyond this (particularly between experimental designs) may not be appropriate.

Inferences of the true numbers of ganglion cells subserving crowding zones are limited by the assumption of an elliptical crowding zone shape with 2:1 radial-tangential extent ratio. As the radial extent was not measured experimentally, this ratio was chosen both to follow the method of Kwon and Liu (2019) (though their experiment utilised radially-spaced flankers, reflected in their ellipse area calculation), and to approximate the range of radial-tangential extent ratios reported in the literature (Kwon *et al.* 2014; Toet and Levi 1992; Nandy and Tjan 2012; Bex, Dakin and Simmers 2003; Petrov, Popple and McKee 2007). The overall pattern of results was unaffected by changing the scaling ratio between radial and tangential extents, but the calculated numbers of ganglion cells varied dramatically. It is also important to recall that the measures of extent used in this study relate to the midpoint of the spatial profile of crowding, at which spacing crowding effects are already prominent (Figure 6.6). Though this measure may show clearer associations with contributing physiology and other spatial measures, the true full extent of spatial interactions is expected to be much larger. As the predicted numbers of ganglion cells serving the crowding zones were already much higher than those reported by Kwon and Liu (2019), attempts to match their predicted numbers of ganglion cells were not informative. As well as the points mentioned above, differences in the crowding task design and experimental setups

likely contributed to the difference in crowding zone area and calculated numbers of ganglion cell receptive fields.

The findings of this study indicate a non-constant number of retinal ganglion cells are found within crowding zones across increasing target eccentricity. While an association is indicated, RGC density (either from the published values or individualised estimates) does not fully explain the observed increase in crowding zone area. The secondary outcome of this study is the assertion that midpoint estimates of crowding zone extent may be more directly reflective of potentially associated structural measures such as RGC density, than estimates obtained with more typical threshold-based methods. By removing the effect of similarity-dependent aspects of crowding, the spatial extent of the crowding zone may be more directly mapped to physical structures. Therefore, future research should consider how best they might probe the spatial profile of crowding to explore their hypotheses, as disentangled measures of crowding zone extent may enhance the explanatory power of such investigations.

Chapter 8 Thesis conclusions

This thesis set out to investigate the detailed perceptual effects that occur when flankers traverse the edge of the crowding zone. In evaluating the spatial interactions of crowding effects in stimuli defined by orientation, a method was developed to map the spatial profile of crowding. This model of crowding relates the distribution of detailed reports of a crowded target's appearance to the spatial separation between the target and flankers. Experimental data fitted with this model reveal that profiles of crowding share a common spatial characteristic, the midpoint of the function, which increases with target eccentricity but is unaffected by target-flanker similarity. When this midpoint separation is taken as an indicator of crowding zone extent, the area of the crowding zone shows a clear (though imperfect) association with the density of retinal ganglion cell receptive fields at the same target eccentricities. This indicates that for the arrangements of stimuli used, the spatial extent of crowding is associated with low-level structural factors (RGC density) and primarily varies with target eccentricity while remaining invariant of changes in target-flanker similarity. Flanker orientation relative to the target instead affects the span of the transitionary zone between minimal and maximum crowding effects, that is centred on the midpoint separation. When flankers are dissimilar in target appearance to the target, this transitionary zone is narrower, compared to when flankers are similar in appearance to the target. In this thesis, it is proposed that characterising the spatial profile of crowding via these two identifying parameters (the midpoint and transitionary span) provides measures that may be more strongly associated with physiology underpinning the extent of crowding zones by disentangling the effects of flanker appearance on the apparent extent of the crowding zone.

These findings give new perspective on experimental estimates of crowding zone extent and are particularly relevant in instances where the physical structures underpinning visual crowding are the object of interest. Commonly used methods of estimating crowding zone extent (critical spacing and threshold spacing, which typically utilise thresholds above 50%) probe the outer limits of the transitionary zone, which may be simultaneously influenced by the extent of physiological structures facilitating crowding interactions, and perceptual (or decisional) effects arising from flanker appearance. This could weaken comparisons between such estimates of crowding zone extent where it may remain uncertain whether differences are the result of a structurally determined span of interaction (such as the size of a cortical receptive field), or an alteration to the integrative mechanisms occurring within this span. Taking only these confounded estimates of crowding zone extent may also obscure the underlying mechanisms producing differences in crowding with visual disorders, where structural and perceptual factors may both deviate from those expected in healthy vision. This thesis demonstrated a methodological format which may help to address these confounds and could provide new insight into crowding in both healthy and abnormal vision. A speculative avenue for future research informed by the findings of this thesis is also proposed, which could potentially provide a step towards a unifying structural account for visual crowding. It is anticipated that the findings of this thesis will also help to inform the design of future experiments by emphasising the importance of considering which aspects of crowding are targeted by different methodological approaches.

8.1 Review of experimental findings

After establishing the technological setup, participant criteria and initial experimental method in Chapter 2, Chapter 3 sought to optimise stimulus scaling to the peripheral acuity of individual participants. The results support the established understanding that crowding zone extent is invariant of target size (Levi, Hariharan and Klein 2002b; Tripathy and Cavanagh 2002; Strasburger, Harvey and Rentschler 1991) and showed that setting the size of stimuli individually for each participant to ensure they were above individual acuity thresholds would be valid with this method. However, the bimodal distributions of some groups of data indicated that more information could be gained with a change to the methods of data collection and analysis. While the initial method focussed on the overall spread of errors made due to crowding, further leveraging the systematic nature of crowded responses had the potential to provide insight into the spatial dependencies of crowding interactions.

In Chapter 4, the limitations of the initial method were presented; as well as the assumptions and required methodological decisions; and the reasons a change in method would be beneficial. A new analytical method was developed to take full advantage of the systematic patterns of errors observed under visual crowding and more thoroughly investigate how the distributions of these errors changed as flankers varied in spacing from the target. This new method utilises a population pooling model to quantify the proportion of responses remaining centred at the target orientation in the presence of flankers. Applying this method of analysis to the data that had already been collected up to this point proved unsuccessful for much of the data. Therefore, a change in experimental method was designed both to overcome the limitations of the previous method, and to compliment the newly developed analysis techniques.

Chapter 5 presented two experiments, each with a related research question: Does unequal cortical magnification of radially spaced flankers contribute to the in-out anisotropy frequently reported in crowding research? Study 1 (section 5.2was conducted with a cohort of untrained participants utilising the initial experimental method. The results suggested that scaling flankers according to their eccentricity with a general cortical magnification function had little impact on the estimated extent of the crowding zone. Study 2 (section 5.3 examined this question further by asking whether modelling each observer's own cortical magnification function and scaling flankers individually for each participant would reveal a potential effect. Implementing the newly developed experimental method, the distributions of errors under crowding were found to be very similar between scaling conditions. This is despite altered edge-to-edge spacing between targets and flankers arising from changing flanker diameter, indicating it is the centre-to-centre separation of target and flankers that mediates the magnitude of crowding effects in this stimulus arrangement. The results of both Study 1 and Study 2 suggested that scaling stimuli to account for cortical magnification (to equate the cortical representation of stimuli along the radial axis) had little impact on the observed effects of crowding.

The overall aim of the experiments outlined in Chapter 6 was to investigate the simultaneous influences of eccentricity and target-flanker similarity on the distributions of errors made under crowding. This investigation established the ability of the method (outlined in section 4.5) to disentangle similarity-dependent influences on apparent crowding zone extent from factors that are independent of target-flanker similarity. Quantifying proportions of target- and flanker-centred reports of perceived target orientation as target-flanker spacing was altered revealed a systematic pattern in the change in responses. Responses shift from being target-centred when flankers are

distant to being mostly centred at the flanker orientation when flankers are positioned close to the target. Modelling this shift in responses as a logistic function showed that changing target-flanker orientation difference altered the rate at which responses shifted as flankers approached the target in visual space. When flankers are offset in orientation by a small amount, the shift in responses occurs over a wide transitionary span, while flankers oriented further away from the target orientation induced more concentrated, 'step-like' shifts in responses (see Figure 6.6). The key finding was that these functions shared the same midpoint, dependent on their eccentricity. That is, the spacing at which the orientation of the target was equally likely to be reported at or around the orientation of the target or the flankers was unaffected by the actual orientation difference between them. This spacing was found to change with target eccentricity, being smaller at more central eccentricities and larger in peripheral vision (see Figure 6.9), which is a long-established hallmark of crowding zones (Bouma 1970; Toet and Levi 1992). Taken together, these inferences reveal a profoundly different way of defining the spatial extent of the crowding zone; using the midpoint of the spatial profile of crowding provides a measure of zone extent which is unaffected by feature-dependent influences on perception of the crowded target. Such feature-dependent effects were revealed by the target-flanker orientation difference in this experiment to affect the span of the transitionary zone in which the shift in perceptual reports occurs, but the location of the zone was unaltered. The modulating effect of target-flanker similarity on the span of the transitionary zone was found to scale consistently with the location (midpoint) of the spatial profile over three levels of eccentricity, shown in Figure 6.9. These influences are likely confounded in most typical methods of estimating crowding zone extent. Disentangling these aspects of crowding is made possible by systematic and comprehensive collection of detailed

reports of target appearance, and the novel method of quantifying responses under visual crowding, which permits profiling the edge of the crowding zone.

In Chapter 7, the midpoint of the spatial profile of crowding was utilised as an indicator of crowding zone extent to calculate crowding zone area. This was then used to investigate whether the change in crowding zone area over eccentricity could be associated with decreasing retinal ganglion cell (RGC) receptive field density. Combining estimates of the midpoint at three levels of target eccentricity with individual measures of RGC receptive field density at corresponding retinal locations, the calculated number of RGCs within the area of the crowding zone was found to increase with eccentricity. This is at odds with the published proposal of a constant number of RGCs within crowding zones across the visual field by Kwon and Liu, (2019), though their study infers this largely from simulations and did not observe a constant number across eccentricity in their experimental data.

In Chapter 7, the resulting counts of RGCs within crowding zones measured at the midpoint of the spatial profile, and from a more conventional definition of threshold-spacing with a high performance criterion, were compared. The results showed a closer association between RGC receptive field density and midpoint-based estimates of crowding extent, as compared to threshold estimates associated with a higher criterion (see section 7.3). This supports the proposal that the midpoint of the spatial profile of crowding is more closely related to underlying physiological structures. However, the non-constant number of RGC receptive fields within crowding zones across levels of eccentricity suggests that RGC density may not be the primary explanatory factor determining crowding zone area. The proposal is also supported by the finding that a more conventional definition of crowding zone extent led to the illogical result that very different numbers of RGCs are employed when target-flanker

similarity is altered. Structural and perceptual factors associated with crowding are confounded if the threshold criterion is above the midpoint. Hypothetically, if fewer numbers of RGCs were truly employed when targets and flankers are dissimilar (as would be suggested by common threshold-spacing estimates and critical spacing), then a common midpoint in the spatial profiles of crowding obtained with similar and dissimilar flankers would not be expected. Instead, the spatial profile of crowding with dissimilar flankers would be expected to be more simply translated along the separation axis, reducing the target-flanker separation corresponding to the midpoint. Therefore, the spatial extent of crowding (which can be indirectly estimated from the midpoint of the spatial profile of crowding) is associated with structural factors related to the density of RGC receptive fields, which may subsequently drive the size of receptive fields in the cortical region responsible for crowding. Higher visual areas with non-constant confluence of RGC input (Harvey and Dumoulin 2011) may potentially show a more complete relationship.

Overall, the findings of the thesis show that while common psychophysical estimates of crowding zone extent are influenced by various factors (van den Berg, Roerdink and Cornelissen 2007), these may reflect changes to both the location (midpoint) and span of the spatial profile of crowding. These differentiable elements of crowding behaviours remain confounded by frequently reported measures of crowding zone extent (both critical spacing and threshold spacing), but each may have very different associations with underlying physiology. This poses a potential problem to the inferences gained from comparisons of such measures, particularly in instances where assumptions about the structures and mechanisms that produce crowding effects may not hold (e.g., in the presence of pathology).

The thesis also reaffirms several commonly understood views of crowding effects, while also presenting a new perspective on the properties and physiology of crowding zones. Crowding leads to systematic errors in the perceived appearance of a target (Greenwood, Bex and Dakin 2010; Harrison and Bex 2015) which occur over a target-flanker distance strongly linked to target eccentricity (Bouma 1970; Toet and Levi 1992) and reports of target appearance are strongly influenced by flanker appearance and similarity to that of the target (Ester, Klee and Awh 2014; Ester, Zilber and Serences 2015; Kalpadakis-Smith *et al.* 2022).

8.2 Overall findings

This thesis presents a novel model of the edge of the crowding zone, the spatial profile of crowding, characterised by two key parameters: the location (or, midpoint) of the profile, and the span of the transitionary zone. While commonly used methods of estimating crowding zone extent probe the outer limit of the transitionary zone, instead assessing the location and spread of the spatial profile (both of which contribute to measures like critical-spacing) provides a novel perspective on crowding behaviour.

A key aspect which differentiates the spatial profile from standard psychometric data and functions presented in some studies (Kooi *et al.* 1994; Flom, Weymouth and Kahneman 1963) is that the spatial profile is developed from modelling detailed distributions of reports of target appearance. Gaining participant reports of perceived target appearance in this way prevents effects arising from a limited number of response alternatives, which may produce misleading results when observers have no option to report the appearance of a flanker at the target location (Reuther and Chakravarthi 2020). This also avoids the need for a response criterion to determine

‘correct’ or ‘incorrect’ responses which may be inappropriate for the mixtures of response types reported in similar data (Harrison and Bex 2017). Providing a fine-grain response scale also effectively removes the lower bound of expected performance produced by the false-positive reporting of target details in trials where poor performance is expected (these differences are discussed in more depth in section 4.3 The overall benefit is that this construction of the spatial profile of crowding can be related to the weighted pooling model fitted to participant reports to predict the expected distribution of reports at different target-flanker spacings and relative orientations of flankers to the target. Quantifying crowded reports as the proportion of responses corresponding to target appearance in the weighted pooling model gives logical upper and lower bounds to the crowding metric – greater than 100%, or fewer than 0%, target responses are impossible but 100% target-centred and 100% flanker centred responses are seen in a number of datasets (see Figure 6.6). Therefore, fitting a spatial profile of crowding between these bounds describes the observed patterns of responses well and produces two identifying parameters which can be individually investigated: the location (or, midpoint) of the spatial profile, and its gradient (which translates to the spread of the transitionary zone between minimal and maximum effects of crowding). Current literature primarily utilises either only the threshold-separation of a psychometric function (Kooi *et al.* 1994) while the gradient of spatial psychometric functions receives little attention, or uses critical-spacing to infer an outermost limit of the observed crowding zone (Pelli, Palomares and Majaj 2004). Neither of these approaches can predict perceived target appearance with varying target-flanker separation, and both achieve only single samples of the outer edge of the spatial profile of crowding. As a result, such measures may overlook how aspects

of the spatial profile of crowding can vary when used as a primary outcome measure in experiments.

Evaluating the spatial profile may be particularly helpful when drawing connections to underlying physiology and information pathways, such as relating crowding zone extent to retinal ganglion cell density (Kwon and Liu 2019) or the span of cortical receptive fields (Freeman and Simoncelli 2011; He, Wang and Fang 2019). The experiment in Chapter 6demonstrated that changes in target-flanker similarity can modulate the spread of the spatial profile while the midpoint remains unchanged (see Figure 6.6 Figure 6.7). Conversely, increasing target eccentricity moved the location of the spatial profile further from the target and increased the spread of the spatial profile simultaneously. The results of Chapter 7 indicate that the shift in midpoint with target eccentricity was more closely associated with the density of underlying RGC receptive fields, as compared to threshold-spacing estimates with high performance criteria. Therefore, the use of such threshold-spacings or critical-spacings alone may obfuscate inferences relating to underlying physiology. Instead, measures of the spatial profile of crowding may be more indicative of the extent of spatial interactions determined by associated physiology independently of target-flanker similarity. The following section (8.3Implications for crowding research) will discuss the predictions of this hypothesis with respect to research in typical and atypical vision.

There are three main caveats to the hypothesis that the location of the spatial profile of crowding is invariant for target-flanker similarity and indicative of underlying physiology.

The values of the location and gradient of the spatial profile of crowding may be specific to the stimuli and crowded features used in the thesis. Evidence that crowding

effects across different stimulus features can be dissociated (Greenwood and Parsons 2020) suggests that different stimulus features undergo crowding independently. Therefore, tasks requiring participants to report different aspects of a target (such as orientation and colour hue) may produce different spatial profiles of crowding, even if stimulus features were otherwise identical between tasks. Therefore, while the principle of the similarity-invariant midpoint may be expected to generalise to other stimulus features demonstrating crowding, it is presently unknown whether their spatial profiles may share the same fixed midpoint or patterns of similarity-based modulation as observed here with oriented Landolt-Cs.

Modulation of the spatial profile seen in Chapter 6 results from quite small alterations to flanker appearance (i.e., orientation only, as opposed to changing shape entirely). Flanker appearance was also altered in the same feature that participants were asked to report, as opposed to another feature such as colour. More drastic changes in flanker appearance, or alterations in features not reported by observers, may produce a range of shifts in both the gradient and location of the spatial profile produced (as seen in the findings of Kooi *et al.*, (1994), see discussion in section 6.4.2).

As the spatial profile is fitted to subjectively acquired data (participants must consciously choose an orientation for each response). It is difficult to differentiate a true perceptual effect from a possible influence at the decision-making stage. Studies have noted that reported orientation of the target influenced subsequent reports of the flanker orientation (Harrison and Bex 2015), as observers were less likely to report the same orientation for both. This study only required observers to report the target orientation, but a shallower spatial profile may theoretically reflect uncertainty in orientation reporting when targets and flankers are similar, leading to strategic reporting of an intermediate orientation. However, all participants in the studies

presented in Chapters 6 and 7 were psychophysically experienced and were periodically reminded to report only the perceived orientation at the target location. Other reports using similar experimental setups also consistently support a perceptual effect over decisional influences in this regard (Kalpadakis-Smith *et al.* 2022; Greenwood, Bex and Dakin 2010).

The span of the transitionary zone (resulting from the gradient of the spatial profile) has so far been related to the similarity between target and flanker appearance. This measure could be interpreted as an indicator of the spatial selectivity of the feature-dependent mechanism of crowding, in addition to the midpoint of the profile which indicates the feature-independent spatial selectivity of crowding. This distinction appears slight but has important ramifications in the application of the spatial profile idea to the results of present literature and future investigations. While a shared spatial profile location for all possible stimuli is unlikely (Kooi *et al.* 1994), the finding that this location is shared for sufficiently similar targets and flankers suggests the existence of two origins of spatial selectivity in visual crowding. One, indicated by the midpoint of the spatial profile, varies dependent on more general factors such as target eccentricity (see Figure 6.7) and when large disparities between target and flanker appearance are present (Kooi *et al.* 1994). The indicated association with low-level physiological structures (retinal ganglion cell receptive field density – Figure 7.4) showed differences in midpoint may indicate differences in structural pathways facilitating crowding interactions. Therefore changes in the location of midpoint may be the psychophysical indicator of different visual areas being utilised, or acting as a limiting factor, in different stimulus arrangements and experimental setups (Chaney, Fischer and Whitney 2014), or alternatively be an indicator of a varying ‘odd-one-out’ cue reducing uncertainty with highly dissimilar flankers (Rosenholtz, Yu and Keshvari

2019). Meanwhile, the second instance of spatial selectivity in crowding is indicated by the span of the transitionary zone. This span is centred on the midpoint of the spatial profile and is influenced by finer discrepancies in target-flanker similarity such as relative orientation (see 6.4.2), so conveys the spatial-interaction of feature-specific crowding mechanisms, provided overall similarity is sufficient.

8.3 Implications for crowding research

The spatial profile model suggests most estimates of crowding zone extent (both critical-spacing and threshold-spacing based measures) may be viewed as sampling a point of the transitionary zone that may be simultaneously influenced by structural factors (determining the location of the spatial profile) and featural factors (determining the spread of the transition zone) – see Figure 6.11. Therefore, inferences based upon critical-spacing or threshold-spacing based estimates of the outer edge of the crowding zone should consider that changes in these estimates may come about through shifts in either the location or spread of the spatial profile. While a shift in such measures is undoubtedly a change in the observed spatial extent of crowding, the evidence presented in this thesis indicates that each parameter of the spatial profile may be related to different aspects of crowding mechanisms – the spread of the spatial profile may be indicative of feature-dependent integrative processes (see section 6.4.2) while the location of the profile is more associated with low-level structural factors (see 7.4).

8.3.1 Studies in typical vision

In the light of the thesis' findings, conclusions about crowding zone 'extent' in the literature may (possibly unknowingly) rely on one of two implicit assumptions:

One factor or the other remains unchanged between experimental conditions or participant groups, therefore a change in extent measure results wholly from shifts either in the location of the profile (indicating physiological/pathway differences) or the spread of the profile (indicating processing/mechanism differences).

Location and spread of the profile are linked such that they consistently covary and would not necessarily need to be differentiated – a greater spacing of the midpoint of the spatial profile is always accompanied by a greater spread and independent varying of each is not expected.

Investigators typically seek to control the potential impact of target-flanker similarity either by keeping target and flanker appearance consistent, or randomising appearance of flankers (Harrison and Bex 2015; Harrison and Bex 2017) or the target (Kwon and Liu 2019) equally between different experimental conditions and groups; the reason being that controlling target-flanker similarity in this way permits either of the above assumptions – the spread of the profile is either fixed or is sufficiently linked to the location of the profile, such that differences between experimental conditions are purely indicative of differences in underlying physiology. The finding that target-flanker similarity modulates the spread of the profile consistently at different target eccentricities (see Figure 6.9) suggests this method is valid for studies in orientation – the experiment effectively samples the 'average' spatial profile of crowding, so observed differences arise from consistently linked shifts in both location and average spread of the profile (above assumption 2 is upheld). However, there is currently

insufficient evidence to say conclusively whether this is also the case for studies with other stimuli. This covariation may also still have the potential to weaken inferences related to other measures such as physiological structures (see section 6.4.3).

In the case of letters, evidence exists that equally confusable letters may vary in crowding impact at differing eccentricities (Zahabi and Arguin 2014) and an interaction with letter complexity and similarity may also exist (Bernard and Chung 2011). It is expected that this confusability between letters should primarily influence the spread of the spatial profile that would be observed, though extreme differences may also shift the location of the profile (Kooi *et al.* 1994). It is difficult to conceive a reason why these effects should not give a consistent average spread over conditions in which the location of the spatial profile alters (e.g., changing target eccentricity), which permits assumption 2 as above when target-flanker similarity is controlled with randomisation. Nevertheless, without clearer evidence this will remain an assumption. Such evidence could be acquired by using the method of Chapter 6 (explained in section 6.2.1) with pairs of letter stimuli and considering each potential pair of letters as a level of target-flanker similarity. However, to cover the entire alphabet this way would be unfeasible given the length of time required to undertake such an experiment, and investigating a subsection of letters may introduce unintended effects from limiting potential responses (Reuther and Chakravarthi 2020).

8.3.2 Studies in atypical vision

The same requirement of assumptions described above in relation to typical vision, can be extended to studies in atypical vision in which the assumption of consistent featural-effects may be less secure. In particular, the assumption that the spread of the spatial profile may be unchanged between observers with typical and atypical

vision warrants attention. Conditions in which enlarged crowding zones have been found (Levi, Hariharan and Klein 2002a; Ogata *et al.* 2019) may produce a range of other deficits in visual function which could differentially impact on crowding effects. For example, consider amblyopia and glaucoma, both of which have been associated with enlarged crowding zones (Levi and Klein 1985; Levi, Hariharan and Klein 2002a; Ogata *et al.* 2019) and have been the focus of studies investigating structural explanations for psychophysically observed effects (Stringham *et al.* 2020; Clavagnier, Dumoulin and Hess 2015). The primary site of pathological disturbance in glaucoma is the retina, with potential cortical impacts (Chang and Goldberg 2012), but amblyopic pathology is cortical (Clavagnier, Dumoulin and Hess 2015). Despite quite different aetiology, both conditions are also associated with enlarged regions of complete spatial summation (Redmond *et al.* 2010a; Je *et al.* 2018). Recent work has indicated amblyopic crowding shares a common mechanism with normal crowding in peripheral vision (Kalpadakis-Smith *et al.* 2022), allowing some inferences regarding the systematic nature of crowded perception from studies in typical vision to be extended to amblyopia, but a question remains: what aspects of the spatial profile of crowding differ in atypical vision to result in enlarged crowding zones?

Through the lens of the spatial profile of crowding, three potential alterations could equally result in an enlarged crowding zone extent (when estimated via threshold- or critical-spacing).

A shift in midpoint, but unchanged span of the transition zone of the spatial profile. This would suggest the spatial dependence of the integrative mechanism producing crowding (i.e., pooling) is unaltered but is taking effect at a greater distance from the target.

The midpoint of the spatial profile may remain unchanged, and the spread of the transitionary zone increases. Such a change would indicate a greater weighting of responses to flankers at more distant spacings, but also a lower weighing of more closely spaced flankers (in comparison to steeper spatial profiles). This could potentially arise from a disturbance to the mechanisms that produce the effects of target-flanker similarity observed in Figure 6.7).

A third possible alteration to the spatial profile is a combination of the two above: the location of the profile is shifted further from the target and the transitionary span is simultaneously widened. This might the most expected of the three alternatives as this is the change seen in typical vision with increasing target eccentricity (see Figure 6.9), and abnormal crowding in amblyopia is sometimes compared to a translation of normal peripheral crowding effects to more central locations (Levi and Klein 1985).

Note: the above speculations refer to the weighting of responses in a population-pooling model, as implemented in this thesis, but could alternatively be interpreted as a change in probability of substitution responses. Distinguishing between pooling and substitution models of crowding was not in the aims of this thesis, though substitution models may fail to describe averaging effects often seen in crowding studies of orientation (Harrison and Bex 2017; Greenwood, Bex and Dakin 2009; Kalpadakis-Smith *et al.* 2022). Therefore, a weighted pooling model was determined to be the preferable approach for the presented work.

A further consideration relates to controlling target-flanker similarity, as mentioned in section 8.3.1above. While controlling target-flanker similarity may be sufficient in studies of typical vision, the presence of pathology may disrupt the perception of similarity between targets and flankers in ways that may be more difficult to predict or

control. Randomising target-flanker similarity between trials should theoretically mean that a typical estimate of crowding zone extent represents a sample of the spatial profile with an average transitionary zone span. In normal vision this may be expected to be reasonably consistent between experimental conditions, meaning observed differences in estimates of zone extent are more likely to be the result of shifts in the location of the spatial profile. However, when comparing typical and atypical vision, there is currently limited evidence that such average spans of the transitionary zone would be comparable in the presence of pathology. Though the physically presented similarity is the same for both participant groups, the similarity-dependent integration may not follow identical patterns.

8.4 Directions for future work

The findings presented in the thesis are a promising step towards furthering the current understanding of the spatial dynamics of crowding. However, it is prudent to continue to explore alternative possibilities for the analysis of the present data in addition to planning future studies. Further steps towards this will include alternative parameterisations of the model fitted to error distributions, which may allow the peak orientation of the 'target' and 'flanker' centred responses to vary and to quantify randomly oriented responses. Further exploration of how best to model the spatial profile is also possible, including weighting values of p(Target) by how well the fitted model of response errors represents the collected response data. Investigating such alternatives is useful in order to further test the current proposals and consider other potential interpretations.

The proposed model of the spatial profile of crowding, whose midpoint and gradient may be taken as distinguishable indicators of factors contributing to the extent of the crowding zone, presents several new avenues for future research. Various characteristics of visual crowding in typical vision may be elaborated on through characterisation of the visual profile of crowding, which could provide clues as to how these characteristics develop. Similarly, investigating how the spatial profile varies with different types and arrangements of stimuli may be helpful in determining the cortical area (or areas) that give rise to crowding effects.

In atypical vision, reported differences in crowding zone extent could potentially arise from changes in either the midpoint or span of the spatial extent of crowding (or both). Characterising the precise changes in the spatial profile of crowding which lead to these differences may provide new insight into the effects and pathophysiology of conditions that have been shown to affect crowding zones (Levi and Klein 1985; Ogata *et al.* 2019; Kalpadakis-Smith *et al.* 2022).

8.5 Conclusion

This thesis presents new perspective on the patterns of interactions that occur within the crowding zone. Using Landolt-Cs defined in orientation, the impact of flanker appearance and spacing was assessed through detailed reports of perceived target orientation. This work took the view of flankers adding a secondary signal to a pooled population response, and (in later studies) fitted a weighted pooling model to the distributions of responses provided. Systematic probing of the edge of the crowding zone revealed that target representation in the distribution of responses could be mapped to target-flanker similarity and spacing following a variable ‘spatial profile of

crowding'. Fitting this spatial profile model to the experimental data revealed an unexpected spatial characteristic that is shared across levels of target-flanker similarity. Rather than simply shrinking or expanding in extent with respect to target-flanker similarity, the edge of the crowding zone appears to pivot in gradient around a spacing at which target and flanker orientations are equally represented in crowded responses. This spacing, defined as the 'location' of the spatial profile of crowding, was shown to be potentially useful as an indicator of the physiological limits of the spatial extent of crowding interactions. Meanwhile, the apparent extent of crowding effects observed psychophysically is simultaneously influenced by target-flanker similarity. Differentiating these two influences on the spatial extent of crowding provides new insight into the physiology underpinning visual crowding and provides a new lens through which future research may be developed.

In summary, the variable nature of the spatial profile of crowding suggests that the employment of some common methods intended for measuring the extent of the crowding zone in typical and atypical vision may lead to some fundamental physiological features and pathological effects being overlooked. This thesis offers an alternative approach to measuring crowding that disentangles the feature-independent location of the transitionary zone from the feature-dependent modulation of the span between minimum and maximum effects of crowding. A new perspective on the dynamic nature of the edge of the crowding zone may help to improve the design of future investigations and resolve apparent discrepancies present in the literature.

Appendix 1. Alternative analyses of RGC density

Additional investigation of the association with midget retinal ganglion cell receptive field density and the extent of Ricco's are and crowding zones, referenced in Chapter 7.

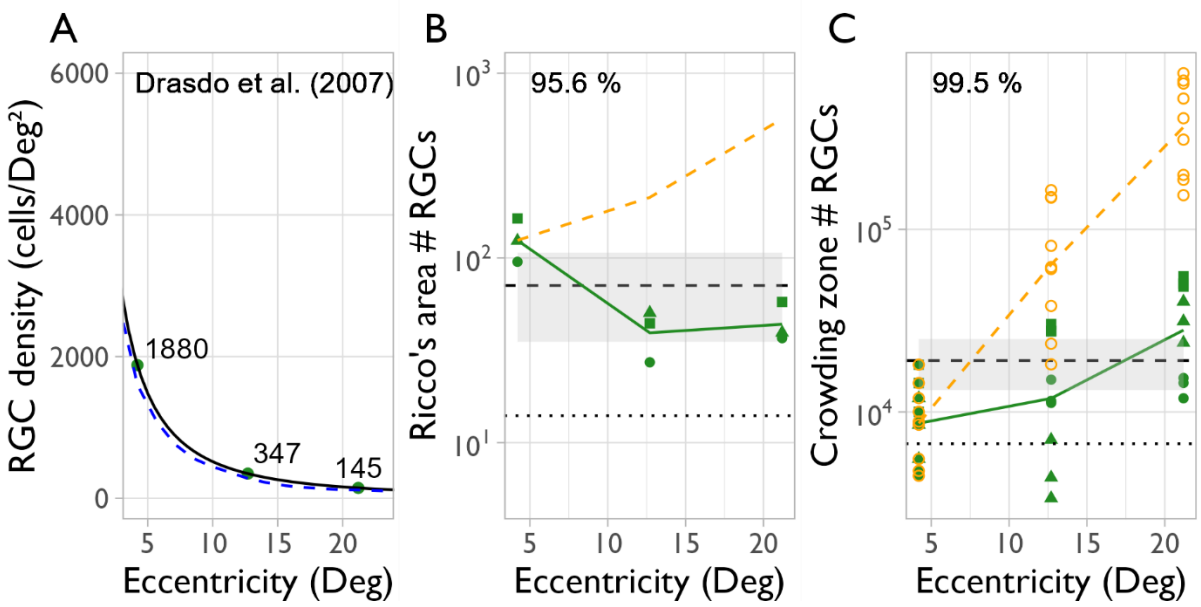

Figure A1.1 - Receptive field counts recalculated with density values from Drasdo et al. (2007)

A) Density of retinal ganglion cell receptive fields estimated with the calculations of Drasdo et al (2007) at the target locations used. The solid black line shows the Drasdo model, while the blue dashed line shows the model of Montesano et al. (2020) as utilised above, for comparison. The two right plots show the number of RGC receptive fields underlying Ricco's area (A) and crowding zones (B) calculated with these density values. The slight difference in density values did not significantly change the calculated numbers of receptive fields, or the percentage contribution of underlying RGC density (Kwon & Liu 2019) to the variance in extent of either measure.

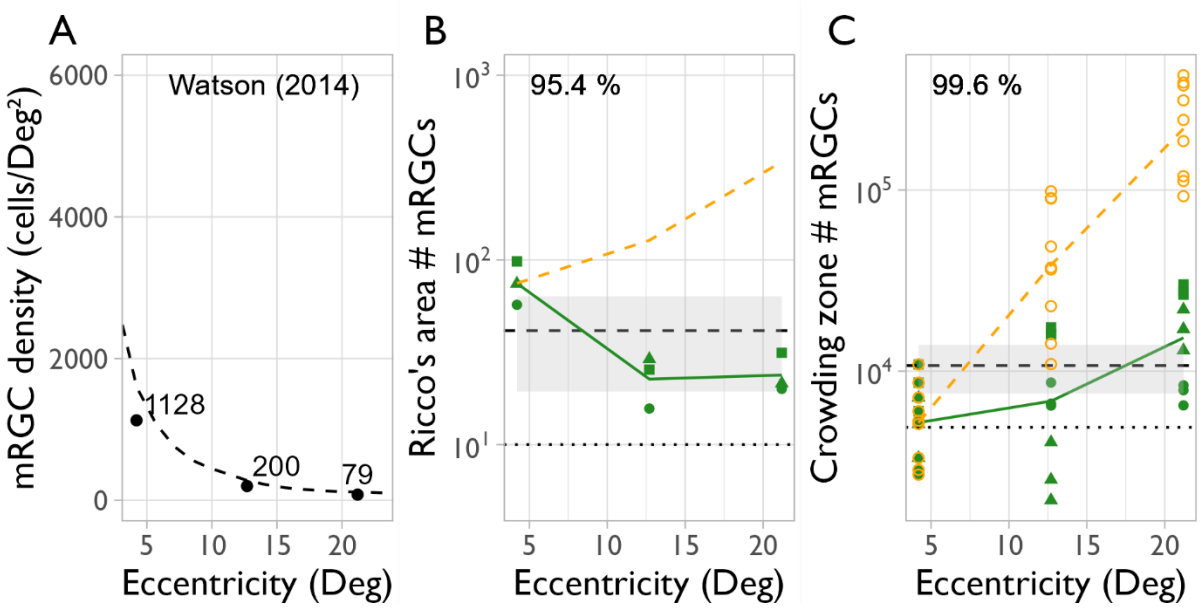

Figure A1.2 - mGRC receptive field counts recalculated with density values from Watson (2014)

A) Density of midget retinal ganglion cell receptive fields estimated with the calculations of Watson (2014) at the target locations used. The blue dashed line shows the model of RGC receptive field density by Montesano et al. (2020) as utilised above, for comparison. The two right plots show the number of mRGC receptive fields underlying Ricco's area (A) and crowding zones (B) calculated with these density values. The calculated numbers of receptive fields within Ricco's area and crowding zones are lower, but the overall patterns of the data are unchanged from the above analyses.

Appendix 2. Investigation into stimulus presentation duration

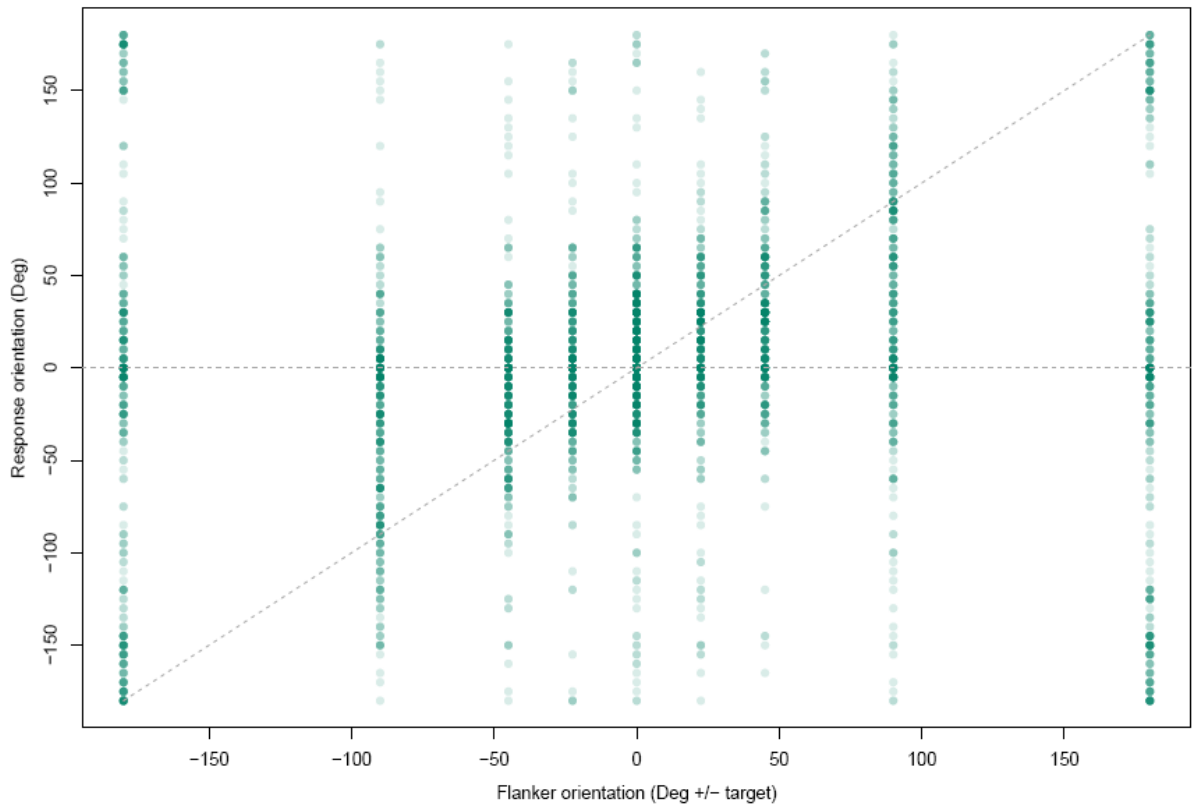

Figure A2.1 - Stimulus presentation for 60ms

Crowding experiment protocol is as described in Chapter 6 Study 1, except stimuli were presented for 60ms. While responses do appear to cluster at the target (horizontal line) and flanker (diagonal line), the spread of errors is very large

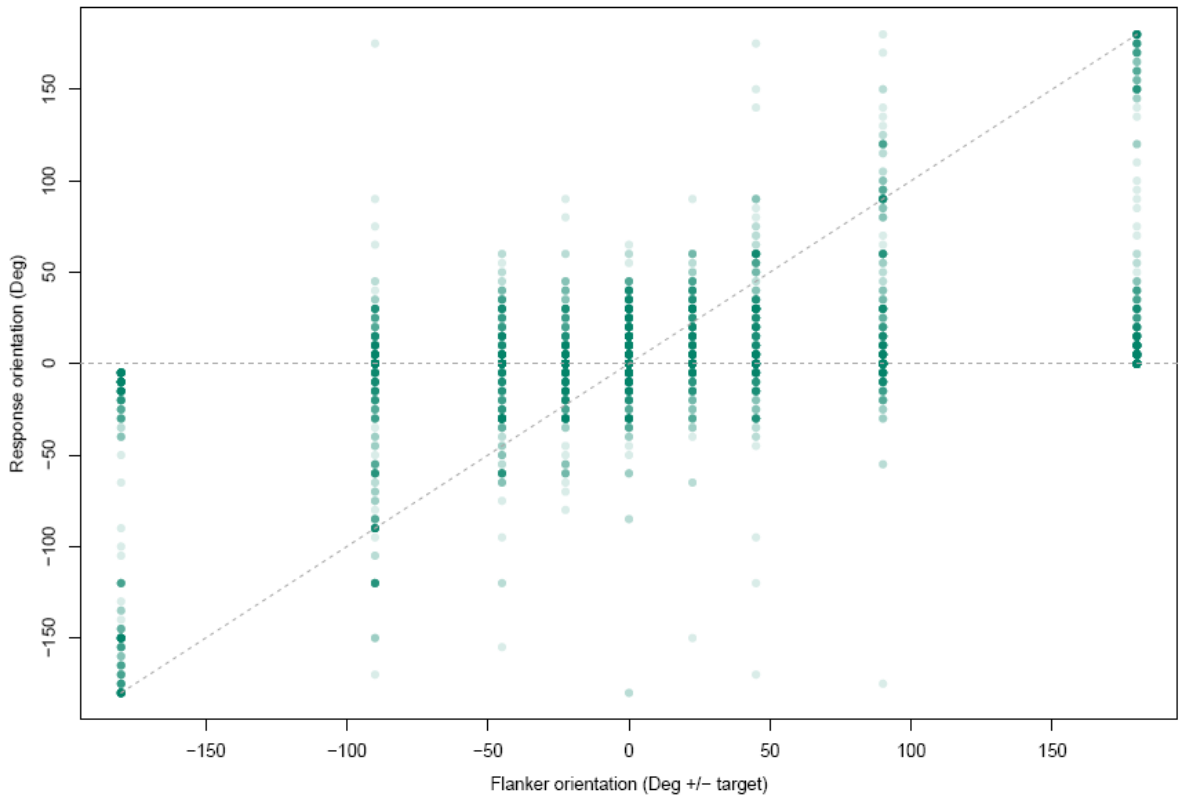

Figure A2.2 - Stimulus presentation for 500ms

Crowding task protocol was as described in Chapter 6 study 1, bust stimuli were presented for 500ms. The spread of responses is noticeable smaller compared to the data collected with 60ms presentation time. However, it took additional effort to avoid unintentionally 'peeking' at the target during such long presentations. Therefore 280ms was selected as the stimulus presentation time for studies presented in Chapter 6.

References

Agaoglu MN and Chung STL (2016) Can (should) theories of crowding be unified? *Journal of Vision* **16**: 1–22.

Agostinelli C and Lund U (2022) R package 'circular': Circular Statistics (version 0.4-95).

Anderson EJ, Dakin SC, Schwarzkopf DS, Rees G and Greenwood JA (2012) The neural correlates of crowding-induced changes in appearance. *Current Biology* **22**: 1199–1206.

Anderson RS, Zlatkova MB and Demirel S (2002) What limits detection and resolution of short-wavelength sinusoidal gratings across the retina? *Vision Research* **42**: 981–990.

Andriessen JJ and Bouma H (1976) Eccentric vision: Adverse interactions between line segments. *Vision Research* **16**: 71–78.

Balas B, Nakano L and Rosenholtz R (2009) A summary-statistic representation in peripheral vision explains visual crowding. *Journal of Vision* **9**: 13–13.

Baldassi S, Megna N and Burr DC (2006) Visual Clutter Causes High-Magnitude Errors. *PLoS Biology* **4**: e56.

Banks WP, Larson DW and Prinzmetal W (1979) Asymmetry of visual interference. *Perception & Psychophysics* **25**: 447–456.

Barlow HB (1958) Temporal and spatial summation in human vision at different background intensities. *The Journal of Physiology* **141**: 337.

Barollo M, Contemori G, Battaglini L, Pavan A and Casco C (2017) Perceptual learning improves contrast sensitivity, visual acuity, and foveal crowding in amblyopia. *Restorative Neurology and Neuroscience* **35**: 483–496.

Baumgardt E (1959) Visual Spatial and Temporal Summation. *Nature 1959 184:4703* **184**: 1951–1952.

van den Berg R, Roerdink JBTM and Cornelissen FW (2007) On the generality of crowding: Visual crowding in size, saturation, and hue compared to orientation. *Journal of Vision* **7**: 1–11.

Van Den Berg R, Roerdink JBTM and Cornelissen FW (2010) A neurophysiologically plausible population code model for feature integration explains visual crowding. *PLoS Computational Biology* **6**:

Bernard JB and Chung STL (2011) The dependence of crowding on flanker complexity and target-flanker similarity. *Journal of Vision* **11**: 1–16.

Bex PJ and Dakin SC (2005) Spatial interference among moving targets. *Vision Research* **45**: 1385–1398.

Bex PJ, Dakin SC and Simmers AJ (2003) The shape and size of crowding for moving targets. *Vision Research* **43**: 2895–2904.

Bouma H (1970) Interaction effects in parafoveal letter recognition. *Nature* **226(49)**: 177–178.

Bouma H (1973) Visual interference in the parafoveal recognition of initial and final letters of words. *Vision Research* **13**: 767–782.

Boyd Taylor HG, Puckett AM, Isherwood ZJ and Schira MM (2019) Vascular effects on the BOLD response and the retinotopic mapping of hV4. *PLOS ONE* **14**: e0204388.

Brainard DH (1997) The Psychophysics Toolbox. *Spatial Vision* **10**: 433–436.

Van der Burg E, Olivers CNL and Cass J (2017) Evolving the keys to visual crowding. *Journal of Experimental Psychology: Human Perception and Performance* **43**: 690–699.

Cao Y and Grossberg S (2005) A laminar cortical model of stereopsis and 3D surface perception: closure and da Vinci stereopsis. *Spatial vision* **18**: 515–578.

Chakravarthi R, Rubruck J, Kipling N and Clarke ADF (2021) Characterizing the in-out asymmetry in visual crowding. *Journal of Vision* **21**: 1–14.

Chaney W, Fischer J and Whitney D (2014) The hierarchical sparse selection model of visual crowding. *Frontiers in Integrative Neuroscience* **8**: 73.

Chang EE and Goldberg JL (2012) Glaucoma 2.0: Neuroprotection, neuroregeneration, neuroenhancement. *Ophthalmology* **119**: 979–986.

Chastain G (1982) Confusability and interference between members of parafoveal letter pairs. *Perception & Psychophysics* **32**: 576–580.

Chung STL and Bedell HE (1995) Effect of retinal image motion on visual acuity and contour interaction in congenital nystagmus. *Vision Research* **35**: 3071–3082.

Chung STL, Levi DM and Legge GE (2001) Spatial-frequency and contrast properties of crowding. *Vision Research* **41**: 1833–1850.

Chung STL and Tjan BS (2007) Shift in spatial scale in identifying crowded letters. *Vision Research* **47**: 437–451.

Clarke AM, Herzog MH and Francis G (2014) Visual crowding illustrates the inadequacy of local versus global and feedforward versus feedback distinctions in modelling visual perception. *Frontiers in Psychology* **5**: 1–12.

Clavagnier S, Dumoulin SO and Hess RF (2015) Is the cortical deficit in amblyopia due to reduced cortical magnification, loss of neural resolution, or neural disorganization? *Journal of Neuroscience* **35**: 14740–14755.

Coates DR, Levi DM, Touch P and Sabesan R (2018) Foveal Crowding Resolved. *Scientific Reports* **8**: 1–12.

Crutch S and Warrington E (2007) Foveal crowding in posterior cortical atrophy: A specific early-visual-processing deficit affecting word reading. *Cognitive Neuropsychology* **24**: 843–866.

Curcio CA and Allen KA (1990) Topography of ganglion cells in human retina. *Journal of Comparative Neurology* **300**: 5–25.

Dakin SC, Bex PJ, Cass JR and Watt RJ (2009) Dissociable effects of attention and crowding on orientation averaging. *Journal of Vision* **9**: 28–28.

Dakin SC, Cass J, Greenwood JA and Bex PJ (2010) Probabilistic, positional averaging predicts object-level crowding effects with letter-like stimuli. *Journal of Vision* **10**: 1–16.

Dakin SC, Greenwood JA, Carlson TA and Bex PJ (2011) Crowding is tuned for perceived (not physical) location. *Journal of Vision* **11**: 1–13.

Dayan P and Solomon JA (2010) Selective Bayes: Attentional load and crowding. *Vision Research* **50**: 2248–2260.

Doerig A, Bornet A, Rosenholtz R, Francis G, Clarke AM and Herzog MH (2019) Beyond Bouma's window: How to explain global aspects of crowding? *PLoS Computational Biology* **15**: e1006580.

Drasdo N and Fowler CW (1974) Non-linear projection of the retinal image in a wide-angle schematic eye. *British Journal of Ophthalmology* **58**: 709–714.

Drasdo N, Millican CL, Katholi CR and Curcio CA (2007) The length of Henle fibers in the human retina and a model of ganglion receptive field density in the visual field. *Vision Research* **47**: 2901–2911.

Ehlers H (1953) Clinical testing of visual acuity. *A.M.A. Archives of Ophthalmology* **49**: 431–434.

Ehlers H (1936) The movements of the eyes during reading. *Acta Ophthalmologica* **14**: 56–63.

Ellis WD (1938) *A source book of Gestalt psychology*. Ellis WD ed. London, England: Kegan Paul, Trench, Trubner & Company.

Eriksen CW and St. James JD (1986) Visual attention within and around the field of focal attention: A zoom lens model. *Perception & Psychophysics* **40**: 225–240.

Ester EF, Klee D and Awh E (2014) Visual crowding cannot be wholly explained by feature pooling. *Journal of Experimental Psychology: Human Perception and Performance* **40**: 1022–1033.

Ester EF, Zilber E and Serences JT (2015) Substitution and pooling in visual crowding induced by similar and dissimilar distractors. *Journal of Vision* **15**: 1–12.

Farell B and Pelli DG (1998) Psychophysical methods, or how to measure a threshold, and why Carpenter R and Robson J eds. *Vision Research: A Practical Guide to Laboratory Methods*, pp. 129–136.

Fechner GT (1860) *Elemente der Psychophysik*. Leipzig: Breitkopf und Härtel.

Fischer J, Spotswood N and Whitney D (2011) The Emergence of Perceived Position

in the Visual System. *Journal of Cognitive Neuroscience* **23**: 119–136.

Flom MC, Heath GG and Takahashi E (1963) Contour Interaction and Visual Resolution: Contralateral Effects. *Science* **142**: 979–980.

Flom MC, Weymouth FW and Kahneman D (1963) Visual Resolution and Contour Interaction. *Journal of the Optical Society of America* **53**: 1026–1032.

Francis G, Manassi M and Herzog MH (2017) Neural dynamics of grouping and segmentation explain properties of visual crowding. *Psychological Review* **124**: 483–504.

Freeman J, Chakravarthi R and Pelli DG (2012) Substitution and pooling in crowding. *Attention, Perception, and Psychophysics* **74**: 379–396.

Freeman J and Simoncelli EP (2011) Metamers of the ventral stream. *Nature Neuroscience* **14**: 1195–1204.

Gheri C and Baldassi S (2008) Non-linear integration of crowded orientation signals. *Vision Research* **48**: 2352–2358.

Greenwood J (2021) Eccentric Vision Toolbox [Computer software] .

Greenwood JA, Bex PJ and Dakin SC (2010) Crowding Changes Appearance. *Current Biology*

Greenwood JA, Bex PJ and Dakin SC (2009) Positional averaging explains crowding with letter-like stimuli. *Proceedings of the National Academy of Sciences of the United States of America* **106**: 13130–13135.

Greenwood JA and Parsons MJ (2020) Dissociable effects of visual crowding on the perception of color and motion. *Proceedings of the National Academy of Sciences of the United States of America* **117**: 8196–8202.

Greenwood JA, Szinte M, Sayim B and Cavanagh P (2017) Variations in crowding, saccadic precision, and spatial localization reveal the shared topology of spatial vision. *Proceedings of the National Academy of Sciences of the United States of America* **114**: E3573–E3582.

Greenwood JA, Tailor VK, Sloper JJ, Simmers AJ, Bex PJ and Dakin SC (2012) Visual acuity, crowding, and stereo-vision are linked in children with and without amblyopia. *Investigative Ophthalmology and Visual Science* **53**: 7655–7665.

Gurnsey R, Roddy G and Chanab W (2011) Crowding is size and eccentricity dependent. *Journal of Vision* **11**: 15.

Hanus D and Vul E (2013) Quantifying error distributions in crowding. *Journal of Vision* **13**: 1–27.

Harrison WJ and Bex PJ (2015) A Unifying Model of Orientation Crowding in Peripheral Vision. *Current Biology* **25**: 3213–3219.

Harrison WJ and Bex PJ (2016) Reply to Pachai et al. *Current Biology* **26**: R353–R354.

Harrison WJ and Bex PJ (2017) Visual crowding is a combination of an increase of positional uncertainty, source confusion, and featural averaging. *Scientific Reports* **7**: 1–9.

Harvey BM and Dumoulin SO (2011) The relationship between cortical magnification factor and population receptive field size in human visual cortex: Constancies in cortical architecture. *Journal of Neuroscience* **31**: 13604–13612.

Hayashi D and Ohnishi M (2019) Influence of Multiple Types of Proximity on the Degree of Visual Crowding Effects Within a Single Gap Detection Task. *i-Perception* **10**: 2–9.

He D, Wang Y and Fang F (2019) The Critical Role of V2 Population Receptive Fields in Visual Orientation Crowding. *Current Biology* **29**: 2229-2236.e3.

He S, Cavanagh P and Intriligator J (1996) Attentional resolution and the locus of visual awareness. *Nature* **383**: 334–337.

Heijl A, Lindgren G and Olsson J (1987) Normal Variability Of Static Perimetric Threshold Values Across The Central Visual Field. *Archives of Ophthalmology* **105**: 1544–1549.

Herzog MH (2018) Perceptual grouping. *Current Biology* **28**: R687–R688.

Herzog MH, Sayim B, Chicherov V and Manassi M (2015) Crowding, grouping, and object recognition: A matter of appearance. *Journal of Vision* **15**: 1–18.

Himmelberg MM, Kurzawski JW, Benson NC, Pelli DG, Carrasco M and Winawer J (2021) Cross-dataset reproducibility of human retinotopic maps. *NeuroImage* **244**: 0–59.

Horton JC and Hoyt WF (1991) The Representation of the Visual Field in Human Striate Cortex: A Revision of the Classic Holmes Map. *Archives of Ophthalmology* **109**: 816–824.

Hubel DH and Wiesel TN (1962) Receptive fields, binocular interaction and functional architecture in the cat's visual cortex. *The Journal of Physiology* **160**: 106–154.

Huckauf A and Heller D (2002) What various kinds of errors tell us about lateral masking effects. *Visual Cognition* **9**: 889–910.

Huurneman B, Boonstra FN, Cox RF, Cillessen AH and Van Rens G (2012) A systematic review on foveal crowding in visually impaired children and perceptual learning as a method to reduce crowding. *BMC Ophthalmology* 12(1).

Intriligator J and Cavanagh P (2001) The Spatial Resolution of Visual Attention. *Cognitive Psychology* **43**: 171–216.

Jacobson L, Ek U, Fernell E, Flodmark O and Broberger U (1996) Visual impairment in preterm children with periventricular leukomalacia - Visual, cognitive and

neuropaediatric characteristics related to cerebral imaging. *Developmental Medicine and Child Neurology* **38**: 724–735.

Jammaladak SR (2001) *Topics in Circular Statistics, Volume 5*. River Edge, N.J.: World Scientific.

Je S, Ennis FA, Woodhouse JM, Sengpiel F and Redmond T (2018) Spatial summation across the visual field in strabismic and anisometropic amblyopia. *Scientific Reports* **8**: 3858.

Kalpadakis-Smith A V., Goffaux V and Greenwood JA (2018) Crowding for faces is determined by visual (not holistic) similarity: Evidence from judgements of eye position. *Scientific Reports 2018 8:1* **8**: 1–14.

Kalpadakis-Smith A V., Tailor VK, Dahlmann-Noor AH and Greenwood JA (2022) Crowding changes appearance systematically in peripheral, amblyopic, and developing vision. *Journal of Vision* **22**: 3.

Kennedy GJ and Whitaker D (2010) The chromatic selectivity of visual crowding. *Journal of Vision* **10**: 15–15.

Keshvari S and Rosenholtz R (2016) Pooling of continuous features provides a unifying account of crowding. *Journal of Vision* **16**: 1–15.

Kim SG and Ogawa S (2012) Biophysical and physiological origins of blood oxygenation level-dependent fMRI signals. *Journal of Cerebral Blood Flow and*

Metabolism 32(7), pp. 1188–1206.

King WM, Sarup V, Sauvé Y, Moreland CM, Carpenter DO and Sharma SC (2006) Expansion of visual receptive fields in experimental glaucoma. *Visual Neuroscience* **23**: 137–142.

Kooi FL, Toet A, Tripathy SP and Levi DM (1994) The effect of Similarity and Duration on Spatial Interaction in Peripheral Vision. *Spatial Vision* **8**: 255–279.

Korte W (1923) Über die Gestaltauffassung im indirekten Sehen [On the apprehension of Gestalt in indirect vision]. *Zeitschrift für Psychologie* **93**: 17–82.

Kothe AC and Regan D (1990) Crowding depends on contrast. *Optometry and vision science : official publication of the American Academy of Optometry* **67**: 283–286.

Kravitz DJ and Behrmann M (2011) Space-, object-, and feature-based attention interact to organize visual scenes. *Attention, Perception, and Psychophysics* **73**: 2434–2447.

Kurzawski JW, Burchell A, Thapa D, Majaj NJ, Jonathan A, Winawer JA and Pelli DG (2021) An enhanced Bouma model fits a hundred people's visual crowding. *bioRxiv* 2021.04.12.439570.

Kurzawski JW, Pelli DG and Winawer JA (2021) Conservation across individuals of cortical crowding distance in human V4. *Journal of Vision* **21**: 2675.

Kwon MY, Bao P, Millin R and Tjan BS (2014) Radial-tangential anisotropy of crowding in the early visual areas. *Journal of Neurophysiology* **112**: 2413–2422.

Kwon MY and Liu R (2019) Linkage between retinal ganglion cell density and the nonuniform spatial integration across the visual field. *Proceedings of the National Academy of Sciences of the United States of America* **116**: 3827–3836.

Leek MR (2001) Adaptive Psychophysical Procedures. *Perception & Psychophysics* **63**: 1279–1292.

Lev M, Yehezkel O and Polat U (2014) Uncovering foveal crowding? *Scientific Reports* **4**: 4067.

Levi DM (2008) Crowding-An essential bottleneck for object recognition: A mini-review. *Vision Research* 48(5), pp. 635–654.

Levi DM and Carney T (2009) Crowding in Peripheral Vision: Why Bigger Is Better. *Current Biology* **19**: 1988–1993.

Levi DM and Carney T (2011) The effect of flankers on three tasks in central, peripheral, and amblyopic vision. *Journal of Vision* **11**: 10–10.

Levi DM, Hariharan S and Klein SA (2002a) Suppressive and facilitatory spatial interactions in amblyopic vision. *Vision Research* **42**: 1379–1394.

Levi DM, Hariharan S and Klein SA (2002b) Suppressive and facilitatory spatial

interactions in peripheral vision: Peripheral crowding is neither size invariant nor simple contrast masking. *Journal of Vision* **2**: 167–177.

Levi DM and Klein SA (1990) Equivalent intrinsic blur in spatial vision. *Vision Research* **30**: 1971–1993.

Levi DM and Klein SA (1985) Vernier acuity, crowding and amblyopia. *Vision Research* **25**: 979–991.

Levi DM, Klein SA and Aitsebaomo AP (1985) Vernier acuity, crowding and cortical magnification. *Vision Research* **25**: 963–977.

Levi DM, Klein SA and Carney T (2000) Unmasking the mechanisms for Vernier acuity: evidence for a template model for Vernier acuity. *Vision Research* **40**: 951–972.

Levi DM, Klein SA and Hariharan S (2002) Suppressive and facilitatory spatial interactions in foveal vision: Foveal crowding is simple contrast masking. *Journal of Vision* **2**: 140–166.

Levi DM, Klein SA and Yen Lee Yap (1987) Positional uncertainty in peripheral and amblyopic vision. *Vision Research* **27**: 581–597.

Levitt H (1971) Transformed Up-Down Methods in Psychoacoustics. *Journal of the Acoustical Society of America* 49, pp. 467–477.

Liu T, Jiang Y, Sun X and He S (2009) Reduction of the Crowding Effect in Spatially Adjacent but Cortically Remote Visual Stimuli. *Current Biology* **19**: 127–132.

Livingstone M and Hubel D (1988) Segregation of form, color, movement, and depth: Anatomy, physiology, and perception. *Science* **240**: 740–749.

Mackworth NH (1965) Visual noise causes tunnel vision. *Psychonomic Science* **3**: 67–68.

Malania M, Herzog MH and Westheimer G (2007) Grouping of contextual elements that affect vernier thresholds. *Journal of Vision* **7**: 1–7.

Manassi M, France BS and Herzog MH (2012) Grouping, pooling, and when bigger is better in visual crowding. *Journal of Vision* **12**: 13–13.

Manassi M, Sayim B and Herzog MH (2013) When crowding of crowding leads to uncrowding. *Journal of Vision* **13**: 1–10.

Mareschal I, Morgan MJ and Solomon JA (2010a) Attentional modulation of crowding. *Vision Research* **50**: 805–809.

Mareschal I, Morgan MJ and Solomon JA (2008) Contextual effects on decision templates for parafoveal orientation identification. *Vision Research* **48**: 2689–2695.

Mareschal I, Morgan MJ and Solomon JA (2010b) Cortical distance determines whether flankers cause crowding or the tilt illusion. *Journal of Vision* **10**: 1–14.

Martelli M, Di Filippo G, Spinelli D and Zoccolotti P (2009) Crowding, reading, and developmental dyslexia. *Journal of Vision* **9**: 14–14.

Martelli M, Majaj NJ and Pelli DG (2005) Are faces processed like words? A diagnostic test for recognition by parts. *Journal of Vision* **5**: 6–6.

Marten-Ellis SM and Bedell HE (2021) A comparison of foveal and peripheral contour interaction and crowding. *Optometry and Vision Science* **98**: 41–50.

Michelson AA (1927) *Studies in Optics*. Chicago: University of Chicago Press.

Millin R, Arman AC, Chung STL and Tjan BS (2014) Visual crowding in V1. *Cerebral Cortex* **24**: 3107–3115.

Montesano G, Ometto G, Hogg RE, Rossetti LM, Garway-Heath DF and Crabb DP (2020) Revisiting the drasdo model: Implications for structure-function analysis of the macular region. *Translational Vision Science and Technology* **9**: 1–15.

Motter BC (2009) Central V4 Receptive Fields Are Scaled by the V1 Cortical Magnification and Correspond to a Constant-Sized Sampling of the V1 Surface. *Journal of Neuroscience* **29**: 5749–5757.

Motter BC (2018) Stimulus conflation and tuning selectivity in V4 neurons: A model of visual crowding. *Journal of Vision* **18**: 15–15.

Motter BC and Simoni DA (2007) The roles of cortical image separation and size in

active visual search performance. *Journal of Vision* **7**: 6–6.

Movshon JA and Simoncelli EP (2014) Representation of naturalistic image structure in the primate visual cortex. *Cold Spring Harbor Symposia on Quantitative Biology* **79**: 115–122.

Nandy AS and Tjan BS (2012) Saccade-confounded image statistics explain visual crowding. *Nature Neuroscience* **15**: 463–469.

Nandy AS and Tjan BS (2007) The nature of letter crowding as revealed by first- and second-order classification images. *Journal of Vision* **7**: 5.1-26.

Ogata NG, Boer ER, Daga FB, Jammal AA, Stringham JM and Medeiros FA (2019) Visual crowding in glaucoma. *Investigative Ophthalmology and Visual Science* **60**: 538–543.

Owen WG (1972) Spatio-temporal integration in the human peripheral retina. *Vision Research* **12**: 1011–1026.

Ozkirli A, Jastrzębowska MA, Draganski B and Herzog MH (2021) Isolate or combine: population receptive field size in (un)crowding. *Journal of Vision* **21**: 2196–2196.

Pachai M V., Doerig AC and Herzog MH (2016) How best to unify crowding? *Current Biology* **26**: R352–R353.

Pan F and Swanson WH (2006) A cortical pooling model of spatial summation for

perimetric stimuli. *Journal of Vision* **6**: 1159–1171.

Pan F, Swanson WH, Dul MW, F. P and W.H. S (2006) Evaluation of a two-stage neural model of glaucomatous defect: An approach to reduce test-retest variability. *Optometry and Vision Science* **83**: 499–511.

Parkes L, Lund J, Angelucci A, Solomon JA and Morgan M (2001) Compulsory averaging of crowded orientation signals in human vision. *Nature Neuroscience* **4**: 739–744.

Pascal E and Abadi R V. (1995) Contour interaction in the presence of congenital nystagmus. *Vision Research* **35**: 1785–1789.

Pelli DG (2008) Crowding: a cortical constraint on object recognition. *Current Opinion in Neurobiology* **18**: 445–451.

Pelli DG (1987) The ideal psychometric procedure. *Investigative Ophthalmology & Visual Science* 366.

Pelli DG, Palomares M and Majaj NJ (2004) Crowding is unlike ordinary masking: Distinguishing feature integration from detection. *Journal of Vision* **4**: 1136–1169.

Pelli DG and Tillman KA (2008) The uncrowded window of object recognition. *Nature Neuroscience* **11**: 1129–1135.

Petrov Y and Meleshkevich O (2011a) Asymmetries and idiosyncratic hot spots in

crowding. *Vision Research* **51**: 1117–1123.

Petrov Y and Meleshkevich O (2011b) Locus of spatial attention determines inward-outward anisotropy in crowding. *Journal of Vision* **11**: 1–1.

Petrov Y, Popple A V. and McKee SP (2007) Crowding and surround suppression: Not to be confused. *Journal of Vision* **7**: 12.1–9.

Pike MG, Holmstrom G, de Vries LS, Pennock JM, Drew KJ, Sonksen PM and Dubowitz LMS (1994) Patterns Of Visual Impairment Associated With Lesions Of The Preterm Infant Bran. *Developmental Medicine & Child Neurology* **36**: 849–862.

Põder E (2007) Effect of colour pop-out on the recognition of letters in crowding conditions. *Psychological Research* **71**: 641–645.

Põder E (2012) On the rules of integration of crowded orientation signals. *i-Perception* **3**: 440–454.

Põder E and Wagemans J (2007) Crowding with conjunctions of simple features. *Journal of Vision* **7**: 23.1–12.

Portilla J and Simoncelli EP (2000) Parametric texture model based on joint statistics of complex wavelet coefficients. *International Journal of Computer Vision* **40**: 49–71.

Pouget A, Dayan P and Zemel R (2000) Information processing with population codes. *Nature Reviews Neuroscience 2000 1:2* **1**: 125–132.

R Core Team (2021) R: A Language and Environment for Statistical Computing.

Raizada RDS and Grossberg S (2001) Context-sensitive binding by the laminar circuits of V1 and V2: A unified model of perceptual grouping, attention, and orientation contrast. *Visual Cognition* **8**: 431–466.

Raizada RDS and Grossberg S (2003) Towards a Theory of the Laminar Architecture of Cerebral Cortex: Computational Clues from the Visual System. *Cerebral Cortex* **13**: 100–113.

Redmond T, Anderson RS, Russell RA and Garway-Heath DF (2013) Relating retinal nerve fiber layer thickness and functional estimates of ganglion cell sampling density in healthy eyes and in early glaucoma. *Investigative Ophthalmology and Visual Science* **54**: 2153–2162.

Redmond T, Garway-Heath DF, Zlatkova MB and Anderson RS (2010a) Sensitivity loss in early glaucoma can be mapped to an enlargement of the area of complete spatial summation. *Investigative Ophthalmology and Visual Science* **51**: 6540–6548.

Redmond T, Zlatkova MB, Garway-Heath DF and Anderson RS (2010b) The effect of age on the area of complete spatial summation for chromatic and achromatic stimuli. *Investigative Ophthalmology and Visual Science* **51**: 6533–6539.

Rentschler I and Treutwein B (1985) Loss of spatial phase relationships in extrafoveal vision. *Nature* **313**: 308–310.

Reuther J and Chakravarthi R (2020) Response selection modulates crowding: a cautionary tale for invoking top-down explanations. *Attention, Perception, and Psychophysics* **82**: 1763–1778.

Riccò A (1877) Relazione fra il minimo angolo visuale e l'intensità luminosa. *Memorie della Societa Degli Spettroscopisti Italiani* **6**: B29–B58.

Ringach DL (2002) Spatial structure and symmetry of simple-cell receptive fields in macaque primary visual cortex. *Journal of Neurophysiology* **88**: 455–463.

Roelfsema PR and Houtkamp R (2011) Incremental grouping of image elements in vision. *Attention, Perception, and Psychophysics* **73**: 2542–2572.

Rosen S, Chakravarthi R and Pelli DG (2014) The Bouma law of crowding, revised: critical spacing is equal across parts, not objects. *Journal of Vision* **14**: 10.

Rosenholtz R (2016) Capabilities and Limitations of Peripheral Vision. *Annual Review of Vision Science* **2**: 437–457.

Rosenholtz R, Huang J, Raj A, Balas BJ and Ilie L (2012) A summary statistic representation in peripheral vision explains visual search. *Journal of Vision* **12**: 1–17.

Rosenholtz R, Yu D and Keshvari S (2019) Challenges to pooling models of crowding: Implications for visual mechanisms. *Journal of Vision* **19**: 1–25.

Rummens K and Sayim B (2021) Broad attention uncovers benefits of stimulus

uniformity in visual crowding. *Scientific Reports* **11**: 1–13.

Sabra AI (1989) *The Optics of Ibn Al-Haytham: Books I-III : on Direct Vision*. London: Warburg Institute, University of London.

Seber GAF and Wild CJ (2005) *Nonlinear Regression*. New York: Wiley.

Shamsi F, Liu R and Kwon MY (2022) Binocularly Asymmetric Crowding in Glaucoma and a Lack of Binocular Summation in Crowding. *Investigative Ophthalmology and Visual Science* **63**: 36.

Shechter A and Yashar A (2021) Mixture model investigation of the inner–outer asymmetry in visual crowding reveals a heavier weight towards the visual periphery. *Scientific Reports* **11**: 1–12.

Shin K, Chung STLL and Tjan BS (2017) Crowding, visual awareness, and their respective neural loci. *Journal of Vision* **17**: 18–18.

Simmers AJ, Gray LS, McGraw P V. and Winn B (1999) Contour interaction for high and low contrast optotypes in normal and amblyopic observers. *Ophthalmic and Physiological Optics* **19**: 253–260.

Solomon JA, Felisberti FM and Morgan MJ (2004) Crowding and the tilt illusion: Toward a unified account. *Journal of Vision* **4**: 500–508.

Song S, Levi DM and Pelli DG (2014) A double dissociation of the acuity and crowding

limits to letter identification, and the promise of improved visual screening. *Journal of Vision* **14**: 1–37.

Stoffer TH (1994) Attentional zooming and the global-dominance phenomenon: Effects of level-specific cueing and abrupt visual onset. *Psychological Research* **56**: 83–98.

Strasburger H (2022) On the cortical mapping function – Visual space, cortical space, and crowding. *Vision Research* **194**: 107972.

Strasburger H (2020) Seven Myths on Crowding and Peripheral Vision. *i-Perception* **11**:

Strasburger H (2005) Unfocussed spatial attention underlies the crowding effect in indirect form vision. *Journal of Vision* **5**: 8–8.

Strasburger H, Harvey LO and Rentschler I (1991) Contrast thresholds for identification of numeric characters in direct and eccentric view. *Perception & Psychophysics* **49**: 495–508.

Strasburger H and Wade NJ (2015) James Jurin (1684-1750): A pioneer of crowding research? *Journal of Vision* **15**: 1–7.

Stringham J, Jammal AA, Mariottoni EB, Estrela T, Urata C, Shigueoka L, Ogata N, Tseng H and Medeiros F (2020) Visual Crowding in Glaucoma: Structural and Functional Relationships. *Investigative Ophthalmology & Visual Science* **61**: 3214–

3214.

Stuart JA and Burian HM (1962) A study of separation difficulty. Its relationship to visual acuity in normal and amblyopic eyes. *American Journal of Ophthalmology* **53**: 471–477.

Swanson WH, Felius J and Pan F (2004) Perimetric Defects and Ganglion Cell Damage: Interpreting Linear Relations Using a Two-Stage Neural Model. *Investigative Ophthalmology and Visual Science* **45**: 466–472.

Tailor VK, Theodorou M, Dahlmann-Noor AH, Dekker TM and Greenwood JA (2021) Eye movements elevate crowding in idiopathic infantile nystagmus syndrome. *Journal of Vision* **21**: 1–23.

Thibos LN, Cheney FE and Walsh DJ (1987) Retinal limits to the detection and resolution of gratings. *Journal of the Optical Society of America. A, Optics and image science* **4**: 1524.

Tkacz-Domb S and Yeshurun Y (2021) Temporal crowding is a unique phenomenon reflecting impaired target encoding over large temporal intervals. *Psychonomic bulletin & review* **28**: 1885–1893.

Toet A and Levi DM (1992) The two-dimensional shape of spatial interaction zones in the parafovea. *Vision Research* **32**: 1349–1357.

Tribble JR, Vasalauskaite A, Redmond T, Young RD, Hassan S, Fautsch MP,

Sengpiel F, Williams PA and Morgan JE (2019) Midget retinal ganglion cell dendritic and mitochondrial degeneration is an early feature of human glaucoma. *Brain Communications* **1**:

Tripathy SP and Cavanagh P (2002) The extent of crowding in peripheral vision does not scale with target size. *Vision Research* **42**: 2357–2369.

Tripathy SP, Cavanagh P and Bedell HE (2014) Large crowding zones in peripheral vision for briefly presented stimuli. *Journal of Vision* **14**:

Tripathy SP and Levi DM (1994) Long-range dichoptic interactions in the human visual cortex in the region corresponding to the blind spot. *Vision Research* **34**: 1127–1138.

Turpin A, Artes PH and McKendrick AM (2012) The open perimetry interface: An enabling tool for clinical visual psychophysics. *Journal of Vision* **12**: 22–22.

De Valois RL, Morgan H and Snodderly DM (1974) Psychophysical studies of monkey Vision-III. Spatial luminance contrast sensitivity tests of macaque and human observers. *Vision Research* **14**: 75–81.

Vassilev A, Ivanov I, Zlatkova MB and Anderson RS (2005) Human S-cone vision: Relationship between perceptive field and ganglion cell dendritic field. *Journal of Vision* **5**: 823–833.

Vassilev A, Mihaylova MS, Racheva K, Zlatkova M and Anderson RS (2003) Spatial summation of S-cone ON and OFF signals: Effects of retinal eccentricity. *Vision*

Research **43**: 2875–2884.

Vickery TJ, Shim WM, Chakravarthi R, Jiang Y V. and Luedeman R (2009) Supercrowding: Weakly masking a target expands the range of crowding. *Journal of Vision* **9**: 1–15.

Van Vliet AGM (1982) Nystagmus. *Documenta Ophthalmologica* **52**: 435–446.

Volbrecht VJ, Shrago EE, Schefrin BE and Werner JS (2000) Spatial summation in human cone mechanisms from 0° to 20° in the superior retina. *Journal of the Optical Society of America A* **17**: 641.

Wallis TS, Funke CM, Ecker AS, Gatys LA, Wichmann FA and Bethge M (2019) Image content is more important than Bouma's law for scene metamers. *eLife* **8**:

Watson AB. and Pelli D (1983) QUEST: A Bayesian adaptive psychophysical method. *Perception & Psychophysics* **33**: 113–120.

Watson AB (2014) A formula for human retinal ganglion cell receptive field density as a function of visual field location. *Journal of Vision* **14**: 15–15.

Wertheimer M (1923) Laws of organization in perceptual forms. *Psycologische Forschung* **4**:

Whitney D and Levi DM (2011) Visual crowding: A fundamental limit on conscious perception and object recognition. *Trends in Cognitive Sciences* 15(4), pp. 160–168.

Wichmann FA and Hill NJ (2001) The psychometric function: I. Fitting, sampling, and goodness of fit. *Perception and Psychophysics* **63**: 1293–1313.

Wickham H, Averick M, Bryan J, Chang W, McGowan L, François R, Grolemund G, Hayes A, Henry L, Hester J, Kuhn M, Pedersen T, Miller E, Bache S, Müller K, Ooms J, Robinson D, Seidel D, Spinu V, Takahashi K, Vaughan D, Wilke C, Woo K and Yutani H (2019) Welcome to the Tidyverse. *Journal of Open Source Software* **4**: 1686.

Wilkinson F, Wilson HR and Ellemberg D (1997) Lateral interactions in peripherally viewed texture arrays. *Journal of the Optical Society of America A* **14**: 2057.

Wilson ME (1970) Invariant features of spatial summation with changing locus in the visual field. *The Journal of Physiology* **207**: 611–622.

Wolford G (1975) Perturbation model for letter identification. *Psychological Review* **82**: 184–199.

Wright M (2021) An investigation into the contribution of receptive fields in the visual cortex to altered perimetric spatial summation in glaucoma. Cardiff University.

Yehezkel O, Sterkin A, Lev M and Polat U (2015) Crowding is proportional to visual acuity in young and aging eyes. *Journal of Vision* **15**: 23.

Zahabi S and Arguin M (2014) A crowdful of letters: disentangling the role of similarity, eccentricity and spatial frequencies in letter crowding. *Vision research* **97**: 45–51.

Zemel RS, Dayan P and Pouget A (1998) Probabilistic Interpretation of Population Codes. *Neural Computation* **10**: 403–430.

Zhang JY, Zhang GL, Liu L and Yu C (2012) Whole report uncovers correctly identified but incorrectly placed target information under visual crowding. *Journal of Vision* **12**: 5–5.

Zhang JY, Zhang T, Xue F, Liu L and Yu C (2009) Legibility of Chinese characters in peripheral vision and the top-down influences on crowding. *Vision Research* **49**: 44–53.

Zhou W, Muir ER, Nagi KS, Chalfin S, Rodriguez P and Duong TQ (2017) Retinotopic fMRI Reveals Visual Dysfunction and Functional Reorganization in the Visual Cortex of Mild to Moderate Glaucoma Patients. *Journal of Glaucoma* **26**: 430–437.